Y 3. At 7:
36/7-3

POWER REACTOR TECHNOLOGY

A Quarterly Technical Progress Review

Prepared for DIVISION OF TECHNICAL INFORMATION, USAEC, by
W. H. ZINN and J. R. DIETRICH, GENERAL NUCLEAR ENGINEERING CORPORATION

Summer 1964

● VOLUME 7

● NUMBER 3

ILLINOIS STATE LIBRARY
AUG 25 1964
U. S. Supt. of Documents Deposit

TECHNICAL PROGRESS REVIEWS

To meet the needs of industry for concise summaries of current atomic developments, the Atomic Energy Commission is publishing this series, Technical Progress Reviews. Issued quarterly, each of the reviews digests and evaluates the latest findings in a specific area of nuclear technology and science.

The five journals published in this series are:

Isotopes and Radiation Technology, P. S. Baker, A. F. Rupp, and associates, Oak Ridge National Laboratory

Nuclear Safety, Wm. B. Cottrell, W. H. Jordan, and associates, Oak Ridge National Laboratory

Power Reactor Technology, W. H. Zinn and J. R. Dietrich, General Nuclear Engineering Corporation

Reactor Fuel Processing, Stephen Lawroski and associates, Chemical Engineering Division, Argonne National Laboratory

Reactor Materials, R. W. Dayton, E. M. Simons, and associates, Battelle Memorial Institute

Each journal may be purchased from the Superintendent of Documents, U. S. Government Printing Office, Washington, D. C., 20402. *Isotopes and Radiation Technology* at $2.00 per year for subscription or $0.55 for individual issues; the other four journals at $2.50 per year and $0.70 per issue. See back cover for remittance instructions and foreign postage requirements.

The views expressed in this publication do not necessarily represent those of the United States Atomic Energy Commission, its divisions or offices, or of any Commission advisory committee or contractor.

Availability of Reports Cited in This Review

Unclassified AEC reports are available for inspection at AEC depository libraries and are sold by the Office of Technical Services, Department of Commerce, Washington, D. C., 20230. Some of the reports cited are not available owing to their preliminary nature; however, the information contained in them will eventually be made available in formal progress or topical reports.

Unclassified reports issued by other Government agencies or private organizations should be requested from the originator.

Unclassified British and Canadian reports may be inspected at AEC depository libraries. British reports are sold by the British Information Service, 45 Rockefeller Plaza, New York, N. Y.; Canadian reports (AECL series) are sold by the Scientific Document Distribution Office, Atomic Energy of Canada, Ltd., Chalk River, Ontario, Canada.

Classified U. S. and foreign reports identified in this journal as Classified may be purchased by properly cleared Access Permit Holders from the Division of Technical Information Extension, U. S. Atomic Energy Commission, P. O. Box 1001, Oak Ridge, Tenn., 37831. Such reports may be inspected at classified AEC depository libraries.

POWER REACTOR TECHNOLOGY

A REVIEW OF RECENT DEVELOPMENTS

Prepared for DIVISION OF TECHNICAL INFORMATION, USAEC,
by W. H. ZINN and J. R. DIETRICH,
GENERAL NUCLEAR ENGINEERING CORPORATION

SUMMER 1964

VOLUME 7

NUMBER 3

Foreword

This quarterly review of reactor development has been prepared at the request of the Division of Technical Information of the U. S. Atomic Energy Commission. Its purpose is to assist interested organizations in the task of keeping abreast of new results in reactor technology for civilian application.

Power Reactor Technology contains reviews of selected recently published reports that are judged noteworthy in the fields of power-reactor research and development, power-reactor applications, design practice, and operating experience. It is not meant to be a comprehensive abstract of all material published during the quarter, nor is it meant to be a treatise on any part of the subject. However, related reports from different sources are often treated together to yield reviews having some breadth of scope, and background material may be added to place recent developments in perspective. Occasionally the reviews are written by guest authors. Reviews having unusual breadth or significance are placed at the front of the issue as Feature Articles.

The intention is to cover the various areas of reactor development from the general viewpoint of the reactor designer rather than from the more detailed points of view of specialists in the individual areas. To whatever extent the coverage of *Power Reactor Technology* may occasionally overlap the fields of the other Technical Progress Reviews, the overlaps will be motivated by this objective of viewing current progress through the eyes of the reactor designer.

A degree of critical appraisal and some interpretation of results are often necessary to define the significance of reported work. Any such appraisal or interpretation represents only the opinion of the reviewer and (in the usual case, when the review is written by General Nuclear Engineering Corporation staff) the Editor. When the review is predominantly interpretive, the reviewer is named; unless identified as a guest author, he is a member of the General Nuclear Engineering Corporation staff. Readers are urged to consult the original references to obtain all the background of the work reported and to obtain the interpretation of the results given by the original authors.

For timely coverage, *Power Reactor Technology* must often review fragmentary material. The fixed subject headings listed below have been adopted in the hope of maintaining some continuity and order in the material from one issue to another: all reviews except Feature Articles will be arranged under these headings. A particular issue will not necessarily contain all the headings but only those under which material is reviewed.

Economics, Applications, Programs
Resources and Fuel Cycles
Physics
Fluid and Thermal Technology
Fuel Elements
Materials
Control and Dynamics
Containment, Radiation Control, and Siting
Systems Technology
Components
Design and Construction Practice
Operating Experience
Specific Reactor Types
Specific Applications
Unconventional Approaches

W. H. Zinn, President
J. R. Dietrich, Vice-President and Editor
General Nuclear Engineering Corporation

Y 3. At 7:
36/7-3

Contents

I Resources and Fuel Cycles 201
Fuel Management 201
References 205

II Physics 206
Critical and Exponential Experiments . . 206
Physics of Heavy-Water Lattices . . . 212
Resonance Integrals in Fertile Isotopes 214
Effective Cross Sections 215
Physics of Control Materials 216
Shielding 218
References 220

III Fluid and Thermal Technology . . . 223
Burnout Correlations from the Russian Literature 223
References 235

IV Fuel Elements 237
Fabrication by Novel Methods 237
References 246

V Control and Dynamics 248
Conference on Noise Analysis in Nuclear Systems 248
References 263

VI Containment, Radiation Control, and Siting 265
Vented-Containment Concept for the New Production Reactor 265
References 267

VII Components 269
Pumps for Liquid Metal 269
Flow Controller for Sodium Service . . 271
Control Rods and Drives 271
References 275

VIII Design and Construction Practice: Pathfinder and BONUS 276
Introduction 276
Pathfinder Atomic Power Plant 276
BONUS Power Station 292
Discussion 310
References 312

IX Operating Experience 313
Consolidated Edison Nuclear Steam Generating Station 313
Plutonium Recycle Test Reactor: Primary Coolant Pumps . . 315
Heavy-Water Components Test Reactor: Control- and Safety-Rod Drive Systems 316
Performance of the EBWR at Powers Up to 100 Mw(t). 317
References 320

X Specific Reactor Types 322
Pressurized Water: Study of Zircaloy Core Structure for N.S. *Savannah* . . 322
Organic-Cooled Reactors: The Tripartite Meeting 324
References 326

Issued quarterly by the Atomic Energy Commission. Use of funds for printing this publication approved by the Director of the Bureau of the Budget on October 14, 1963.

Section

I

Power Reactor Technology

Resources and Fuel Cycles

Fuel Management

The proceedings of a fuel management symposium that was held at the New York Operations Office of the AEC on Sept. 27, 1962, have been published.[1] Although considerable time has elapsed since the symposium, the material is still of interest, and selected results are noted briefly below.

The benefits to be derived from a program of partial-core reloading were studied in a project carried out by Jackson and Moreland, Inc., and Allis-Chalmers Mfg. Co. under AEC-Euratom sponsorship. The study was made in terms of the SENN reactor,[2] a dual-cycle boiling-water reactor which was designed by the General Electric Company and which is nearly identical to the Dresden reactor.

Of the refueling programs investigated, the out-in refueling shuffle proved most attractive. This involves unloading fuel from the centermost region of the core, shifting the remaining, partially exposed fuel inward to occupy the unloaded region, and adding fresh fuel in the resulting empty peripheral core positions. The advantage of partial reloading is an increase in the reactivity lifetime for a given feed enrichment (or for a given control capability), and the out-in shuffle gives the further advantage of flattening the radial power distribution by placing the most highly exposed fuel elements near the center of the core. The first of these advantages increases continuously, but at a decreasing rate, as the frequency of refueling is increased and the size of the reload batch is decreased. The second advantage increases with the frequency of refueling, at least up to a point, although there may be an optimum frequency for this effect, depending on the feed enrichment and the resulting fuel lifetime.

These relations are illustrated in Fig. I-1, which shows the power peaking factors and the discharge exposure of the fuel in the equilibrium cycle as functions of the number of reload batches into which the core is divided. The feed enrichment is held constant at 1.84% ^{235}U. Up to three or four batches, both the radial and axial peaking factors decrease as the number of batches is increased. Presumably the improvement in the axial factor is due partly

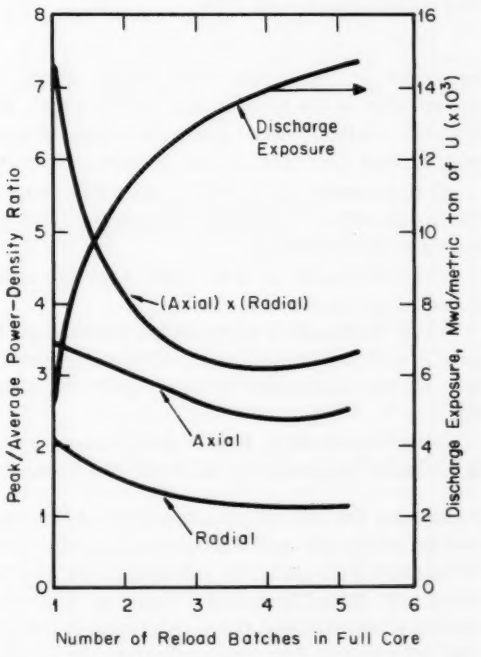

Fig. I-1 The fuel exposure at discharge and the power peaking factors calculated for the SENN reactor with out-in partial-core reloading.[3] The feed enrichment is held constant at 1.84% ^{235}U. All control rods are operated as a bank, and the curves apply to the equilibrium reloading cycle.

to the decreasing depth of insertion of the control rods (which are assumed to be operated as a bank) as the reactivity swing between loadings is reduced and partly to the increasing self-flattening by preferential fuel burnup as the fuel exposure increases. Eventually the exposure

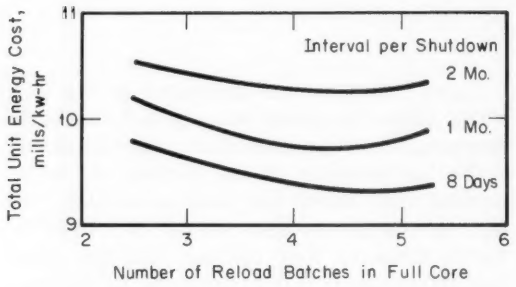

Fig. I-2 Calculated effect of the number of reload batches per core on total power-generation cost in the SENN reactor, for out-in reloading with constant feed enrichment of 1.84% ^{235}U.

becomes so high that the power drops off drastically in the most highly exposed fuel, and both the radial and axial factors increase slightly with further increases in the number of batches.

As the number of reload batches is increased, the main effects on the total power-generation cost are the following:

—the decrease in fuel-cycle cost due to the increasing exposure at discharge

—the decrease in capital cost component (up to the point of minimum power peaking factor) due to the increasing power capability of the reactor

—the decrease in plant factor caused by the increasing frequency of shutdown for reloading

In Fig. I-2 the net effect of energy cost has been estimated for three different values of the shutdown time required per refueling. The importance of this shutdown time is apparent. Crowley[3] emphasized the importance of designing the reactor for rapid refueling. In the discussion following the presentation of his paper, he indicated that, although refueling times from four to eight days have been used as "reference" values for some reactors, they have not yet been achieved. He did consider it reasonable, however, to consider routine refueling operations of one-month duration as compatible with the present state of the art.

In a study carried out at the Massachusetts Institute of Technology,[4] fuel cycles in the Canadian CANDU reactor were investigated. The CANDU reactor is a pressure-tube heavy-water type designed for fueling with natural uranium. The basic cost assumptions used are listed in Table I-1. For the study the enrichment of the fuel was considered to be open to variation, and one of the questions investigated was the effect of enrichment on fuel-cycle cost and total energy cost in the basic CANDU fuel management program of bidirectional push-through. The results are given in Table I-2.

As the fuel enrichment is changed, the degree of power flattening attainable in the equilibrium reactor, by adjusting the rate of push-through to give higher average exposure in the central region of the reactor, is changed. This is taken into account in the total (overall) power cost by assuming that the reactor size, and hence the capital cost, can be adjusted to take advantage of the maximum attainable power flattening. The study did not consider, however, any other changes in design variables, such as changes in lattice pitch.

In Table I-2 it is shown that one of the methods investigated for achieving the desired feed enrichment is by blending. This method is attractive primarily because the Canadian price for natural uranium is lower than the natural-uranium price used in fixing the price scale for

Table I-1 PRINCIPAL COST BASES FOR STUDY OF FUEL MANAGEMENT IN THE CANDU REACTOR[4]

Natural UO_2, \$/kg U	13.55
Enriched UF_6	USAEC price scale, 7/1/62
Plutonium nitrate credit, \$/g Pu	8.00
Conversion of UF_6 to UO_2, \$/kg U	12.50
Fabrication of fuel from UO_2, \$/kg U	42.78
Shipping of irradiated fuel, \$/kg U	15.45
Reprocessing of fuel to nitrates, \$/kg U	20.68
Conversion of UNH to UF_6, \$/kg U	5.60
Annual charges on	
Fuel fabrication working capital, %/yr	4.5
Uranium, %/yr	4.5
Plant investment, %/yr	7.76
Operation and maintenance, mills/kw-hr	1.02

slightly enriched uranium in the United States. The blending scheme involves mixing uranium of 3.2% enrichment, purchased in the United States, with Canadian natural uranium to produce uranium of the desired enrichment. This possibility involves both technical and regulatory problems that have not been explored in practice. In Table I-2 it is shown that the optimum enrichment for overall power cost is about 1.0%. This is true whether or not blending is used,

The paper by Puechl[5] of Nuclear Materials & Equipment Corporation is worthy of particular attention; this paper is more readily available, and in greater detail, in Refs. 6 and 7. The paper is a fuel management study of water-moderated reactors fueled with mixtures of natural uranium and plutonium isotopes. The plutonium mixtures considered are typical of those discharged from thermal power reactors and contain substantial fractions of ^{240}Pu. The

Table I-2 CALCULATED EFFECTS OF FUEL COST VARIABLES ON POWER COSTS IN THE CANDU REACTOR, WITH CONTINUOUS BIDIRECTIONAL FUELING[4]

Fuel enrichment	Fuel prepared by blending		Fuel not prepared by blending	
	Fuel reprocessed	Fuel not reprocessed	Fuel reprocessed	Fuel not reprocessed
	Fuel-cycle costs, mills/kw-hr			
Natural U			(1.03)*	0.99
1.0 at.% ^{235}U	0.83	0.89	0.99	1.05
1.3 at.% ^{235}U	0.86	0.92	0.93	0.99
1.5 at.% ^{235}U	0.93	0.96	0.97	1.00
	Overall power costs, mills/kw-hr			
Natural U			(6.56)	6.52
1.0 at.% ^{235}U	6.21	6.27	6.37	6.43
1.3 at.% ^{235}U	6.30	6.36	6.38	6.44
1.5 at.% ^{235}U	6.45	6.48	6.50	6.53

*Numbers in parentheses are for cases where reprocessing is not economically justified.

although the improvement is large only for the blending case. A comparable or somewhat greater improvement would, of course, be available without blending if the U. S. enriched-fuel price schedule were based upon the Canadian price for natural uranium.

Table I-3 shows the results of the investigation of other refueling methods in the CANDU reactor. For each of these cases, an investigation similar to that recorded in Table I-2 was carried out. In Table I-3 the results are recorded for the enrichments calculated to give the minimum total power cost in each case. The advantage of the bidirectional push-through program appears to be clearly confirmed, although it must be remembered that the study was confined to the basic CANDU design, and no investigation was made of qualitative variations in the plant design which might turn the other fuel-cycle approaches to particular advantage.

author points out that quite long reactivity lifetimes can be achieved with these mixtures at relatively modest values of initial excess reactivity. Basically this is because the ^{240}Pu acts in much the same way as a burnable poison, but with the accentuated effect, since the absorption of a neutron in ^{240}Pu not only removes a ^{240}Pu atom (a poison) but also produces a fissile atom of ^{241}Pu. The effect, however, is a complex one since the cross sections of both ^{239}Pu and ^{240}Pu vary strongly with neutron energy and, therefore, the behavior of the neutron energy spectrum during the fuel exposure is important. Figure I-3 shows the computed reactivity lifetimes for two different cases, and in each the initial plutonium loading contained 12% ^{240}Pu. The details of these cases are given in Table I-4.

Puechl[5] also shows that the reactivity lifetime is quite sensitive to the fuel-to-moderator ratio and that the optimum ratios tend to be

Table I-3 CALCULATED EFFECTS OF DIFFERENT REFUELING METHODS ON POWER COSTS IN THE CANDU REACTOR[4]

	Fuel prepared by blending		Fuel not prepared by blending	
	Fuel re-processed	Fuel not reprocessed	Fuel re-processed	Fuel not reprocessed
Continuous bidirectional refueling				
Feed enrichment for lowest power cost,* % ^{235}U	1.0	1.0	1.0	1.0
Fuel-cycle cost for lowest power cost, mills/kw-hr	0.83	0.89	0.99	1.05
Lowest total power cost, mills/kw-hr	6.21	6.27	6.37	6.43
Discontinuous out-in refueling				
Feed enrichment for lowest power cost,* % ^{235}U	1.3	1.3	1.3	1.3
Fuel-cycle cost for lowest power cost, mills/kw-hr	1.33	1.34	1.44	1.45
Lowest total power cost, mills/kw-hr	6.78	6.79	6.89	6.90
Single-batch refueling				
Seed enrichment for lowest power cost,* % ^{235}U	1.75	1.75	1.75	1.75
Fuel-cycle cost for lowest power cost, mills/kw-hr	1.74	1.75	1.79	1.80
Lowest total power cost, mills/kw-hr	7.18	7.18	7.23	7.23

*The enrichments considered were natural uranium, 1.0%, 1.3%, 1.5%, and 1.75%.

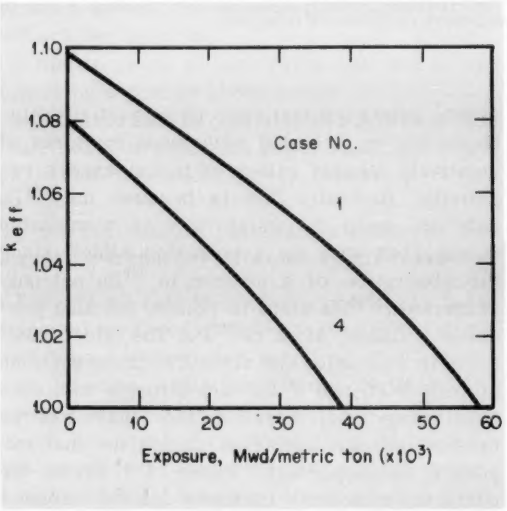

Fig. I-3 Reactivity lifetimes[5] of two H_2O-moderated cores fueled with natural uranium plus plutonium containing 12% ^{240}Pu. See Table I-4 for further characteristics.

Table I-4 CHARACTERISTICS OF THE PLUTONIUM-FUELED CORES[5] GIVING REACTIVITY LIFETIMES SHOWN IN FIG. I-3

	Case 1	Case 4
Surface-to-volume ratio of fuel elements, cm^{-1}	5.36	7.00
Moderating ratio, $\xi\Sigma_s$ per fuel* atom, barns	150	150
Σ_a (moderator) per fuel* atom, barns	2.84	2.84
Σ_a (cladding) per fuel* atom, barns	3.0	3.92
Core life, Mwd/metric ton	57,500	39,400
Initial k_{eff}	1.0983	1.0806
Initial Pu content of fuel,* at.%	7.84	6.33
Final Pu content of fuel,* at.%	5.52	4.90
Final isotopic composition of Pu, at.%		
^{239}Pu	49.6	53.6
^{240}Pu	22.4	20.8
^{241}Pu	19.0	19.0
^{242}Pu	9.0	6.6
Initial U enrichment	Natural	Natural
Final U enrichment, (atoms ^{235}U/atoms U) × 100	0.346	0.413
Net Pu change, kg/metric ton	26.9	17.3
Net U change, kg/metric ton	28	24

*The "fuel" comprises all the uranium and plutonium present.

lower than is desirable from the point of view of power density in the reactor core. Another point that is suggested by Table I-4 is that the loss of reactivity which does occur is due not so much to the net burnup of plutonium but to the degradation of the plutonium isotope mixture to one which contains a higher percentage of nonfissile isotopes. One wonders what method would be optimum for reenriching the discharged fuel for further recycle.

Puechl[5] suggests that the recycle of plutonium is not simply a matter of producing plutonium-bearing fuel elements but that there may be unique advantages to be exploited in the plutonium-fuel concept, as well as unique considerations of reactor design to be taken into account.

References

1. Fuel Management Symposium Held at New York Operations Office, New York, N.Y., September 27, 1962, USAEC Report TID-7665, October 1963.
2. C. Matteini, The Garigliano Nuclear Power Station, *Nucl. Eng.*, 4(38): 200-203 (May 1959).
3. J. H. Crowley, Fuel Management Study of the SENN Reactor, in Fuel Management Symposium Held at New York Operations Office, New York, N. Y., September 27, 1962, USAEC Report TID-7665, pp. 1-12, October 1963.
4. M. Benedict, Physics Model for Fuel Management Study of the Spectral Shift Reactor and Recalculations of Costs of the Heavy Water Reactor, in Fuel Management Symposium Held at New York Operations Office, New York, N.Y., September 27, 1962, USAEC Report TID-7665, pp. 40-56, October 1963.
5. K. Puechl, Fuel Management Study of a Water Moderated UO_2PuO_2 System, in Fuel Management Symposium Held at New York Operations Office, New York, N. Y., September 27, 1962, USAEC Report TID-7665, pp. 103-137, October 1963.
6. K. H. Puechl, The Potential of Plutonium as a Fuel in Near-Thermal Converter Reactors, *Nucl. Sci. Eng.*, 12(2): 135 (February 1962).
7. K. H. Puechl, The Potential of Plutonium as a Fuel in Near-Thermal Burner Reactors, *Nucl. Sci. Eng.*, 12(2): 151 (February 1962).

Section

II

Power Reactor Technology

Physics

Critical and Exponential Experiments

Boiling Reactors

Experiments relating to exponential work on the BORAX-V reactor were cited in *Power Reactor Technology*, 7(1): 7. Further work on this reactor, covering the zero-power critical experiments performed with boiling core B-1, is recorded in Ref. 1. The fuel rods for core B-1 consist of type 304 stainless-steel tubes with an outside diameter of 0.375 in. and a wall thickness of 0.015 in. These rods contain UO_2 that is enriched to 4.95 wt.% ^{235}U. The active fuel height is 2 ft. The square fuel bundles, $3\frac{7}{8}$ in. on a side, may contain any number of fuel rods from 0 to 49. The full core (Fig. II-1) contains 60 fuel bundles on an 8 by 8 array, with the corner bundles missing, and has an effective diameter of 39 in. Poison rods having the same dimensions as the fuel rods could be substituted for fuel rods for flux-flattening purposes and to control excess reactivity. The core contained nine control rods of boral canned in stainless steel; the central rod and four intermediate rods were cruciform in shape, and the four outer rods were T shaped. The zero-power experiments covered the range from room temperature to the operating condition at 489°F and 600 psig. The major core characteristics measured included critical mass, control-rod calibrations, excess reactivity, shutdown reactivity margin, reactivity effects of various core components, reactivity effects of temperature and voids, neutron-flux and power distributions, and cadmium ratios. Also, some development work was done on a rotating oscillator rod that was installed toward the end of the experimental program.

The experiments indicated that the available excess reactivity at 489°F and 600 psig was 3.2%. Because the void coefficient measurements were made at room temperature and it was expected that the void worth would be higher at operating temperature, it was estimated that the rated full power of 20 Mw(t) could not be achieved. This condition resulted from the requirement that the reactor must be subcritical, in its most reactive state, with eight control rods inserted fully and the ninth control rod withdrawn fully. To accomplish this, a number of boron–stainless-steel poison rods were substituted for fuel rods, thus reducing the reactivity available for power operation. As a result of this, the planned power operation of the core was canceled and changes in the design of core B-2 were undertaken to achieve more excess reactivity.

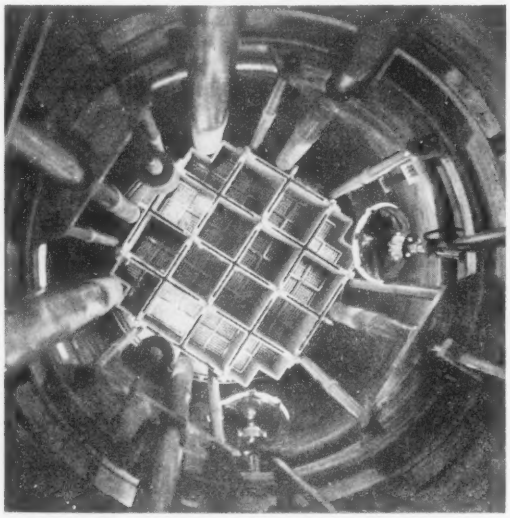

Fig. II-1 Boiling core B-1 of BORAX-V.[1]

Experiments to provide tests of analytical techniques used for predicting reactivity coefficients, detailed power distributions, and spectral variations, with special emphasis on control augmentation in boiling-water reactors, were performed at Vallecitos by the General Electric Company.[2] It is pointed out in Ref. 2 that the control augmentation is sought in order to improve power-reactor designs in the following areas:

1. Reduction in the worth of the movable control required, which in turn leads to increased plant safety
2. Extension of the average fuel exposure made possible with the increased reactivity in the initial core load
3. Flattening of the power distribution by more desirable control distribution

The particular method of control augmentation investigated utilized temporary poison slabs of boron steel. The core characteristics of interest were measured for a range of poison concentrations in the slabs. Two types of fuel rods were used in these experiments. The central zone of the core contained type 304 stainless-steel tubes that had an outside diameter of 0.500 in. and a wall thickness of 0.028 in. The tubes were filled with UO_2 pellets enriched to 2.01 wt.% U. The pellet density was 9.41 g/cm^3, and the pellet outside diameter was 0.444 in. The active fuel height was 67 in. In experiments requiring a driver region, the central core region was surrounded by fuel tubes made of 2S aluminum. The driver tubes had an outside diameter of 0.502 in.; the UO_2 pellets had an outside diameter of 0.491 in., a density of 10.0 g/cm^3, and an enrichment of 1.6 wt.% ^{235}U. The active fuel height in these tubes was 48.0 in. A typical core arrangement is shown in Fig. II-2. The core configurations studied were typical of boiling-water reactor lattices and included assemblies with black and gray absorbing slabs and control-rod cruciforms. Differential reactivity and spectrum effects were investigated for various poison and void tube perturbations. The spatial variation of the neutron spectrum and density in a typical boiling-water lattice was studied by means of the resonance spectral indicator method. This method utilizes foils of materials with well-defined resonances in the energy range of 0.5 to 5.0 ev. Strong spectral variations across the fuel bundles were observed. These variations exist in power reactors and are important in reactor design.

Light-Water-Moderated Assemblies

Critical approach and exponential experiments were performed by General Electric at Hanford on 1.82 wt.% plutonium-aluminum fuel rods. The purpose of these experiments was to determine the effect on criticality of small differences in the concentration of the ^{240}Pu isotope. Reference 3 describes the cylindrical lattice array that was studied. The fuel rods used in this experiment were 0.500 in. in diameter and 44 in. in length. They were sealed in Zircaloy-2 tubes that had an outside diameter of 0.566 in. and a wall thickness of 0.030 in. The average plutonium content was 7.12 g per rod. The amount of the ^{240}Pu isotope varied, but there were two principal groups of rods. One group contained an average of 5.05 wt.% ^{240}Pu in the plutonium, and the other group contained an average of 6.0 wt.% ^{240}Pu. Experiments were performed with the two groups of rods alternately in either an inner or outer

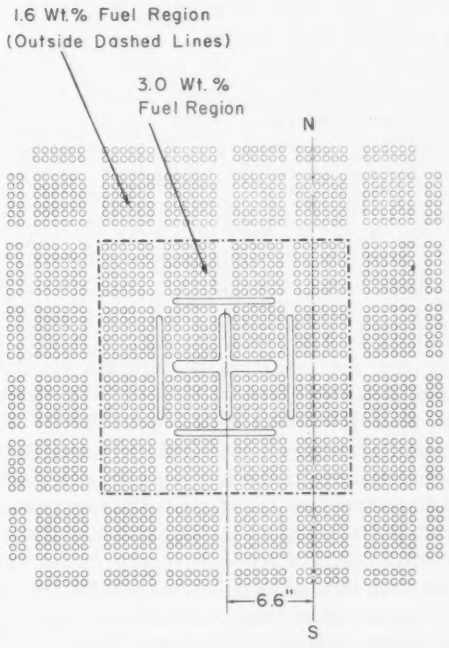

Fig. II-2 Fuel regions for the poison-curtain study.[2]

zone. Calculations were fitted to those two experiments to yield an average ^{240}Pu concentration that could be associated with each experiment; i.e., an average ^{240}Pu concentration was specified as a function of the critical number of rods in both cases. A plot was made of the number of fuel rods vs. ^{240}Pu content and extrapolated linearly to the number of rods for criticality of the mixed loading. The number of rods for criticality of a loading that contained a mixed ^{240}Pu content is also reported in Ref. 3. This extrapolation indicated that the average ^{240}Pu content in the mixed loading was greater than that for any rod in the mixed lattice. It is concluded that either there is a systematic error that has not been detected in the results from the mixed loadings or that the critical mass of plutonium varies more strongly with ^{240}Pu concentration than the calculations predict.

Also given in Ref. 3 are the results of measurements of the relative plutonium content of plutonium-aluminum fuel elements using reactivity coefficients measured in the Physical Constants Testing Reactor (PCTR). These measurements were compared with chemical analysis, and rods were selected on this basis for use in lattice experiments.

Results of critical and exponential experiments performed on small, highly enriched light-water-moderated cores are given in Ref. 4. The fuel elements for these experiments were formed by bolting together 3- by 12- by 0.018-in. plates of uranium-aluminum alloy and 3- by 12- by 0.30-in. plates of stainless steel. High-density polythene washers were used to separate the plates for the required metal-to-water volume ratios. Each fuel plate contained 11 g of 93 wt.% enriched uranium. To allow for the insertion of cadmium shutdown plates, a lattice pitch of 0.35 in. was chosen. This pitch left water gaps approximately 0.35 in. wide between adjacent fuel elements. Critical and exponential bucklings as well as gross- and fine-structure flux distributions were measured. An analysis of the experiments utilizing the MUFT-SOFOCATE few-group model indicates that this method is adequate for the calculation of the critical size of highly absorbing light-water-moderated lattices. Other conclusions inferred from these experiments are

(b) In reactor systems with critical heights down to a minimum of 12 in. there is no evidence that separation of spatial variable in the macroscopic flux distribution is invalid to within the experimental accuracies of ±1 cm. (vertical) and ±1.5 cm. (horizontal) in the determination of the extrapolated core dimensions.

(c) The theoretical mode underestimates thermal flux peaking due to wide water gaps (0.35 in.) in the core. Although this may be significant in calculations of fuel power peaking, the theoretical predictions are adequate to provide "flux weighting factors" for the calculation of reactivity and critical size.

(d) Measurements of material buckling and thermal fine structure can be made in light water moderated exponential assemblies as small as 12 in. sq. and 24 in. high.* Measurements in smaller assemblies diverge significantly from the critical determinations.

*In terms of migration lengths these dimensions are equivalent to five migration lengths square and ten migration lengths high.

A report of a panel on light-water lattices held in Vienna May 28–June 1, 1962, is given in Ref. 5. Physicists from most of the well-known laboratories in the field attended this meeting. The formal papers prepared for the meeting were not read but rather served as a basis for information discussion in which other relevant matters could be introduced which had not been formally prepared. The formal papers are, however, printed in their entirety in Ref. 5. Most of the experimental work cited has been reviewed either in *Power Reactor Technology* or elsewhere, and no attempt will be made here to describe each of the experiments. However, the reader should consult Ref. 5 for a systematic tabulation of experimental results on light-water lattices. It was pointed out in the discussions that reasonably uniform practices are used at the present time for the calculation of light-water lattices, and toward the end of the discussion the panel tried to estimate the uncertainties in the calculation of eigenvalues. These uncertainties depend on such things as the water-to-fuel ratio, the rod size, and the fuel enrichment. Although the estimates of uncertainties were largely intuitive, they are of interest (see Table II-1). If these uncertainties were really present and if they all acted in the same direction, they would amount to 3.1% in the eigenvalue. If they were combined statistically (being nearly independent), they would amount to 1.3%. The observed difference between calculation and experiment is somewhat smaller than the 1.3%, indicating that there is

Table II-1 EFFECT OF UNCERTAINTIES ON THE EIGENVALUE[5]

Source of uncertainty	Effect on eigenvalue, %
Resonance absorption	0.5
Thermal-flux spatial distribution	0.3
Thermal η (^{235}U)	0.7
Fast fission factor calculation	0.3
Leakage calculation	0.5
Epithermal η (^{235}U)	0.7
Cross sections used in thermal utilization	0.1

either a canceling of errors in the calculations or that overestimates are given in Table II-1.

Heavy-Water Assemblies

Critical bucklings were measured for heavy-water-moderated lattices of natural-uranium-metal rod clusters in the Process Development Pile at Savannah River Laboratory. The results of these measurements are given in Ref. 6. Fuel for these assemblies consisted of uranium-metal slugs having a diameter of 0.988 in. The slugs were 8.07 in. long and had an average density of 18.9 g/cm^3; they were loaded into air-filled aluminum tubes 12 ft long, with outside and inside diameters of 1.090 and 1.026 in., respectively. These rods were suspended in the reactor tank either individually or in clusters of 3, 7, or 19 rods. With one exception the rods in each cluster were spaced in a triangular array on 1.5-in. centers. The exception was a special 7-rod cluster in which the rods were spaced on 2.0-in. centers. The fuel assemblies were loaded in the reactor on triangular pitches ranging from 7.0 in. to 21.0 in.

Reference 6*a* presents the results of material buckling measurements with the same rods. These measurements were made in an exponential facility, and the results were compared with measurements in the critical facility. A systematic difference in the bucklings was noted. Although the exact nature of the processes involved are not well understood, the effect has been shown (see Ref. 22) to be systematic changes in the exponential buckling which exceed those that can be calculated from simple two-group theory.

Reference 7 gives the results of critical buckling measurements of 25 heavy-water-moderated lattices of natural-uranium oxide rod clusters. These measurements were made in the Process Development Pile at Savannah River. The fuel rods consisted of 9-ft-long aluminum tubes that had an outside diameter of 0.547 in. and a wall thickness of 0.02 in. These tubes were filled with sintered uranium oxide pellets which were $\frac{1}{2}$ in. in diameter and which had an average density of 10.4 g/cm^3. Fuel assemblies containing 19, 31, and 48 rods were built up from the fuel rods. The assemblies were loaded in the reactor on triangular lattice pitches that ranged from 8.08 to 16.17 in. In some experiments the fuel clusters were encased in housing tubes made of aluminum, with outside diameters of 4.00, 5.00, and 6.00 in. and wall thicknesses of 0.054, 0.056, and 0.058 in., respectively. Migration areas were also measured. This was accomplished by measuring the pile periods resulting from small increases in water height, converting these periods to changes in k_{eff} by means of the inhour equation, and then using two-group theory to calculate the migration area from the $\Delta k_{eff}/\Delta B^2$ values. It is pointed out that the buckling measurements should be accurate to about 1% and that the measured migration areas are in good agreement with those obtained from the Benoist theory. (The appropriate references for the Benoist theory are Refs. 8 and 9).

Measurements of initial conversion ratios and fast fission factors at five hexagonal lattice spacings in a 19-element UO_2 CANDU type fuel bundle have been made in a ZED-II lattice at Chalk River. The fuel bundles contained cold D_2O coolant. Reference 10 describes the details of the measurements. One conclusion reached was that a previous model used by Duret and Marriott,* which assumed the fast fission factor to be independent of lattice spacing, should be modified to account for the variation shown by the experiments.

Graphite-Moderated Assemblies

Reference 11 gives the results of critical measurements on systems that are thorium loaded, graphite moderated, and oralloy fueled (93.16% ^{235}U). These experiments are a part of a program to study the characteristics of long-life high-temperature gas-cooled reactors. In particular, the experiments were designed for the comparison of graphite-moderated critical

*The model used by Duret and Marriott is described in the Canadian Report CRRP-873, A Computer Program for Reactor Studies, 1959.

assemblies with and without thorium, in hopes that the effects of uncertainties in uranium cross sections would cancel to yield more accurate information about resonance capture in thorium. The assembly for these experiments consisted of a lattice of thin oralloy foils equally spaced between graphite moderator blocks 0.5 and 1.0 in. thick. Thorium-metal foils that had the same dimensions as the oralloy foils were also placed within the assembly at regular intervals. Results of the experiments were compared with earlier experiments that had the same composition except for the thorium foils. Resonance group cross sections are deduced from the experiments and are compared with calculations from basic resonance parameter data.

The PCTR small-lattice techniques have been discussed in earlier issues of *Power Reactor Technology*, in particular 7(1): 4 and 8. Reference 12 gives results of PCTR measurements on the lattice of the Experimental Gas-Cooled Reactor being built at Oak Ridge. The fuel assembly is a cluster of seven uranium oxide rods clad with stainless steel. The steel cladding has an outside diameter of 0.705 in. and a wall thickness of 0.020 in. The fuel consists of UO_2 pellets, enriched in the ^{235}U isotope, having an outside diameter of 0.323 in. and a density of 10.4 g/cm^3. Two fuel enrichments were studied: 1.8 and 2.5 wt.% ^{235}U. The fuel rods were spaced on an 8-in.-square pitch in a graphite moderator. The infinite multiplication factor and thermal utilization were measured for both enrichments. In addition, both the resonance escape probability and the fast fission factor were measured for the 1.8% enrichment. Results of this work provide a basis for reactor calculations on lattices of this type.

Results of similar measurements utilizing the PCTR techniques are given in Ref. 13 for lattice parameters of solid and concentric tubes of natural-uranium fuel in graphite lattices. The basic measurements were made for the concentric tube in a 10.5-in. graphite lattice as well as in an 8.375-in. lattice. Measurements were made with both water and air in the coolant channels for the 10.5-in. lattice and with water only in the smaller lattice. Basic measurements on the solid fuel were limited to the 10.5-in. water- and air-cooled lattice. Fuel dimensions and associated data are given in Table II-2.

Table II-2 DIMENSIONS AND RELATED DATA ON LATTICES STUDIED IN REF. 13

	Concentric tube fuel		Solid fuel	
Radii of cell components, cm				
	Inside	Outside	Inside	Outside
Fuel	1.422	2.108		
	2.540	3.175		3.175
Cladding	1.237	1.400		
	2.133	2.205		
	2.439	2.528		
	3.189	3.278	3.189	3.273
Coolant tube	3.840	4.003	3.840	4.003
Graphite				
10.5-in. lattice	4.035	15.050*	4.035	15.050*
8.375-in. lattice	4.035	12.001*		
Densities, g/cm^3				
Fuel	18.81		18.86	
Aluminum	2.7		2.7	
Graphite	1.615		1.610	
Water	1.0		1.0	
Weights in central cell, g				
Fuel	18,164		30,347	
Cladding	755.5		255.9	
Process tube	531.0		531.0	
Water	1,060		631.0	
Graphite				
10.5-in. lattice	54,193		54,007	
8.375-in. lattice	32,874			

*Radius of cylindrical cell of equal area.

Zirconium Hydride Assemblies

Critical experiments performed to evaluate results of the consequences of water immersion of SNAP-2/10A reactor cores are given in Ref. 14. The fuel for these experiments was an alloy of zirconium–10 wt.% (93.2% enriched) uranium, hydrided to a concentration of 6.5×10^{22} atoms of hydrogen/cm^3. The fuel rods were clad with Hastelloy that had an outside diameter of 1.250 in. and a wall thickness of 0.011. The fuel diameter was 1.212 in., and the rod length was 12.225 in. The rods were arranged on a triangular pitch of 1.260 in. in the full core, which contained 37 fuel rods and was hexagonal in shape. The coolant for the SNAP-2/10A reactors normally is NaK, but the experiments reported on in Ref. 14 were conducted with the core flooded with water or voided with the aid of Styrofoam displacers. To simulate immersion the core was surrounded by several tanks which could be filled with water to various levels. Pulsed-neutron techniques were used to measure the excess reactivity of the fully loaded, fully water-reflected assemblies that were studied. The measurements were compared with diffusion theory and transport calculations. It was shown that much better agreement was obtained between theory and experiment when the experiments were compared with transport calculations that assumed anisotropic scattering rather than diffusion theory or transport theory with isotropic scattering.

Fast-Neutron Assemblies

The ZPR-III critical facility was described in *Power Reactor Technology*, 7(1): 11. Reference 15 gives a further comparison of experimental parameters of assemblies studied in this facility with calculations utilizing a set of cross sections deduced from the published set by Yiftah et al.* Critical masses of a large number of assemblies were calculated to an accuracy of about 5%. Other conclusions are quoted as follows:[15]

(2) The calculated relative fission rates of U^{233}, Pu^{239}, Pu^{240}, U^{236}, and U^{238} are in good agreement with the measured data, but the calculated rates for U^{235} and U^{234} are 6% low and 7% high, respectively, relative to those of the other five isotopes. The disagreement between the calculated and experimental fission rates of U^{235} and those of U^{233} and Pu^{239} is insensitive to errors in the calculated spectrum and may be due to erroneous intercalibration of these chambers. This uncertainty regarding the intercalibration of the fission chambers must be removed before the fission-ratio data can be interpreted.

(3) In every case examined, the experimental prompt-neutron lifetime was larger than the calculated value. On the average, the experimental value was 34% greater than the calculated and was moderately constant for all the assemblies, with extreme values of 24% and 48%. The discrepancy is too large to be attributed to experimental errors, and it appears that all the calculated spectra are too hard.

(4) The lack of data on the effect of the sample size upon the measured central reactivities is held to be a serious drawback to the interpretation of much of the reactivity data. It is argued that this should not be important in the comparison of the relative reactivity effects of U^{233}, U^{235}, and Pu^{239}, and also should not affect the general conclusions to be drawn from cases such as carbon and boron-10 in which the discrepancies between experiment and calculation are very large.

(5) The calculated relative central reactivities of U^{233}, U^{235}, and Pu^{239} are in moderately good agreement with experimental data. These data are not sensitive to the calculated spectra. The agreement indicates that the assumed nuclear data for these isotopes are reasonably accurate.

(6) The reactivity effects of the scatterers carbon, oxygen, aluminum, and sodium are shown to be principally dependent upon the importance spectrum and, hence, can be considered as principally importance-spectrum indices. There are large discrepancies between the experimental and calculated reactivities, particularly in the systems with soft importance spectra, and it is inferred that the calculated importance spectra are too hard.

(7) The experimental and calculated central reactivities of steel are in excellent agreement, and those for zirconium are in quite good agreement. In view of the evidence of appreciable errors in the calculated real flux and importance spectra, it appears that this agreement might be fortuitous.

(8) There are large discrepancies between the experimental and calculated central reactivities of the heavy absorbers Mo, Nb, Ta, Th^{232} and B^{10}. Of particular note is the experimental reactivity of B^{10}, 31% greater than calculated. Since the $\sigma(n,\alpha)$ for B^{10} is roughly $1/v$ in dependence, this is strong corroboration of the prompt-neutron lifetime data for which the discrepancy is 34%. Thus, the B^{10} central reactivity data also show that the calculated spectra are too hard.

*These cross sections appear in: S. Yiftah, D. Okrent, and P. A. Moldauer, *Fast Reactor Cross Sections*, Pergamon Press, Inc., New York, 1960.

The data for Mo, Nb, Ta and Th^{232} do not generally support the B^{10} data, but it is suggested that this may be due to uncertainty in the knowledge of $\sigma(n,\gamma)$ for these materials.

(9) The calculation of the reactivity effect of U^{238} is shown to be quite sensitive to the assumed cross sections due to competing reactions, and it is not possible to identify errors in U^{238} data. The agreement between results of experiment and calculation would be improved if the calculated spectrum were not so hard.

Spectral Shift

Experimental work under the Spectral Shift Control Reactor (SSCR) Basic Physics Program was reviewed in *Power Reactor Technology*, 5(4): 17; 6(2): 13; 6(3): 81; and 7(1): 8. References 16 to 19 are topical reports containing summaries of the experimental work as well as some analysis and interpretation of the experiments. Reference 16 summarizes results of 20 uniform lattice measurements that utilize 4.02% enriched UO_2 clad in stainless steel as fuel as well as 2.46% enriched UO_2 clad in aluminum. Lattice nonmoderator-to-moderator volume ratios varied from 0.65 to 1.2. The moderator mixtures of light and heavy water ranged from 0 to 77 mole % D_2O. Theoretical interpretation has shown that these systems are very sensitive to the resonance integral of ^{238}U. Also, it was pointed out that the multiregion, few-group diffusion model provides an adequate means of predicting lattice criticality as well as space and energy flux distributions over a large range of lattice parameters.

Reference 17 gives a summary of the perturbation experiments as well as an analysis of these experiments. The PDQ-4 four-group two-dimensional code and the TKO four-group three-dimensional code were used for the analysis. Coefficients for the diffusion equation were calculated utilizing the BPG computer code. In general, the agreement between calculations and experiment is good.

Reference 18 is a summary of the small-lattice work. In addition to the work reviewed in *Power Reactor Technology*, 7(1): 8, lattice parameters for fuel rods containing thorium as the fertile material were measured at two heavy-water concentrations, namely, 70.4 and 80.4 mole %. Although critical experiments were not available for comparison as was the case with the UO_2 measurements, the results appear to be consistent and are in reasonably good agreement with theoretical predictions.

In spectral shift reactors the large epithermal absorption by the fertile material leads to cadmium ratios close to unity for this material. Errors in cadmium ratios of this magnitude lead to very large errors in ρ_{28}, the ratio of epicadmium to subcadmium absorptions. This has given incentive for the development of a method of measuring this quantity with some degree of accuracy. Reference 19 describes such a technique, which has been demonstrated by measurements to 1% in 12 water-moderated lattices. The principal advantages of the method are[19]

1. Uranium activities are measured by chemically processing the irradiated fuel to avoid problems associated with the use of ^{238}U foils.
2. Cadmium-covered uranium measurements are eliminated to avoid cadmium perturbations.
3. ρ_{28} is obtained directly, rather than by the difference between the cadmium ratio and unity, to avoid large errors when the cadmium ratio approaches unity.

Physics of Heavy-Water Lattices

Several analytical schemes have been employed in the past to determine D_2O lattice bucklings from test-lattice data obtained by fuel assembly substitution measurements. Reference 20 presents a comparison between experiment and predictions of three such analytical schemes for test lattices that have bucklings known from previous one-region pile measurements.

A typical substitution measurement of a lattice buckling has three steps: (1) a reference measurement in a one-region lattice, (2) the substitution of one or more test fuel assemblies for reference fuel assemblies, and (3) a remeasurement in the mixed lattice. Three methods of analysis are described and compared with experiment. The first is a one-group three-region perturbation method (after Persson)* which requires experimental data for test regions of at least two different sizes. These results are then used to extrapolate to the case in which the test lattice extends through

*Persson's work is referenced in the following report: R. Persson, One-Group Perturbation Theory Applied to Substitution Measurements with Void, Swedish Report RFX-74, 1961.

the pile. The second method is a two-region two-group approach which utilizes a single measurement of the critical moderator height with test assemblies present and a measurement of the critical moderator height with the one-region reference loading. This analysis requires a knowledge of the fast and slow diffusion coefficients, the fast and slow migration areas, and the resonance escape probability for both the reference and test lattices. The third method involves two-group three-region calculations and thus combines features of the two preceding methods. At least two differently sized substitution loadings are made and the results analyzed in concert by two-group theory to eliminate the effect of the intermediate zone of immediately adjoining test and reference fuel assemblies while obtaining the buckling for the test region.

All experimental measurements were performed in the Process Development Pile on a 9.33-in. triangular pitch. The fuel assemblies employed in the test lattices were of four types: (1) a 31-element UO_2 rod cluster in a 5-in.-OD aluminum housing tube (0.056 in. thick); (2) a 19-element UO_2 rod cluster in a 4-in.-OD aluminum housing tube (0.054 in. thick); (3) a 19-element UO_2 rod cluster in a 5-in.-OD aluminum housing tube (0.056 in. thick); and (4) a single natural-uranium-metal rod. The 0.50-in.-OD natural-UO_2 columns had a density of 10.4 g/cm^3, were clad in a 0.547-in.-OD 0.02-in.-thick 6063 aluminum tube, and were spaced on a 0.650-in. triangular pitch within a cluster. The 0.998-in.-OD metal rod was clad in a 1.090-in.-OD 0.032-in.-wall 6063 aluminum tube. Reference fuel assemblies consisted of the 31-element UO_2 rod clusters with either D_2O or air-filled housing tubes. Extrapolated pile radii and vertical extrapolation distances were measured by the flux profile method. The perturbation method included measurements of the change in diffusion coefficients, $\delta D_z/D_z$, resulting from voiding the coolant channels of test assemblies. Conclusions on the applicability of the analytical methods were as follows: (1) the successive-substitution one-group perturbation method gave satisfactory results in all cases; (2) the two-region two-group method gave satisfactory results under limited conditions; and (3) the three-region two-group method worked well but did not offer any advantage over the one-group perturbation method to justify its greater complexity.

Further comparisons between experiment and predicted reactivity parameters for clusters of natural-uranium and oxide rods are presented in Ref. 21. The first part of this report is concerned with a comparison between the present calculational method employed at United Nuclear Corp. and two other methods in use during the period around 1959, i.e., prior to the existence of reliable data (k_∞ and B^2) on large clusters of natural-uranium rods, for normalization of calculational methods over the complete range of practical interest. The results of the three calculational methods are compared over the relatively broad range of parameters contained in the following experimental data: (1) measurements of k_∞ and material buckling for D_2O-cooled 7- and 19-element metal rod (0.515-in. diameter) and UO_2 rod (0.520-in. diameter) clusters at the Zero Energy Experimental Pile, Chalk River; (2) measurements of k_∞ for D_2O- and air-cooled 19-element UO_2 rod (0.504-in. diameter) clusters at the PCTR, Hanford; (3) measurements of material buckling for D_2O-cooled 7-element metal rod (1.0-in. diameter) clusters at the Process Development Pile, Savannah River; and (4) measurements of k_∞ for 19-, 31-, and 37-element UO_2 rod (0.5-in. diameter) clusters at the Pawling Lattice Test Rig (PLATR), United Nuclear Corp. In the latter group the experiments were chosen to check the ability of the calculational methods to calculate: k_∞ for D_2O-cooled lattices, coolant density coefficients, and the effect of replacing D_2O with low-density H_2O.

The second part of the report[21] contains a comparison between predictions of the calculational method presently employed at United Nuclear Corp. and the results of measurements of thermal utilization and k_∞ made in the PLATR. The latter facility was specially constructed for D_2O studies; k_∞ measurements are performed by the void-substitution or null-reactivity technique, similar to the method employed at the PCTR. Results are presented for 19-, 31-, and 37-element clusters of 0.5-in.-diameter UO_2 rods, for a series of experiments with fuel elements consisting of concentric tubes of UO_2 (inside diameters of 0.56, 1.24, 1.54, 2.52, 2.52, and 3.50 in. and outside diameters of 1.06, 2.04, 2.04, 3.02, 3.32, and 4.00 in., respectively), and 7-, 19-, and 31-element clusters of 0.5-in.-diameter UC rods. Coolants used include air, D_2O, low-density H_2O (fog), and organic (Dowtherm A).

Reference 22 provides a review of the requirements, methods, and accuracy of experimental physics studies performed on heavy-water lattices. The types of measurements discussed include those of buckling, multiplication constant, intracell lattice parameter, migration area, spectrum, and operating coefficients. Within each category the experimental methods and accuracy of measurement are discussed, and, where possible, the discussion is illustrated with examples taken from the heavy-water power-reactor studies at the Savannah River Laboratory. A broad spectrum of experimental methods and their interpretation is covered in a concise manner with a minimum of mathematical detail. An extensive bibliography is provided to supplement the mathematical aspects of the subject.

Resonance Integrals in Fertile Isotopes

Because the results of measurements of resonance integrals as a function of rod size have been sufficiently inconsistent to indicate the presence of large systematic errors in some of the measurements or in some of the interpretations, Pettus et al.[23,24] have measured the effective resonance integrals for the two fertile isotopes, ^{238}U and ^{232}Th, in both their metal and oxide forms as functions of lump size in the Lynchburg Pool Reactor at the Babcock & Wilcox Co. Nuclear Development Center. See Figs. II-3 to II-5. In addition to the resonance-integral measurements, Refs. 23 and 24 give measurements of temperature effects and determinations of the Dancoff factor. The Dancoff factor measurements substantiate calculations that utilize the Bell[25] approximation.

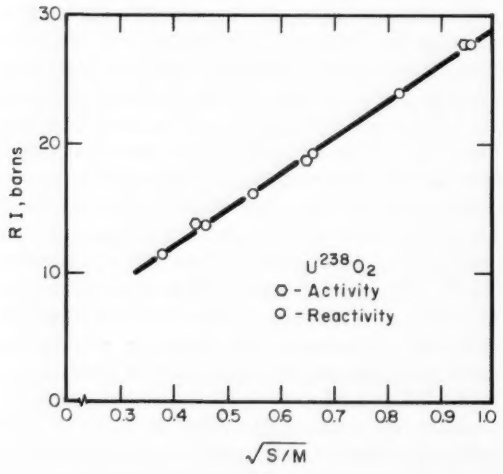

Fig. II-3 Uranium oxide effective resonance integral (RI) vs. $\sqrt{S/M}$.[23]

It is of particular interest that both activation and reactivity techniques were used to measure the resonance integrals independently and that results of the two techniques compared favorably. Apparently no comparable work using both techniques at the same facility has been reported. Linear fits to results obtained for the resonance integrals as a function of the square root of the surface-to-mass ratio are given below:

$$^{238}\text{U (metal)}\ RI = 2.4 + 26.2\sqrt{S/M}$$

$$^{238}\text{U (oxide)}\ RI = 0.8 + 28.2\sqrt{S/M}$$

$$^{232}\text{Th (metal)}\ RI = 3.91 + 14.81\sqrt{S/M}$$

$$^{232}\text{Th (oxide)}\ RI = 3.41 + 17.32\sqrt{S/M}$$

Note that no $1/v$ contributions are included in these expressions. The formulas for uranium were obtained from fits to both the reactivity and activation measurements, whereas the formulas for thorium are from the activation results only. The activation results are preferred because many complex calculations are required for the proper interpretation of the reactivity measurements. In particular, the neutron spectrum as well as the importance function must be calculated as a function of the lethargy within the cadmium sleeve where the measurements are made.

As an indication of the agreement between the activation and reactivity measurements, results are presented for uranium oxide in Fig. II-3. A comparison of this work on uranium with other recent measurements (Refs. 26 and 27 cited for comparison purposes) indicates that the uranium-metal results are in good agreement but that the uranium oxide results are systematically several barns lower. Although the differences in the uranium oxide results are not fully explained, note that in this work the same ratio of oxide-to-metal capture was obtained by both activation and reactivity measurements and that this ratio is independent of calibration errors. A comparison of the

results for thorium metal and oxide with recent measurements at other facilities is given in Figs. II-4 and II-5.

Reference 23 gives the results of measurement of the uranium metal and uranium oxide resonance integrals by activation techniques. A comparison of this work with previous measurements of Hellstrand indicates good agreement for uranium oxide and poorer agreement for uranium metal. It is pointed out,[28] however, that the difference between results for uranium metal is judged to be within the over-all uncertainty. Results of these measurements are given below.

For ^{238}U (metal):

$$RI = 6.09 + 24.8\sqrt{S/M} \qquad 0.4 < \sqrt{S/M} < 0.75$$

For ^{238}U (oxide):

$$RI = 3.91 + 27.8\sqrt{S/M} \qquad 0.2 < \sqrt{S/M} < 0.6$$

The $1/v$ part of the integral is included in these expressions.

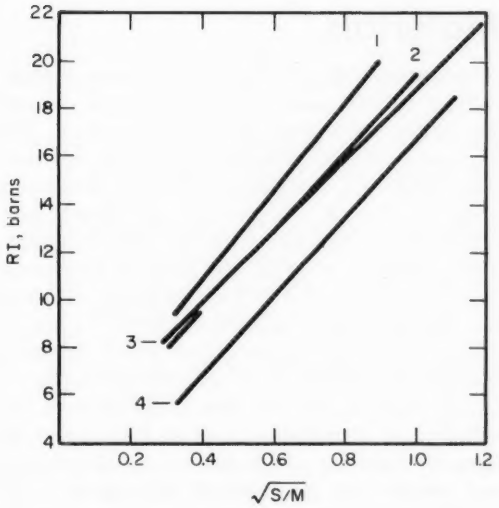

1. - Moore et al, British Report AEEW - R 57, 1961
2. - Hellstrand and Weitman, Swedish Report AE-99, 1962
3. - Present Work
4. - Rothman and Ward, Nuc. Sci. & Eng., 1; 293, 1962

Fig. II-4 Comparison of thorium-metal results with other recent measurements.[24]

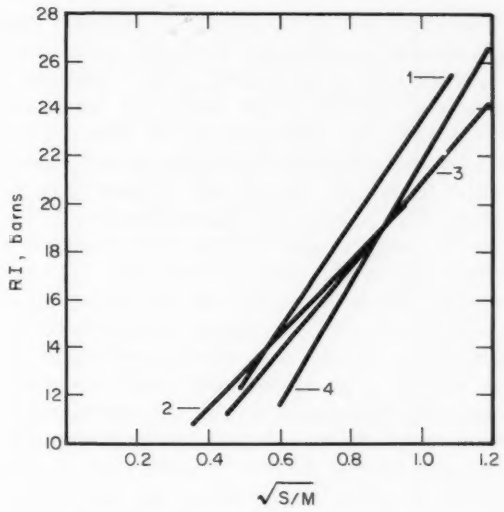

1. - Moore, et al, British Report AEEW-R57, 1961
2. - Hellstrand and Weitman, Swedish Report AE-99, 1962
3. - Present Work
4. - Thie, "Heavy Water Exponential Expts. Using ThO_2 and UO_2", Pergamon Press, 1961

Fig. II-5 Comparison of thorium oxide results with other recent measurements.[24]

Recent measurements of the effective resonance integral of thorium oxide rods are reported in Ref. 29. In the activation technique used, activities obtained in thermal and slowing-down neutron fluxes were compared and gold was utilized as a standard. The results of these thorium oxide measurements are expressed by:

$$RI = (4.9 + 15.5\sqrt{S/M}) \pm 5.0\%$$

The $1/v$ part of the integral is excluded from this expression.

Effective Cross Sections

The need for an accurate description of the time-dependent concentrations of fission products and their macroscopic cross sections prompted the formulation of the CINDER one-point depletion and fission-product program. Reference 30 presents the analytical and physical basis for this program and a comparison with experimental results for enriched-uranium samples exposed to a fuel depletion of 87%.

An exact analytical method is outlined[30] for calculating the detailed time-dependent concentration of each fission product and other generated nuclides. The analytical treatment is general and applicable to all fuels. It includes the formation of nuclides by both radioactive decay (β^- and γ) and neutron capture. Flexibility is built into the calculation by the use of linear chains coupling each nuclide to a single parent (contains no branches). This approach results in a unique set of coupled equations which can be solved independently of particular nuclide parameters and which can be applied to all chains. The chains are independent in the sense that the concentrations in each chain can be calculated without regard to the other chains; the total concentration of each nuclide is given by the sum of the partial concentrations from each chain. The CINDER program embodies this approach in determining the concentration of the nth nuclide, assuming a constant flux and an average fission rate during a given time increment. The program employs one to four arbitrary energy groups and will handle up to 300 nuclides grouped into linear chains as specified by the requester. Up to 99 fission-product chains and 40 fuel chains containing a maximum of 15 nuclides each are permitted. The direct fission yields for the nuclides in the fission-product chains can be specified for up to 10 fissile nuclides appearing in the fuel chains. These limitations are arbitrary and readily changed. The calculation is performed in a sequence of time increments with each increment being of arbitrary length. At each of these increments, the power density (or, optionally, the thermal flux), the fast-to-thermal flux ratios, a thermal spectrum (or shielding) factor, and an epithermal shielding factor (per nuclide) can be specified. The parameters needed to calculate the concentrations, i.e., decay constants, cross sections, type of coupling, yields, etc., must be specified by the requester. At the end of each time step, the program output provides the individual nuclide concentrations, the barns per fission and macroscopic absorption cross sections in each energy group (total and summed over selected nuclides), and other quantities of interest. Given is a recommended set of data (cross sections, half-lives, yield fractions, and nuclide chains) necessary to describe the products resulting from fission of ^{235}U, ^{238}U, and ^{239}Pu. The tabulation includes 67 chains and 256 nuclides of which only 163 are actually different nuclides. The more important nuclides and chains are discussed in detail.

The calculational method is demonstrated by calculating both the individual and total thermal and resonance cross sections per fission of 163 fission products from ^{235}U, natural uranium, enriched uranium, and ^{239}Pu, in a variety of irradiation flux histories and spectra. All known fission products of significance are included in the analysis, i.e., those formed by direct fission yields and by neutron absorption and radioactive decay. A comparison of the aggregate absorption cross sections, determined by both calculation and experiment for a highly enriched sample, shows agreement to within 2% thermally and 15% epithermally.

Reference 31 presents a compilation of neutron cross sections for 6-, 16-, 18-, 24-, and 25-group problems, with neutron energies ranging from fast to thermal. A conspicuous feature of this report is the lack of definitions, discussion, source of contents, and references.

Physics of Control Materials

Reference 32 is a topical report on the absorber burnup experimental program carried out at the Vallecitos Atomic Laboratory. The purpose of the program is to provide information about the change in effective absorption cross section of reactor control-element materials due to transmutation by neutron capture. Test samples were in the form of cylinders, $\frac{1}{4}$ in. in diameter and 2 in. in length. Most of the absorber materials were diluted in glass to provide samples of three different self-shielding factors for each element (corresponding to $\Sigma_a l$ of ~0.2, 1, and 5). The samples were irradiated in a region adjacent to the core of the General Electric Test Reactor pool facility, and the flux was monitored by aluminum-cobalt wires. After each irradiation the reactivity effect due to the individual samples was measured by pile oscillator techniques in the General Electric Nuclear Test Reactor. Resonance and subcadmium effects were measured by oscillating the samples with and without a fixed 20-mil cadmium sleeve. A detailed description of the experimental technique and method of interpreting the experimental data is given for each element investigated. Figure II-6

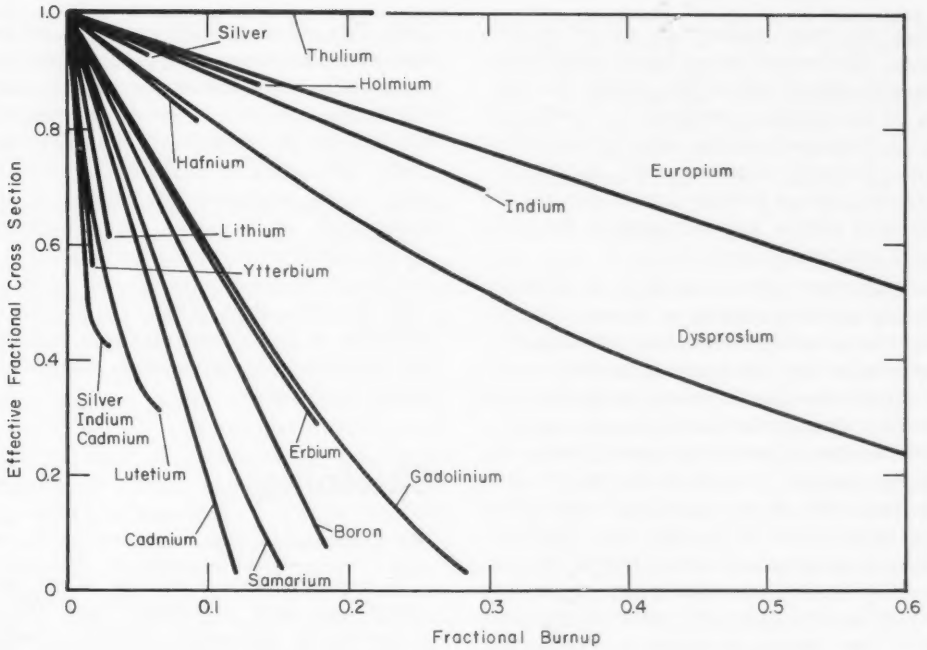

Fig. II-6 Fractional cross section vs. fractional burnup.[32]

presents curves of the effective fractional cross section, $\sigma(n)/\sigma(0)$, vs. fractional burnup, n/N_0, where

$\sigma(n)$ = isotopically weighted element cross section after capturing n neutrons per atom

$\sigma(0)$ = isotopically weighted element cross section for no irradiation

n = number of neutrons captured by the absorbing element (per atom of the element)

N_0 = number of initial atoms of a given element

The curves neglect all resonance capture effects. They are computed on the basis of thermal burnup, and the experimental verification was with a thermal flux.

A theoretical investigation has been made regarding the effect of binary poison mixtures on the temperature defect and temperature coefficient with a simple reactor model.[33] The poison mixtures investigated were Gd-Er, Gd-Eu, Eu-Er, and Eu-Cd. The reactor model consists of an infinite homogeneous mixture of ^{235}U, carbon, and poison, thus eliminating the need for consideration of lattice effects. The change in an operating characteristic at a given operating temperature is defined in terms of the behavior of the reactor system poisoned with the binary mixture relative to one poisoned with boron. Both reactors use the same fuel and structure density and the same multiplication factor at operating temperature; consequently both reactors have the same percentage of parasitic absorption. To simplify computations the Westcott scheme for computing reaction rates was adopted. All materials other than ^{235}U and the binary poison mixtures were assumed to have cross sections of the $1/v$ type.

In the analytical model adopted, changes in the poison cross section are dependent solely on changes in the moderator temperature. Restrictions on the temperature dependence of the poison cross sections necessary to give a decrease in both the temperature defect and temperature coefficient were derived. It was found, for a fixed macroscopic poison cross section, that the largest decrease in the temperature coefficient is produced by the element or isotope having the largest value of $d\sigma/(\sigma dT)$, whereas the poison that gives the largest decrease in the temperature defect is one having the highest ratio of cross section at room tem-

perature to cross section at operating temperature. This result seems hardly surprising. It was also found that in this model the magnitude of the negative temperature coefficient could be increased and the temperature defect could be decreased simultaneously, and a suitably selected binary mixture could decrease the temperature defect without changing the temperature coefficient of reactivity.

One objective when selecting a burnable poison for use in a reactor is to match the reactivity curve throughout the life of the reactor. In many cases not only does a mismatch occur, but a sizable residue of poison remains at the end of life. These effects are of particular importance for the case of slightly enriched cores, where the desired burnout curve departs quite widely from that of an unshielded poison. Reference 34 presents the results of an investigation to find a burnable poison element that can be used to match essentially any decreasing reactivity curve and still have a tolerable residue. The approach taken by the author exploits geometrical effects for highly self-shielded poison materials rather than adjustment of unshielded elemental cross sections. The use of highly self-shielded poisons allows the shape of the burnout curve to be nearly independent of the particular (high cross section) element used.

It is assumed in the analysis that the total effective cross section is proportional to the absorber surface, and, for the case of cylinders or slabs, one dimension (optical thickness) is smaller than the other dimensions. With these assumptions it is shown that spherical particles yield little improvement over an unshielded poison, that cylinders are limited to a linear reactivity shape, but that slabs allow the synthesis of any decreasing burnout characteristics by a combination of samples with different initial blackness factors. Typical fuel cycles were evaluated to determine additional requirements on the burnable poison; both irradiation lifetime and burnout shape were determined. The physical characteristics of four poison materials (cadmium, samarium, europium, and gadolinium) were examined, and gadolinium was selected for further investigation. To retain the desirable geometric properties associated with a slab geometry as well as the requirement of a high neutron absorption cross section, the actual shape of the absorber lumps was taken to be that of a right-circular disk. The effect of disk geometry on both the self-shielding factor and external medium was investigated first for monoenergetic reactions; the analysis was then extended to include spectral effects. The dependence of the self-shielding factor and effective cross section (on irradiation) were evaluated for disks of different dimensions. Experiments were performed to obtain information on (1) the amount of poison residue from gadolinium, (2) self-shielding factors for gadolinium disks, and (3) the burnout behavior of gadolinium disks. A description of the experimental procedures and data interpretation are given.

Shielding

ML-1 Shield Design

A complete report on the ML-1 radiation shield has been published.[35] The ML-1 is a closed-cycle gas-cooled nuclear power plant developed to demonstrate the feasibility of using such a plant in the field; it was reviewed in *Power Reactor Technology*, 6(3): 57-60. Since the plant was to be transportable, the shielding was designed primarily to allow access around the reactor after shutdown. Accordingly it is of interest to review the field operating characteristics of the plant:[35]

> The plant unit (connected reactor and power conversion packages) shall be assembled on a standard military semi-trailer... and all preparations completed for relocation to an operating site within six (6) hours after unloading from any aircraft.
>
> The plant shall be capable of being installed and delivering rated power within twelve (12) hours after arrival at an operating site.
>
> The plant shall be capable of relocation to a new site beginning twenty-four (24) hours after reactor shutdown following operation for extended periods at full power. Completion of disassembly and loading shall be within thirty-six (36) hours after reactor shutdown.
>
> Nuclear radiation allowed: (1) Allowable radiation, twenty-four (24) hours after shutdown at twenty-five (25) ft from the reactor in the direction of the (truck) cab (without water shield), is fifteen (15) mr/hr with the power conversion package in place. (2) No personnel shall receive greater than 3 rem/quarter.
>
> During plant operation, radiation shielding integral to the plant may be supplemented by field expedient materials (earth, gravel, wood, water) sufficient to reduce radiation levels outside the

combined shield to within dosage levels prescribed by the Surgeon General D/A. The integral plant shield (excluding supplemental expedient shielding) shall be adequate to reduce the residual radiation level following full power operation for extended periods to safe levels in time to permit relocation twenty-four (24) hours after reactor shutdown.

A discussion of the shield design changes that took place as the reactor system was developed is presented[35] in chronological order with a listing of the reasons for each significant change in design. The reasons include a change in performance specifications, unacceptable materials, and the incorporation of Lid Tank Shielding Facility (LTSF) test results into the final shield design. The original shield design, for example, used canned crystalline ammonium pentaborate as a solid shielding material, but during testing it was found not acceptable because of deterioration under thermal cycling and radiation. Ammonium pentaborate in aqueous solution was considered; however, during testing it was found to be unacceptable because it was corrosive to aluminum alloys and unstable above 150°F. The final choice was a boric acid solution.

The complete analysis of the final shield design, as shown in Fig. II-7, is presented in the report. The analysis is in two parts. One part deals with the after-shutdown dose rate, which is of prime importance in this shield design, and the other part deals with the expected dose rates during reactor operation. An outline of the methods used in these calculations is presented. The report also presents the data from a series of experiments which were conducted in the LTSF at Oak Ridge National Laboratory in support of the ML-1 shield design. The tests included both operational and shutdown measurements. Also included were variations of the shielding materials, changing of shielding-material thicknesses, and variation of boron content in the water annulus.

Of particular interest is the operational dose-rate data taken during power runs of the ML-1 system. The shielding was that of the reference design (Fig. II-7), with the exception that an expedient shield consisting of 17½ in. of wood (Douglas fir) was positioned directly over the reactor to help reduce the air-scattered dose rate. The operational data agreed fairly well with the analysis and proved that the system

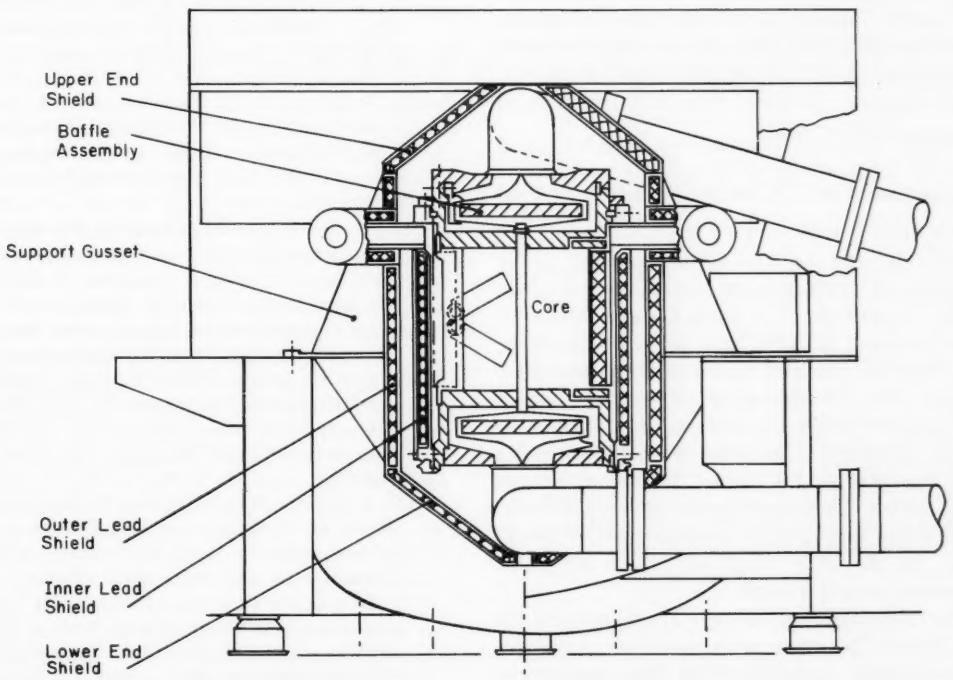

Fig. II-7 Final design of the ML-1 shield.[35]

could operate in the field without exceeding the dose-rate limits set forth in the specifications.

Geometrical Attenuation Factors

The analysis of many shielding problems can be reduced to surface sources that require only a geometrical attenuation factor to determine the radiation flux at the detector location. There are actually very few instances in which a true surface source exists, but there are several instances in which a volume source can be represented as a surface source. As an aid in quickly determining the radiation flux from either a cylindrical or concave spherical surface source, a recent report[36] presents the geometrical attenuation factors in the form of sets of curves. The attenuation factors are plotted as functions of the ratio $d:R$, where d is the source-detector separation distance and R is the radius of the source. The cylindrical source data are further broken down into separate curves for different length-to-radius ratios. Curves are also presented for concave spherical surfaces with different polar angles. For the two geometries, curves are presented for both isotropic and cosine source distributions. The choice of which set of curves to use is left to the user's discretion. A true surface source would be isotropic, but, when a volume source is replaced by an "equivalent" surface source, representation by either distribution will be an approximation at best.

Measurement of $^{16}O(n, p)^{16}N$ Cross Section

In water-cooled reactors the most significant activity as far as biological shielding of the primary coolant pipes and systems is concerned is the ^{16}N activity. The ^{16}N is formed in or very near the reactor core by a fast-neutron reaction with ^{16}O, which is the most abundant oxygen isotope. The ^{16}N decays by β emission with a half-life of 7.35 sec, releasing several high-energy gammas. The most important gammas have energies of 6.13 and 7.11 Mev and occur in 69 and 5% of the disintegrations, respectively. It is these high-energy gammas which determine the shielding requirements of the water or steam coolant system.

The measurement of the cross section for the $^{16}O(n,p)^{16}N$ reaction is therefore very important. Until recently there has been some discrepancy in the cross section at about 14.7 Mev. To resolve the discrepancies an experiment was run to remeasure the cross section between the neutron energies of 12.6 and 16.3 Mev.[37] When these cross sections were combined with previously measured cross sections from 10.24 Mev (the reaction threshold) to 12.6 Mev,[38] a curve was obtained which could be integrated over the Watt fission spectrum to yield an effective cross section for fission neutrons. This effective cross section was evaluated as 19.5 μb, an effective cross section in agreement with most previously calculated and measured effective values. Care is necessary in the choice of fits to the Watt spectrum as this alone can vary the effective cross section from 16.5 μb to 24.3 μb.

References

1. Argonne National Laboratory, Zero-Power Experiments with Boiling Core B-1, BORAX-V, USAEC Report ANL-6689, June 1963.
2. T. R. Jaworowski, P. G. Aline, and H. D. Kosanke, Control Augmentation Critical Experiments, USAEC Report APED-4236, Vallecitos Atomic Laboratory, July 15, 1963.
3. F. G. Dawson, Jr., J. L. Carter, W. A. Reardon, J. E. Faulkner, E. D. Clayton, R. E. Heineman, H. L. Henry, and B. R. Leonard, Jr., Physics Research Quarterly Report, October–December 1962, USAEC Report HW-76128, Hanford Atomic Products Operation, Jan. 15, 1963.
4. I. Johnstone, W. H. Taylor, and S. K. Wallace, Critical Size and Flux Distribution Measurements in Highly Enriched, Light Water Moderated Lattices, *J. Brit. Nucl. Energy Soc.*, 2(4): 379 (October 1963).
5. *Light Water Lattices*, Technical Reports Series No. 12, International Atomic Energy Agency, 1962.
6. T. J. Hurley, Jr., H. R. Fike, and G. F. O'Neill, Experimental Bucklings of Heavy Water Moderated Lattices of Natural Uranium Metal Rod Clusters, *Nucl. Sci. Eng.*, 12(3): 341 (March 1962).
   a. E. E. Wingfield and E. J. Hennelly, Exponential Measurements of Natural Uranium Rods in Heavy Water and Comparisons with Critical Experiments, *Nucl. Sci. Eng.*, 12(3): 348 (March 1962).
7. W. E. Graves, H. R. Fike, and F. G. O'Neill, Experimental Bucklings and Void Effects in Heavy Water Lattices of Natural Uranium Oxide Rod Clusters, *Nucl. Sci. Eng.*, 16(2): 186 (June 1963).
8. P. Benoist, General Formulation of the Diffusion Coefficient in a Heterogeneous Medium Allowing Cavities, Report SPM-522, Commissariat à l'Énergie Atomique, Dec. 2, 1958.
9. P. Benoist, A Simple New Expression of the Radial Diffusion Coefficient for Fueled Channels,

Report SPM-710, Commissariat à l'Énergie Atomique, 1962.

10. B. G. Chidley, T. J. Manuel, and P. R. Tunnicliffe, Initial Conversion Ratios and Fast Fission Factors in Heavy-Water Natural-Uranium Lattices Using 19-Element UO_2 Fuel Rods, *Nucl. Sci. Eng.*, 17(1): 47 (September 1963).
11. G. M. Benson and R. H. Fox, Room Temperature Critical Measurements on Thorium-Loaded, Graphite-Moderated, Oralloy-Fueled Systems, USAEC Report UCRL-6901, University of California, Lawrence Radiation Laboratory, June 30, 1962.
12. P. F. Nichols, J. R. Worden, F. C. Engesser, and R. E. Heineman, The Measurement of the Lattice Parameters of a Gas Cooled Reactor Lattice, *Nucl. Sci. Eng.*, 15(3): 233 (March 1963).
13. D. E. Wood, K. R. Birney, and E. Z. Block, Lattice-Parameter Measurements for Solid and Concentric Tubes of Uranium Fuel in Graphite Lattices, *Nucl. Sci. Eng.*, 18(1): 116 (January 1964).
14. L. I. Moss, Experiments with Water-Reflected, Undermoderated, Zirconium Hydride Critical Assemblies, USAEC Report NAA-SR-8490, Atomics International, Sept. 15, 1963.
15. W. G. Davey, A Comparison of Experimental and Calculated Prompt Neutron Lifetimes and Central Reactivity Coefficients in ZPR-III Assemblies and Their Relationship to Other Reactor Parameters, USAEC Report ANL-6682, Argonne National Laboratory, June 1963.
16. T. C. Engelder, R. H. Clark, M. N. Baldwin, E. J. DeRoche, G. T. Fairburn, J. W. Hallam, D. H. Roy, N. Vutz, and T. M. Schuler, Spectral Shift Control Reactor Basic Physics Program. Measurement and Analysis of Uniform Lattices of Slightly Enriched UO_2 Moderated by D_2O-H_2O Mixtures, USAEC Report BAW-1273, The Babcock & Wilcox Co., November 1963.
17. T. C. Engelder, R. H. Clark, E. J. DeRoche, G. T. Fairburn, J. W. Hallam, D. R. Hostetler, and C. B. Woodhall, Spectral Shift Control Reactor Basic Physics Program. Measurement and Analysis of Perturbed Lattices of Slightly Enriched UO_2 Moderated by D_2O-H_2O Mixtures, USAEC Report BAW-1274, The Babcock & Wilcox Co., October 1963.
18. T. C. Engelder, N. L. Snidow, D. M. Roberts, G. T. Fairburn, and D. H. Roy, Spectral Shift Control Reactor Basic Physics Program. Measurement of k_∞ and Other Lattice Parameters by the Small Lattice Experiment Technique, USAEC Report BAW-1283, The Babcock & Wilcox Co., November 1963.
19. R. H. Lewis, T. C. Engelder, D. M. Roberts, and D. B. Wehmeyer, Thermal Activation Method for ρ_{28} Measurements in Slightly Enriched Uranium Oxide Lattices, USAEC Report BAW-1268, The Babcock & Wilcox Co., May 1963.
20. W. E. Graves, Analysis of the Substitution Technique for the Determination of D_2O Lattice Bucklings, USAEC Report DP-832, Savannah River Laboratory, June 1963.
21. W. L. Brooks, M. Raber, and G. Sofer, Present Status of Calculation and Experiment for D_2O-Moderated Natural Uranium Lattices, Report UNC-5062, United Nuclear Corp., Sept. 13, 1963.
22. J. L. Crandall, Efficacy of Experimental Physics Studies on Heavy Water Lattices, USAEC Report DP-833, Savannah River Laboratory, July 1963.
23. W. G. Pettus, M. N. Baldwin, and C. Samuel, Resonance Absorption in U^{238} Metal and Oxide Rods, USAEC Report BAW-1244, The Babcock & Wilcox Co., April 1962.
24. W. G. Pettus, M. N. Baldwin, and C. Samuel, Resonance Absorption in Thorium Metal and Oxide Rods, Final Report, USAEC Report BAW-1286, The Babcock & Wilcox Co., November 1963.
25. G. I. Bell, A Simple Treatment for Effective Resonance Absorption Cross Sections in Dense Lattices, *Nucl. Sci. Eng.*, 5(2): 138 (February 1959).
26. E. Hellstrand, Measurements of the Effective Resonance Integral in Uranium Metal and Oxide in Different Geometries, *J. Appl. Phys.*, 28: 1493-1502 (December 1957).
27. P. G. F. Moore, S. K. Pattenden, and R. B. Tattersall, The Measurement of the Effective Resonance Integrals of Uranium and Thorium Using the Pile Oscillator Operating Inside a Cadmium Tube, British Report AEEW-R-57, August 1961.
28. J. Hardy, Jr., G. G. Smith, and D. Klein, The Effective U-238 Resonance Capture Integrals of Uranium Metal and UO_2 Rods, *Nucl. Sci. Eng.*, 14(4): 358 (December 1962).
29. J. Weitman, The Effective Resonance Integral of Thorium Oxide Rods, *Nucl. Sci. Eng.*, 18(2): 246 (February 1964).
30. T. R. England, Time-Dependent Fission-Product Thermal and Resonance Absorption Cross Sections, USAEC Report WAPD-TM-333, Westinghouse Electric Corp., Bettis Atomic Power Laboratory, November 1962.
31. L. D. Connolly, Los Alamos Group-Averaged Cross Sections, USAEC Report LAMS-2941, Los Alamos Scientific Laboratory, July 1963.
32. J. L. Russell, Jr., M. R. Carrothers, and W. V. Mosgovoy, Absorber Burn-up Experiment, USAEC Report GEAP-4017, General Electric Company, Atomic Power Equipment Department, April 1962.
33. J. H. Bick, Poison Mixtures Which Improve Thermal Reactor Operating Characteristics, USAEC Report NAA-SR-8225, Atomics International, June 30, 1963.
34. R. J. Holl, Highly Self-Shielded Burnable Poisons, USAEC Report ACNP-63003, Allis-Chalmers Mfg. Co., Mar. 6, 1963.
35. Aerojet-General Nucleonics, Army Gas-Cooled Reactor Systems Program. ML-1 Shielding De-

sign Report, USAEC Report IDO-28609, October 1963.

36. K. M. Campe, Geometrical Attenuation Factors for Gamma Radiation from Cylindrical and Spherical Surface Sources, USAEC Report PWAC-397, Pratt & Whitney Aircraft, Sept. 15, 1962.
37. K. W. Seemann and W. E. Moore, The $O^{16}(n,p)N^{16}$ Cross Section from 12.6 to 16.3 Mev, USAEC Report KAPL-2214, Knolls Atomic Power Laboratory, Sept. 21, 1962.
38. J. A. DeJuren, R. W. Stooksberry, and M. Wallis, Measurement of the $O^{16}(n,p)N^{16}$ Cross Section from 11 to 19 MeV, *Phys. Rev.*, 127(4): 1229 (Aug. 15, 1962).

Section

III

Power Reactor Technology

Fluid and Thermal Technology

Burnout Correlations from the Russian Literature

By John S. Wiley

In an earlier discussion of burnout limits [*Power Reactor Technology*, 7(1): 14-26], two circumstances were pointed out which are well known to heat-transfer investigators but which may not be emphasized strongly enough when thermal limits are set for a particular reactor. They are:

— Burnout correlations that are arrived at empirically to cover a wide range of operating variables provide no means of distinguishing between deviations which result from experimental errors and those which result from true functional relations neglected in the correlation.

— The burnout ratio, as ordinarily used in reactor design, represents not so much a safety factor on reactor heat flux (and hence on reactor power) as an uncertainty factor, related to the uncertainty as to whether the burnout correlation used is truly applicable to the situation in the reactor core.

Both of these considerations emphasize the desirability of comparing correlations and burnout data that have been developed by investigators who are widely separated in background and in approach. The Russian work provides a useful comparison of this kind with the U. S. work that has been reviewed more frequently in *Power Reactor Technology*. The purpose of this review is to make such a comparison. Some work by British investigators is also covered[21] because it illuminates the effect of length and diameter on the burnout heat flux in tubular test sections, a question that has particular significance in the comparison.

Table III-1 RUSSIAN BURNOUT CORRELATIONS EXAMINED

Correlator	Reference
Kutateladze	1
Ornatskii and Kichigin	2
Povarnin and Semenov	3
Zenkevich	4,5
Zenkevich and Subbotin	6

Burnout Correlations for Subcooled Water: Tubular Geometry

The correlations considered here are listed in Table III-1. It is not clear whether U. S. burnout data were used to any important extent in developing the correlations. Direct references to data from USAEC documents are not often cited in the Russian heat-transfer literature, although there are references to journals of the U. S. technical societies, such as the American Society of Mechanical Engineers and the American Institute of Chemical Engineers.

One of the surprising things discovered was that those correlations in which the surface tension of water was a parameter were quite dependent on the value of surface tension used, particularly at pressures approaching the critical pressure where the surface tension approaches zero. Accordingly values of surface tension were taken from Ref. 7. At pressures approaching critical the Russian values differ appreciably from numbers in the *International Critical Tables*, at least as presented in Ref. 8.

Another difficulty in comparing the various correlations arises in converting pressure from metric to British units. The usual unit used in the Russian literature is the atmosphere, which is defined in either of two ways:[7]

$$1 \text{ atm} = 1 \text{ kg/cm}^2 = 735.6 \text{ mm Hg}$$

$$1 \text{ atm(phys)} = 1.034 \text{ kg/cm}^2 = 760 \text{ mm Hg}$$

The former definition (1 atm = 1 kg/cm^2) seems, on the basis of some spot checks of saturation-pressure data, to be the one most often used in the Russian literature, and it was used for the conversions made in this review.

The correlation by Zenkevich and Subbotin is stated[4] to lie within ±10% of the Zenkevich correlation, and attention will therefore be devoted to the latter. The Zenkevich correlation is as follows:

$$K = K_1^{0.65}\,(95 + 420K_2) \times \left(1 + \frac{0.32 \times 10^6}{R^{1.1} + 2.6K_1 + 0.9K_2}\right)(10^{-5}) \qquad (1)$$

where $K = \dfrac{q_{cr}}{r}\left(\dfrac{\nu}{\sigma g\, W_g}\right)^{1/2}$

$$K_1 = \gamma''/\gamma_{sub}$$

$$K_2 = \frac{i_{sat} - i_{sub}}{r}$$

$$R = \frac{W_g\,[\sigma/(\gamma' - \gamma'')]^{1/2}}{\gamma_{sub}\,\nu}$$

The definitions of K, K_1, K_2, and R involve the Russian symbols usually found in their heat-transfer–fluid-dynamics technical articles. A list of these symbols and their usual U. S. equivalents is given in Table III-2. In correlations like that of Zenkevich, Eq. 1, where dimensionless groupings are utilized, it is relatively easy to handle the units. On the other hand, strictly empirical correlations, typified by that of Zenkevich and Subbotin,* require careful attention to the units to ensure correct answers.

The correlation of Zenkevich is plotted in Figs. III-1 and III-2. Again the concept of steam-energy flow (SEF) is utilized to compare the correlation with data given in *Power Reactor Technology*, 7(1): 14-26. SEF is calculated as the product of the mass flow through the test section and the difference between the enthalpy at the burnout point and that of saturated water at the test-section pressure. Also plotted in Figs. III-1 and III-2 are (dotted) DNB-1 lines for corresponding pressures taken from *Power Reactor Technology*, 7(1). The agreement between the solid and dotted lines (which are based on Ref. 9 data) is fairly good. Data of Buchberg were used in developing the Zenkevich correlation; Ref. 10 contains these data in graphs, and Zenkevich states that the graphs were used in the development of Eq. 1. These data are given as "UCLA burnout data for subcooled water at tube exit" in Table II of Ref. 11 and finally appear in Table 12 of Ref. 9. For some reason, however, the Table 12 data are

Table III-2 LIST OF SYMBOLS USED BY ZENKEVICH

Russian symbol	Definition	Units	USA symbol
q_{cr}	Critical heat flux	kcal/(hr)(m^2)	ϕ_{BO}, etc.
r	Vaporization enthalpy	kcal/kg	h_{fg}
ν	Kinematic viscosity*	m^2/hr	μ/ρ
σ	Surface tension†	kg/m	σ
W_g	Mass velocity	kg/(hr)(m^2)	G
γ'	Density of water at saturation temperature	kg/m^3	$1/v_f$
γ''	Density of steam at saturation temperature	kg/m^3	$1/v_g$
γ_{sub}	Density of water*	kg/m^3	ρ
i_{sat}	Enthalpy of saturated water	kcal/kg	h_f
i_{sub}	Enthalpy of subcooled water*	kcal/kg	h

*Taken for mean water temperature at test-section exit.
†Taken at saturation temperature.

*The Zenkevich-Subbotin correlation is as follows:

$$q_c = 590\, W_g^{1/2}\, \Delta t_H^{1/3} \left(\frac{v''}{v'' - v'}\right)^{-1.8} \qquad (2)$$

where Δt_H = subcooling at point of burnout, °C
v'' = specific volume of saturated steam at test-section pressure, m^3/kg
v' = specific volume of saturated water at test-section pressure, m^3/kg

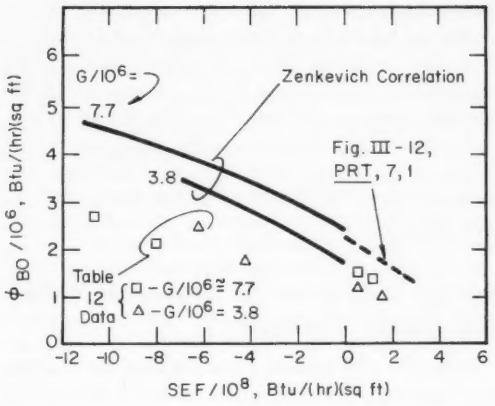

Fig. III-1 Comparison of correlation of Zenkevich[4,5] with data appearing in Table 12 of Ref. 9. Also plotted is a curve taken from Fig. III-12, *Power Reactor Technology*, 7(1): 22. Pressure = 1000 psia.

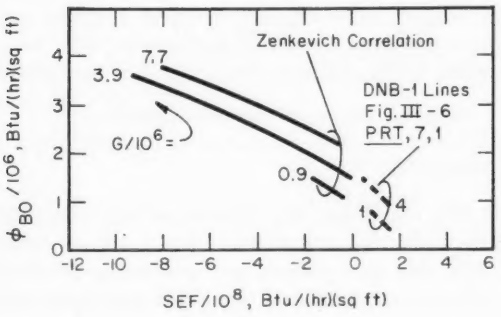

Fig. III-2 Comparison of correlation of Zenkevich[4,5] with data taken from Fig. III-6, *Power Reactor Technology*, 7(1): 18. Pressure = 2000 psia.

slightly different from the data that originally appeared in Ref. 10.

One wonders why, if Zenkevich used Buchberg's data in developing his correlation, the correlation does not agree more closely with the Buchberg data. A comparison is given in Table III-3, and Fig. III-1 also shows Table 12 data of Ref. 9. It can be seen that the Zenkevich correlation overpredicts ϕ_{BO} by as much as a factor of 2. It is possible that only the 2000-psia data of Buchberg were used by Zenkevich, since the agreement for the 2000-psia data is relatively good (as shown in Table III-3). Figure 3 of Ref. 4, page 139, shows a comparison of Buchberg's data with Eq. 1, and a total of 26 points is shown. Table 12 of Ref. 9 contains results of 27 experiments at 2000 psia in the subcooled regime. In addition, Zenkevich concluded that the critical heat flux is not affected by tube diameter in the range from 4 to 12 mm. This is questioned in Ref. 12. The diameter effect will be considered in this article in a later section.

Several correlations, which are listed in Table III-4, are compared in Fig. III-3. The correlation of U. S. origin (WCAP) is included for purposes of comparison. It is believed likely that the differences in the values of ϕ_{BO} predicted by the various correlations is primarily due to a lack of inclusion (or improper inclusion) of terms for the effect of L and D. The values of L and D used by the various experimenters are indicated on Fig. III-3, and it is evident that Ornatskii and Kichigin achieve quite high values of ϕ_{BO} with their short, small-diameter tube. Interestingly, Kutateladze in writing his correlation stated that he used data

Table III-3 COMPARISON OF ZENKEVICH CORRELATION WITH TABLE 12 DATA OF REF. 9

Table 12* run No.	Pressure, psia	Mass flow, lb/(hr)(sq ft) $\times 10^{-6}$	Burnout enthalpy, experimental, Btu/lb	$\phi_{BO_{predicted}}$, Btu/(hr)(sq ft) $\times 10^{-6}$	$\phi_{BO_{experimental}}$, Btu/(hr)(sq ft) $\times 10^{-6}$	$\frac{\phi_{BO_{experimental}} - \phi_{BO_{predicted}}}{\phi_{BO_{experimental}}}$, %
002	500	3.87	390	1.76	2.68	34
006	500	3.87	434	1.51	2.28	34
012	500	7.73	438	2.09	2.04	−2.5
008	500	7.65	398	2.42	2.70	10.4
023	1000	3.87	385	3.29	2.54	−30
026	1000	3.84	436	2.89	1.77	−63
027	1000	7.71	404	4.46	2.74	−63
029	1000	7.65	437	4.07	2.05	−99
038	2000	3.95	473	3.42	2.96	−16
054	2000	3.88	659	1.63	1.42	−15
049	2000	7.74	573	3.66	3.34	−10
055	2000	7.76	652	2.44	2.28	−7

*Table 12 of Ref. 9.

of Zenkevich, Zenkevich and Subbotin, and Buchberg, although the publications of the first two experimenters do not seem to be any of those cited in this article. Note that the correlations of Povarnin and Semenov[3] and of Kutateladze,[1] as given in the cited references, involved the flow velocity rather than the mass flow W_g, as shown in Table III-4. Kutateladze[1] calls this, in fact, the "reduced flow velocity of liquid." The substitution of the term W_g/γ_{sub} was done by the present author and may involve some error, since the flow velocity varies along the entire length of the heated test section. A few data are included from Table 12 of Ref. 8 for comparative purposes.

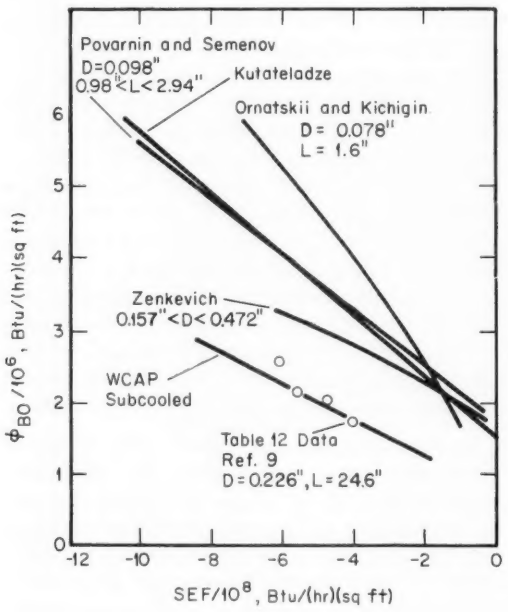

Fig. III-3 Comparison of various burnout heat-flux correlations. Pressure = 1000 psia, $G = 3.7 \times 10^6$ lb/(hr)(sq ft).

Burnout Correlations for Subcooled Water: Rod–Bundle Geometry

Reference 13 contains the results of one of the few experiments conducted to study burnout in the subcooled regime with a bundle of heated rods. The bundle consisted of 7 or 19 rods having an outside diameter of 5 mm (0.197 in.) on a triangular pitch of 6 mm (0.236 in.). A cross section of the bundle is given in part *a* of Fig. III-4, and an individual heater element is shown in part *b* of Fig. III-4. Burnout-detecting thermocouples were attached to the central rod and three peripheral rods. Experiments were conducted within the following ranges of variables:

Pressure: 180 to 210 atm (2560 to 2987 psia)
Flow rate: 0.65 to 4.65 m/sec (2.1 to 15.3 ft/sec)
Subcooling (exit): 10 to 40°C

It was found that the data were correlated by the Zenkevich correlation, Eq. 1. Some difficulty was experienced in reproducing the data when a fresh bundle of tubes was tested, and the

Table III-4 BURNOUT CORRELATIONS PLOTTED IN FIG. III-3

Correlator	Correlation
Povarnin and Semenov[3] (metric units)	$q_{cr} = 2.85 \times 10^6 (1 + 0.017\ \Delta t_{sub}) \left(1 + \frac{W_g}{24{,}660\ \gamma_{sub}}\right)^{0.8}$ (3)
Ornatskii and Kichigin[2] (metric units)	$q_{cr} = 2.5 \times 10^4\ W_g^{0.44}\ \Delta t_{sub}^{0.6}$ (4)
Kutateladze[1] (metric units)	$\frac{q_{cr}}{r\sqrt{g\gamma''}\sqrt[4]{\sigma(\gamma' - \gamma'')}} = 0.023 \left(\frac{W_g}{3600\ \gamma_{sub}} \sqrt[4]{\frac{\gamma' - \gamma''}{g^2\ \sigma}}\right)^{0.5} \times \left[1 + 0.45 \left(\frac{\gamma'}{\gamma''}\right)^{0.85} \left(\frac{i_{sat} - i_{sub}}{r}\right)\right]$ (5)
WCAP* subcooled[14] (British units)	$\phi_{BO} = (0.23 \times 10^6 + 0.094\ G)\ (3 + 0.01\ \Delta T_{sub}) \times (0.435 + 1.23\ e^{-0.0093 L/D_e})\ (1.7 - 1.4\ e^{-a})$ (6)
	where: $a = (0.532)\ [(H_f - H_{in})/H_{fg}]^{1/4} \left(\frac{\rho_g}{\rho_f}\right)^{-1/4}$

*The term *a* in this correlation has been given three different definitions.[14–16] The particular form used above is the one published first and appears in Ref. 14. Reference 16 presumably corrected the definition given in Ref. 15 but gave the constant as 0.0532.

authors state that "... after several successive transitions (of regime in boiling), the critical heat flux q_{cr} attained a steady value."

What is not clear, however, is how the subcooling was measured. The following quotation serves to illustrate this:[13]

> The results are in satisfactory agreement with the equation, although there are marked differences in the patterns of water flow for the bundles of seven and nineteen tubes. This agreement is probably related to the discrepancy for both types of bundle(s) between the mean temperature of the water after mixing at the exit of the bundle and the temperature actually measured.

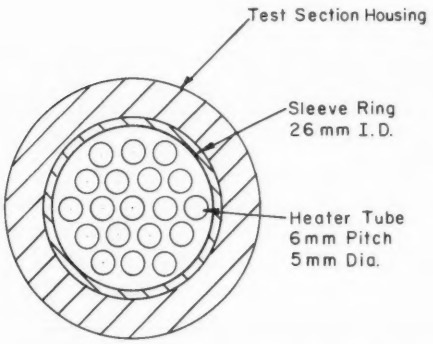

A. Cross Section of 19-Rod Bundle.

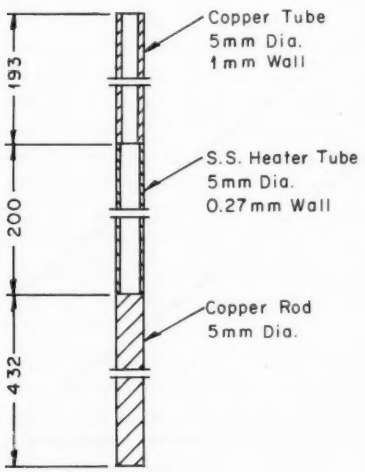

B. Cross Section of Heater Tube Used in 19-Rod Bundle.

Fig. III-4 Details of test section used to take data appearing in Ref. 13.

The quotation suggests that subcooling was measured at the location of burnout with a waterside thermocouple and that the exit, mixed-mean water temperature was not used. This is a somewhat crucial point, of course. The importance of mixing was discussed in Sec. III of the last issue of *Power Reactor Technology*.

Reference 17 contains the results of burnout experiments that were run with a test section which had a cross section as shown in Fig. III-5. This test section is, of course, a mockup of a rod bundle, at least of the central and surrounding rods. The inner and outer walls could be heated independently, and the data plotted in Fig. III-5 are for $\phi_{exterior}$ both zero and finite. The heated exterior walls apparently act like a film tripper and promote transfer of liquid from the walls to the central rod. The improvement in ϕ_{BO} caused by heating the exterior walls is of the same order of magnitude as that obtained[18] by placing washers on the unheated (outer) flow tube in annular geometry. Reference 18 was reviewed in *Power Reactor Technology*, 6(3): 10. The beneficial effect on ϕ_{BO} of bilateral heating has also been observed in annular geometry. The following is quoted from Collier[19] (page 16):

> The Italian ... and Swedish ... experiments with annuli heated on both walls have indicated that the heating of the external surface of the annulus causes an increase in the burnout heat flux value of the inner surface at the same nominal channel exit conditions ... The increase appears to be proportional to the value of the heat flux applied to the secondary surface.

Burnout Correlations for Net Boiling: Tubular Geometry

The correlations of interest for the net boiling region are those of Kon'kov and Modnikova,[20] Ivashkevich,[21,22] and Shitsman.[23] Also included for comparative purposes is a recently developed correlation by British experimenters Lee and Obertelli.[24]

The Kon'kov and Modnikova correlation is quite a specialized one, dealing with the phenomenon of the deterioration of heat transfer during the flow of a steam-water mixture in vertical, tubular test sections. The original article (or translation) should be consulted for details on this phenomenon, but, briefly, it involves the breaking-away of the film of water on the internal surface of the tube during annular flow. The following quotation serves to define this phenomenon more fully.[20]

... the wall temperature is initially almost constant and only differs by a few degrees from the saturation temperature. When the steam content reaches a certain level, the wall temperature rises sharply, reaches a maximum and then falls, the magnitude of the maximum rise being a function of the flow rate, the specific heat load and the pressure. The reduction in the wall temperature after the maximum is apparently to be explained by the increase in the flow rate as a result of the evaporation of the liquid phase in the flow.

In contrast to the experiments with film boiling, where as a rule very large temperature jumps occur and the destruction of the tube makes it impossible to determine the maximum temperature, in our present experiments the temperature jumps varied from t = 25°C to t = 300°C.

The correlation is as follows:

$$x_d = \left[\frac{q}{r\gamma''}\frac{\left(\frac{\sigma}{\gamma'-\gamma''}\right)^{1/2}}{\nu'}\right]^{-0.125}\left(\mathrm{Pr}_{\mathrm{liquid}}\right)^{-0.5}\left(\frac{\mu'}{\mu''}\right)^{-0.2} \times\left[\frac{d}{\left(\frac{\sigma}{\gamma'-\gamma''}\right)^{1/2}}\right]^{0.2}\left(\frac{500}{\mathrm{Re}_{\mathrm{liquid}}\,\frac{\gamma''}{\gamma'}+350}+0.35\right) \quad (7)$$

The units employed in Eq. 7 have been defined in Table III-2 with only a few exceptions. The term d is the diameter of the tube, and $\mathrm{Pr}_{\mathrm{liquid}}$ is obvious. The term $\mathrm{Re}_{\mathrm{liquid}}$ is called the "Reynolds number for the liquid film, on the assumption that the liquid phase is flowing wholly along the surface of the tube":

$$\mathrm{Re}_{\mathrm{liquid}} = \frac{M(1-x_{\mathrm{mean}})\,v'}{\pi d_{\mathrm{internal}}\,\nu'} \quad (8)$$

where M = flow rate (mass of steam-water mixture, kg/hr
$v' = 1/\gamma'$, m^3/kg
ν' = kinematic viscosity of saturated water, m^2/hr

The term x_d is the quality at which the deterioration of heat transfer takes place, and, if x_{mean} (which is not defined in either translation cited as Ref. 20) can be taken as x_d, then Eq. 8 becomes

$$\mathrm{Re}_{\mathrm{liquid}} = \frac{dW_g\,(1-x_d)}{4\mu'} \quad (9)$$

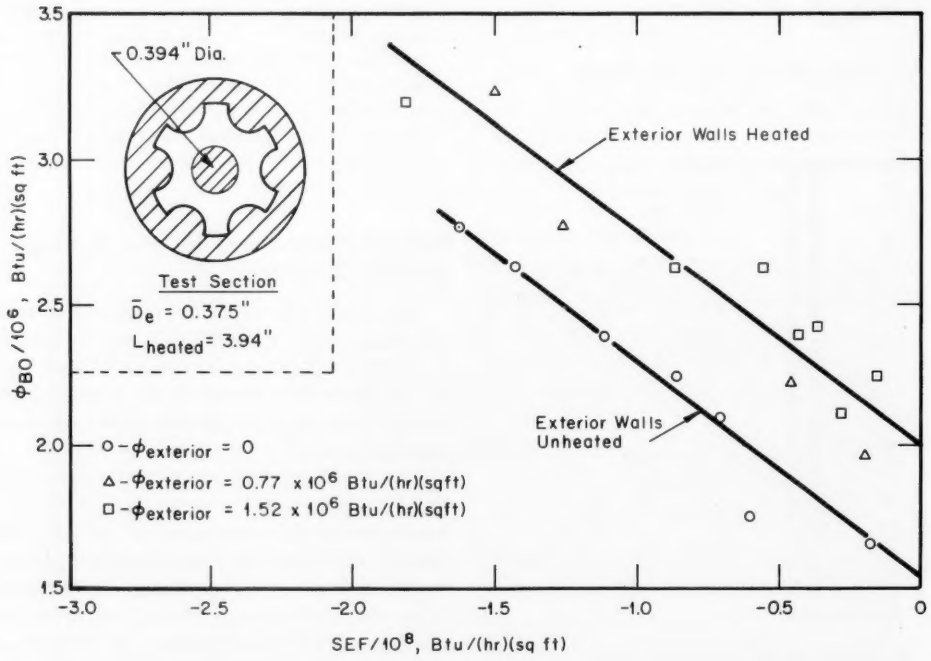

Fig. III-5 SEF plot of data of Alad'yev and Dodonov. Data taken from Table 2 of Ref. 17. Pressure = 1421 psia; ϕ_{exterior} = heat flux impressed on scalloped flow tube; ϕ_{BO} = burnout heat flux for center rod; and $G \cong 0.6 \times 10^6$ lb/(hr)(sq ft).

Table III-5 VALUES OF x_d PREDICTED BY KON'KOV-MODNIKOVA CORRELATION

Mass flow, lb/(hr)(sq ft)	x_d, lb/lb
Pressure = 2000 psia	
0.5×10^6	0.27
1.0×10^6	0.21
2.0×10^6	0.18
Pressure = 1000 psia	
0.5×10^6	0.66
1.0×10^6	0.45
2.0×10^6	0.32

where μ' equals $\nu'\gamma'$. The units on M are not given in Ref. 20, and in fact the translations show this symbol as G; the units for M were derived by the present author to make the Reynolds number of Eq. 8 dimensionless.

Equation 9 was substituted in Eq. 7, and values of x_d were calculated by trial and error for various pressures and values of W_g. These are shown in Table III-5.

The phenomenon of disruption of a thin liquid flowing in the annular regime has been discussed in Ref. 25, which was reviewed in *Power Reactor Technology*, 5(2): 17-18. What appears to correspond to the values of x_d for an internally heated annular test section appear in Table II-7 of that issue of *Power Reactor Technology*, and, in general, they are somewhat lower than the values shown in Table III-5. In any case the values shown in Table III-5 are considerably higher than typical qualities used in boiling-water reactors designed in the USA, although they are about right for exit qualities from proposed fog-cooled reactors. The Russian experiments were done with both steam-water mixtures or water alone fed to the test section, and the following conclusion was reached:[20]

> ... No effect on the conditions of deterioration of heat transfer could be detected as a result of the different methods.

The correlations of Ivashkevich[21,22] allow for nonuniform heating of the test section, but the present discussion will be restricted to the form applicable directly to uniform heating.[21] The correlation is as follows:

$$\frac{q_c}{r^*\,(g\gamma'')^{1/2}\,[\sigma(\gamma'-\gamma'')]^{1/4}} = \frac{1.9\times10^{-5}\,R_e}{1+1.8\times10^{-6}\,[K_3(1+K_2)+K_4]\,R_e} \qquad (10)$$

where $K_2 = \dfrac{i_{sat}-i_c}{r}$

$$K_3 = l_1\left(\frac{\gamma'-\gamma''}{\sigma}\right)^{1/2}$$

$$K_4 = l_2/d$$

$$R_e = \frac{w}{\nu'}\left(\frac{\sigma}{\gamma'-\gamma''}\right)^{1/2} \quad \text{when } \frac{d}{2}\left(\frac{\gamma'-\gamma''}{\sigma}\right)^{1/2} \geq 1$$

$$= \frac{wd}{2\nu'} \quad \text{when } \frac{d}{2}\left(\frac{\gamma'-\gamma''}{\sigma}\right)^{1/2} < 1$$

$$r^* = r\,(1-x) \text{ for } x \geq 0$$

$$r^* = r\,[1 + A\,(i_{sat}-i_c)/r] \quad \text{for } T_z < T_{sat}$$

$$A = 1 + 0.065\,(\gamma'/\gamma'')^{0.8}$$

The preceding units are consistent with those given in Table III-2. Two of the terms not yet defined are i_c and T_z, which are the enthalpy and temperature, respectively, of the liquid at the center of the stream. Thus, for net vapor generation, $i_c = i_{sat}$ and K_2 is zero. The term l_1 is defined as the "distance between section at which surface boiling begins and section under consideration ...," and l_2 is the "... distance between section at which $x = 0$ and section under consideration ..." The only other term open to question is w. In Ref. 22 this is termed the velocity of the liquid, and in Ref. 21 it is termed the velocity of flow. For purposes of this review, the term w will be set equal to W_g/γ'.

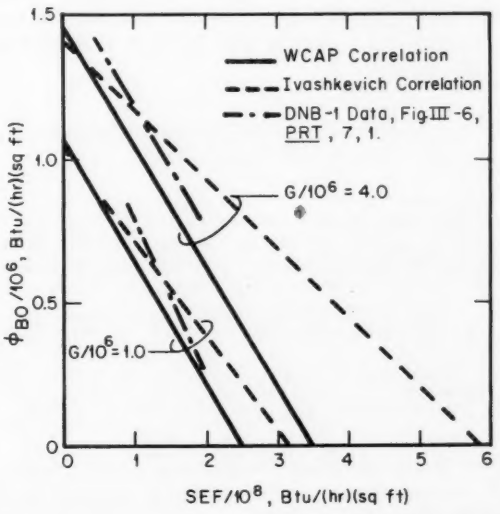

Fig. III-6 Comparison of correlation of Ivashkevich (Eq. 10) with the WCAP correlation (Table III-6). Pressure = 2000 psia. Also shown are DNB-1 data from Fig. III-6, *Power Reactor Technology*, 7(1): 18.

The constant K_3 has an upper limit of 50 and is related to the velocity profile. The constant involves a determination of the position where subcooled boiling is initiated. Fortunately for runs employing net steam generation over only a few inches of test-section length, the value of 50 is quickly achieved. The constant K_4 is the ratio of the boiling length to the test-section diameter. This ratio† can be shown to be

$$L_B/D = \text{SEF}/4\phi \tag{11}$$

For the moment attention is restricted to the net quality regime where

$$r^* = r(1 - x) \tag{12}$$

and to tubular test sections with an internal diameter of 0.18 in. At pressures between 1000 and 2000 psia, the parameter

$$\frac{d}{2}\left(\frac{\gamma' - \gamma''}{\sigma}\right)^{1/2}$$

exceeds unity; the value of Reynolds number is as follows:

$$\text{Re} = \frac{W_g}{\gamma'\nu'}\left(\frac{\sigma}{\gamma' - \gamma''}\right)^{1/2} \tag{13}$$

Substitution of physical property data, a value of 50 for K_3, and Eqs. 11 to 13 into Eq. 10, and rearranging,‡ yields Eq. 14 at a pressure of 2000 psia,

$$\phi_{BO} = \frac{0.5309G - (1.15 \times 10^{-4} + 1.647 \times 10^{-9}G)\ \text{SEF}}{0.1907 + 3.294 \times 10^{-4}G} \tag{14}$$

†The heat balance across a uniformly heated test section can be written as follows: [See Fig. III-1, *Power Reactor Technology*, 7(1), for nomenclature.]

$$\phi = \frac{GD}{4L}(x_e H_{fg} + H_f - H_{in}) = \frac{D}{4L}[\text{SEF} + G\ (H_f - H_{in})]$$

Therefore

$$H_f - H_{in} = \frac{4\phi L}{GD} - \frac{\text{SEF}}{G}$$

if $H_{in} = H_f$, $L = L_B$. Hence

$$\frac{L_B}{D} = \frac{\text{SEF}}{4\phi}$$

‡The system of units in Eqs. 14 and 15 is British.

and Eq. 15 at a pressure of 1000 psia,

$$\phi_{BO} = \frac{1.484G - (2.285 \times 10^{-3} + 2.385 \times 10^{-9}G)\ \text{SEF}}{0.233 + 4.77 \times 10^{-4}G} \tag{15}$$

Equations 14 and 15 have been plotted in Figs. III-6 and III-7. Also plotted in these figures is the so-called "WCAP correlation" in the form used in *Power Reactor Technology*, 7(1). Another comparison is in Table III-6.

When Figs. III-6 and III-7 are considered, it is important to remember that the burnout correlations illustrated are equations, and that actually very few burnout data exist at high SEF's such as those in the vicinity of the intersections of the correlations with the SEF axis. The reason for this is probably best explained by considering Eq. 11. If one attempts to explore the region around an SEF of 5×10^8 and a ϕ_{BO} of 0.5×10^6 (see Fig. III-7), then L_B/D must be equal to 250. Not many test sections employing only single-phase water as feed have been

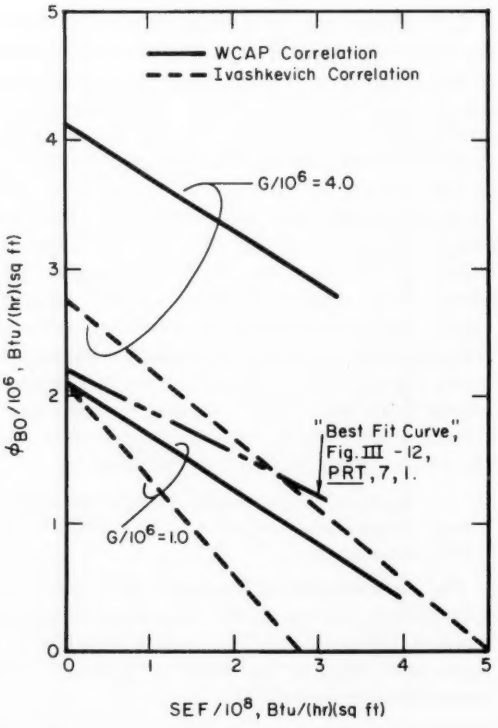

Fig. III-7 Comparison of correlation of Ivashkevich (Eq. 10) with the WCAP correlation (Table III-6). Pressure = 1000 psia. Also shown is the curve from Fig. III-12, *Power Reactor Technology*, 7(1): 22.

operated with such a large value of L_B/D to produce DNB-1 data. In particular, Tables 13 and 23 of Ref. 9 contain data taken with test sections that had values of L_T/D of 365 and 242, respectively. The data shown in Table 13, however, were taken in the subcooled region, whereas the data in Table 23 plot as DNB-2 curves. The reader's attention is directed to Fig. III-12, which will be discussed later. The data shown thereon were taken in a tubular test section with a total length-to-diameter ratio, L_T/D, of about 151. At the high mass velocities employed for some of the experiments, it can be seen that the DNB-1 line eventually becomes about parallel with the x axis as SEF increases. This behavior is not predicted by either the WCAP or Ivashkevich correlations, but then neither is the existence of the DNB-2 lines such as are shown in Fig. III-6, *Power Reactor Technology*, 7(1).

Table III-6 COMPARISON OF WCAP BURNOUT CORRELATION WITH THE CORRELATION OF IVASHKEVICH

Mass flow (G), lb/(hr)(sq ft)	WCAP* correlation	Ivashkevich correlation
	Pressure = 2000 psia	
1.0×10^6	$\phi_{BO} = 1.12 \times 10^6 - 0.0042$ SEF	$\phi_{BO} = 1.02 \times 10^6 - 0.0034$ SEF
4.0×10^6	$\phi_{BO} = 1.47 \times 10^6 - 0.0042$ SEF	$\phi_{BO} = 1.41 \times 10^6 - 0.0024$ SEF
	Pressure = 1000 psia	
1.0×10^6	$\phi_{BO} = 2.07 \times 10^6 - 0.0042$ SEF	$\phi_{BO} = 2.09 \times 10^6 - 0.0074$ SEF
4.0×10^6	$\phi_{BO} = 4.09 \times 10^6 - 0.0042$ SEF	$\phi_{BO} = 2.77 \times 10^6 - 0.0055$ SEF

*These are taken from Fig. III-11 and Table III-2 (bottom equation) of *Power Reactor Technology*, 7(1).

The correlation by Shitsman[23] is as follows:

$$q_c/q_0 = 1/[1 + K(L_B/D)^{0.8}] \qquad (16)$$

where q_c = critical heat flux, kcal/(m²)(hr)

$$K = 2.2\, D^{0.8} \exp\left(\frac{0.1}{1 - \frac{P_{crit}}{P}}\right) \qquad (17)$$

P_{crit} = critical pressure, kg/cm²
P = system pressure, kg/cm²
L_B = boiling length, m
D = tube diameter, m
q_0 = constant, kcal/(m²)(hr)

Values of the constant q_0 are given in Ref. 23 as a function of pressure and mass flow. These data are reproduced in Fig. III-8. Substitution of Eq. 11 into Eq. 16 yields the equations shown in Table III-7. Figure III-9 illustrates Eqs. 18 and 19 and compares them with data previously cited in Sec. III of *Power Reactor Technology*, 7(1). The Shitsman correlation reproduces the illustrated Ref. 9 data quite well at a diameter of 0.18 in., but the dependence of ϕ_{BO} on diameter as given in Eq. 17 does not agree with the data as the quality (or SEF) approaches zero.

Table III-7 SHITSMAN BURNOUT CORRELATIONS

[Pressure = 1000 psia, and q_0 Is Taken as 6×10^6 kcal/(hr)(m²)]

Tube diameter, in./mm	Correlation*	
0.18/4.57	$\phi_{BO} = \dfrac{2.21 \times 10^6}{1 + 0.0282\left(\dfrac{SEF}{\phi_{BO}}\right)^{0.8}}$	(18)
0.32/8.13	$\phi_{BO} = \dfrac{2.21 \times 10^6}{1 + 0.0448\left(\dfrac{SEF}{\phi_{BO}}\right)^{0.8}}$	(19)

*Units on ϕ and SEF are Btu/(hr)(sq ft).

The Lee-Obertelli correlation is given as an appendix to Ref. 24. It is as follows:

$$q_{BO}/10^6 = 0.45\left(1 + \frac{0.546}{G/10^6}\right)\left(\frac{H_{BO}}{10^3}\right)^{-2} \frac{e^{-0.00165L/D}}{0.77 + 12D} \qquad (20)$$

The units are straightforward and are in terms of British thermal units, pounds, hours, and feet. The heat balance across the test section can be written as follows:

$$H_{exit} \equiv H_{BO} = \frac{4\phi_{BO}L}{GD} + (H_{in} - H_f) + H_f \qquad (21)$$

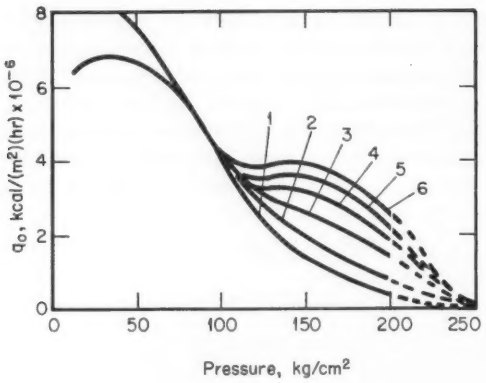

Curve	Mass flow, kg/(sec)(m²)	Mass flow, lb/(hr)(sq ft) × 10⁶
❶	500	0.37
❷	1000	0.74
❸	2000	1.47
❹	3000	2.21
❺	4000	2.95
❻	5000	3.68

Fig. III-8 The functional relation between the constant q_0 and pressure. (Taken from Ref. 23.)

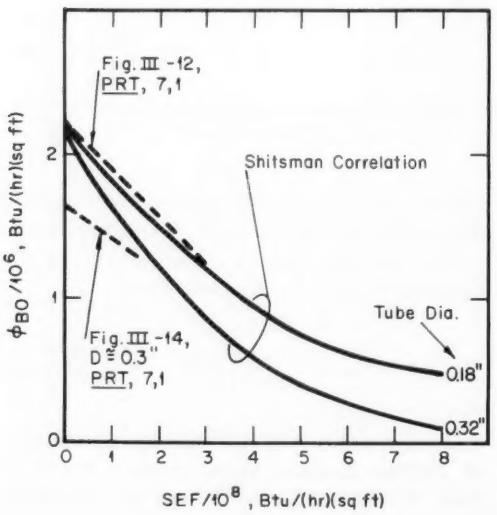

Fig. III-9 Comparison of the Shitsman correlation[23] with data taken from Sec. III of *Power Reactor Technology*, 7(1). Pressure = 1000 psia.

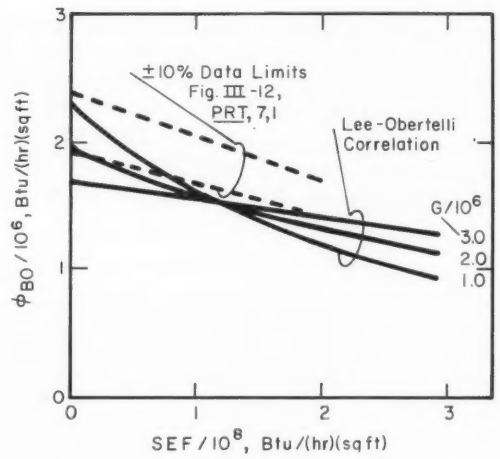

Fig. III-10 Comparison of the Lee-Obertelli correlation[24] with data taken from Fig. III-12, *Power Reactor Technology*, 7(1): 22. Pressure = 1000 psia.

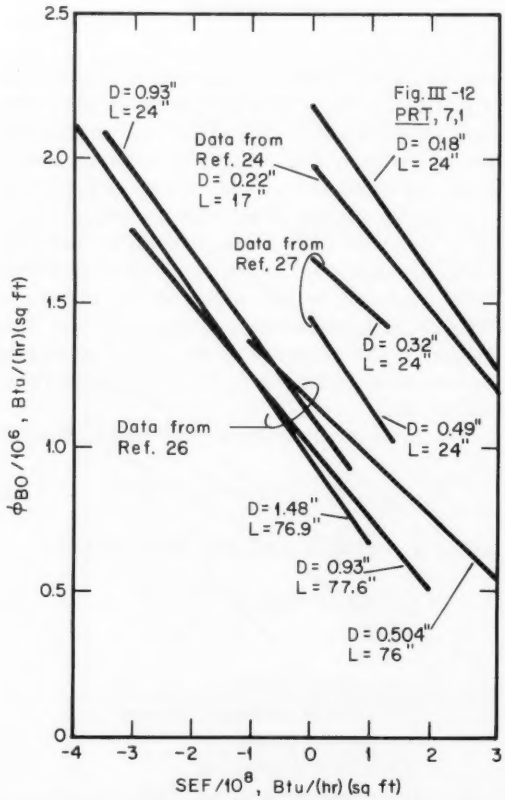
D = 0.93" L = 24"
Data from Ref. 24 D = 0.22" L = 17"
Fig. III-12 PRT, 7,1 D = 0.18" L = 24"
Data from Ref. 27
D = 0.32" L = 24"
Data from Ref. 26
D = 0.49" L = 24"
D = 1.48" L = 76.9"
D = 0.93" L = 77.6"
D = 0.504" L = 76"
ϕ_{BO} /10⁶, Btu/(hr)(sq ft)
SEF/10⁸, Btu/(hr) (sq ft)

Fig. III-11 Comparison of data from various sources showing effects of length and diameter changes on ϕ_{BO}. Pressure = 1000 psia.

Table III-8 COMMENTS ON DATA PLOTTED IN FIG. III-11

(Pressure = 1000 psia)

Source	Diameter, in.	Length, in.	Effect of G on DNB-1 line position on SEF plot	ϕ_{BO} at SEF = 0, Btu/(hr)(sq ft)*
Reference 24, runs 56 to 90	0.22	17.0	None for $0.7 \times 10^6 < G < 3 \times 10^6$	1.99×10^6
Reference 26, runs C-1 to C-2	0.504	76.0	Some effect for $5.5 \times 10^6 < G < 10 \times 10^6$ None for $0.7 \times 10^6 < G < 4 \times 10^6$	1.18×10^6
Reference 26, runs B-1 to B-49	0.93	77.62	None for $0.5 \times 10^6 < G < 4 \times 10^6$	1.01×10^6
Reference 26, runs D-1 to D-38	0.93	24.0	Some effect for $0.5 \times 10^6 < G < 1 \times 10^6$ and $5.5 \times 10^6 < G < 7 \times 10^6$ None for $1.4 \times 10^6 < G < 4 \times 10^6$	1.12×10^6
Reference 26, runs A-1 to A-47	1.475	76.88	Some effect for $0.7 \times 10^6 < G < 1 \times 10^6$ None for $1.4 \times 10^6 < G < 4 \times 10^6$	0.91×10^6
Reference 27	0.32 (av.)	24	None for† $1.2 \times 10^6 < G < 1.9 \times 10^6$	1.66×10^6
Reference 27	0.49 (av.)	24	Some effect for $G = 0.5 \times 10^6$ None for† $1 \times 10^6 < G < 2 \times 10^6$	1.44×10^6

*These data are taken from Fig. III-11.
†Upper limit on G was about 2×10^6.

Substitution of the second equation in the footnote on page 230 for $H_{in} - H_f$ yields

$$H_{BO} = H_f + \frac{SEF}{G} \tag{22}$$

If Eq. 22 is substituted in Eq. 20, rearrangement yields

$$\phi_{BO} = \frac{0.45 \times 10^{12} \, (G^2 + 0.546 \times 10^6 G) \, f(D,L/D)}{G^2 H_f^2 + 2(GH_f)\,(SEF) + SEF^2} \tag{23}$$

where

$$f(D,L/D) = \frac{e^{-0.00165 L/D}}{0.77 + 12D} \tag{24}$$

Equation 23 is plotted in Fig. III-10 for a pressure of 1000 psia with $f(D,L/D)$ taken as 0.95 (the value of 0.95 is an average of the f values for the dimensions of the test sections used to obtain data in Tables 3, 5, and 8 of Ref. 9). Also plotted are the data-limit lines taken from an earlier *Power Reactor Technology* article. The correlation predicts ϕ_{BO} quite well. The effect of G shown by the correlation is approximately within the ±10% scatter of the experimental data plotted in Fig. III-12, *Power Reactor Technology*, 7(1). The correlation is somewhat under the experimental data, but the authors mention that the correlation (in the form given by Eq. 20) also underpredicted ϕ_{BO} for their own data at a diameter of 0.22 in. and total lengths of 8.5 and 17 in.

The $f(D,L/D)$ function is very interesting, and its application is one of the few where such a correction has been attempted. Accordingly an attempt was made by the present author to ascertain its accuracy when applied to other data, since the Lee-Obertelli correlation was developed by the authors from their own data by modifying a correlation presented in Ref. 9. The data that were used for comparative purposes are shown in Fig. III-11 and originate from the sources indicated in Table III-8. This table shows that there is a wide

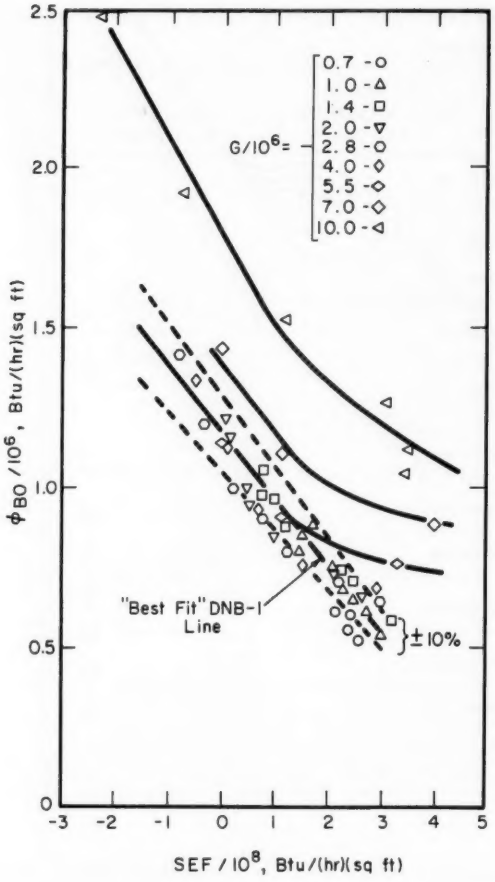

Fig. III-12 Burnout heat-flux data from Ref. 26. Pressure = 1000 psia. Test-section length is 76 in. Test-section diameter is 0.504 in. (tubular).

range of mass flow, G, over which the position of the DNB-1 line is independent of G. The range is roughly from 1×10^6 to 4×10^6 lb/(hr)(sq ft). This G-independent range is illustrated in Fig. III-12 for one of the test sections used to take data appearing in Ref. 26. A variation of $G/10^6$ between 0.7 and 4.0 affects the position of the DNB-1 line within ±10% as $G/10^6$ is increased to a value of 10.0, the position of the DNB-1 line is affected markedly. Figure III-11, therefore, is a collection of the G-independent DNB-1 curves. The intersection of these DNB-1 lines with the SEF-equals-zero axis yields a value termed $\phi_{BOSEF=0}$, and these values are shown in Table III-8.

If, in Eq. 23, SEF is taken as zero, then ϕ_{BO} becomes a function of $f(D,L/D)$ and, according to the correlation, of G. What we have just done, however, is assemble some data where ϕ_{BO} is not a function of G within certain ranges, and let us pretend that the Lee-Obertelli correlation says this, i.e.,

$$\phi_{BOSEF=0} = f(D,L/D) \times (\text{constant}) \qquad (25)$$

The comparison of the Lee-Obertelli $f(D,L/D)$ term with the burnout data shown in Fig. III-11 is illustrated in the last two columns of Table III-9. The f term correlates the data, at least at SEF = 0, to within ±10%, which is about the spread in ϕ_{BO} anyway.

Discussion and Conclusions

Figures III-1 and III-2 show that, if the correlation of Zenkevich were extrapolated into the

Table III-9 APPLICATION OF THE LEE-OBERTELLI $f(D,L/D)$ TERM TO DATA APPEARING IN REFERENCES 9, 24, 27, AND 26

Test-section length (L), in.	Test-section diameter (D), in.	$f(D,L/D)$	ϕ_{BO} at SEF = 0, Btu/(hr)(sq ft)	$\frac{\phi_{BOSEF=0}}{f(D,L/D)}$	$\frac{\phi_{BOSEF=0}}{f(D,L/D)} - \left[\frac{\phi_{BOSEF=0}}{f(D,L/D)}\right]_{av.}$ / $\left[\frac{\phi_{BOSEF=0}}{f(D,L/D)}\right]_{av.}$
12	0.18	0.943	2.20×10^6	2.33×10^6	0.11
17	0.22	0.889	1.99×10^6	2.24×10^6	0.07
76	0.504	0.612	1.18×10^6	1.93×10^6	−0.08
77.6	0.93	0.513	1.01×10^6	1.97×10^6	−0.06
76.9	1.48	0.409	0.91×10^6	2.22×10^6	0.06
24	0.93	0.564	1.12×10^6	1.99×10^6	−0.05
24	0.32	0.811	1.66×10^6	2.05×10^6	−0.02
24	0.49	0.732	1.44×10^6	1.97×10^6	−0.06
			$\left[\frac{\phi_{BOSEF=0}}{f(D,L/D)}\right]_{av.} = 2.09 \times 10^6$		

quality range, it would agree fairly well with the DNB-1 data plotted thereon from Ref. 9, especially at 2000 psia. Zenkevich did use a few data that now appear in Ref. 9, and it is of interest to speculate whether Ref. 9 was available in the Soviet Union when Zenkevich was deriving his correlation. If it was, the "agreement" may be less significant. The remaining correlations shown in Fig. III-3 illustrate the confusion arising from lack of inclusion of a term dealing with a length and diameter effect on ϕ_{BO}. If the data, taken with the exterior walls heated, were plotted from Fig. III-5 to Fig. III-3, they would lie above even the correlation of Ornatskii and Kichigin. Again this is believed to be the result of working with a short test section.

The agreement between the correlations of Ivashkevich and WCAP is rather remarkable and illustrates the utility of an SEF treatment for comparing rather difficult correlations. At 2000 psia (Fig. III-6) both correlations do well with respect to the Ref. 9 data that were plotted; at 1000 psia (Fig. III-7) both correlations do less well. This might be because the functional form of the correlations was developed from the 2000-psia, or at least the relatively higher pressure, data.

The correlations of Shitsman and Lee-Obertelli are in rather good agreement for a tube diameter of 0.18 in. (Figs. III-9 and III-10), although the diameter effect predicted by the former correlation is not correct at SEF's approaching zero. Shitsman predicts no effect of mass flow on burnout for pressures between about 70 and 100 kg/cm^2 (Fig. III-8), and this is substantiated by data plotted in Fig. III-12, *Power Reactor Technology*, 7(1). The $f(D,L/D)$ term suggested by Lee-Obertelli to account for the effect of these variables on ϕ_{BO} is quite good, as is evidenced by the last column of Table III-9.

References

1. S. S. Kutateladze, Critical Heat Fluxes in the Flow of a Wetting Liquid with the Core (of the Stream) Below the Saturation Temperature, USAEC Translation AEC-tr-5518, Aug. 28, 1962. [Translated from *Nauchn. Dokl. Vysshei Shkoly, Energ.*, 2: 229-239 (1959).]
2. A. P. Ornatskii and A. M. Kichigin, An Investigation of the Dependence of the Critical Heat Load on Mass Flow Rate, Subcooling, and Pressure, USAEC Translation AEC-tr-5710. [Translated from *Teploenerg.*, 8(2): 75-79 (1961).]
3. P. I. Povarnin and S. T. Semenov, An Investigation of Burnout During the Flow of Subcooled Water Through Small-Diameter Tubes at High Pressures, USAEC Translation AEC-tr-5602. [Translated from *Teploenerg.*, 7(1): 79-85 (1960).]
4. B. A. Zenkevich, Similarity Criteria for Critical Heat Loading in Forced Liquid Flow, *J. Nucl. Energy: Pt. B*, 1(2): 137 (August 1959).
5. B. A. Zenkevich, The Generalization of Experimental Data on Critical Heat Fluxes in Forced Convection of Subcooled Water, *J. Nucl. Energy: Pt. B*, 1(2): 130 (August 1959).
6. B. A. Zenkevich and B. I. Subbotin, Critical Heat Fluxes in Subcooled Water with Forced Circulation, *J. Nucl. Energy: Pt. B*, 1(2): 134 (August 1959).
7. S. S. Kutateladze and V. M. Borishanskii, Handbook of Heat Transfer, Translation NP-tr-917, Aug. 16, 1962. (Translation of *Spravochnik po Teploperedache*, State Publishing House of Power Engineering, Moscow, 1958.)
8. Knolls Atomic Power Laboratory, Basic Sub-Cooled Light Water Properties, USAEC Report KAPL-M-SMS-3, April 1955 (reissued October 1959).
9. R. A. DeBortoli, S. J. Green, B. W. LeTourneau, M. Troy, and A. Weiss, Forced-Convection Heat Transfer Burnout Studies for Water in Rectangular Channels and Round Tubes at Pressures Above 500 Psia, USAEC Report WAPD-188, Westinghouse Electric Corp., Bettis Plant, October 1958.
10. H. Buchberg et al., Final Report on Studies in Boiling Heat Transfer, USAEC Report COO-24, University of California, March 1951.
11. W. H. Jens and P. A. Lottes, Analysis of Heat Transfer, Burnout, Pressure Drop, and Density Data for High-Pressure Water, USAEC Report ANL-4627, Argonne National Laboratory, May 1, 1951.
12. I. T. Alad'yev, L. D. Dodonov, and V. S. Udalov, Critical Heat Fluxes for Water Flowing in Tubes, *J. Nucl. Energy: Pt. B*, 1(3): 181 (March 1960).
13. B. A. Zenkevich, V. I. Subbotin, and M. F. Troyanov, Critical Heat Fluxes for a Bundle of Tubes Cooled in Pressurized Water, *J. Nucl. Energy: Pt. B*, 1(3): 197 (March 1960).
14. L. S. Tong, H. B. Currin, and A. G. Thorp II, New DNB (Burnout) Correlations, USAEC Report WCAP-1997(Rev.), Westinghouse Electric Corp., Atomic Power Division, September 1962.
15. L. S. Tong, H. B. Currin, and A. G. Thorp II, New Correlations Predict DNB Conditions, *Nucleonics*, 21(5): 43 (May 1963).
16. L. S. Tong, H. B. Currin, and A. G. Thorp II, Comments on Letter by W. R. Gambill, *Nucleonics*, 21(7): 7 (July 1963).
17. I. T. Alad'yev and L. D. Dodonov, Critical Heat Flows in the Boiling of Underheated Water in Channels of Complex Shape (Pressure 100 atm

abs), in Convection and Radiation Heat Transfer. Translation of *Konvektiviyy I Luchistyy Teploobmen*. Report FTD-TT-61-395, pp. 79-99 (a publication of Publishing House of the Academy of Sciences, USSR, Moscow, 1960).

18. J. A. Hodde (Ed.), Fuel Cycle Program. A Boiling Water Reactor Research and Development Program, Quarterly Report No. 5, July 1961–September 1961, USAEC Report GEAP-3835, General Electric Company, Atomic Power Equipment Department, Oct. 10, 1961.
19. J. G. Collier, Heat Transfer and Fluid Dynamic Research as Applied to Fog Cooled Power Reactors, Canadian Report AECL-1631, June 1962.
20. A. S. Kon'kov and V. V. Modnikova, Experimental Investigation of the Conditions of Deterioration of Heat Transfer During Boiling in Tubes, USAEC Translation AEC-tr-5539 [Translated from *Teploenerg.*, 9(8): 77-81 (1962).] See also the Central Electricity Generating Board (British) translation, C.E. Trans. 2932, O.T.S. Document 63-23966.
21. A. A. Ivashkevich, Critical Heat Flux and Heat Transfer Coefficient During Boiling of Liquids in Channels Under Conditions of Forced Flow, USAEC Translation AEC-tr-5038. [Translated from *Teploenerg.*, 8(10): 74-78 (1961).]
22. A. A. Ivashkevich, Critical Heat Fluxes for Forced Convection of Liquid in Channels, *J. Nucl. Energy: Pts. A & B*, 16: 171 (March 1962).
23. M. E. Shitsman, Heat-Transfer Crisis in Steam-Generating Channels, British Report TRG Information Series 267(R). [Translated from *Inzh.-Fiz. Zhur., Akad. Nauk Belorussk. SSR*, 5(9): 9-15 (1962).
24. D. H. Lee and J. D. Obertelli, An Experimental Investigation of Forced Convection Burnout in High-Pressure Water, Part I. Round Tubes with Uniform Flux Distribution, British Report AEEW-R-213, August 1963.
25. A. W. Bennett, J. G. Collier, and P. M. C. Lacey, Heat Transfer to Mixtures of High Pressure Steam and Water in an Annulus, Part II. The Effect of Steam Quality and Mass Velocity on the "Burnout" Heat Flux for an Internally Heated Unit at 1000 psia, British Report AERE-R-3804, August 1961.
26. R. R. Hood and L. Isakoff (Comps.), Heavy Water Moderated Power Reactors Progress Report, May–June 1963, USAEC Report DP-855, E. I. du Pont de Nemours & Co., Inc., August 1963.
27. R. R. Hood and L. Isakoff (Comps.), Heavy Water Moderated Power Reactors Progress Report, June 1962, USAEC Report DP-755, E. I. du Pont de Nemours & Co., Inc., July 1962.

Section

IV

Power Reactor Technology

Fuel Elements

Fabrication by Novel Methods

The oxide-bearing fuel elements in currently operating water-cooled power reactors have all been fabricated by the technique of loading pressed-and-sintered pellets of UO_2 into cladding tubes and welding end caps onto the ends of the tubes for sealing purposes. Research has continued, however, into alternate methods of fabricating fuel elements, and the purpose of this review is to discuss several recent publications dealing with these novel methods. For supporting background information the reader may wish to consult the following articles published in *Power Reactor Technology*, 6(1): 26-37 and 6(2): 28-42.

References 1 through 3 are recent Battelle Memorial Institute reports concerned with fabrication details of several different fuel elements. The references report on work done to develop fabrication techniques for producing low-cost fuel elements of specific types. As such, applications to specific reactors are not discussed; the work, however, is of general interest because of the variety of fabrication methods studied. Of the two elements described in Ref. 1, emphasis herein will be placed on the so-called "concentric-component" element, as this was the most successful. The concentric-component element is of tubular geometry and employs a UO_2–stainless-steel cermet as "meat," clad on both sides with stainless steel. The core materials were 20 and 30 wt.% loadings of −325-mesh, spherical UO_2 particles in a matrix of −325-mesh, type 316 stainless-steel powder. The cladding material was 0.006-in. type 316 stainless steel, and the end plugs were also made of type 316 stainless steel.

Attempts were made to incorporate a plastic binder into the core material to allow for forming or extruding into a tubular shape, but the final elements were made by the loading of loose powder into the annular space formed between the concentric stainless-steel cladding tubes. As-loaded densities from 50 to 60% were attained. Tamp packing, powder wetting after partial loading, vibrational packing, and step packing with periodic thermal cycling of the tubes were studied to try to attain a uniform loading density.

When loading was completed, a consolidation and bonding step was accomplished. This was designed to densify the fuel cermet, size the fuel element, and form a bond between the meat and the cladding. Three processes were considered: (1) explosive compaction, (2) cold hydrostatic pressing, and (3) gas-pressure bonding. These processes were employed either singly or in combination. Figure IV-1 shows a schematic view of an assembled specimen ready for implosive consolidation. In this process a sheet of explosive (PETN) was wrapped around the outside jacket and detonated in a housing submerged in a tank of water. The mild-steel jackets were then removed by an acid bath. Experiments were also done using a backup die with the explosive charge (Primacord) placed inside the tube. A mild-steel insert was used between the specimen and the explosive to smooth out the shock wave.

Cold hydrostatic pressing was accomplished at 100,000 psi. No mandrels were necessary because the outer tube yielded before the inner cladding tube, and densification of the meat took place from the outside in. The gas-pressure bonding was done at 2100°F and 10,000 psi for 3 hr.

Test elements of lengths 6 and 10 in. were made by combinations of the above-discussed fabrication techniques, and full-scale elements having an outside diameter of $\frac{3}{4}$ in. and a length

of 27 in. also were fabricated. The conclusions are quoted[1] as follows:

> (1) Tubular fuel elements approximately $^3/_4$ in. in diameter and 27 in. long can be fabricated by the assembly, consolidation, and bonding of concentric components.
>
> (2) These elements possess dense fuel cores and almost complete core-cladding bonding when explosively sized and gas-pressure bonded.
>
> (3) Additional study is needed to optimize the blending and loading procedures to insure a uniform dispersion of UO_2 in the stainless steel matrix and to achieve a uniform loading density along the length of the elements, which later influences the surface condition of the bonded elements.
>
> (4) A densification step after powder loading is needed to attain sufficient density in the fuel annulus to prevent wrinkling of the outside cladding during pressure bonding of the element.

References 2 and 3 deal with fabrication techniques applicable to the production of UO_2-fueled rods. Specifically, the work was done as a part of the USAEC Fuel-Cycle Development Program. Reference 2 describes a fabrication technique that is a combination of vibrational compaction and gas-pressure bonding. The fuel material was UO_2, consisting of high-density particles of coarse sizings mixed with varying amounts of micronized UO_2. The latter material is a powder prepared by a fluid jet-grinding process to reduce the particle size.[4] The coarse particles included fused, high-energy-impacted, and electrodeposited oxides. The cladding materials included Zircaloy, types 304L and 406 stainless steel, and Inconel X, with cladding thicknesses varying from 0.007 in. (304L) to 0.030 in. (Zircaloy).

Some results of the program are given in Table IV-1. An improvement was achieved by the use of an intermediate swage to increase the prebonded density to the point where pleating and surface roughening would not occur during the gas-pressure bonding step. The effect of intermediate swaging is shown in Table IV-2. To summarize:

> The swaging operation was found to be particularly advantageous in the aforementioned work and its combination with vibrational compaction, using inexpensive vibrational equipment and pressure bonding may be advantageous although somewhat more involved. These studies have shown, however, that gas-pressure bonding following a single-step preliminary densification by vibrational compaction is feasible. The requirements for fabricating stainless steel-clad UO_2 rods by the combined processes are:
>
> (1) Oxide mixtures of fused and Micronized UO_2 in which the high-surface-area Micronized UO_2 constitutes approximately 30 to 40 w/o

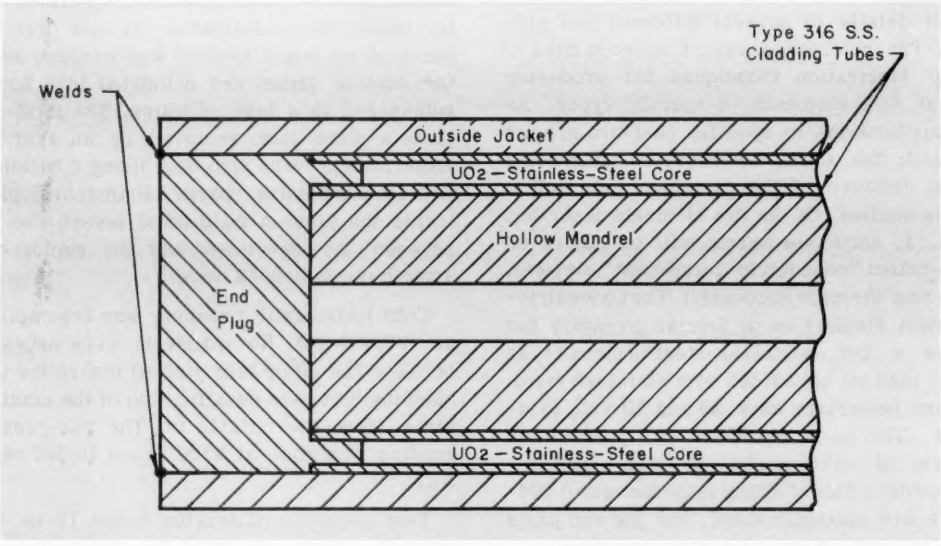

Fig. IV-1 Schematic of assembled specimen for implosive consolidation.[1] Explosive sheet is wrapped around the outside jacket to the desired charge density, and the fuel annulus is densified from the outside in.

Table IV-1 EFFECTS OF FUSED PARTICLE-SIZE VARIATIONS ON VIBRATIONALLY COMPACTED AND PRESSURE-BONDED RODS[2]

Oxide composition			Average density after vibrational compaction, % of theoretical	Results of gas-pressure bonding 3 hr at 2100°F and 10,000 psi			
Amount, wt.%	Type of powder	Mesh size		Rod appearance	Outside diameter, in.	Oxygen/uranium ratio	Average density, % of theoretical
40	Micronized		64.3	Rods were bowed, and cladding was rough and distorted	Could not be taken	2.007	94.1
60	Fused	−6 +10					
40	Micronized		60.5	Rods were bowed, and cladding was rough and distorted by wrinkling	Could not be taken	2.010	94
40	Fused	−6 +10					
20	Fused	−35 +65					
20	Micronized		73.7	Rods were only slightly bowed and cladding slightly roughened; these were areas where uneven packing was in evidence	0.535 (av.),* rods out of round	2.008	87.7†
60	Fused	−10 +20				2.010	89.0
20	Fused	−35 +65				2.010	86.5
25	Micronized		71.9	Rods were only slightly bowed; cladding was roughened slightly, and there was some evidence of uneven packing	0.536 (av.),* rods out of round	2.006	87.8†
60	Fused	−10 +20				2.006	88.4
15	Fused	−35 +65				2.012	87.4
30	Micronized		66.5	Rods were bowed and badly distorted by wrinkling; there was evidence of uneven packing	Could not be taken	2.008	92.0
50	Fused	−10 +20					
20	Fused	−35 +65					
30	Micronized		70.0	Rods were only slightly bowed, and cladding surfaces were only slightly distorted; there was some wrinkling of the cladding	0.532 (av.), rods slightly out of round	2.002	93.5
70	Fused	−20 +35					
20	Micronized		74.2	Rods retained a high degree of straightness, and cladding was only slightly distorted	0.563 (av.)	2.004	92.4
70	Fused	−20 +35					
10	Fused	−35 +65					
25	Micronized		72.2	Rods retained a high degree of straightness, and cladding was only slightly distorted	0.562 (av.)	2.003	94.3
60	Fused	−20 +35					
15	Fused	−65 +200					

*All oxide materials were contained in 0.563-in.-OD type 304L stainless-steel tubes with a 0.015-in. wall.
†Samples taken at three locations down the length of the rod.

Table IV-2 EFFECTS OF INTERMEDIATE SWAGING ON VIBRATIONALLY COMPACTED AND PRESSURE-BONDED RODS[2]

Oxide composition			Prefabrication method	Type 304L cladding diameter prior to bonding, in.			Cladding wall thickness, in.	Average density before bonding, % of theoretical			Results of gas-pressure bonding 3 hr at 2100°F and 10,000 psi			
Amount, wt.%	Type of powder	Mesh size		Vibratory packed	Cold swaged	Hot swaged		Vibratory packed	Cold swaged	Hot swaged	Rod appearance	Outside diameter, in.	Oxygen/ uranium ratio	Average density, % of theoretical
30 70	Micronized Fused	−20 +200	Vibrationally compacted and cold swaged	0.590	0.563		0.007	64.9	71.7		Rods retained straightness, but there was some surface roughness and a wrinkle down entire length of cladding	5.515 (av.) (wrinkled)	2.001	95.4
30 70	Micronized Fused	−35 +65	Vibrationally compacted and cold swaged	0.750	0.575		0.010		81.0		Rods retained straightness, and cladding remained smooth	5.568 (av.)	2.006 2.006 2.004	95.4* 95.1 94.5
30 70	Micronized Fused	−100 +200	Vibrationally compacted and cold swaged	0.750	0.573		0.010	58.0	72.0		Rods remained straight and had smooth surfaces	0.555 (av.)	2.017	96.3
30 70	Micronized Fused	−20	Vibrationally compacted, cold swaged, and hot swaged	0.750		0.570	0.010			84.0	Rods were slightly bowed, but cladding retained a smooth surface	0.547 (av.)	2.014 2.012 2.000	95.6* 96.3 95.3
30 70	Micronized Fused	−65 +100	Vibrationally compacted, cold swaged, and hot swaged	0.750		0.573	0.010			84.6	Rods were slightly bowed, but cladding retained a smooth surface	0.552 (av.)	2.012 2.016 2.004	95.2* 94.5 92.6
30 70	Micronized Fused	−100 +200	Vibrationally compacted, cold swaged, and hot swaged	0.750		0.573	0.010			83.3	Rod retained its straightness and smooth surface	0.550 (av.)	2.002 2.010 2.006	95.6* 95.1 94.3

*Samples taken at three locations down the length of the rod.

Fig. IV-2 Cross section of an annular multitube element.[5] In the particular application envisioned in Ref. 5, water is boiled on the inner and outer cladding surfaces, and steam is superheated within the steam tubes.

(2) A maximum fused UO_2 particle size of minus 20 plus 35 mesh and uniform bulk densities of 75 per cent of theoretical or greater

(3) A pressure-bonding cycle consisting of pressurizing to approximately 6,000 psi prior to heating to 2100 F and holding for 3 hr at 2100 F and 10,000 psi.

The reference[2] concludes with a discussion of the effect of pressure bonding on the cladding.

Reference 5 describes developmental work leading to the fabrication of an "annular multitube fuel element." A cross section of the element is shown in Fig. IV-2. The element is quite specialized, in that it was designed to be used with an integral boiling-superheating reactor. Fuel elements for steam-cooled reactors have been discussed in *Power Reactor Technology*, 6(2): 75-80. The small tubes serve as flow channels for steam, whereas boiling takes place on the external and internal heat-transfer surfaces of the annulus itself. The element represents the application of vibrational compaction to the fabrication of a fuel element of a relatively complex shape.

The fuel powder used was vacuum-outgassed arc-fused UO_2 having a particle density greater than or equal to 98% of theoretical. Several blends were tried, but the final experiments were done with powder that was 60% $^{8}/_{16}$ mesh, 15% $^{30}/_{100}$ mesh, and 25% 200 mesh. The fuel subassembly ready for loading is shown in Fig. IV-3. Details for the welding of the various tubes into the bottom tube sheet are given in the reference[5] but will not be discussed here.

The assembly at the top is not part of the fuel element proper but was utilized to ensure that the steam tubes retained their proper relative positions with respect to each other and to the internal and external cladding tubes. The tension rods (carbon steel) were inserted through the steam tubes and held in tension by tightening the locknuts. The center column absorbed

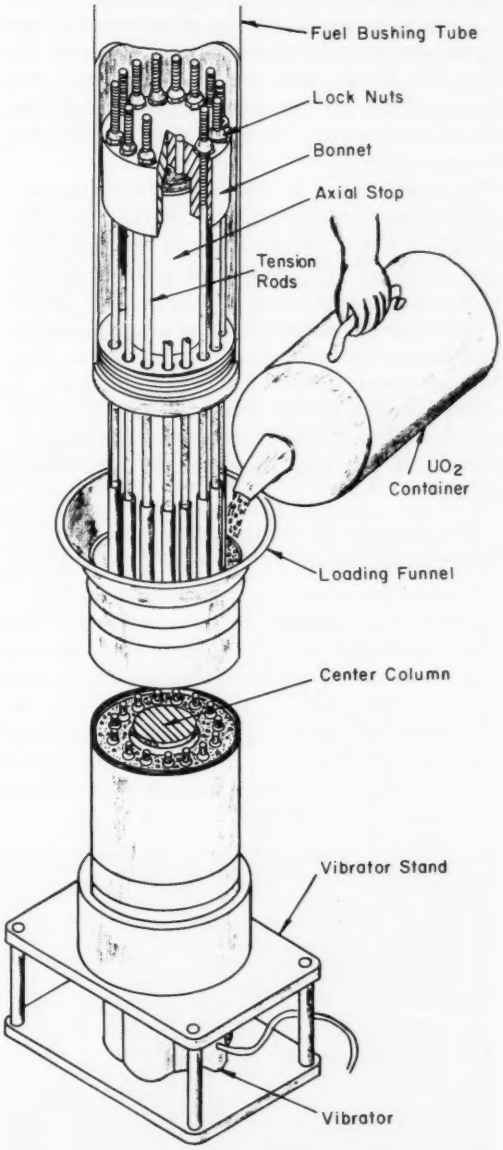

Fig. IV-3 The UO_2 fuel loading of multitube shell subassembly.[5]

the load developed by the tension rods and provided the basis for straightness of the whole subassembly.

The maximum density attained during the compaction step was 84.3% and was accomplished by dividing the fuel charge into eight equal increments. Dimensional inspection indicated that the small tubes were within ±0.030 in. from their intended axes. The ovality of the outside cladding was reduced from about 0.020 in. initially to about 0.010 in. after compaction, and the assembly had a runout of about 0.010 in. along the 36-in. fuel length. The upper end closure of the fuel element is peculiar to the boiling-superheating function and will not be discussed here.

The fabrication of fuel rods clad with Al-Al_2O_3 [sintered aluminum powder (SAP)] is described in Ref. 6. Fuel elements clad with SAP have potential application in organic-cooled reactors; the reader may wish to consult Sec. X of this issue for a discussion of organic-cooled heavy-water-moderated power reactors. The cladding material, SAP 930, was in the form of 8-finned tubing and is shown in Fig. IV-4. A magnetic-pulse forming machine,[6] the Magneform Mark I, was used in the fabrication process.

The operation of Magneform is based upon the discharge of electrical energy from a capacitor bank through a coil. The collapsing magnetic field causes eddy currents to be induced into a conductive workpiece placed in, around, or near the coil. This results in a repulsive force between the coil and the workpiece due to the interaction of their magnetic fields, in accordance with Lenz's law. Various forming operations are possible depending on the location of the coil with respect to the workpiece. For example, coils may be selected for swaging and expanding of tubular shapes and forming all sheet materials. Coils for magnetic pulse forming must be rigidly constructed to withstand the force equal and opposite to that exerted on the workpiece.

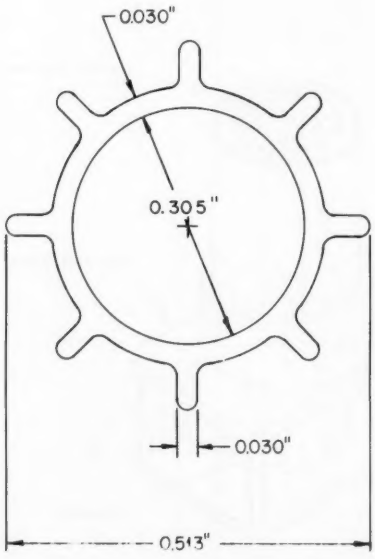

Fig. IV-4 Cross-sectional dimensions of SAP extruded tubing.[6]

Table IV-3 SPECIFICATIONS FOR MAGNEFORM MARK I MAGNETIC-PULSE FORMING MACHINE[6]

Power consumption	220 volts, 60 cps, single phase, 1500 watts (maximum average)
Maximum energy released per pulse	6000 joules
Maximum input current to work coil	90,000 amp
Maximum pulse rate at maximum power	10/min
Operating-level control	Continuously adjustable
Maximum pressure on workpiece	$\frac{4 \times 10^6}{\text{Work area, sq in.}}$ psi
Time of applied pressure	10 to 100 μsec, depending on coil and workpiece

Work-coil application	Work-coil size
Swaging	4- and 6-in. in inside diameter (with corresponding field shapers)
Expanding	1 in. in outside diameter (minimum)
Flat forming	3- and 6-in.-diameter "pancake" coils

The specifications for the machine are given in Table IV-3.

The study of magnetic swaging was initiated to develop techniques for producing fuel rods with cladding-to-fuel contact in order to improve heat transfer between the fuel and cladding. A design of an organic-moderated reactor which is briefly mentioned in the reference specifies a fuel-to-cladding annulus of 0.0015 in. This was stated[6] to be difficult to obtain over the design fueled length of 96 in. because of diametral variations in the components, chipping of the fuel pellets, and internal galling of the cladding. Various techniques were considered for collapsing the cladding onto the pellets, and

the magnetic swaging was selected for investigation as the most promising. The swaging reduces the fuel-to-cladding clearance to approximately zero, which should produce a higher gap conductance than the 0.0015-in. annulus, but the reference states that little is known of the overall heat-transfer effect of having no clearance between fuel and cladding.

Table IV-4 SIMULATED FUEL-ROD COMPONENTS[6]

	Rod 1	Rod 2	Rod 3
Pellet material	Stainless steel	Grade A Lavite	Natural UO_2
Pellet diameter, in.	0.300 ± 0.001	$0.300\ ^{+0.001}_{-0.000}$	$0.300\ ^{+0.001}_{-0.000}$
Pellet length, in.	1.000	0.500	0.350
Number of pellets	32	64	90
Pellet column length, in.	32	32	31.5
Tube length, in.	40	40	40

Several simulated fuel rods were fabricated, and dimensional details are given in Table IV-4. Figure IV-5 shows the simulated fuel rod undergoing the swaging step in the Magneform machine. The operation was done at room temperature. Swaging of rods 2 and 3 (Table IV-4) took place in increments of $\frac{3}{8}$ in., and swaging was extended about $\frac{1}{2}$ in. beyond the ends of each pellet column. Rod 3 was filled with helium, sealed with hot, pressure-bonded aluminum end plugs, and thermal cycled between 350 and 900°F in a vacuum retort. No leaks were detected. The conclusions are as follows:

> It is concluded that magnetic pulse swaging is a feasible method of reducing the fuel-cladding annuli in APM-clad UO_2 fuel rods to essentially zero. Intimate fuel-cladding contact is retained after thermal cycling, and is believed to be a result of tensile hoop stresses remaining in the Magneformed cladding.

Reference 7 gives comparative cost data for various processes used to fabricate fuel elements for the General Electric High Power Density Development Project. This project was discussed in *Power Reactor Technology*, 7(1): 34-42. The processes are as follows:

Pellet Fuel

Ground pellet, cladding-to-pellet gap of 4 to 9 mils
Ground pellet, gap reduced by swaging
Unground pellet, gap reduced by swaging

Compacted Powder Fuel

Two-pass cold-swaged powder
Three-pass cold-swaged powder
Three-pass hot-swaged powder
Tandem-rolled powder
Vibratory-compacted powder

Fabrication flow sheets are shown[7] for the various processes, and Fig. IV-6 illustrates the three-pass swaged-powder fuel method. The fuel-fabrication costs were those associated with the process from the receipt of tubing and fuel, through the fabrication of fuel segments, loading of rods into a fuel assembly, and packing for shipment. The bases for the cost figures are quoted as follows:

> ... Costs are based on actual labor measurements made during semi-production laboratory fabrication of two and three-pass swaged powder fuel and swaged ground and unground pellet fuel. The unmeasured fabrication steps of the tandem rolling and the vibratory compaction processes are estimated based on laboratory fabrication experience.

Table IV-5 shows a breakdown for the labor for the three-pass cold-swaged-powder fuel-fabrication process. Similar tables are given for the other processes. Table IV-6 summarizes the various fuel-fabrication processes and their relative labor requirements. It must be remembered that the cost of direct labor is only a portion of the cost of the final fuel element, even if the fuel rods fabricated by the various processes had identical in-core lifetimes. Besides overhead charges on the direct labor, the cost of amortizing capital equipment must be included. Losses may also be an important cost consideration, and the unit fabrication cost increases with the enrichment of the fuel.[7]

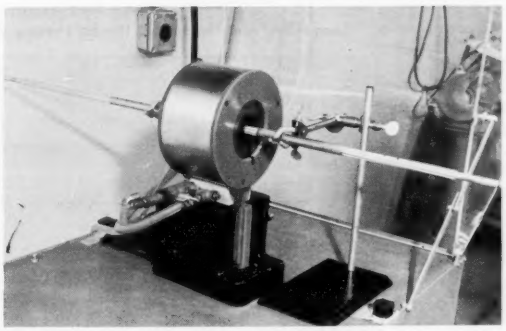

Fig. IV-5 Swaging simulated APM-UO_2 fuel rod.[6]

Interestingly, almost any fabrication process appears to be cheaper labor-wise than assembly of a ground pellet into a clad tube. Whether the less expensive processes can be used, however, depends on their in-reactor performance. One of the objectives of the High Power Density Development Project is to obtain in-pile performance data. Although a large number of fuel assemblies have been classed as failed,[8] the reasons for these failures do not appear to be known and may or may not be related to the various fabrication procedures used.

The remaining reports deal with two fuel-element components, the cladding tubing and the end closures.[9,10] The importance of maintaining cladding integrity in an operating fuel element is obvious. The tubing evaluation program outlined in Ref. 9 had the following objectives:

1. Determine the influence of defects upon tubing burst strengths and thereby define an "acceptable defect." This information is necessary to establish an inspection procedure for tubing quality control.
2. Determine the "expected defect level" of commercial tubing as indicated by ultrasonic testing techniques, thus allowing a correlation between the expected and acceptable defect levels.
3. Determine tubing tensile properties at elevated temperatures and thus provide information applicable to fuel geometries desired for nuclear superheat designs.

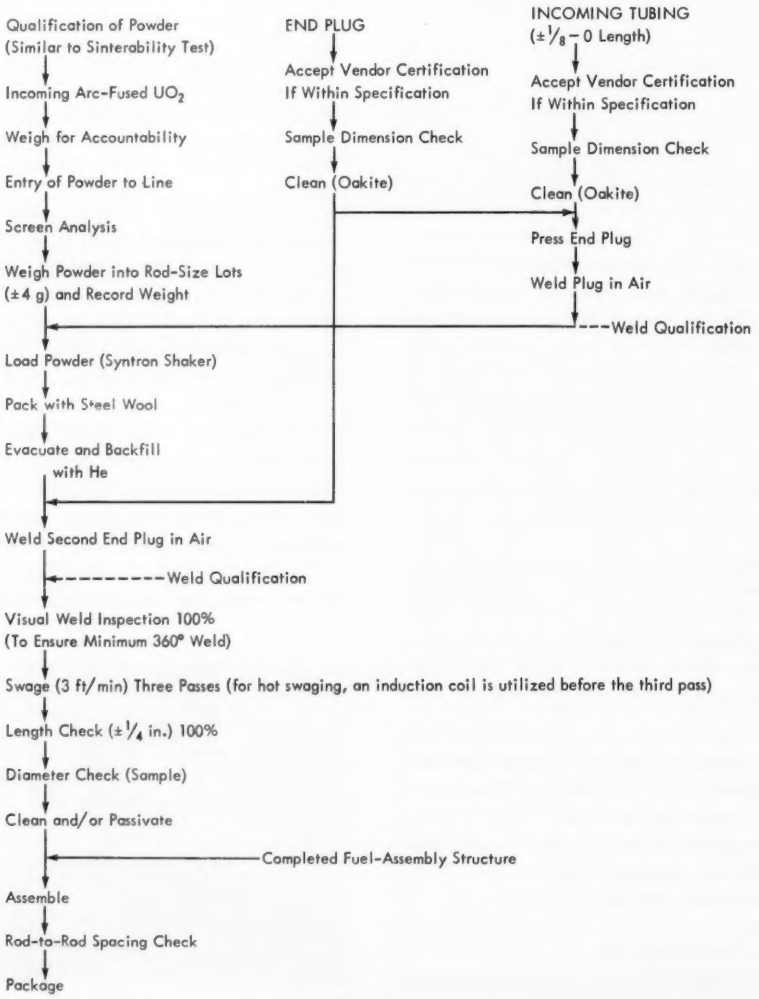

Fig. IV-6 Three-pass swaged powder fuel.[7]

Table IV-5 LABOR REQUIRED IN FABRICATING THREE-PASS COLD-SWAGED-POWDER FUEL[7]

Process step	Labor man-hours/ pound of uranium
Sample; weigh; crush; screen; weigh for accountability; blend	0.166
Fuel transfer and accountability; clean tubing (ultrasonic); cut tube to length; press and weld first end plug	0.020 0.101
Load, vibrate, and compact	0.140
Helium backfill; press and weld second end plug	0.104
Swage (3 pass)	0.164
Check diameter and length	0.088
Leak check	0.022
Assemble	0.023
Package	0.024
Total process	0.852

A number of feet of types 304, 316, and 316L stainless-steel tubing were purchased from several manufacturers. The tubes were subject to burst and tensile tests and given ultrasonic inspections. Since the tubing evaluation program was done in support of the Nuclear Superheater Development Effort, the burst and tensile tests were done at about 1300°F. The ultrasonic evaluation was done by the immersion-ultrasonic method using equipment calibrated to detect longitudinally oriented defects on the outer and inner wall surfaces of the tubing. The results of the ultrasonic evaluation are shown in Table IV-7. The conclusions of the study are quoted as follows:[9]

1. Tubing defects which are 10 percent of the wall thickness or less do not significantly affect the location of tubing failures induced in a laboratory burst test apparatus. In other words, there is not a direct correspondence between burst test failures and location of tubing defects if the defects are 10 percent or less of the tubing wall thickness.

2. Artificially defecting tubing to less than 20 percent of the wall thickness does not affect the average burst strength but tends to reduce the minimum in a group of data points. This may be explained by the low probability of coinciding the defect with the weakest portion of the tube.

3. Defects greater than 20 percent of the tubing wall will cause a reduction in the average ultimate tubing strength with the defect serving as the point of initial failure.

4. Differences in tubing geometry, temper, and type material appear to have no significant effect upon the quality of the tubing as determined by ultrasonic methods.

5. The average expected rate of occurrence of defects in commercial tubing is one defect in 22 feet of tubing for those defects greater than 5 percent of the wall, and one defect in 50 feet for those in excess of 10 percent.

6. In view of the data obtained from this study, a realistic acceptance limit has been established for incoming tubing slated for fuel element fabrication. This limit (defects having a magnitude not greater than 10 percent of the wall thickness) can be used in tubing inspection practices where the ultrasonic technique is recommended. The cost penalty that such a specification may incur is expected to be minimum based on results obtained from a sampling of tubing purchased from representative qualified tube vendors using a variety of in-plant non-destructive testing techniques.

Reference 10 is somewhat specialized, dealing with end-closure development for the superheater fuel rods for the Pathfinder reactor. The Pathfinder reactor is discussed in detail in Sec. VIII of this issue. The report does bring attention to bear on the many details that may be important in producing satisfactory fuel

Table IV-6 RELATIVE LABOR REQUIREMENTS FOR VARIOUS UO_2 FUEL-FABRICATION PROCESSES[7]

Process	Man-hours/lb U	Large core (25,000 lb U), man-hours/lb U*	Very large core (352,000 lb U), man-hours/lb U†
Tandem rolled	0.689	0.459	0.306
Three-pass swaged powder	0.852	0.568	0.379
Three-pass hot swaged powder	0.853	0.569	0.379
Swaged unground pellet	0.972	0.648	0.432
Two-pass swaged powder	0.978	0.652	0.435
Vibratory compacted	1.026	0.684	0.456
Ground pellet with gap	1.106	0.737	0.491
Swaged ground pellet	1.172	0.781	0.521

*A 33% labor and overhead decrease from the value shown in column 2.
†A 33% labor and overhead decrease from the value shown in column 3.

Table IV-7 ULTRASONIC EVALUATION OF STAINLESS-STEEL TUBING–SUMMARY SHEET[9]

Vendor	Wall thickness, in.	Outside diameter, in.	Type material	Quantity tested, ft	Number of defects		Defects/ft of tubing
					Greater than 5% of wall	Greater than 10% of wall	
A	0.028	3/4	304L	34	1	1	1/17
A	0.028	3/4	316L	36	1	1	1/18
A	0.028	5/8	304	22	0	0	0/22
A	0.028	5/8	316L	48	2	0	1/24
B	0.028	1 1/4	304L	32	0	0	0/32
A	0.016	3/4	304L	48	1	1	1/24
A	0.016	3/4	316L	42	0	0	0/42
B	0.016	5/8	304	168	8	7	1/11.2
A	0.010	3/4	304	36	1	2	1/12
D	0.010	7/16	304	48	3	1	1/12
C	0.010	3/8	316 annealed	48	0	0	0/48
C	0.010	3/8	316 1/8 hard	36	0	1	1/36
C	0.010	3/8	316 1/4 hard	42	0	0	0/42
C	0.008	3/8	316 annealed	48	1	2	1/16
C	0.008	3/8	316 1/8 hard	18	0	0	0/18
C	0.008	3/8	316 1/4 hard	54	0	0	0/54

rods. The end-cap designs studied are shown in Fig. IV-7. The conclusions are quoted as follows:

1. Design is one of the major considerations for welding components which have large mass differences. Proper attention to heat balance of components at the design stage can mean the difference between a process which is hypercritical to parameter variation and one which provides a practical latitude for production application.

2. Weld puddle geometry and weld microstructure can be greatly improved with the proper use of chills on the fuel tube. An integral chill which rotates with the tube during welding is the most effective.

3. Entrapped air or gas between the end plug and fuel can cause serious weld defects if heat buildup becomes great during welding. This can be minimized by venting, increasing weld speed or reducing the welding mass by end cap design. The most satisfactory method was found to be a combination of speed and design.

4. Preheat and decay cycles change outer appearances, but do not significantly affect weld penetration in the range studied ... in the case of this material and this geometry.

5. Satisfactory welds can be made on Pathfinder-type fuel rods by using straight plug caps with vent holes, reduced shoulder caps or cup caps. The plug caps, however, are the most sensitive to welding parameters.

6. Both the reduced shoulder and the cup-cap end closures are relatively insensitive to process variations. From a design standpoint the reduced shoulder cap is most desirable for Pathfinder.

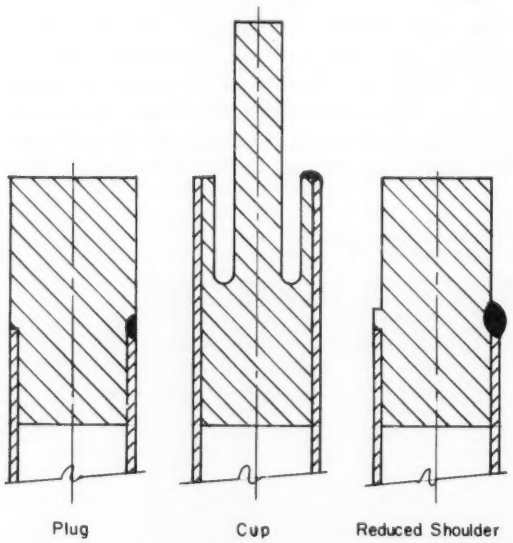

Fig. IV-7 Schematic of modified end caps with improved heat balance.[10]

References

1. E. S. Hodge, R. J. Carlson, and E. G. Smith, Jr., Investigation of Fabrication Techniques for Tubular Fuel Elements, USAEC Report BMI-1652, Battelle Memorial Institute, Oct. 28, 1963.

2. S. W. Porembka, C. B. Boyer, and J. J. Hauth, Fabrication of UO_2 Fuel Rods by Vibrational Compaction and Pressure Bonding, USAEC Report BMI-1637, Battelle Memorial Institute, June 28, 1963.
3. E. S. Hodge, S. W. Porembka, C. B. Boyer, and R. J. Diersing, Use of Agglomerated UO_2 in Pressure-Bonded Stainless Steel-Clad Fuel Rods, USAEC Report BMI-1640, Battelle Memorial Institute, July 23, 1963.
4. G. R. Cole, Evaluation of Fused UO_2, USAEC Report DP-819, Savannah River Laboratory, April 1963.
5. H. V. Lichtenberger, C. D. Sedlak, and B. E. Murtha, Annular Multitube Fuel Element Design and Development, USAEC Report CEND-187, Combustion Engineering, Inc., Apr. 30, 1963.
6. E. C. Supan, Magnetic Pulse Swaging of APM-UO_2 Fuel Rods, USAEC Report NAA-SR-8263, Atomics International, Sept. 30, 1963.
7. R. B. Hoffman, Economic Comparison of Fuel Fabrication Processes Used in the High Power Density Program, USAEC Report GEAP-4294, General Electric Company, Atomic Power Equipment Department, June 25, 1963.
8. R. L. Holladay (Comp.), High Power Density Development Project Fourteenth Quarterly Progress Report July–September 1963, USAEC Report GEAP-4391, General Electric Company, Atomic Power Equipment Department, Sept. 1, 1963.
9. R. F. Kirby, Evaluation of 300 Series Stainless Steel Tubing for Fuel Cladding, USAEC Report GEAP-4095, General Electric Company, Atomic Power Equipment Department, October 1962.
10. R. A. Boschke and R. J. Wiggins, Pathfinder Atomic Power Plant. End Closure Development for Low Enrichment Superheater Fuel Rods, USAEC Report ACNP-63023, Allis-Chalmers Mfg. Co., July 30, 1963.

Section

V

Power Reactor Technology

Control and Dynamics

Conference on Noise Analysis in Nuclear Systems

By M. F. Valerino

On November 4–6, 1963, a symposium on Noise Analysis in Nuclear Systems was held at the University of Florida, Gainesville. The objectives of the symposium were to define the present state of the art and to stimulate maximum exchange of ideas and information through informal discussions. From the proceedings it was evident that the field of reactor noise analysis has steadily grown to the point that routine noise measurements are now generally accepted as part of power-reactor startup procedures, although the results have not proved to be useful in all cases. Noise measurements have been made as part of the standard operational analyses performed on such power reactors as the Saxton, Savannah, Consolidated Edison, Yankee, and Dresden reactors. From an overall consideration, it was apparent that much exploratory experimentation remains to be done in order to realize the full potentialities of noise-analysis techniques.

Data-handling systems have been developed for rapid acquisition and digitizing of the data for processing with digital computer codes. The use of commercially available electronic analyzers (on-line or off-line in conjunction with the tape-recorded noise fluctuations) have proved to be highly satisfactory in the analysis of the noise data.

The fundamental soundness of noise-analysis techniques, from both the theoretical and experimental points of view, has been amply tested by extensive measurements on numerous zero-power reactors and subcritical assemblies whose dynamic characteristics are thoroughly understood. Hence a firm foundation exists for extension of present noise-analysis techniques to the study and physical interpretations of the variety of noise sources prevalent in reactor power-plant systems. The interacting dynamics of the numerous components of the reactor power-plant system, as ultimately reflected in the reactor through the various reactivity coefficients, result in an extremely complicated behavior of the overall system which, in most cases, cannot be analyzed in terms of the individual physical processes involved. In general, the additional understanding obtained by application of current noise-analysis techniques and interpretations has been more qualitative than quantitative. This limitation reflects the existing limitation on the amount of useful information contained in the noise signals which can presently be extracted and reliably interpreted in terms of system kinetic parameters, however, it has not prevented the acquisition of useful results in a number of important cases. In several instances extrapolation of the results of noise measurements clearly indicated the reactor operating conditions for onset of instability. In the Saxton power reactor, an empirical correlation was obtained between the area under a well-defined resonance in the power spectra and the fraction of the reactor heat-transfer surface over which nucleate boiling is occurring. This unexpected result demonstrates the fact that the full potentialities of noise-measurement results are currently being realized as continued experimentation is under way in the application and further refinement of presently developed methods.

Development work on reactor noise analyses utilizing zero-power reactors and subcritical assemblies is continuing in several important areas. In particular, investigations of spatial

effects upon the noise measurements are currently being emphasized, which involve considerations of such basic phenomena as neutron-wave propagation and the associated spatially dependent impulse and transfer functions. Several methods for generating neutron-source driving functions having a random or pseudo-random output are in various stages of practical development for use in noise experiments. A coordinated effort is presently under way to improve on the noise measurements for specific determination of reactor shutdown margin.

The underlying principles of random-noise theory have been formulated on a sound mathematical basis and are well documented in the scientific literature. Applications of the theory have been carried out in the fields of communication engineering, systems analyses, automatic controls, meterology, etc. References 1 through 12 represent a portion of the bibliography on this subject. The recently published book *Reactor Noise*, by J. A. Thie,[1] presents a thorough and concise exposition of the fundamentals of noise analysis and of the important reactor noise experiments performed up to 1962.

A brief review is presented herein of the papers given at the Conference on Noise Analysis in Nuclear Systems. Abstracts of these papers are published in Ref. 13. Prior to the review, the general methods of noise analysis are briefly described to provide background information on the subject. For a comprehensive treatment of noise analysis, reference should be made to the literature, notably Thie's book[1] (and references listed therein) for the specific application to reactors.

Methods of Reactor Noise Analysis

Analysis of a stationary random process is performed by means of various characteristic functions that describe in a statistical manner the regularity of the process. Repeated measurements of a stationary random process under identical conditions would reveal no apparent similarity in the instantaneous variations (wave form) of the random function with time. However, the characteristic functions calculated from the different wave forms would be closely similar (within a statistically defined precision) and hence would reveal that the different wave forms were indeed member functions of the same stationary random process. Two characteristic functions, which have proven to be highly useful in the analysis of random functions, are the autocorrelation function and the power spectral density. These two functions are determinable one from the other. In the case of two stationary random processes that are in some manner related to each other, the comparable characteristic functions calculated from the two wave forms are the cross-correlation function and the cross power spectral density.

AUTO- AND CROSS-CORRELATION FUNCTIONS

Assume that $x(t)$ is some frequency-rich random disturbance in some system variable, such as fission rate, control-rod position, coolant flow rate, coolant inlet temperature, or void density, which is being generated either intrinsically within the system or by some external source. Let $y(t)$ be the observed system response signal, such as neutron level, coolant outlet temperature, or fuel temperature. The autocorrelation function of the measured output signal is defined as

$$C_y(\tau) = \lim_{T\to\infty} \frac{1}{T} \int_{-T/2}^{T/2} y(t)\ y(t+\tau)\, dt \qquad (1)$$

In practice, a finite number of data of total time duration T are treated. The data record is subdivided by N equally spaced discrete points of time interval Δt, where $T = N\ \Delta t$. The lag time τ is then represented by a shift of m points (so as to equal $m\ \Delta t$) up to the maximum lag time $\tau_m = M\ \Delta t$, where $M < N$. It is evident that with this method of treatment the continuous data record is handled in a digitized manner over the finite time T. The expression for the approximation to the autocorrelation function defined in Eq. 1 is hence given as

$$C_y(\tau) = \frac{1}{N - \frac{\tau}{\Delta t}} \sum_{j=1}^{N-\frac{\tau}{\Delta t}} y_j y_j + \frac{\tau}{\Delta t} \qquad (2)$$

The autocorrelation function is a measure of the degree of correlation present in successive values of $y(t)$. If the function is normalized to $C_y(0) = 1$, strong correlation exists between the signal variations occurring at time interval τ apart when $C_y(\tau) \approx 1$. Zero correlation exists when $C_y(\tau) = 0$.

The cross-correlation function of output y on input x is defined in a similar manner as

$$C_{xy} = \lim_{T\to\infty} \frac{1}{T} \int_{-T/2}^{T/2} x(t)\, y(t+\tau)\, dt \qquad (3)$$

In practice, data records of $x(t)$ and $y(t)$ are digitized and the cross-correlation function is obtained in the same way as indicated by Eq. 2 for the autocorrelation function. The cross-correlation function is a measure of the interrelation between two random variables. Figure V-1 is a plot of the cross-correlation function

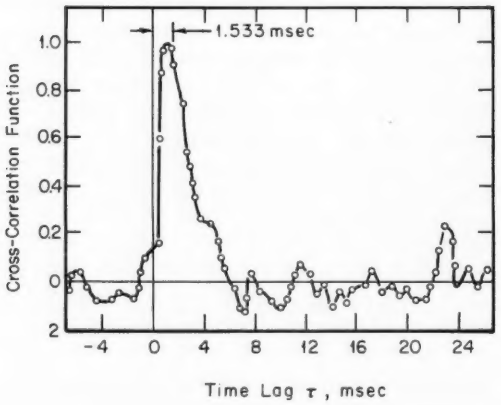

Fig. V-1 Cross correlations between source and detector, with detector located 32.6 cm from source.[19]

between input-source and output-detector random signals obtained in noise measurements at the University of Florida. The input variations are mainly felt by the detector at a time 1.533 msec later. In this particular application (study of space-dependent kinetics), the lag time is related to the time for neutron-wave propagation between source and detector in the critical assembly. Thie[1] gives other examples of cross correlations which have been obtained from noise measurements, e.g., between reactor power and primary steam flow in the Halden Boiling-Water Reactor.

POWER SPECTRAL DENSITY

The correlation functions, which are in the time domain, may be Fourier analyzed to obtain corresponding functions in the frequency domain. For the more familiar case of a periodic function $f(t)$, the Fourier representation is given by

$$f(t) = \sum_{n=-\infty}^{\infty} F(n) \exp\,(jn\omega_1 t) \qquad (4)$$

where ω_1 is the fundamental frequency $2\pi/T$ and $F(n)$ is the complex Fourier amplitude at frequency $n\omega_1$, which is given by

$$F(n) = \frac{1}{T} \int_{-T/2}^{T/2} f(t) \exp\,(-jn\omega_1 t)\, dt \qquad (5)$$

Here $f(t)$ is simply characterized by a superposition of sine waves at various frequencies $n\omega_1$ with appropriate amplitudes and phase angles given by $F(n)$. If $f(t)$ is considered to be a time-varying current through a unit resistance, it can be shown[1] that the total dissipated power is simply given by

$$P_t = \sum_{n=-\infty}^{\infty} |F(n)|^2 \qquad (6)$$

Here $|F(n)|^2$ represents the square of the magnitude of the Fourier amplitude for frequency $n\omega_1$. A plot of the individual values of $|F(n)|^2$ vs. integer n displays the spectrum of the power, i.e., the frequency-dependent power spectra for $f(t)$.

As opposed to the discrete line-spectral characteristic of periodic functions, continuous frequency distributions are required to represent nonperiodic functions of time, e.g., random-noise functions from which any periodicities present in the fluctuations have been removed. For the random function of time $y(t)$, the Fourier series representation becomes a Fourier integral representation.

$$y(t) = \int_{-\infty}^{\infty} Y(f) \exp\,(j\omega t)\, df \qquad (7)$$

Here $\omega = 2\pi f$. Equation 7 differs from Eq. 4 only in that the summation over discrete frequencies is replaced by integration over a continuous frequency spectrum.

An extremely useful result is obtained by Fourier analysis of the autocorrelation function.

$$C_y(\tau) = \int_{-\infty}^{\infty} P_y(f) \exp\,(j\omega\tau)\, df \qquad (8)$$

It has been proved that the Fourier amplitude $P_y(f)$ of the autocorrelation function $C_y(\tau)$ is the frequency-dependent power spectral density of

the original random function $y(t)$. This important result is known as Wiener's theorem.[14]

The total power in the random-noise fluctuations (the analogy that $y(t)$ represents a current through a unit resistor is retained throughout) is given by

$$P_t = \int_{-\infty}^{\infty} P_y(f)\, df \tag{9}$$

A plot of $P_y(f)/P_t$ vs. f gives the normalized power spectral density for the noise fluctuations. Obviously, if the resulting plot is peaked at, say, frequency f_0 over a narrow frequency bandwidth Δf, a resonance is indicated in the system behavior for $f = f_0$.

To evaluate $P_y(f)$ from knowledge of $C_y(\tau)$, the Fourier theorem analogous to Eq. 5 for periodic functions is applied. In this case the relation is

$$P_y(f) = \int_{-\infty}^{\infty} C_y(\tau) \exp(-j\omega\tau)\, d\tau \tag{10}$$

Note that in the analysis of data by digital methods, the integral is actually approximated as a sum of discrete values. Because of the finite length of the signal analyzed in any practical digital application, the summation is terminated over some finite time interval T. Thie[1] discusses the general effects of these and other analysis approximations on such factors as precision, frequency resolution, and high-frequency cutoff of the calculated results.

Fourier analysis of the cross-correlation function C_{xy} gives similar results; in this case the cross power spectral density $P_{xy}(f)$ is obtained rather than $P_y(f)$ as indicated above for the autocorrelation function. An important difference between $P_y(f)$ and $P_{xy}(f)$ is that $P_{xy}(f)$ is complex and contains important phase information, whereas $P_y(f)$ is real and so actually represents only the magnitude of the power as a function of frequency.

TRANSFER FUNCTION

The transfer function between output $y(t)$ and input $x(t)$ relates the amplitudes and the phase-angle differences of the input and output signals as a function of input-signal frequency. The transfer function can be obtained from noise measurements by application of the cross-correlation technique to the random-noise signals. The result obtained is

$$H(f) = \frac{P_{xy}(f)}{P_x(f)} \tag{11}$$

where $H(f)$ is the desired transfer function, $P_x(f)$ is the power spectral density of the input noise signal, and $P_{xy}(f)$ is the cross power spectral density.

In the practical application of noise-analysis techniques, the effect on the correlation results of extraneous system noises or disturbances, $n(t)$, must be considered. The sources for $n(t)$ could be instrumentation noise or system noise generated by some unknown driving function. Obviously $n(t)$ affects the observed signal $y(t)$.

If the fluctuations $x(t)$ and $n(t)$, which determine $y(t)$, are completely unrelated so that they are mutually nondependent variations, then the fluctuations $x(t)$ and $n(t)$ are statistically uncorrelated with each other, i.e., $C_{xn}(\tau) = 0$. In this case the input-output cross-correlation function obtained is independent of the presence of the uncorrelated noise $n(t)$ and hence is actually equal to $C_{xy}(\tau)$. As a result, the cross power spectral density $P_{xy}(f)$, and hence the transfer function $H(f)$, does not reflect the existence of the uncorrelated noise $n(t)$.

Generally, it is much easier to measure the power spectral density of the output, $P_y(f)$, rather than the cross power spectral density, $P_{xy}(f)$. For no extraneous noise in the system, the amplitude of the transfer function of the system, $|H(f)|$, is given by the following relation:

$$|H(f)|^2 = \frac{P_y(f)}{P_x(f)} \tag{12}$$

If, further, $P_x(f)$ is white, i.e., is frequency independent over the range of frequencies of interest, then $\sqrt{P_y(f)}$ is directly proportional to the amplitude of the transfer function.[15]

In the presence of extraneous noise sources, reliable and meaningful interpretation of the noise measurements requires that either the unwanted noise be negligible, i.e., $P_n(f) \ll P_y(f)$, or that the experiment be designed so that the uncorrelated noise component can be determined and accounted for in obtaining the final results. Further, it is important that the frequency response of the instrumentation system be reasonably flat over the range of frequencies of interest in the investigation. The instrumentation frequency response can be measured

to thereby permit appropriate corrections for the instrumentation effects.

NOISE SOURCES

In zero-power reactors and subcritical assemblies, two important noise sources are detected,[16,17] namely, (1) the natural statistical fluctuations of the neutron-chain reaction as filtered by the reactor transfer function and (2) the random neutron bombardment of the detector. The first noise source contains information on the reactor transfer function and, accordingly, is referred to as the correlated noise component of the detector output. The second noise source represents an interfering background noise and, accordingly, is referred to as the white- or uncorrelated-noise component of the detector output. To satisfactorily determine the reactor transfer function (and associated reactor characteristics, such as the neutron lifetime and degree of subcriticality), it is necessary to have a high ratio of correlated to white-noise content in the detector output. This ratio is proportional to the detector efficiency ϵ, which is defined as the number of detector pulse counts per reactor fission. For suitable measurements ϵ must be at least 10^{-4} and preferably greater. To meet this requirement the detection chambers are heavily loaded with ^{10}B and are placed within or at the edge of the active core.

In power reactors, additional reactivity noise sources, $\rho_{in}(f)$, are usually present to excite the reactor. These reactivity variations may arise as the result of random fluctuations in coolant temperature, coolant flow, steam-void content, electrical signal actuating the control rods, etc. The neutron detectors in power reactors are generally far removed from the reactor core so that the natural statistical fluctuations of the chain reaction are masked by the white noise. Useful information can be obtained if the noise component at the detector output associated with the random driving function, $\rho_{in}(f)$, is sufficiently large compared to the white-noise component discussed above. Thie[1] obtains an estimate of the order of magnitude of reactivity fluctuations required to observe the correlated-noise component for a typical case. Thie's estimate indicates, for example, that random coolant-temperature fluctuations of the order of 0.1°C, as typically producing about a 0.1-cent reactivity effect, would provide a suitably strong signal at the detector output (above the white-noise component) for observing the spectrum of the reactivity driving function as filtered by the reactor transfer function. In the typically noisy boiling-water reactors, reactivity excitations of the order of 1 cent are obtained from the random steam-void fluctuations.

Recent Work on Noise Analysis

A review of the conference papers follows. Reference is made to the individual papers by using the conference-assigned paper number, which was retained in the abstracts published in Ref. 13.

NOISE MEASUREMENTS IN ZERO-POWER REACTORS

D. H. Bryce[18] described how measurements of neutron-detection probabilities (defined as the probability per unit time of detecting a neutron at time t following detection of an arbitrary neutron at time $t = 0$) were utilized in zero-power experiments on the Cornell University reactor to obtain subcritical calibration of control elements, to measure shutdown margin, and to estimate detector efficiency (and hence reactor power). The measurements were made using a neutron-triggered time-sequenced multiple-scaler system, the output of which permitted construction of a quantity proportional to the neutron-detection probability function. A heavily loaded BF_3 detector was mounted at the periphery of the small-diameter core so as to obtain the high detector efficiency required for reliable interpretation of the measurements. The estimated detector efficiency was about 10^{-2} (believed accurate to within a factor of 2). The measured control-rod worth vs. rod position was found to agree well with results obtained by the inhour method. Good agreement of shutdown margin (10 cents reactivity difference for shutdown of 12.70 dollars) was obtained between the measured results and the results of application of other methods, including consideration of the reactivity worths of the individual control rods. Cohn of Argonne National Laboratory cautioned on the interpretation of the measurement results down to large subcriticalities. In particular, he pointed out that the prompt-neutron generation time, which was assumed constant in the data interpretation, is a function of the magnitude of the shutdown reactivity and that changes in generation time

as high as 30% have been calculated for some reactor configurations.

Uhrig[19] described the research program at the University of Florida on noise-analysis techniques, as specifically applied to both critical and subcritical assemblies. This program began about 1957 with attempts to measure the source transfer function, i.e., the output variation of neutron density in a subcritical assembly due to an input variation of neutron-source strength. Mathematically it is readily shown that the frequency-dependent portion of the source transfer function and the frequency-dependent portion of the reactivity transfer function (defined as the output neutron-density variation due to an input reactivity variation) are identical, to a good approximation. For k less than about 0.98, the source transfer function of a subcritical assembly can be represented as

$$\frac{1}{j\omega + \alpha}$$

where

$$\alpha = \frac{1 - k(1 - \beta)}{l}$$

Hence the prompt subcriticality is obtained from the source transfer function if the neutron lifetime, l is known. The ratio β/l can be obtained from reactivity transfer-function measurements performed on the critical assembly; from knowledge of the effective delayed-neutron fraction β, the neutron lifetime is determined.

Uhrig described the details of the power-spectral-density measurements performed in subcritical assemblies. The primary input to the system was the statistical fluctuations in the rate with which neutrons were emitted from the artificial neutron source. The data curves obtained exhibit the shape predicted by theory. Internal consistency between these measurements of $\Delta k/k$ and control-rod calibration was obtained. An absolute comparison was not possible because the reactor would not go critical for the test configuration.

Cross power-spectral-density measurements were carried out in the two-slab critical core of the University of Florida Training Reactor wherein the disturbance input was introduced by a random reactivity generator. The cross power spectral density was measured between the outputs of two ionization chambers located adjacent to the two slabs comprising the reactor core. A mathematical model was formulated for this experimental configuration which includes coupling between the two slabs; the coupling is delayed by a transit time related to the time for neutron-wave propagation between the two slabs. The experimental results support the general features of the proposed model and further show that the frequency dependence of the velocity of the neutron wave must be taken into account.

As a result of the demonstrated importance of the neutron-wave phenomenon, more elaborate experiments were devised to measure the spatially dependent impulse-response function. These measurements were performed on both light- and heavy-water-moderated subcritical assemblies. The results obtained are given in Ref. 20 and are reviewed later. The impulse-response function is proportional to the cross-correlation function between a random input and the output. In these experiments an accelerator type neutron source was used. The input source intensity into the system was of the pseudorandom binary off-on type. Cross correlations were performed between the input source variation and the output neutron flux at several positions in the assembly. Figure V-1 shows the cross-correlation function obtained between the input source and the output of the detector located 32.6 cm above the source in a heavy-water assembly. The peak value of the function is reached in about 1.5 msec, after which it decreases to almost zero and vacillates about the zero value. The reciprocal of the decay constant defining the curve falloff immediately after attainment of the peak value is equal to the effective neutron lifetime. The value indicated by the data curve is in good agreement with the lifetime obtained from pulsed neutron experiments in the same assembly. Present effort at the University of Florida is concentrated on continuation of the theoretical and experimental investigations of the spatially dependent effects.

Kylstra and Uhrig[20] described the results of the measurements of the spatially dependent transfer function between two detectors at different locations in the assembly. For the light-water assembly, reasonable agreement for the amplitude of the transfer function is obtained between the experimental data and a theoretical spatially dependent transfer function which is based on a Fermi-age diffusion-theory point-

source model. The measured phase shift was somewhat less than the theoretical phase shift, although the agreement is still reasonable. The transfer function measured in the heavy-water subcritical assembly agrees very well in both amplitude and phase shift with the theoretical model to 250 cps. At that point other effects become important and cause large changes in the measured transfer function. Selfridge[21] described the details of the mechanized data-handling procedures developed for noise analysis at the University of Florida.

The results of reactor noise and other kinetic experiments are frequently interpreted in terms of the simple point-reactor kinetics model utilizing one neutron energy group. Cohn[22] presented derivations of source transfer functions corresponding to more complex models. The primary interest is to determine what effect departures from the simple model would have on the interpretation of noise measurements, in particular, with respect to the determination of the ratio of delayed-neutron fraction to prompt-neutron lifetime. The more complex models considered were (1) a two-group point-reactor model, (2) a two-region reactor model in which fissions may occur in both regions, and (3) a three-region reactor model in which neutrons could pass between the two multiplying regions by way of a nonmultiplying intermediate region only. The application of these models to the fitting of noise data that were available from appropriate zero-power critical assemblies were presented.

Danofsky[23] described the measurements of the cross power-spectral-density function between the neutron outputs of the two fuel regions of the Iowa State University Training Reactor. The measurements were taken with the reactor critical and no external signal input into either region. In the reactor configuration the two slab fuel regions are surrounded with graphite and separated by approximately 18 in. of graphite. An attempt was made to relate the cross power-spectral-density function between the two fuel regions to the power-spectral-density function of the output of one of the regions. In this relation a coupling term is involved which includes the phase shift resulting from the time lag required for a disturbance to travel between the two fuel regions. A nonspatial model was used for theoretical interpretation of the results, although clearly the problem is one of space-dependent kinetics.

SHUTDOWN REACTIVITY MEASUREMENTS

Schultz[24] described how reactor noise measurements can be utilized to determine shutdown reactivity. The principle involved (limited to the high-frequency range of the output signal) is based on these two facts: (1) the frequency dependence of the reactor power fluctuations on input variations of reactivity and neutron-source strength is the same, and (2) the ratio of reactor power fluctuations (or of the magnitudes of the Fourier amplitudes of the neutron-flux noise) obtained at a high frequency to those obtained at a low frequency (but nevertheless in the high-frequency range) is related to the shutdown reactivity. The theoretical relation is obtained from the zero-power transfer function. The theoretical ratios of the amplitudes of the transfer function, corresponding to various combinations of high- and low-frequency values, are plotted in Fig. V-2 (dashed curves) as a function of subcriticality. To check the practical application of noise techniques for shutdown reactivity measurements, power-spectral-density measurements were accomplished on the cold, clean reactor at the Westinghouse Reactor Evaluation Center Critical Experiment Station (CES), Waltz Mill, Pa., for various amounts of shutdown reactivity and for several source, detector, and control-rod configurations. Initial measurement results

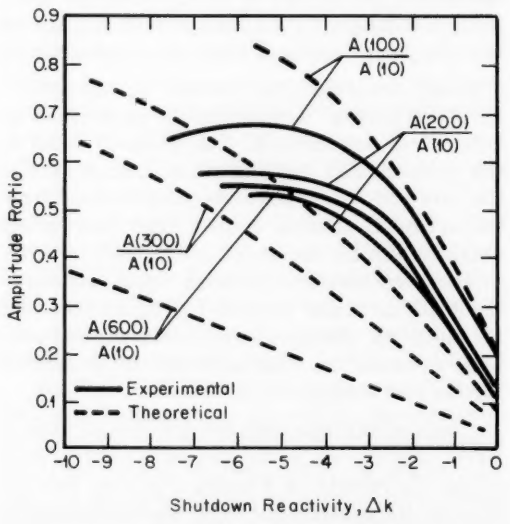

Fig. V-2 Power-spectral-density ratios for various frequency combinations vs. shutdown Δk.[24]

gave extremely poor agreement with the theoretical curves. These results emphasized the importance of decreasing the relative magnitude of the uncorrelated noise in the output signal, particularly if it is desired to infer the shutdown margin from the measurement by use of the theoretical zero-power transfer function. The high level of uncorrelated noise in the system also significantly altered the shape of the experimentally derived curves of amplitude ratio vs. shutdown margin, as compared to the theoretically derived curves.

Uncorrelated noise consists of (1) bombardment noise or counting randomness, (2) neutrons arriving at the detector after such a long distance or after so many interactions that any fission information has been wiped out, and (3) neutrons resulting from (γ, n) reactions that would be uncorrelated with the fission process, as would be the noise arising in the input circuit of the electronic measuring equipment. Because of the small signals generally involved in such measurements, the counting statistics are poor and bombardment noise makes up a large portion of the total uncorrelated noise. In general, detector efficiencies greater than 10^{-4} are required if reactor noise measurements are to be made in the presence of bombardment noise.

Attempts were made to obtain larger useful signals. The solid curves of Fig. V-2 represent the results of measurements taken with the detector in the center of the core. It is seen that the amplitude ratio, $A(100)/A(10)$, closely approximates the theoretical ratio for shutdown reactivities less than about -3%. However, as the magnitude of the shutdown reactivity increased, the amplitude ratios flattened out instead of approaching unity, as indicated by the theory.

In one special set of measurements, wherein two parallel-connected detectors were placed in the center of the core (resulting in a detector efficiency of approximately 10^{-3}), the experimental curves of amplitude ratio vs. shutdown reactivity, as shown in Fig. V-3, are much closer to the theoretical curves. The experimental curves also approached unity as the subcriticality was increased.

In the practical application of the noise techniques to power reactors, the locations at which the detectors can be placed relative to the core are limited so that the attainment of detector efficiencies near the required 10^{-4} value is extremely difficult in any practical installation. The intense fission-product and activation gamma sources prevalent after power operation add to the problem of minimizing the uncorrelated noise relative to the useful fission fluctuation noise.

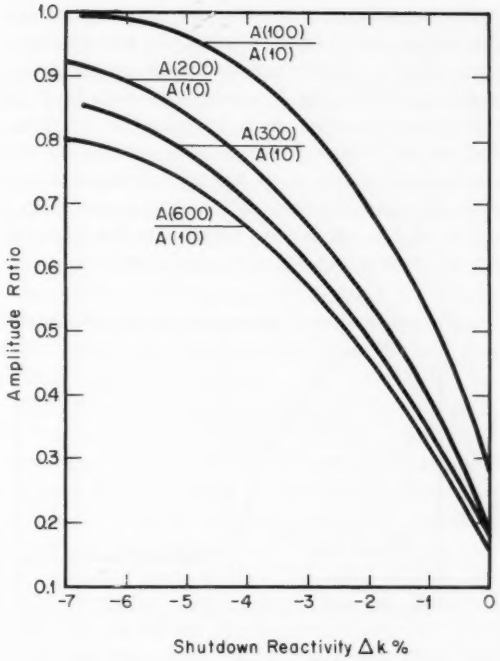

Fig. V-3 Variation of power-spectral-density ratio with Δk, as achieved with two parallel-connected ionization chambers in center of core.[24]

In general, the results presented by Schultz verify the principles involved in the shutdown reactivity measurements and show that even in the presence of a significant amount of uncorrelated noise, a useful reactivity meter might still be derived empirically. This conclusion is illustrated by the experimental results plotted in Fig. V-4, which show that true subcriticality readings were being obtained and that the apparatus was not functioning as a simple counting-rate meter. These results were obtained with the single detector in the center of the core and with the reactor subcritical and later made critical at several different power levels. Once the reactor is critical the amplitude ratio does not change. This characteristic distinguishes the true shutdown reactivity meter from the ordinary counting-rate meter.

The empiricism in the use of a shutdown reactivity meter is introduced by the requirement for a calibration of amplitude ratio vs. shutdown reactivity (as initially measured by other experimental techniques). The calibration curve obtained, which will depend on the geometrical location of the ion chamber in or near the core, is then utilized for future monitoring of the shutdown margin. On the basis of the measurements Schultz concludes that, given

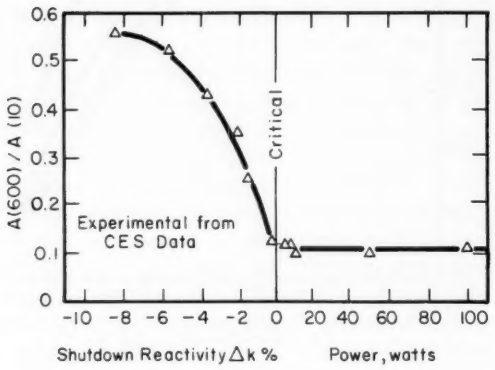

Fig. V-4 Operation of shutdown reactivity meter in subcritical and power ranges.[24]

a favorable detector location, a relatively simple and inexpensive direct-reading shutdown reactivity meter can be built which will operate down to −5% in shutdown reactivity for a cold, clean reactor.

Ricker et al.,[25] described the research program that was set up at the Oak Ridge National Laboratory (ORNL) in order to (1) obtain a more thorough understanding of the nature of the neutron fluctuations in a shutdown reactor, (2) ascertain the need for specialized instrumentation for spectral-density measurements, and (3) acquire the fundamental information necessary for the development of a practical shutdown margin monitor. In the first phase of the program, the fluctuations in a reactor whose physical characteristics are well understood will be investigated. In the final phase various reactor types under normal operating conditions will be investigated. The first phase of research is presently under way. Negative reactivity determinations will be made by using the spectral-density analyzer at the ORNL Pool Critical Assembly, which has been carefully calibrated by pulsed-neutron and distributed-poison techniques. The required specialized instrumentation for accurate analysis of the fluctuations by the spectral-density techniques is being developed and checked.

NOISE MEASUREMENTS IN POWER REACTORS

Randall and Griffith[26] summarized the noise-measurement and -analysis techniques and equipment developed at Atomics International for reactor parameter determinations and dynamic-stability analyses. The mathematical concepts involved in the determination of transfer functions from power spectra were briefly outlined. Wherever extraneous system noise is excessive, the cross power-spectral-density techniques should be used. It is pointed out, however, that, if the spectral density of the disturbance, $P_n(f)$, is a large portion of $P_y(f)$, then even the cross spectral-density technique (expressed by Eq. 11) is subject to serious statistical errors. An expression is given for estimating the relative confidence limits for the phase and gain components of a transfer-function measurement from a finite sample of data. This expression contains the coherence function, $R^2(f)$, the use of which enables qualitative representation of the noise-to-signal ratio for the system.

$$\frac{P_n(f)}{|H(f)|^2 P_x(f)} = \frac{1 - R^2(f)}{R^2(f)} \qquad (13)$$

The characteristic frequency modes of importance in reactor systems lie within the span of 10^{-4} to 10^5 cps. Randall and Griffith divide this wide range into three overlapping regions. The first region, from 1 to 10^5 cps, is that in which prompt-neutron lifetime and reactor shutdown margin are generally determined. The second region, from 0.05 to 50 cps, includes the natural frequency modes of nearly all mechanical components and hydraulic parameters, i.e., mechanical vibrations, fuel bowing, pump oscillations, nucleate boiling, gas entrainment, and hydraulic disturbances. The third region, 10^{-4} to 1 cps, is dominated by the time dependence of the temperature coefficients of reactivity, delayed-neutron effects, and xenon instabilities. Randall and Griffith emphasize that specific techniques and equipment must be considered for application in each frequency region. Each region has certain unique technical problems associated with system excita-

tion, data acquisition, data reduction, and interpretation of results. A brief discussion is presented of each of these technical problems, and experimental examples are described to illustrate the differences in the equipment and techniques used in each frequency region.

As an illustration of inherent system excitation which can be utilized, it is pointed out that transfer functions between flow rate and several output variables (power level, coolant outlet temperature, and fuel temperature) were measured on a SNAP-2 power-reactor system wherein inherent random fluctuations in coolant flow rate provided the only system driving function. However, because of the low driving-function strength, other sources of system noise, such as instrumentation noise, severely limited the accuracy of many of these measurements. Hence a strong incentive exists for perturbing the system with an externally generated random disturbance if accurate noise analyses are desired.

Three stages of data acquisition are involved. These are signal detection, conditioning, and recording. Flow diagrams are presented for the data-acquisition systems used in the high- and low-frequency ranges. Data reduction to obtain the desired power spectral densities from the recorded noise signals is accomplished with either analog or digital techniques. Precise analog measurements can be obtained with a wave-analyzer system that normally operates over the frequency range from 4 to 10^4 cps; the frequency range can be extended from 0.0003 to 10^5 cps by use of signal tape recordings with appropriate speed controls for expanding or compressing the time scale of the data to be analyzed. A sample power-spectral-density measurement of high-frequency noise in the range from 10 to 7×10^4 cps is shown for illustration. The relative standard deviation for statistical errors was less than 1%, and the machine accuracy was also of the order of 1%.

For digital-computer analysis of the data, the noise signals are passed through signal-conditioning networks, coupled to an analog-to-digital converter, and sampled in regular time intervals. As a result, the digital results are recorded on magnetic tape to provide the input information for a cross spectral computer code which calculates the gain, phase, and coherence estimates at each frequency.

Ball[27] described the noise measurements performed on three pressurized-water power reactors. The noise studies were primarily motivated by a desire to check experimentally the stability of the nuclear reactor system in the N.S. *Savannah*. However, the available equipment was also utilized for measurements on the Yankee reactor and on the Indian Point reactor of Consolidated Edison. The ion-chamber signals were amplified, filtered through band-pass filters, and used to provide the integral of the absolute value of the noise at selected frequencies. The resultant output power spectral density represents the combination of the reactivity driving function and the reactor transfer function.

Prior to the noise measurements at power, the zero-power transfer function was measured on a group of N.S. *Savannah* elements to confirm the feasibility of the analog method of analysis. In these measurements the spectral reactivity fluctuations are very small so that the transfer function could be easily masked by the white-noise component of the average current. Hence the ion chamber was located in the center of the zero-power assembly. The data follow the expected transfer-function curve very closely, as shown in Fig. V-5, thereby verifying the technique used.

The power spectral densities measured at power operation indicated no tendency toward instability for any of the three power reactors. The source of the broad-band reactivity driving function was not definitely determined, but the most likely cause in each of the reactor systems is the random fluctuation in water-temperature distribution. Experiments on the N.S.

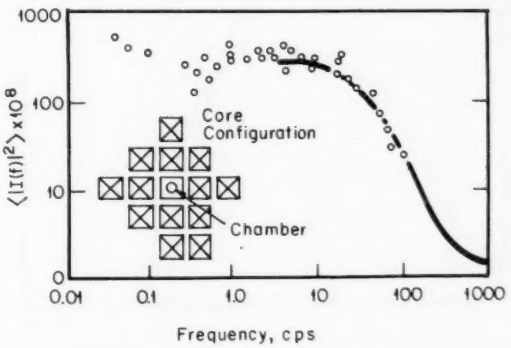

Fig. V-5 Zero-power transfer function obtained from power spectral density.[27] Empirical curve fit, using theoretical form of the functional relation, gives $l/\beta = 0.00394$.

Savannah at 50% power and in a rolling sea (ship gyro stabilizers off) indicated a resonance at the frequency of the ship roll (0.1 cps). The resonance is clearly evident in Fig. V-6, where the product of the spectral density of input reactivity fluctuations and the squared modulus of the reactor transfer function is plotted against frequency. This reactivity driving effect is definitely associated with the side-to-side movement of the control rods ("rod slosh"), occurring in the rolling sea; however, the amplitude of the effect was too small to require any remedial action. In general, no specific application of the information obtained was found insofar as setting operating criteria for these pressurized-water systems. Work at Babcock & Wilcox is presently centered on using the spectral-density change at high powers as an indication of the onset of boiling in pressurized-water systems.

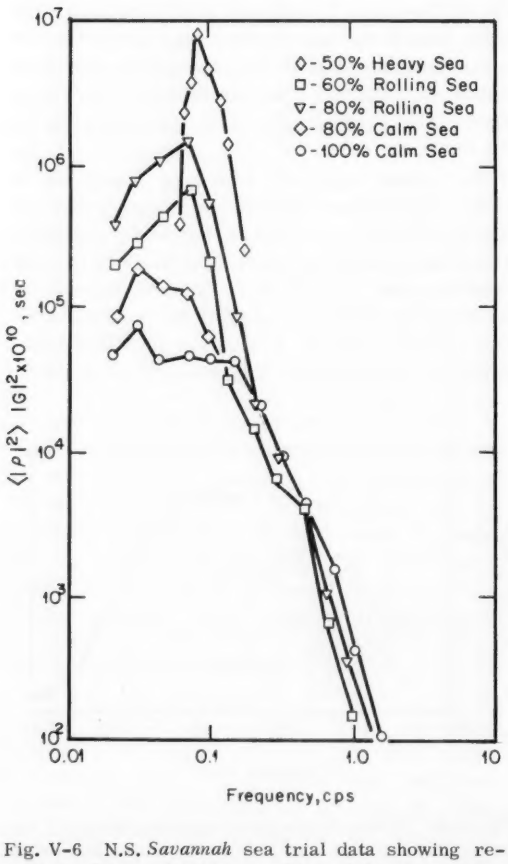

Fig. V-6 N.S. *Savannah* sea trial data showing reactivity driving function as filtered by the reactor transfer function.[27]

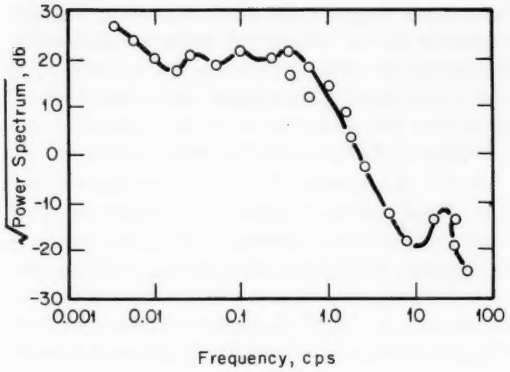

Fig. V-7 Spectrum of nuclear power fluctuations in the Saxton reactor at 20 Mw.[28]

Rajagopal[28] described the noise measurements performed on the Saxton pressurized light-water reactor. The major objectives of the noise studies were to (1) detect nucleate boiling and determine its relation to changes in reactor operating conditions and (2) study the applicability of noise measurements in determining reactor time constants, shutdown reactivity, and any other kinetic parameters.

The primary side of the Saxton reactor is provided with extensive instrumentation, including miniature in-core detectors, instrumented (with cladding thermocouples) fuel rods, Pitot flow tubes at the inlet and outlet nozzles of selected fuel assemblies, and inlet and outlet plenum thermocouples. Standard plant instrumentation, such as the compensated ion chambers and the flow meters, is also available to provide signals for noise measurements. The power spectral and cross power spectral analyses were performed in a commercial electronic spectrum analyzer. Comparison of results obtained from immediately successive measurements demonstrated a surprising degree of resolution and repeatability.

The most interesting results were obtained on the spectral density of the power fluctuations, which exhibit a well-defined resonance between 10 and 20 cps as shown in Fig. V-7. An investigation was therefore conducted to determine the effect on the resonance of reactor power at constant average coolant temperature and of average coolant temperature at constant reactor power. Some of the results obtained are presented in Fig. V-8. Detailed analysis of the resonance at these various reactor operating

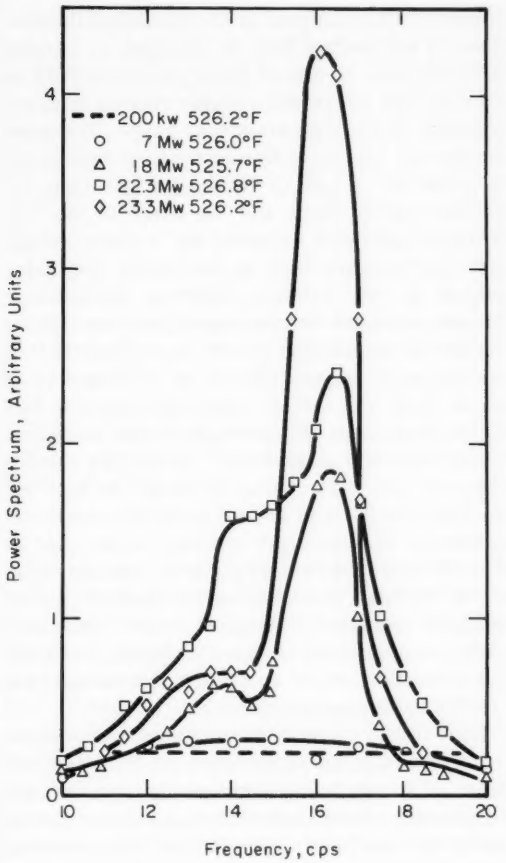

Fig. V-8 Effect of reactor power on resonance present in the power spectrum of the Saxton reactor.[28]

conditions showed that the resonance is related to nucleate boiling. The frequency at which the resonance occurs corresponds to the expected bubble formation and collapse rates at the operating temperature and pressure. In attempts to correlate the measured properties of the resonance with calculations on nucleate boiling, a plot was made of the measured area under the resonance curves vs. the estimated averaged surface area in nucleate boiling (see Fig. V-9). The estimated surface area in nucleate boiling is based on calculations made by an available digital-computer code. The plot shows a linear dependence between the variables. These results indicate that, by power spectral analysis of the fluctuations in nuclear power, it is possible to detect and obtain a relative measure of nucleate boiling occurring in the reactor. In addition to the foregoing analyses, cross power spectral analyses of the various measured signals were performed. It was concluded that significant information and insight as to the dynamic behavior of a power reactor can be obtained by noise analysis.

Pluta[29] summarized the preliminary results of statistical analyses of limited neutron-flux and core-flow noise data taken from the Vallecitos Boiling-Water Reactor. Both digital and Fourier analog analyses of the data were performed; the power-spectral-density functions

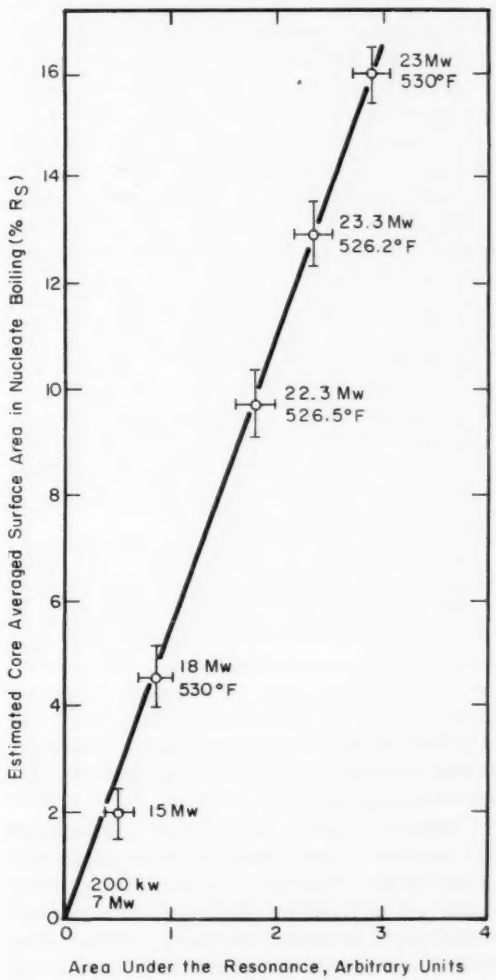

Fig. V-9 Relation between measured resonance and calculated fraction of heat-transfer surface in nucleate boiling for the Saxton reactor.[28]

obtained are in agreement within the statistical confidence associated with the data. Because of the lack of a quantitative model of the reactor kinetic characteristics and the reactivity driving mechanisms, it was not possible to infer the value of a significant system parameter (e.g., the exit steam fraction) from the correlation functions. Hence the results obtained were limited in usefulness.

For the same reactor conditions, measurements were made of (1) the power-spectral-density function of the neutron flux utilizing noise analysis and (2) the closed-loop reactivity-flux transfer function, utilizing a rod oscillator as the reactivity driving function and an in-core ionization chamber for the flux measurements. It had been previously demonstrated that the in-core and out-of-core ionization chambers gave nearly the same noise-analysis results. From the magnitude of the transfer function, $|T(j\omega)|$, and the measured power-spectral-density function of the neutron flux, G, the reactivity driving–power-spectral-density function of the system was determined from the relation $G = |T|^2 G_{\text{driving}}$. The frequency dependence of the reactivity driving function obtained by this procedure is plotted in Fig. V-10. These results demonstrate the fact that the reactivity driving function is not white over the frequency range of interest. Since no techniques are known at this time for predicting G_{driving}, it is not possible to determine $|T|$ from boiling-water reactor-flux noise by means of autocorrelation techniques.

The application of cross-correlation techniques using a known random reactivity function or the classical rod-oscillator experiment is the obvious way to circumvent the lack of a comprehensive theoretical model. The present theoretical background is adequate to justify application of the cross-correlation technique to a boiling-water reactor as a substitute method for obtaining the closed-loop transfer function of the system.

A paper presented by Eurola[30] summarized the reactor noise measurements performed during power operation with the first fuel charge in the Halden Boiling-Water Reactor (HBWR) and described the scope of the noise measurements with the second fuel charge. The HBWR is a D_2O-boiling power reactor, which has been in power operation since October 1960. The primary purpose of the reactor noise measurements was to detect any appearance of substained oscillations in the statistical fluctuations of the neutron flux. In addition, an attempt is being made to utilize these measurements as a tool to get information on the reactor dynamic behavior in the high-frequency range. The measurements conducted during the first fuel charge revealed (1) a kind of hysteresis that made the nuclear power noise and the noise in the differential pressure between the reactor vessel and the primary side of the steam generator behave in two entirely different ways under almost identical reactor conditions and (2) an acoustical oscillation (which was predicted) in the primary steam circuit at a frequency of about 3 cps and with an amplitude reaching 30% of the mean flow. With respect to the measurements with the second fuel charge, the results obtained are still being analyzed so that the information derived to date must be considered tentative. Of particular interest is the plot in Fig. V-11 of the reciprocal mean-square value of the nuclear power noise vs. reactor power. A linear relation is obtained which, when linearly extrapolated to zero ordinate, predicts the instability to be at 16 Mw for the specific conditions of reactor operation.

Boardman[31] described the attempts to analyze the noise from the Dounreay Fast-Breeder Reactor. During a high-power run, recordings were made of the fluctuations in reactor power and in the inlet and outlet coolant temperatures (through plenum thermocouples). The cross-correlation function between reactor power and

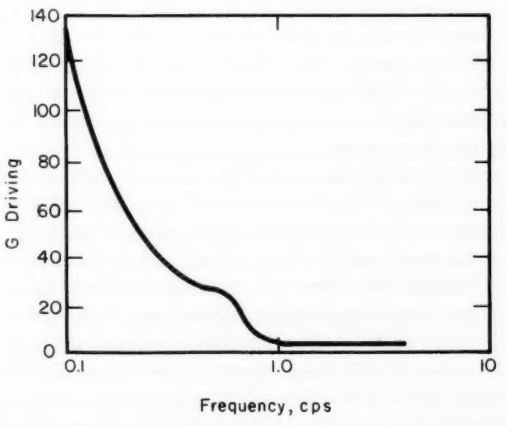

Fig. V-10 Frequency dependence of the reactivity driving function in the Vallecitos Boiling-Water Reactor.[29]

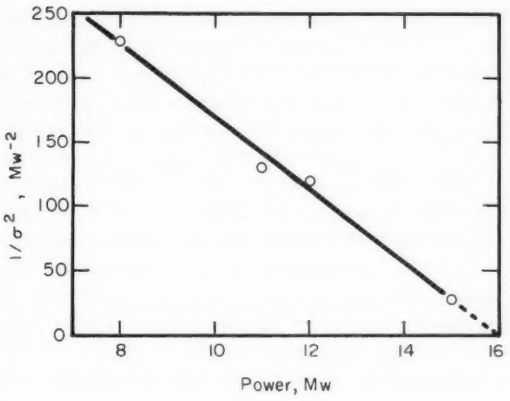

Fig. V-11 Reciprocal of the mean-square value of reactor power noise vs. power level in the Halden Boiling-Water Reactor.[30]

inlet coolant temperature was determined in order to obtain an indication of the mean fraction of the noise in the reactor power which is due to the noise measured by the thermocouple. The very small magnitude of the cross-correlation function indicates that very little of the reactor power fluctuation is actually due to changes in inlet coolant temperature, as measured by the plenum thermocouple. The most significant features of the cross-correlation results are that: (1) the correlation, although small, is positive, thereby implying a positive coefficient of reactivity; and (2) there is no indication of the long-term correlation appearing in the autocorrelation function of the reactor power, which had been previously evaluated. This latter result suggests that the long-term correlation obtained in the autocorrelation function of the reactor power is not due to fluctuations in inlet coolant temperature but rather to some other cause, e.g., reactor operator. On the basis of various reasonable assumptions that were indicated by the overall measurement results, it is suggested that the combined reactivity coefficient of fuel and coolant, α, is about $+5 \times 10^{-6}\,(°C)^{-1}$, as compared with the value of $-1.3 \times 10^{-5}\,(°C)^{-1}$ obtained from oscillator measurements for the combined coefficients averaged over the core. However, because of the approximate nature of the noise-data interpretations, the deduced value of α may have quite a large error. More refined calculations are being carried out. Also, it is recognized that the plenum thermocouple measures only fluctuations in temperature of the coolant in its immediate vicinity and not the average fluctuation over the core.

The possibilities of noise-analysis techniques are discussed in Ref. 31 as: (1) an aid in determining the kinetics of the reactor, e.g., the power feedback mechanism, and (2) an on-line reactor monitor. It is emphasized that much more experience with noise-analysis techniques is required for accurate evaluation and interpretation of reactor noise data of the type obtained on the Dounreay reactor.

A paper by Miida[32] was presented which reviewed the status of noise analysis in nuclear systems in Japan. Considerable activity is under way in research work on noise-analysis techniques and in measurements and analyses of power spectra from operating reactors in Japan. The measurements are directed at obtaining the zero-power transfer function, neutron-generation time, and power spectra of reactors at high power levels for stability information. Combination of the results of noise and pile oscillator measurements performed on a water-boiler reactor revealed that the input noise spectrum had a peak at 0.03 to 0.04 cps; this peak was shown to be associated with the void fluctuations due to radiolytic water decomposition. The results indicated that the void fluctuation noise was nonwhite, i.e., the noise amplitude was sharply peaked at a frequency that was determimed by the void-residence time in the reactor core. Power spectral measurements on a power reactor revealed that the reactor noise increased by a factor of 3 more with coolant flow relative to values without coolant flow. This is mainly due to mechanical vibration of the fuel rods and control rods.

GENERAL INVESTIGATIONS

Osborn and Yip[33] presented a highly theoretical and generalized treatment of the subject of neutron-noise interpretation. The purpose was to develop, from first principles, the theoretical basis underlying the more commonly used phenomenological interpretation of measurements of fluctuations and correlations in neutron distributions. In the reduction of the generally intractable theoretical equations to "working level" equations, which involved the usual "point reactor" approximation, it is demonstrated that the cross sections appearing in the reduced equations differ from those appearing in the

commonly used phenomenological equations. Osborn concludes that the effort to deduce kinetic parameters for reactors from measurements on steady-state systems must proceed with caution.

Moore[34] presented a theoretical paper on the general properties of noise fields in a reactor. In the usual point reactor approximation, the random fluctuations of the neutron population are interpreted in terms of the usual lumped-parameter model. In this case the dynamic characteristics are described by means of the transfer function. Moore points out that in a large reactor the transit time across the reactor for disturbances, such as thermal-neutron-wave propagation, becomes important; hence the random fluctuations of the neutron population can no longer be described by lumped-parameter models, and, instead, the fluctuations in neutron density must be regarded as a stochastic function of both space and time, i.e., a noise field. The general mathematical properties of such fields were presented.[34] The space-time autocorrelation function of any field and the cross correlation between two fields were defined. Relations between the correlation functions were obtained which are generalizations of the usual relations for lumped-parameter systems. In the case of a noise field, the spectral relations are characterized by a dispersion function in a manner analogous to the appearance of the transfer function in the lumped-parameter system. The dispersion function essentially describes how a sharp pulse, initiated at time $t = 0$ and at a given point in the medium, is dispersed (i.e., how the pulse peak is attenuated and the pulse width broadened) as its effects are propagated in time and space.

Balcomb[35] presented a summary of the cross-correlation method for measuring system dynamic response. The use of the method was illustrated by various appropriate examples. One example involved the utilization of a Gaussian input signal. The results were carried through to system transfer functions and included examples both with and without extraneous noise. It was demonstrated that excellent results can be obtained using purely random input signals provided the computations are carried to the frequency domain. Included was a discussion of the use of idealized input signals constructed from special pseudorandom binary sequences. The resulting input signal is a binary square-like wave form which has been modified so that the sign in each time interval is chosen at random. Also included was a discussion of the factors involved in the choice of either the digital or analog method for performing the cross-correlation computations. Valat[36] discussed autocorrelation techniques with random source excitation (random square waves, rectangular Poisson pulses) as means of reducing statistical error in highly negative reactivity measurements. Extraction of the desired information from the measurements is, however, difficult. Encouraging experiments are under way. It is emphasized that a high detector efficiency is essential to significant measurements. Mohler[37] discussed the problems involved in the measurement of power spectrum and in the estimation of power spectral density (average power per unit of frequency bandwidth) from noise records. Error analysis and methods for reducing error in measurement were emphasized.

Gyftopoulos and Hooper[38] described some work on the synthesis of test signals for the measurement of kernels in nonlinear systems. A number of periodic signals have been designed which allow the exact measurement of the linear kernel by means of cross-correlation measurements between input and output. The spectrum of the linear kernel is the transfer function of the first-order approximation of the system. Efforts are currently under way to design signals for the measurement of the linear kernel in the presence of the higher order kernels as well as measurement of the higher order kernels themselves. Surdin and Kassimatis[39] considered, in great detail, the problem of measurement of subcritical reactivity using the correlation functions. Several cases of external source modulation were considered, namely, (1) random short pulses of equal amplitude and m zero crossings; (2) short periodic pulses of large constant amplitude; (3) sinusoidally modulated source; (4) large periodic pulses of constant amplitude. The authors conclude that the possible applications of the correlation functions appear to be more extensive than those specifically treated in the paper.

Kemeny and Murgatroyd[40] were primarily concerned with the formulation of stochastic models to represent some of the important physical aspects of nuclear reactor theory. The noise produced in a zero-power reactor is mainly associated with the neutron-fission fluctuations. For analyses of the physical processes

related to these neutron-fission fluctuations, it is possible to synthesize the stochastic analog of many of the well-known relations of reactor theory. It was pointed out, however, that the principal source of noise produced in power reactors is associated with mechanical vibrations, flow fluctuations, etc. In this case the input noise is not necessarily Gaussian, and it is not known how this affects the interpretation of the noise-analysis results.

Weaver[41] considered the problem of minimizing the mean-square value of the neutron-noise output of a reactor by appropriate design of the control system. By noise minimization it was felt that an increase in reactor stability would be realized. Albrecht[42] derived, by use of a simple model, the general equations for the variance of the neutron density in systems undergoing transient changes, without solving for the distribution itself. The variance is a measure of the statistical uncertainty (i.e., the spread of the data), which is sufficient information for many excursion and pulsed-neutron experiments.

References

1. J. A. Thie, *Reactor Noise*, Rowman and Littlefield, Inc., New York.
2. R. B. Blackman and J. W. Tukey, *The Measurement of Power Spectra*, Dover Publications, Inc., New York.
3. J. S. Bendat, *Principles & Applications of Random Noise Theory*, John Wiley & Sons, Inc., New York.
4. Y. W. Lee, *Statistical Theory of Communication*, John Wiley & Sons, Inc., New York.
5. L. A. Wainstein and V. P. Zubakov, *Extraction of Signals from Noise*, Prentice-Hall, Inc., Englewood Cliffs, N. J.
6. W. R. Bennett, *Electrical Noise*, McGraw-Hill Book Company, Inc., New York.
7. D. K. C. MacDonald, *Noise and Fluctuations: An Introduction*, John Wiley & Sons, Inc., New York.
8. A. M. Yaglom, *An Introduction to the Theory of Stationary Random Functions* (translated by R. A. Silverman), Prentice-Hall, Inc., Englewood Cliffs, N. J., 1962.
9. E. L. Peterson, *Statistical Analysis and Optimization of Systems*, John Wiley & Sons, Inc., New York.
10. S. H. Crandall and W. D. Mark, *Random Vibration in Mechanical Systems*, Academic Press Inc., New York.
11. A. A. Kharkevich, *Spectra and Analysis*, (translated from Russian), Consultants Bureau, New York, 1960.
12. R. C. Jennison, *Fourier Transforms and Convolutions for the Experimentalist*, Pergamon Press, Inc., New York.
13. *J. Nucl. Energy, Pt. A & B*, 18(1): (1964).
14. N. Wiener, Generalized Harmonic Analysis, *Acta Math.*, 55: 117 (1930).
15. M. N. Moore, The Determination of Reactor Transfer Functions from Measurements at Steady Operation, *Nucl. Sci. Eng.*, 3: 387 (1958).
16. C. E. Cohn, A Simplified Theory of Pile Noise, *Nucl. Sci. Eng.*, 7: 472 (1960).
17. F. de Hoffmann, Statistical Aspects of Pile Theory, *The Science and Engineering of Nuclear Power*, Vol. II, edited by Clark Goodman, Addison-Wesley Publishing Company, Inc., Cambridge, Mass., 1949.

References 18 through 42 are papers presented at the Conference on Noise Analysis in Nuclear Systems; these papers will be published as USAEC Report TID-7679.

18. D. H. Bryce, Measurement of Reactivity and Power Through Neutron Detection Probabilities, Paper No. 1-1.
19. R. E. Uhrig, The Nuclear Noise Research Program at the University of Florida, Paper No. 4-3.
20. C. D. Kylstra and R. E. Uhrig, Measurement of the Spatial Dependent Transfer Function of Nuclear Systems by Noise Analysis, Paper No. 4-1.
21. R. G. Selfridge, Digital Data Reduction in Noise Analysis, Paper No. 4-2.
22. C. E. Cohn, Applicability of Simple Reactor Kinetics to the Interpretation of Reactor Noise Experiments, Paper No. 5-2.
23. R. A. Danofsky, Cross-Power Spectral Measurements in the Two Core University Training Reactor-10, Paper No. 3-3.
24. M. A. Schultz, Shutdown Reactivity Measurements Using Noise Techniques, Paper No. 2-3.
25. C. W. Ricker, D. N. Fry, E. R. Mann, and S. H. Hanauer, Investigation of Negative Reactivity Measurement by Neutron Fluctuation Analysis, Paper No. 2-4.
26. R. L. Randall and C. W. Griffith, Application of Power Spectra to Reactor System Analysis, Paper No. 2-2.
27. R. M. Ball, Noise Results on Yankee, Savannah, and Con Ed Reactors, Paper No. 6-1.
28. V. Rajagopal, Noise Measurements on the Saxton Reactor, Paper No. 6-2.
29. P. R. Pluta, Preliminary Results of VBWR Noise Analysis, Paper No. 6-3.
30. T. Eurola, Reactor Noise Experiments on HBWR (Paper No. unassigned).
31. F. D. Boardman, Noise Measurements in the Dounreay Fast Reactor, Paper No. 6-4.
32. J. Miida, A Review of Noise Analysis in Nuclear Systems in Japan (Paper No. unassigned).

33. R. K. Osborn and S. Yip, The Physical Theory of Noise in Reactors and Reactor-Like Systems, Paper No. 1-2.
34. M. N. Moore, The Noise Field of a Reactor, Paper No. 1-3.
35. J. D. Balcomb, The Crosscorrelation Method of Measuring System Dynamic Response, Paper No. 3-1.
36. J. Valat, Negative Reactivity Measurements Using Random Source Excitation and Autocorrelation Techniques, Paper No. 3-2.
37. R. R. Mohler, Power Spectrum Measurement and the Estimation of Power Spectral Density, Paper No. 2-1.
38. E. P. Gyftopoulos and R. J. Hooper, Signals for Transfer Function Measurements in Nonlinear Systems, Paper No. 3-4.
39. M. Surdin and C. Kassimatis, Some Applications of Correlation Functions to Nuclear Reactor Control, Paper No. 3-5.
40. L. G. Kemeny and W. Murgatroyd, Stochastic Models for Fission Reactors, Paper No. 5-1.
41. L. E. Weaver, Minimization of Reactor Noise Through Minimum Bandwidth Control, Paper No. 5-3.
42. R. W. Albrecht, Statistical Uncertainties in Pulsed Neutron and Excursion Experiments, Paper No. 5-4.

Section

VI

Power Reactor Technology

Containment, Radiation Control, and Siting

Vented-Containment Concept for the New Production Reactor

The New Production Reactor (NPR) is a dual-purpose power-plus-plutonium reactor located at Hanford.[1–3] It was briefly discussed in *Power Reactor Technology*, 3(4): 75-76. Reference 1 is a discussion of the containment concept used for the reactor. Although the NPR is a dual-purpose reactor located at a relatively remote site, the technical features of the use of vented containment hold considerable interest for the power-reactor designer.

The NPR is only one of a number of production reactors located at the Hanford site, and none of the others are contained.[1] The author states that a decision was made to open some land across from the site to farming and that this would make it necessary to provide a containment system that would preclude the spread of radioactive contamination in the event of a failure of the reactor cooling system. Since a total containment sphere would have been several hundred feet in diameter, it was decided that the initial pressure surge resulting

Table VI-1 MODES OF OPERATION FOR THE NPR[2]

Phase	Products	Period used as basis of design, years
I	Plutonium	2
II	Plutonium and steam	8 or more
III	Steam	Remaining life

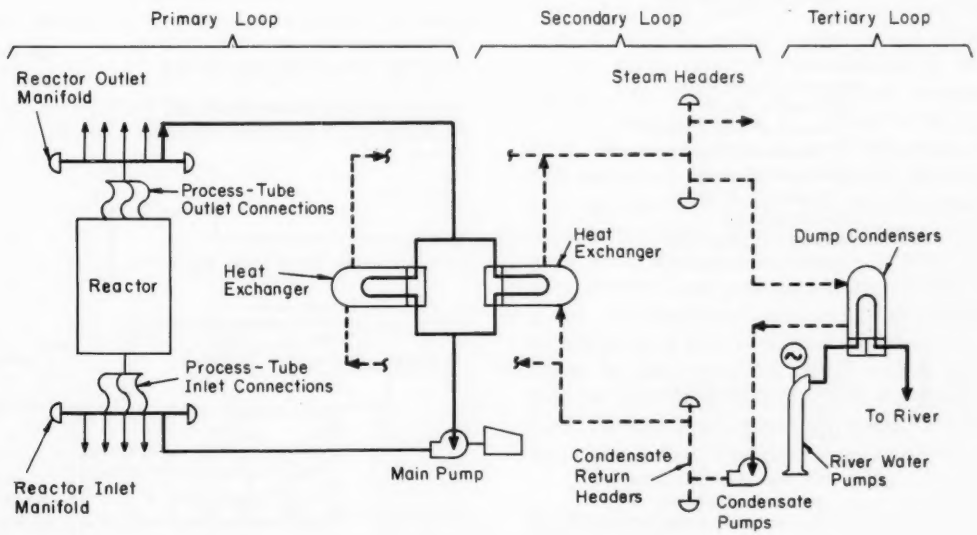

Fig. VI-1 Simplified flow diagram for the NPR.[1]

from a coolant-system failure would be released to the atmosphere. Before release of fission products from the reactor core could occur, a number of pressure-tight valves would be closed to isolate the reactor. The reactor is a pressurized-water-cooled graphite-moderated reactor designed to produce both plutonium and power. The operation of the reactor is divided into phases I, II, and III. The mode of operation during the various phases is shown in Table VI-1. Phase I operation actually will be only for about a year. The NPR was scheduled for final completion[4] in March 1964, and construction of an 800-Mw(e) power plant to utilize the steam is in progress. Completion and operation of the power plant are scheduled for the fall[4] of 1965.

Table VI-2 gives design data on the NPR, and Fig. VI-1 illustrates the simplified NPR flow diagram. The reactor and heat exchangers are arranged in different, adjacent buildings. This is illustrated in Fig. VI-2. The reactor building, pipe gallery, and cells housing individual primary coolant loop components are connected by means of double-hinged flapper-valve type shutters located between the buildings. These shutters ordinarily allow the buildings to maintain their separate identities for ventilation purposes but allow passage of the initial pressure surge in the event of an accident.

The construction material used for the confinement-volume walls, etc. (Fig. VI-2), is reinforced concrete coated with an elastomer.[3] The heat-exchanger cells can withstand an internal pressure of 8 psig. The initial pressure-relief vent valves are located in the pipe-gallery area and in the reactor building. The

Table VI-2 DESIGN DATA FOR THE NPR[2]

Reactor type and size	Pressurized-water-cooled graphite-moderated pressure-tube design; approximate dimensions are 33 by 33 by 39 ft		
Pressure tubes			
Material	Zircaloy-2		
Number	1004		
Inside diameter, in.	2.7		
Wall thickness, in.	0.25		
Lattice spacing, in.	8 by 9		
Controls			
Horizontal rods	87		
Vertical ball channels	108		
Fuel			
Phases I and II	Metallic uranium, Zircaloy-2 cladding		
Phase III	Uranium oxide, Zircaloy-2 cladding		
Heat-dissipation plant			
Number of loops	5 in phase I; 6 in phases II and III		
Number of evaporators	10 in phase I; 12 in phases II and III		
Surface area of each, sq ft	16,000		
Dump condensers	16		
Capacity, lb/hr	12.6×10^6		
Generating plant			
Number of generators	2		
Capacity of each, Mw(e)	400 in phase II; 430 in phase III		
	Operating phase		
	I (5 loops)	II (6 loops)	III (6 loops)
Design capacity, gross			
Mw(t)			3290
Mw(e)	0	800	860
Operating data			
Bulk coolant temperature, °F			
Reactor inlet/outlet			469/572*
Coolant flow, lb/hr			86×10^6
Steam temperature at evaporation, °F	320	359	438
Steam pressure at evaporation, psia	90	150	375
Steam flow, lb/hr			11.4×10^6

*These numbers are reversed in the reference.

thickness of the pipe-gallery roof was sized to withstand 5 psig. These design values resulted from calculations which indicated that a rupture in one of the cells would cause a pressure drop of 3 psi between the cell wherein the rupture occurred and the gallery. In turn, the vent area provided in the pipe-gallery roof was sized to limit the pressure within to a maximum of 5 psig.

The maximum credible accident postulates a complete fracture of a main coolant line and the escape of the entire volume of primary water without condensing. When the pressure within the confinement area builds up to 1 in. of water, the ventilating supply and discharge valves will be closed by pressure switches, thus sealing the ventilation system. When the pressure rises to 2 in., the pressure switches initiate a fog spray that sprays water in the pipe gallery and the cells. The fog-spray pumps are driven by both electric motors and diesels for maximum reliability. At a pressure of 2 psig, the counter-weighted weather hoods on the vent stacks blow off. These stacks are shown in Fig. VI-3. After approximately 300 sec the butterfly valves close automatically, sealing the building and preventing release of any fission products released by fuel meltdown. The fog-spray system starts delivering water about 10 sec after the pressure surge to prevent further pressure buildup within the confined building. This spray system is the only means of preventing excessive pressure buildup.

There are a total of 13 butterfly vent valves (Fig. VI-3), 11 of which are located in the gallery and 2 in the reactor building. The inflatable plastic bag serves as a backup, should the butterfly valve fail to close. A vacuum-breaker system is provided which consists of 4 check valves, 2 in the reactor building and 2 in the heat-exchanger building. These check valves open if the differential pressure exceeds 2 psig.

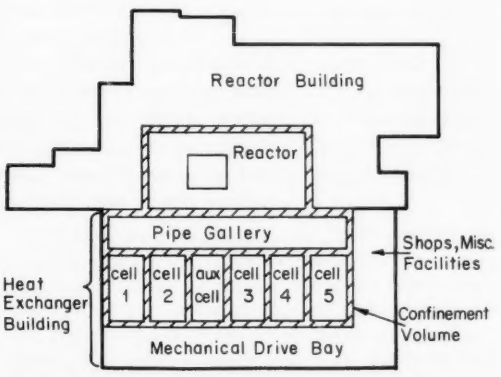

Fig. VI-2 Plan view of reactor and heat-exchanger buildings of the NPR plant.[1]

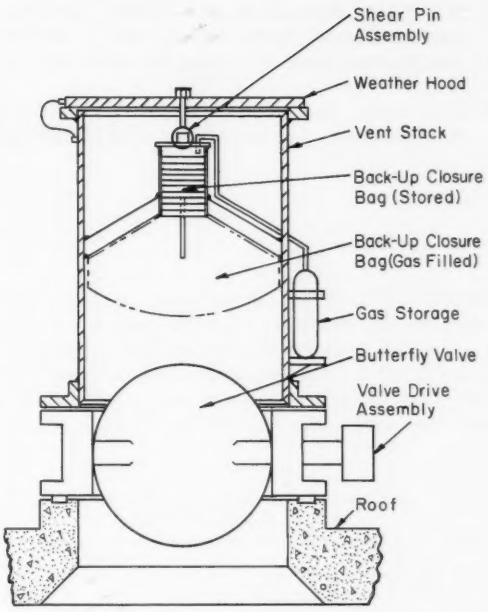

Fig. VI-3 Simplified arrangement of an individual confinement vent-valve assembly.[1]

The whole concept of confinement is tied rather explicitly to an accident wherein no fission products will be liberated during the first 300 sec when the reactor is blowing down. The meltdown of fuel was studied analytically and is reported on in Ref. 3. For the most serious incident studied, a period of 100 sec was available between closure of the building vent valves and potential fission-product release. A containment exhaust system is provided with filters of high particulate efficiency. These would be used after the initial venting and control of building pressure by the fog-spray system. The filtered exhaust air would be released through a 200-ft stack to the atmosphere.

References

1. G. T. Lewis, Jr., The Vented-Containment Concept Used for the New Production Reactor, Paper 63-WA-229 presented at the Winter Annual Meeting of the ASME, November 17–22, 1963.

2. W. J. Dowis, Basis of Design—Hanford New Production Reactor (NPR), USAEC Report HW-SA-2981, Hanford Atomic Products Operation, Apr. 19, 1963.
3. H. S. Davis, D. D. Stepnewski, G. E. Wade, and D. L. Condotta, Fission-Product Confinement for the New Hanford Production Reactor, *Trans. Am. Nucl. Soc.*, 6(1): 118 (June 1963).
4. New Production Reactor, in *Annual Report to Congress of the Atomic Energy Commission for 1963*, p. 46, U. S. Government Printing Office, Washington, January 1964.

Section

VII

Power Reactor Technology

Components

Pumps for Liquid Metal

The Lithium-Cooled Reactor Experiment (LCRE) is an outgrowth of the Aircraft Nuclear Propulsion Program (ANP). References 1 and 2 discuss the design of the primary coolant pump[1] and the reflector coolant pump[2] for the LCRE. The two pumps appear to be quite similar, and only the primary coolant pump will be discussed here. The pumps were designed during the ANP program and incorporate design features of a flight type reactor coolant pump for a nuclear aircraft power plant. The "spin-off" of the ANP technology into other areas is an interesting development, although it must be realized that the design of a liquid-metal pump for a central-station power plant might be different from a pump designed for use in flight.

Table VII-1 lists design characteristics of the primary coolant pump, termed the LP-1. Figure VII-1 shows a simplified section of the liquid lithium pump. The design goal of a 10,000-hr operation without maintenance[1] is not a modest one, and it is of interest to note that four LP-1 test units have accumulated a total of 32,254 hr at design conditions. Two of the units have completed their scheduled 10,000-hr test.[1] Whether these were free of maintenance is not specified in the reference.

The major problem in the design of the pump is the sealing system, which is shown schematically in Fig. VII-1. Figure VII-2 shows additional details of the construction of the dynamic seal. The following quotation[1] serves to explain the operation of the seals:

> A major design feature of the LP-1 pump is the sealing system, which is shown on the simplified schematic in Fig. [VII-1]. The objective of the sealing system is to prevent any contamination of the hot liquid metal with oxygen, moisture, or carbonaceous material. Absolute minimum contamination levels are required to assure proper operation of the pump for the design total operating life of 15,000 hours. Primary sealing of the hot lithium is accomplished by establishing a liquid metal to inert gas interface on the rotating vanes of a radial vaned impeller, termed a dynamic seal, which is located on the shaft above the main pump impeller. The

Table VII-1 SUMMARY OF DESIGN CRITERIA FOR LP-1 PRIMARY COOLANT PUMP[1]

Hydraulic criteria	
Type of pump	Single stage, centrifugal
Fluid	Lithium
Fluid temperature, °F	Maximum, 1600; nominal, 1000
Flow rate, gal/min	390 total; 195 per pump
Head rise, ft	115
Design shaft speed, rpm	4500
Pump hydraulic efficiency, %	69
Inlet pressure, psia	36
Design specific speed	1830
Design suction specific speed	1310
Structural criteria	
Operating life: 15,000 hr total; 1000 hr at design conditions	
Material, predominantly niobium–1% zirconium alloy and type 316 stainless steel	
Radiation dosage	
10^9 rads of gamma; 5×10^{14} fast neutrons/cm^2	
Maximum allowable design-stress levels for niobium–1% zirconium alloy (forgings and extrusions)	
15,200 psi for 10,000-hr operation at 1000°F; 5500 psi for 1000-hr operation at 1600°F	
Mechanical design criteria	
Design critical speed of pump shaft, 11,850 rpm	
Pump mounting: vertical, with two pumps mounted in a common sump	
Pump-shaft bearing support: single roller bearing at top end, duplex ball thrust bearing at lower end	
Pump-shaft sealing system: centrifugal type of dynamic seal for primary liquid-metal seal; helium sweep-gas flow and mechanical shaft face seals for secondary sealing	
Pump thermal insulation: sealed can filled with zirconium wool type insulation	
Pump lubrication system: forced feed; total flow of 2.2 gal/min of MIL-L-7808D oil	
Dry weights: each pump, excluding motor, 226 lb; sump without pumps, 630 lb	
Pump drive-motor design criteria	
Type of drive: two pole, variable frequency, a-c induction motor	
Shaft speed range, 0 to 7200 rpm	
Electrical system: 3 phase; 110 volts at 60 cps; 0 to 120 cps	
Shaft bearing support, single ball bearings at top and lower end	
Drive lubrication system, bearing packed with NRRG 159 grease	
Motor weight, 320 lb	

pump discharge pressure is sealed by permitting the liquid metal to partially flood the vaned side of the rotating dynamic seal impeller to a selected radial interface location where a pressure balance is obtained by utilizing the sweep gas pressure above the dynamic seal, as shown in Fig. [VII-1]. At this equilibrium condition, the sum of the sweep gas pressure plus the pressure rise developed in the rotating annulus of liquid on the dynamic seal impeller vanes is equal to the pressure existing at the top of the impeller due to the pump discharge pressure. The helium sweep gas discharges into the sump at essentially the same pressure as that existing at the interface on the dynamic seal, so that a common inlet pressure is sensed by both the dynamic seal and main pump impellers. In this manner, the dynamic seal interface position is insensitive to the pump shaft speed for a given pump throttle setting as both impellers generate a head rise as a common function of the pump shaft speed. The sweep gas exits from the top of the sump through a vapor trap and then through a pressure regulator, which establishes the pressure level in the sump. From the regulator the helium sweep gas is discharged overboard to the atmosphere.

The secondary sealing of the pump is accomplished by the helium sweep gas flow in conjunction with the cermet faced, bellows mounted mechanical shaft face seals. A single, oil cooled, shaft face seal is located at each end of the pump bearing compartment to effectively seal against leakage of oil or inert gas from the lubrication system and prevent contamination of the inert gas blanketed oil system from the ambient air at the top of the shaft. A dry gas cermet shaft face seal is utilized below the lower shaft face seal to form a purge cavity as indicated in Fig. [VII-1]. A flow of about 6 SCFH of helium is introduced into the purge cavity directly above the dry gas face seal and flows upward through a single tooth shaft labyrinth, which produces an effective acceleration of the helium purge gas to prevent the diffusion of oil vapors below the labyrinth. The purge gas and any oil vapor leakage from the oil cooled face seal are swept overboard to an extennal containment vessel. To prevent gross leakage of oil into the liquid metal region in the

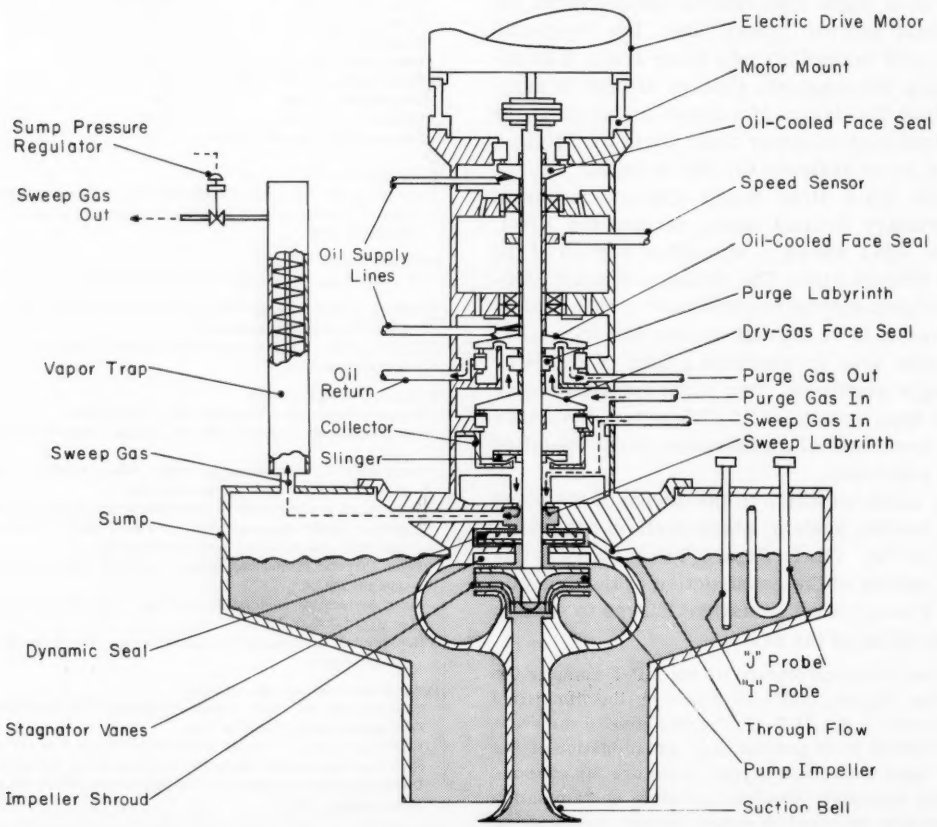

Fig. VII-1 Cross section of the primary coolant pump and sump.[1]

event of a major failure of both lower shaft face seals and the purge gas flow, a secondary dynamic seal, termed a slinger, is installed below the dry gas shaft face seal. The helium sweep gas flow is introduced down the shaft tunnel below the slinger to prevent the diffusion of lithium vapors up the shaft above the single tooth labyrinth shown in Fig. [VII-1]. A sweep gas flow rate of about 25 SCFH is utilized to provide an effective sweep gas velocity through the labyrinth. To prevent the introduction of contaminants into the pump system through the sweep gas circuit, the helium is purified to less than two parts per million of oxygen and two parts per million of moisture contaminants prior to introduction into the pump sealing system.

Two primary pumps are arranged on a common sump, as shown in Fig. VII-3.

Flow Controller for Sodium Service

Reference 3 describes a throttle valve that was constructed for possible use in the primary or secondary systems of a sodium-cooled reactor. The major parts of the controller are the valve body with one entrance and two exit ports, an orifice-closing member or gate, and a torque-tube seal. A cross-sectional view of the valve assembly is shown in Fig. VII-4. Type 304 stainless steel was utilized for the valve parts, and the valve body walls were $\frac{5}{8}$ in. thick. The design of the gate was an important feature of the controller. As the gate rotated, the flow area of one of the exit ports was approximately equal to the area of the other port available for flow. A turn from the fully open to the completely closed position required about a 30° rotation of the gate in either direction from the midposition.

The sealing of the valve was accomplished by means of seal welds as shown in Fig. VII-5. The torque tube allowed the drive shaft to turn within the necessary ±30° swing and still provided a positive barrier between the sodium and the helium fill gas. The sodium freeze seal at the top of the drive shaft was used for backup purposes. In case of rupture or damage of the torque tube, the sodium flowing into the small, annular clearance would freeze and seize the drive shaft.

Table VII-2 DESIGN CHARACTERISTICS FOR HYDRAULIC CONTROL-ROD ACTUATOR[4]

Criterion	Design value
Stroke, in.	60
Scram time, maximum, sec	1
Positioning speeds, in./min	6 and 12
Incremental positioning, in./step	1/8
Rod-position indication, in.	±1/8
System environmental pressure, psig	2000
System environmental temperature, °F	500
Maximum outside diameter, in.	14
Design lifting capacity, lb	2300

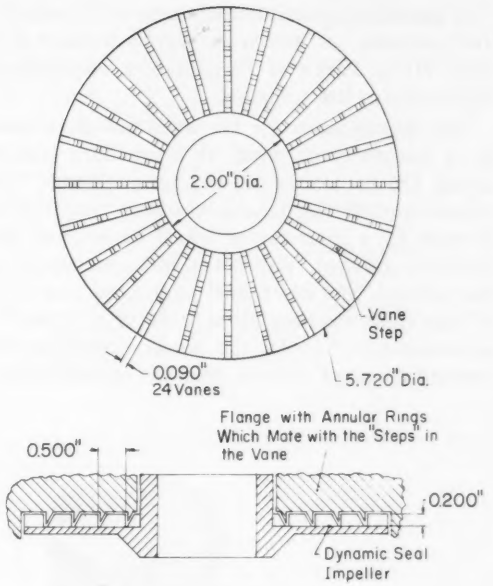

Fig. VII-2 Schematic of the dynamic seal for the primary coolant pump.[1]

The flow controller was tested with flowing sodium in a test loop at flows to 5000 gal/min in the temperature range from 825 to 1000°F. The two exit orifices were contoured, and the flow rate was shown to be nearly linear with respect to the degree of valve opening. Thermal shocking was done to the flow controller by allowing colder sodium to flow through a hot valve. The valve performed satisfactorily for 500 shocks after some modifications to increase clearances between the gate and the bore. The performance of the torque-tube drive-shaft seal was satisfactory.

Control Rods and Drives

A hydraulic control-rod actuator is described in Ref. 4. This mechanism utilizes reactor primary water as an actuating mechanism and has the design characteristics shown in Table VII-2.

The operating principle of the hydraulic control-rod actuator is shown in parts *a* through *d* of Fig. VII-6. Part *e* of Fig. VII-6 is a simplified schematic of the actuator.

The supply water for the actuator is furnished by a canned rotor pump at a pressure that is about 125 psi above the reactor pressure. The linear-motion mechanical-transfer coupling is formed by a shaft having spiral keyways of two different pitches, which are in turn coupled to the pistons. The reference[4] compares the action of this shaft and the pistons to that of a "Yankee" screwdriver: "... As the power piston moves upward the shaft rotates, thus the angular position of the shaft is a function of the power piston position. This rotary motion of the shaft is translated back to a linear motion of the servo piston by the 'Yankee' screwdriver action. The ratio of motion between the pistons is approximately 38 to 1 so that a 3-in. motion of the servo piston represents the full stroke of the power piston." Rod withdrawal is accomplished by driving (or stepping) the control sleeve in an up direction. The increase in the pressure beneath the power piston moves it, and (by means of the transfer coupling) the servo piston, in a withdrawal direction. When the control port is again uncovered the proper amount, the motion ceases

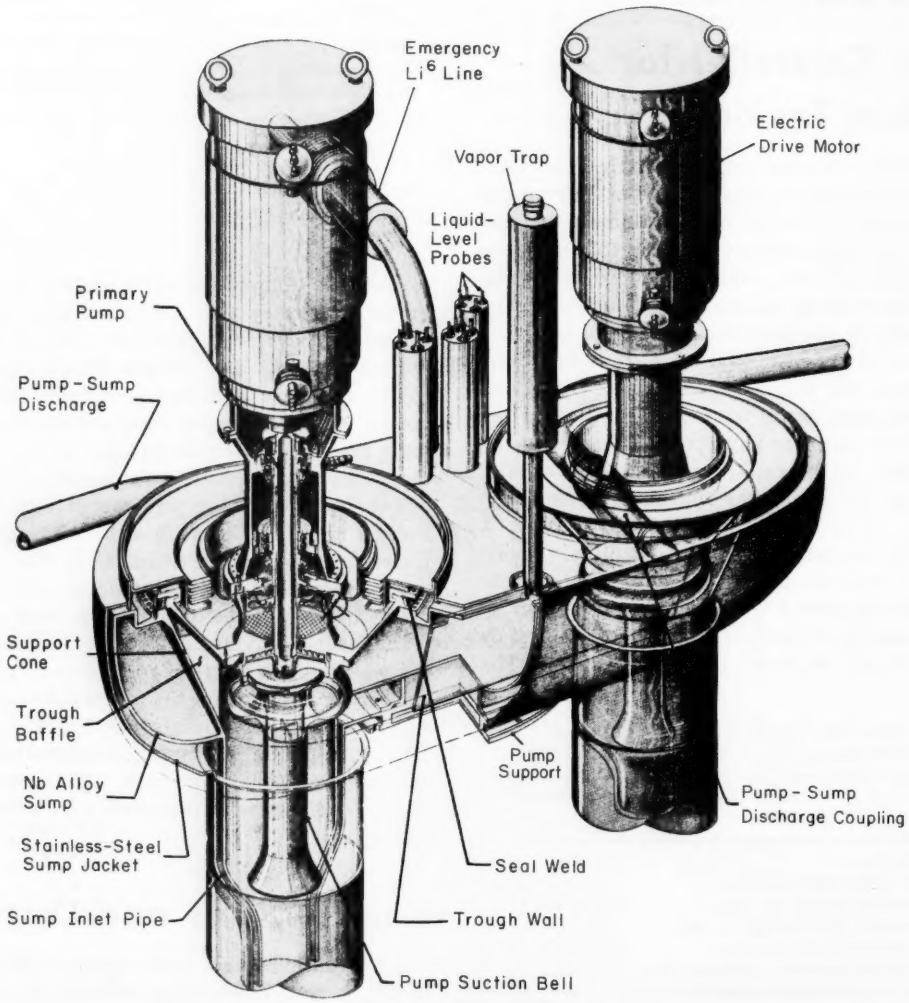

Fig. VII-3 Cutaway illustration of LP-1 pumps and sump.[1]

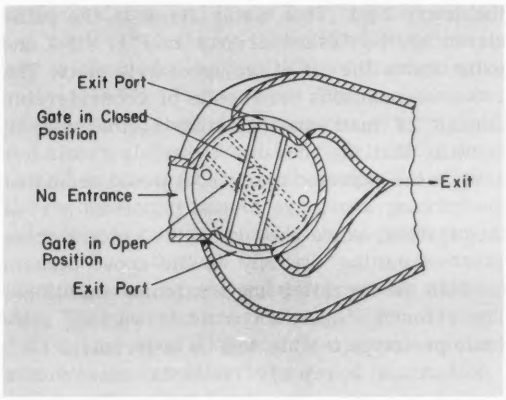

Fig. VII-4 Cross section of the sodium-flow controller valve.[3]

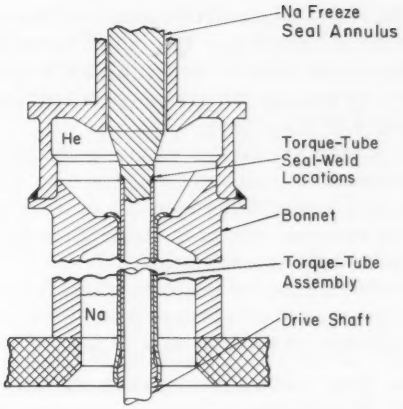

Fig. VII-5 Torque-tube seal and sodium-flow controller valve.[3]

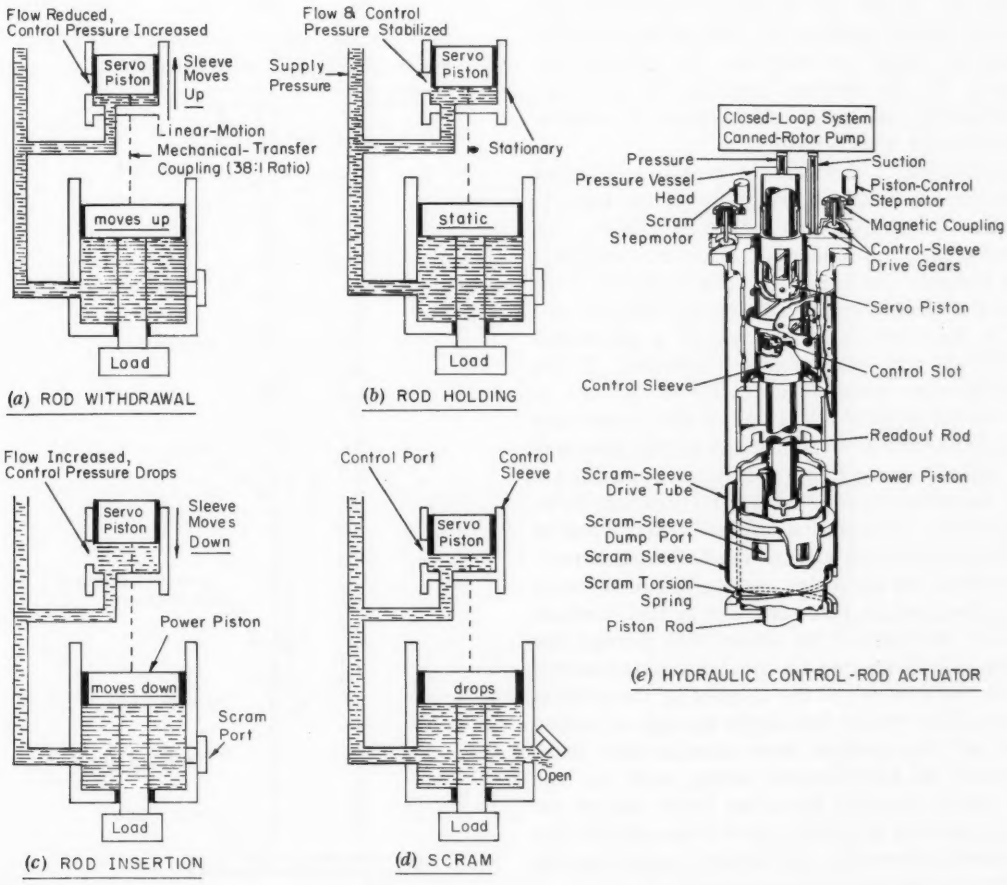

Fig. VII-6 Schematic diagram of the hydraulic control-rod actuator and illustrations of its operating principles.[4]

and the rod is held in a fixed position. The rod is inserted by reversing the initial direction of motion of the control sleeve. Scram is accomplished by opening the scram ports and allowing the water to drain away.

All signals in and out of the mechanism are transmitted by magnetic couplings so that no seals are required between the reactor water and the exterior. Scram is accomplished by any one of the following operations:

— deenergizing the magnetic clutches
— interrupting all electric power
— shutting off the hydraulic supply

In the first two scram options, the magnetic clutch disconnects the scram stepmotor from the scram sleeve-drive gears, and the scram torsion spring rotates the scram sleeve until the scram ports are uncovered. This results in the action shown in part *d* of Fig. VII-6. No controls are moved for the last scram option, and scram occurs at about one-half the normal rate. When pressure is restored, the control rod moves to its original position. A prototype mechanism was built and operated to demonstrate proof of principle.

Reference 5 describes a pressure-balanced control rod, designed originally for the Experimental Organic-Cooled Reactor (EOCR). The reference is an analytical study only and does not describe any hardware. The particular control rod studied employed a fueled follower, and it is this feature which makes a pressure-balanced rod particularly important. If the coolant-flow direction normally is opposite to the direction of rod-fuel motion for scram, then the attainment of an acceptable scram time may be difficult owing to the resistance of passage of the assembly through the relatively rapidly flowing water. The solution offered in Ref. 5 can be explained by study of Fig. VII-7. During normal operation the absorbing section is raised out of the core, and its place is taken by fuel. Coolant enters the side of the lower boot through the slots and flows into an annular passage sealed from the exterior of the element by the rubbing shoes. The coolant then flows through an orifice and into the movable lower plenum; from there it cools the fuel element, exiting at the top into an upper plenum. Since the lower end of the lower plenum is sealed, there is no need for the element to force its way through rapidly moving coolant in the event of a scram.

In the event of scram, the movable assembly displaces the water trapped between itself and the lower boot. This water flows in the paths shown by the dashed arrows in Fig. VII-7 and exits above the top of the upper grid plate. The reference contains the results of a considerable amount of mathematical study of the system, showing that the movable assembly should behave in the expected manner. It would seem that the rubbing shoes are a most important part of the system, since they keep the coolant from short-circuiting directly to the upper plenum for both the operating and scrammed conditions. The reference does not indicate whether full-scale prototype testing will be undertaken.

Reference 6 reports on tests done with a control-rod-drive prototype for the Pathfinder power reactor. The drive system uses a rack-

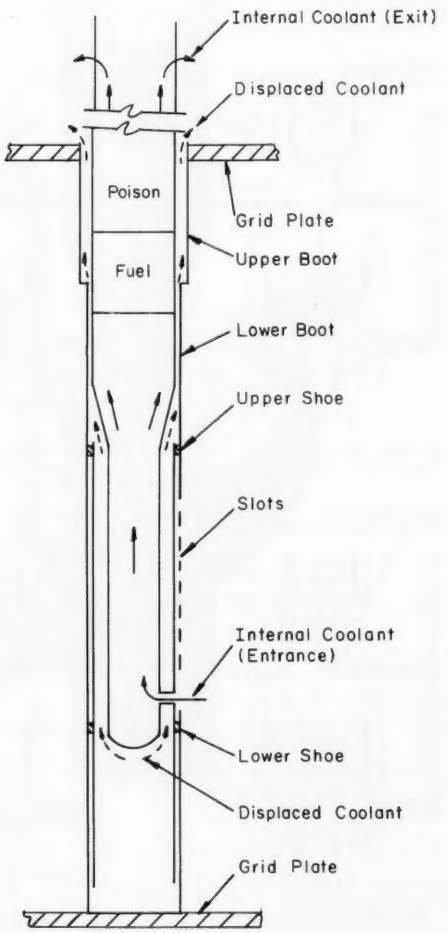

Fig. VII-7 Flow paths for internal coolant and displaced coolant during a scram.[5]

and-pinion drive, and it was designed to operate in a pool of shielding water. The Pathfinder plant is discussed in Sec. VIII of this issue of *Power Reactor Technology*. The installation contains an interesting mechanism to prevent the formation of a void in the rack housing due to rapid removal of the rack during a scram. This mechanism consists of a steam line from the reactor to the upper end of the rack housing; as steam flows through this line during a scram, it is condensed by the relatively cooler shield water. To prevent a convection path from being set up during normal operation, a spring-loaded piston type accumulator is provided near the top of the rack housing. The reference contains the results of a number of tests performed on the rod-drive prototype to demonstrate satisfactory performance under all operating conditions.

References

1. C. Ferguson, L. K. Knudsen, R. P. Lamers, B. R. Lucas, D. V. Manfredi, and H. P. Odom, Design Summary Report of LCRE Primary Coolant Pumps and Sump, USAEC Report PWAC-383, Pratt & Whitney Aircraft Division, United Aircraft Corp., Nov. 22, 1963.
2. C. Ferguson, L. K. Knudsen, R. P. Lamers, B. R. Lucas, D. V. Manfredi, and H. P. Odom, Design Summary Report of LCRE Reflector Coolant Pumps and Sump, USAEC Report PWAC-384, Pratt & Whitney Aircraft Division, United Aircraft Corp., Dec. 6, 1963.
3. R. A. Winborne, Flow Controller Evaluation for Sodium Service, USAEC Report NAA-SR-7534, Atomics International, Nov. 30, 1963.
4. F. C. Legler and R. B. Hussey, A New Hydraulic Control-Rod Actuator for Nuclear-Reactor Power Plants, ASME Paper 63WA88, 1963.
5. F. K. Clements, A. D. Kartchner, R. S. Kerr, and W. B. Lewis, Design of a Pressure Balanced Control Rod, *Nucl. Sci. Eng.*, 18(2): 200 (February 1964).
6. J. Patterson, E. Duewel, R. Kern, M. Jury, R. Grenda, A. McIlheran, and M. McDermott, Control Rod Drive Prototype Test Report, USAEC Report ACNP-63018, Allis-Chalmers Mfg. Co., Oct. 25, 1963.

Section

VIII

Power Reactor Technology

Design and Construction Practice: Pathfinder and BONUS

By Walter Mitchell III

Introduction

The Nuclear Superheat Program of the U. S. Atomic Energy Commission includes the construction of two central-station power reactors, the Pathfinder reactor near Sioux Falls, S. D., and the Boiling Nuclear Superheater (BONUS) reactor at Punta Higuera, P. R. These two reactors are in the process of startup at this writing. If they fulfill expectations, they will establish the feasibility of generating high-temperature steam in water-cooled water-moderated reactors. Since water-reactor technology has so far shown economic promise in the United States, the development of nuclear superheat reactors may have important consequences.

The design approaches to many of the problems of nuclear superheat are different in the two reactors. The designs are described here, in a single review, because their diversity itself serves to illuminate the problems and relations of nuclear superheat. The major part of the review is devoted to summaries of the two designs. A brief discussion of the two in relation to the development of nuclear superheat is given at the end, but any critical comparison given before the establishment of the operating characteristics would be premature.

Pathfinder Atomic Power Plant

The integral nuclear superheat reactor of the Pathfinder Atomic Power Plant[1,2] reached criticality in March 1964. The evolution of the plant type and the administrative organization of the project were described in *Power Reactor Technology*, 2(3): 51; hence the emphasis in this article is on design features and operating parameters. The plant, which is located near Sioux Falls, S. D., was designed and constructed by the Allis-Chalmers Mfg. Co. for the owners and operators, the Northern States Power Co. of Minneapolis, Minn. Architect and engineering services for the project were provided by the Pioneer Service and Engineering Co. of Chicago.

Although a bulk-steam exit temperature of 825°F from the superheater is specified for the reference design, this temperature cannot be realized with the first-core loading. The basis for design of the first core is a 725°F bulk-steam exit temperature from the superheater, and the safeguards report for the plant, as well as the following discussion, is based on the lower value.

The two-region core of the heterogeneous, boiling-water type reactor contains a central superheater region that is surrounded by an annular boiler region. Superheated steam from the reactor is passed directly to a condensing steam turbine, and feedwater from the condensate system is mixed with the boiler recirculated water. Forced, controlled recirculation of water through the boiler region is accomplished by pumps and piping located outside the reactor vessel. The stainless-steel-clad superheater fuel elements contain highly enriched uranium dioxide in a stainless-steel cermet, whereas the Zircaloy-2-clad boiler elements are fueled with slightly enriched uranium dioxide. The steam-generating portion of the plant is housed in a vertical, cylindrical containment vessel, and the power-conversion equipment is located in an adjoining building.

A simplified flow diagram of the plant is given in Fig. VIII-1, and the principal characteristics are listed as follows:

Power, boiler region, kw	157,400
Power, superheater region, kw	31,500
Total core power, kw	188,900

Gross electrical capability, kw	62,500
Gross heat rate, Btu/kw-hr	10,780
Net electrical output, kw	58,500
Net efficiency, %	31
Steam outlet pressure, psig	535
Reactor operating pressure, psig	600
Temperature, boiler region, °F	489
Outlet temperature, superheater region, °F	725
Reactor steam flow at rated power (approximate), lb/hr	616,125
Recirculation rate, gal/min	65,000
Containment vessel size, ft	50 (dia.) by 120
Reactor vessel size, ft	11.5 (OD) by 31.5
Overall core dimensions, height and diameter, ft	6 by 6
Dimensions of superheater region, height and diameter, ft–in.	6 by 30
Fuel, boiler region (Zircaloy-clad)	2.2% enriched UO_2
Fuel, superheater region (S.S.-clad)	93% enriched UO_2–S.S. cermet
Fuel loading, boiler region, kg ^{235}U	144.3
Fuel loading superheater region, kg ^{235}U	50.0
Average heat flux, boiler region, Btu/(hr)(sq ft)	122,000
Average heat flux, superheater region, Btu/(hr)(sq ft)	59,100
Maximum heat flux, boiler region, Btu/(hr)(sq ft)	447,000
Maximum heat flux, superheater region, Btu/(hr)(sq ft)	219,000
Neutron flux, approximate, neutrons/(cm^2)(sec)	3.5×10^{13}

General Reactor Features

The reactor vessel and its internals, the recirculation loops, and the control-rod drives constitute the reactor system. Figure VIII-2, a vertical section through the reactor vessel, shows the arrangement of internal components of the vessel, the mounting position for the control-rod drives, and the connecting points at the vessel for feedwater piping, recirculation water piping, and the main steam line. As shown in the figure, recirculation water enters the reactor vessel at its bottom and flows upward through the annular boiler region. Most of the steam formed in the boiler region continues to flow upward in the pressure vessel and is separated from the water at the steam-water interface located above the active core. The water and some entrained steam flow into steam separators that are located in the annular space between the boiler core and the pressure-vessel wall. The entrained steam is separated from the water, and the water then flows down through the downcomer annulus to the lower portion of the pressure vessel. The steam flows upward into the steam dome, passes through the steam dryer, flows down through the superheater region, and flows out the bottom of the reactor

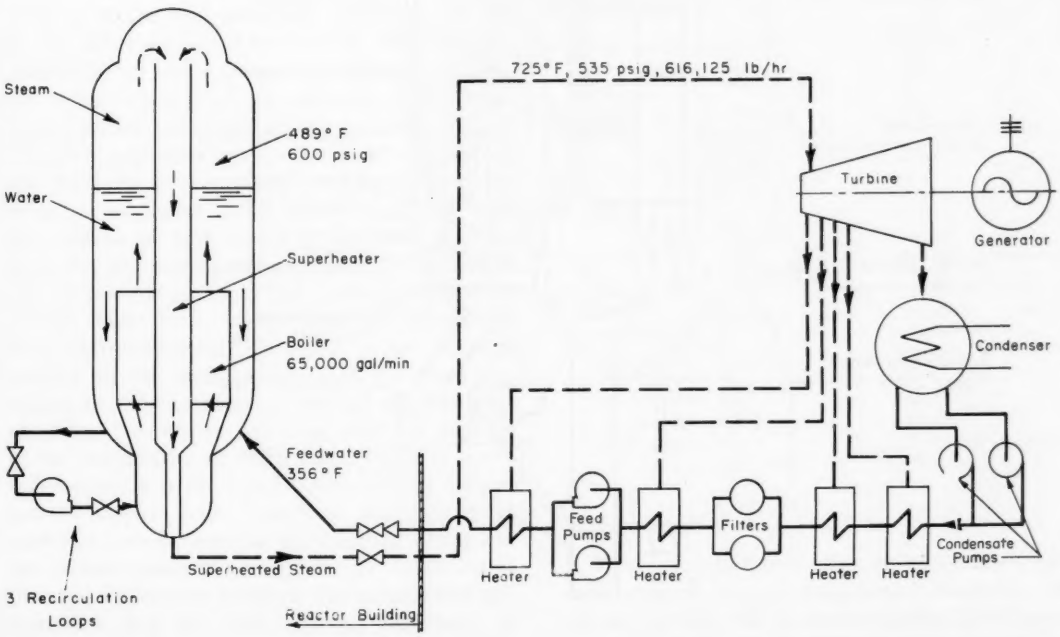

Fig. VIII-1 Simplified flow diagram of the Pathfinder Atomic Power Plant.

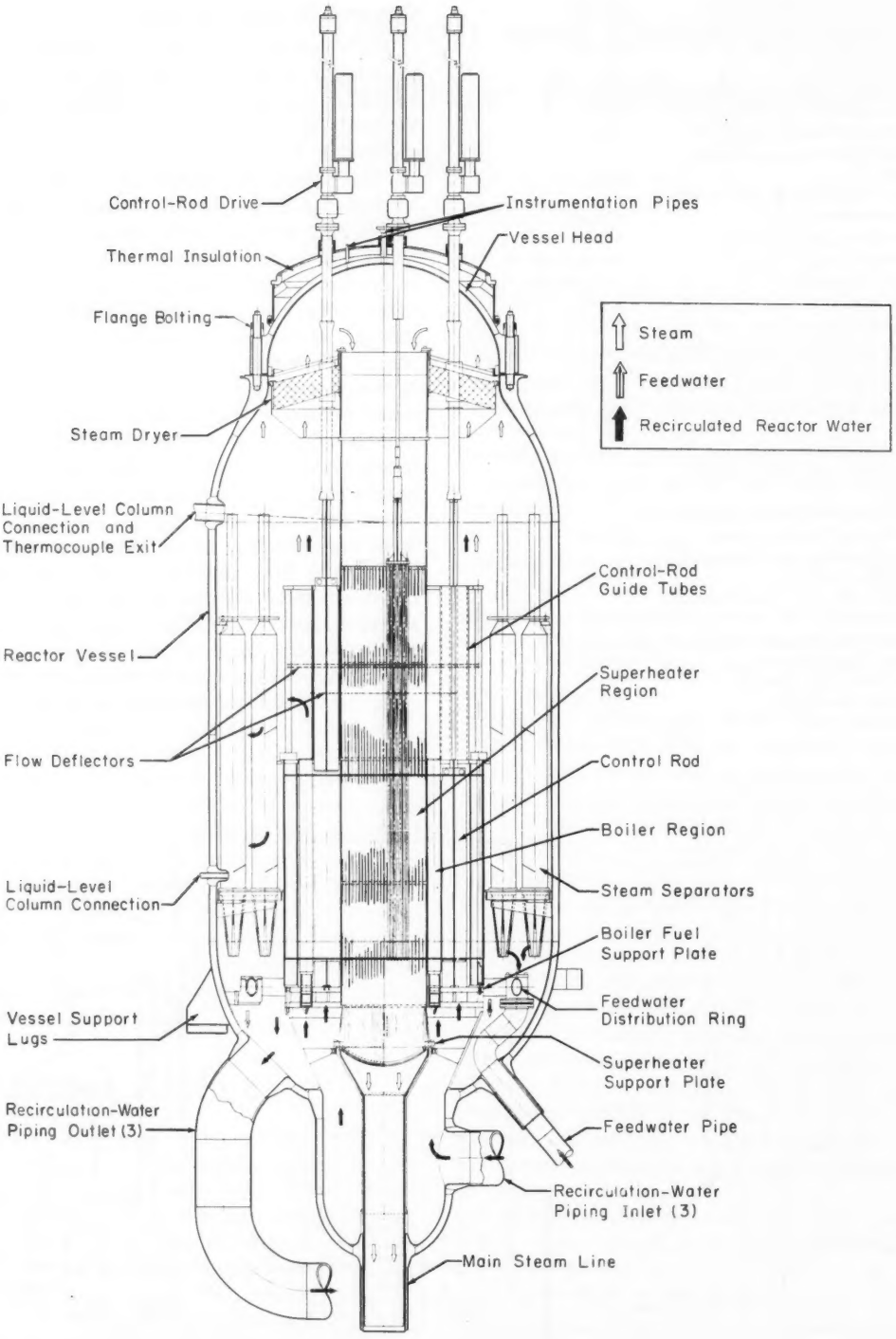

Fig. VIII-2 Vertical section of the Pathfinder reactor.

vessel through the main steam line. Feedwater enters the reactor vessel near its bottom and is mixed with the downcomer flow by means of a sparger shown in Fig. VIII-2. The recirculation flow, which consists of the downcomer flow and the feedwater, leaves the vessel through piping outlets, passes through recirculation pumps where its pressure is raised approximately 25 psi, and then reenters the reactor vessel through the recirculation-water piping inlets.

The boiler region contains 96 fuel-element assemblies, each approximately 5 in. square by 99 in. long overall. The superheater region of the core, which resembles a tube type heat exchanger, contains 412 positions for 1-in.-diameter fuel assemblies. Reactor power level is controlled by a system of rods located in both the boiler and superheater regions of the core. The rack-and-pinion type drives employed for all control rods are mounted on top of the reactor pressure vessel.

The reactor vessel is carbon steel and is internally clad with stainless steel. Internal support structures and baffles are stainless steel, and the recirculation piping is stainless steel or is clad with stainless steel.

Boiler Fuel

Each boiler fuel assembly contains a bundle of 81 fuel rods in a 9 by 9 array, with a nozzle assembly on one end and a handling fitting on the other. Each fuel rod consists of four segments joined end to end as shown in Fig. VIII-3. The two segments that comprise the top half of the fuel rod have a slightly smaller diameter than the segments in the bottom half. The rods are spaced by tube sheets at the joints between fuel-rod segments and by support grids at each end of the rod bundles. The rods are supported on the lower grid, where each rod is fastened by a stainless-steel bolt which, in turn, is tack welded to the grid. Sixteen of the rods are bolted to the top support grid to hold the element together during handling, whereas the tops of the remainder of the rods are free to move independently in the axial direction. The top and bottom support grids, which are stainless-steel castings, are fastened to the handling fitting and the nozzle assembly, respectively. Differential thermal expansion between the boiler fuel assemblies and the core support structure is accommodated at the bottom core support plate by a spring-loaded sliding fit between the fuel-element nozzles and the receiving sleeves in the bottom support structure.

Specifications and performance data for the boiler fuel assemblies and for the boiler region of the reactor are given in the following tabulation:

Core, boiler region		
Mean outside diameter, in.	69.0	
Mean inside diameter, in.	31.3	
Active fuel length, in.	72	
Volume, cu ft	123	
Number of fuel-element assemblies	96	
Average power density, kw/cu ft core volume	1280 (~45 kw/liter)	
Average specific power, kw/kg of uranium	24.0	
Average heat flux, Btu/(hr)(sq ft)	122,000	
Maximum heat flux, Btu/(hr)(sq ft)	447,000	
Steady-state minimum burnout ratio	1.9	
Maximum fuel temperature, °F	4215	
Maximum surface-cladding temperature, °F	514	
Inlet coolant velocity, ft/sec	13.6	
Exit voids, average and maximum, %	45.5 and 56	
Pressure drop, psi	13.6	
Thermal power generated, Mw	157.4	
Thermal power to coolant, Mw	159.1	
Heat-transfer area, sq ft	4397	
Coolant flow area, lower half, sq ft	9.43	
Coolant flow area, upper half, sq ft	10.81	
Fuel burnup, Mwd/ton	10,000	
Core lifetime, year	1.5	
Fuel enrichment ^{235}U, wt.%	2.2	
Fuel loading, uranium, kg	6560	
Boiler fuel-element assemblies		
Bundle size, in. square	4.735	
Number fuel rods per bundle	81	
Rod sections per rod	4	
	Lower sections	Upper sections
Pellet diameter, in.	0.348	0.310
Cladding thickness, in.	0.028	0.026
Rod diameter, in.	0.408	0.367
Box material	Zircaloy-2	
Cladding material	Zircaloy-2	
Fuel material	UO_2	
Fuel density, g/cm^3	10.41	
Nozzle material	Chrome-plated 304L S.S.	

Superheater Fuel

Two concentric fuel tubes form the basic fuel arrangement in each superheater assembly. As shown in Fig. VIII-4, concentricity of the tubes is maintained by full-length straight-wire spacers, and spacing of the assembly proper in pre-

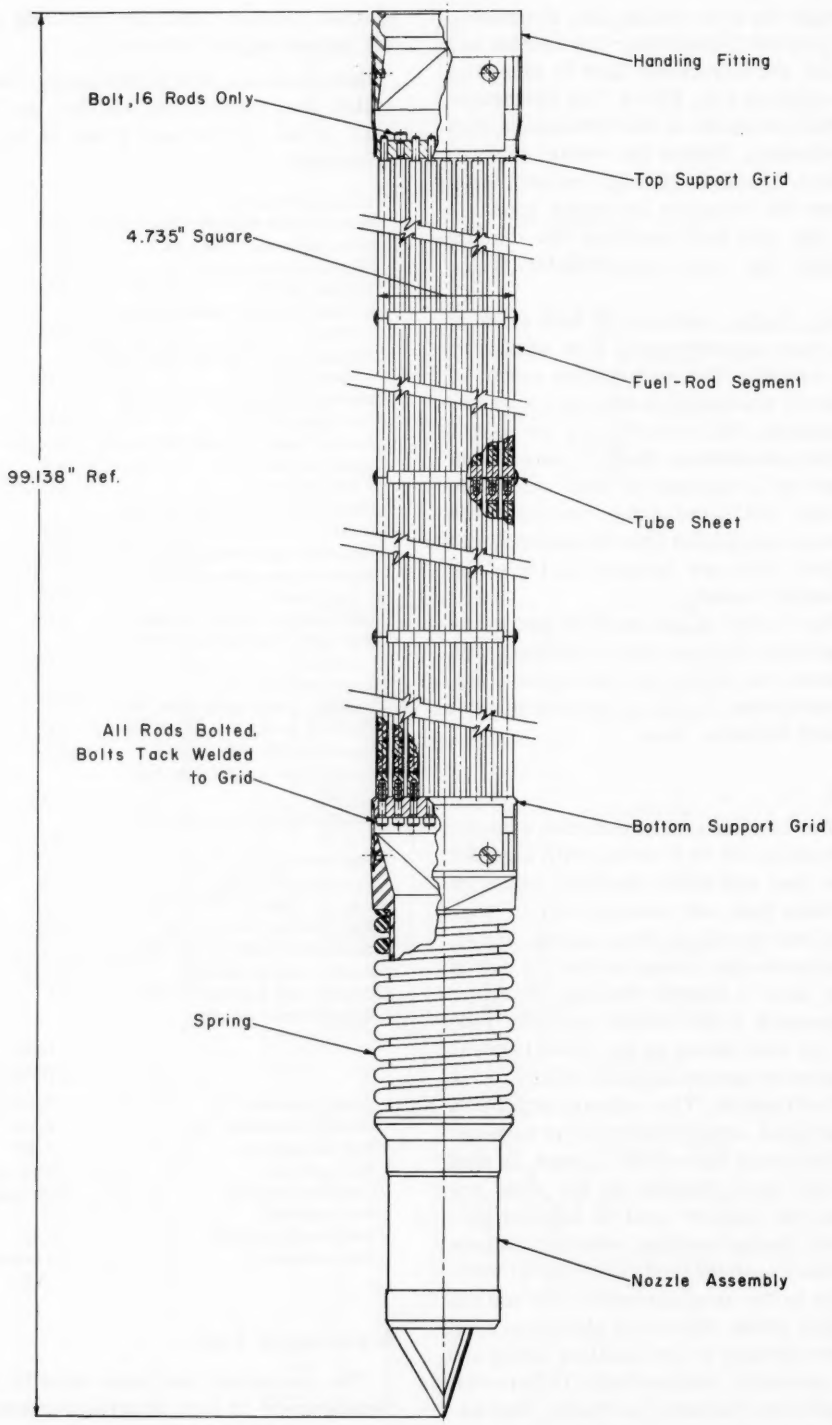

Fig. VIII-3 Boiler fuel assembly of the Pathfinder reactor.

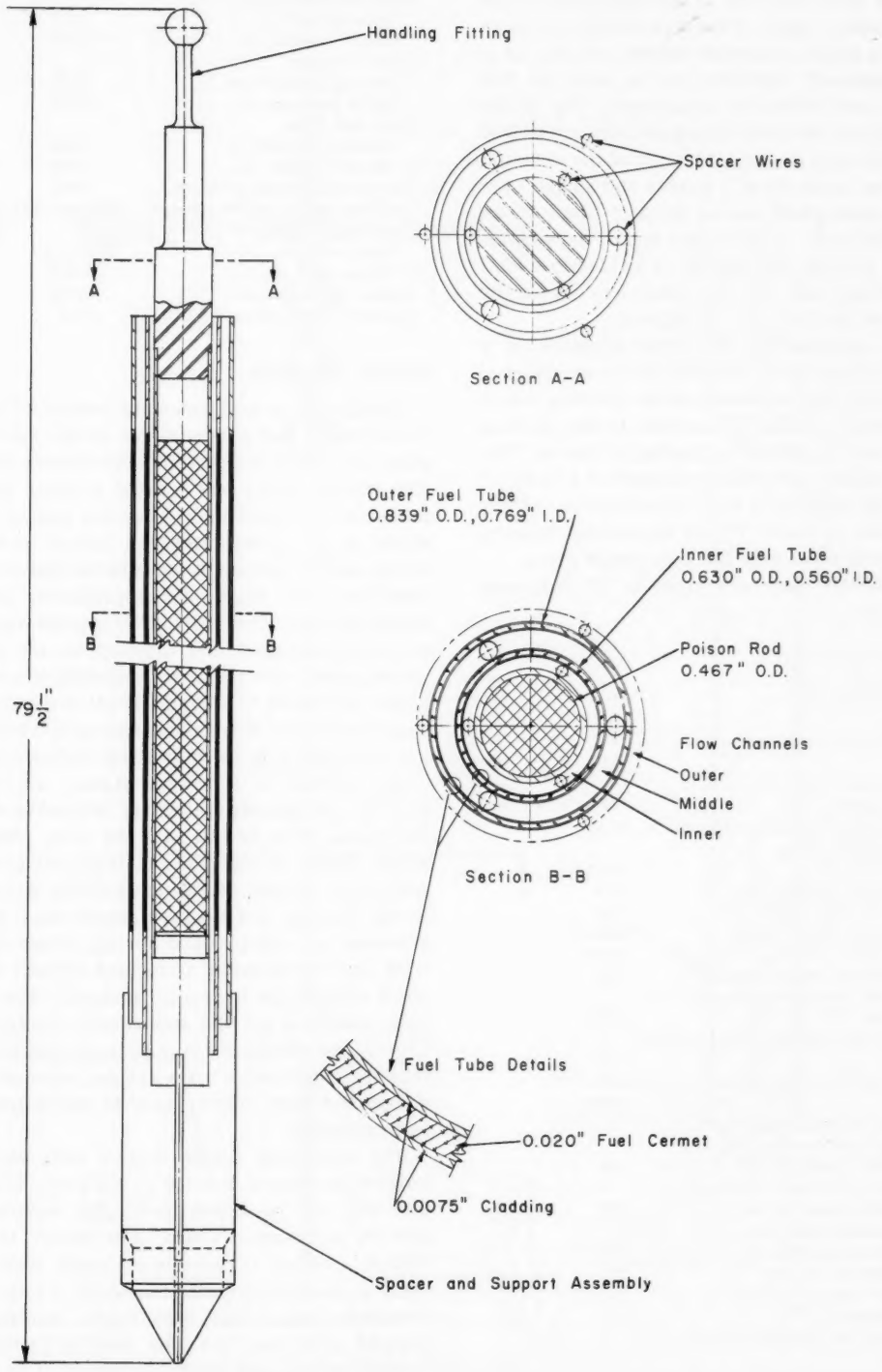

Fig. VIII-4 Superheater fuel assembly of the Pathfinder reactor.

installed flow channels is accomplished in the same manner. Most of the superheater elements contain a central burnable poison rod, but up to 100 unpoisoned elements can be used for flux shaping and reactivity adjustment. The fueled and poisoned sections of each element are welded to end fittings. At the lower end of the element, the fitting consists of a spacer and support assembly that plugs into a support plate in the core structure. At the upper end of the assembly, the central-rod portion is welded to a handling fitting, and the fuel tubes are not axially restrained and are free to expand.

Each superheater fuel tube consists of a UO_2–stainless-steel cermet that is sandwiched between two thin stainless-steel-cladding tubes. Heat transfer from the cermet to the cladding is improved by diffusion bonding of the two. The central poison rod, which consists of a compact containing about 0.35 wt.% natural boron carbide in alumina at about 70% of theoretical density, is clad with relatively thick stainless steel.

Superheater data are given in the following tabulation:

Core, superheater region	
Mean outside diameter, in.	30
Active fuel elength, in.	71.5
Volume, cu ft	32.5
Number of fuel-element assemblies	412
Average power density, kw/cu ft core volume	970 (~34 kw/liter)
Average heat flux, Btu/(hr)(sq ft)	59,100
Maximum heat flux, Btu/(hr)(sq ft)	219,000
Power generated, Mw(t)	31.5
Power to coolant, Mw(t)	29.8
Heat-transfer area, sq ft	1817
Coolant-flow area, sq ft	0.993
Maximum fuel temperature, °F	1280
Maximum cladding surface temperature, °F	1270
Average flow rate in element, lb/hr	1478
Maximum flow rate in element, lb/hr	1626
Average exit bulk temperature, °F	725
Average inlet velocity in coolant channels, steam, ft/sec	128
Average exit velocity in coolant channels, steam, ft/sec	207
Core pressure drop, psi	61
Fuel burnup, average, %	18.5
Core lifetime, months	9
Fuel enrichment, wt.% ^{235}U	93
Fuel loading, kg ^{235}U	50
Superheater fuel-element assemblies	
Outer insulating tubes	
Outside diameter, in.	1.076
Inside diameter, in.	1.024
Inner insulating tubes	
Outside diameter, in.	0.967
Inside diameter, in.	0.937
Outer fuel tubes	
Outside diameter, in.	0.839
Inside diameter, in.	0.769
Inner fuel tubes	
Outside diameter, in.	0.630
Inside diameter, in.	0.560
Poison-tube outside diameter, in.	0.467
Cladding and structural material	Type 316L S.S.
Cladding thickness	
Fuel tubes, in.	0.0075
Poison tube, in.	0.028
Cermet thickness, in.	0.020
Cermet composition, wt.% UO_2	17.5

Control Elements

Pathfinder control elements consist of cruciform blades and poison shims in the boiler region and round rods in the superheater region. The poison shims are located between boiler-fuel-assembly positions. They are locked in position by the assemblies and cannot be moved unless the two adjacent fuel assemblies are first removed. The boiler and superheater control elements are driven by mechanisms mounted on the vessel head, and, although all rod drives are equipped with magnetic clutches, the superheater elements will normally not be scrammed. The drives are of the rack-and-pinion type and are equipped with servo position indicators.

On receipt of a scram signal, the boiler control-rod magnetic clutches release and allow the boiler rods to fall into the core, while the same signal initiates a run-in of all control-rod-drive motors. Those boiler rods which are in the full-out position are accelerated, during a scram by a compressed spring; all scrammed rods are decelerated at the end of their downward strokes by hydraulic dashpots. The magnetic clutches for the superheater control-rod drives are energized by a separate supply, and thus the superheater rods are not automatically scrammed when clutch power to the boiler rods is interrupted.

The cruciform boiler-control rods were described in *Power Reactor Technology*, 5(2): 46, and will not be shown here. The superheater control elements, which are shown in Fig. VIII-5, consist of groups of small rods. The rods in each group are attached to a cruciform structure called the superheater control-rod support yoke, and this yoke, holding 13 rods, is driven by a single drive unit mounted on top of the reactor vessel. There are four such control elements in the superheater region.

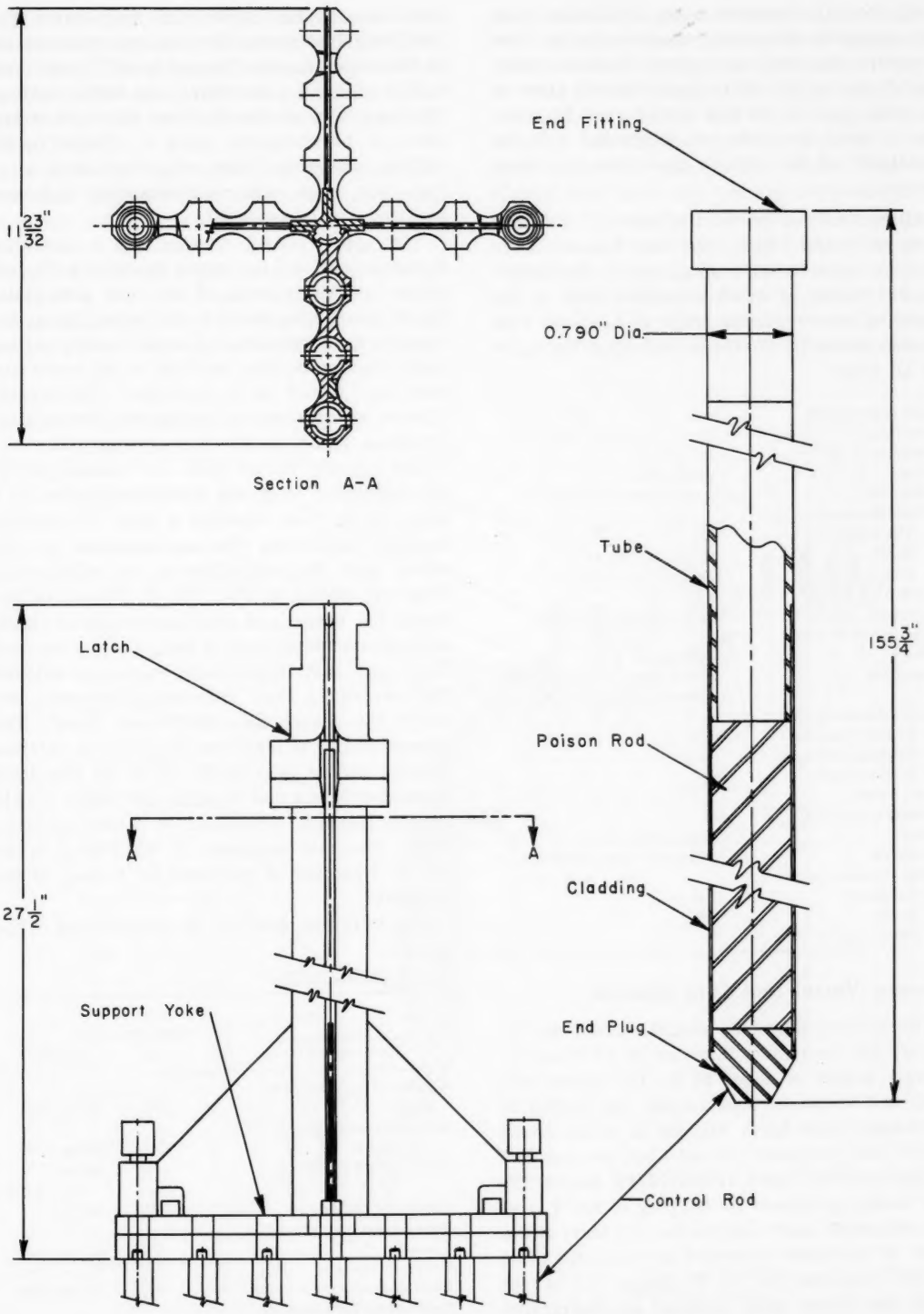

Fig. VIII-5 Superheater control element of the Pathfinder reactor.

All control elements in the Pathfinder core are provided with guide channels in the core structure, and none can contact a fuel assembly. Specifications for the control rods are given in the table that follows this section, and the manner in which the rods are integrated with the remainder of the core is described in a later section.

All control-rod drives are basically the same rack-and-pinion type, but the normal drive speed of those boiler rods closest to the superheater region is about one-third that of the speed of other rods in order to keep the cold startup reactivity-increase rate about the same for all rods.

Boiler control rods	
Number	16
Number of drives	16
Shape	Cruciform
Material	2 wt.% boron in 304 S.S.
Blade dimensions, in.	
Thickness	1/4
Width	10 7/16
Poison length	72
Superheater control rods	
Number	52, ganged into 4 groups
Number of drives	4
Shape	Cylindrical
Material	2 wt.% boron in 304 stainless steel, clad in 304L S.S.
Rod dimensions, in.	
Poison diameter	0.75
Cladding thickness	0.020
Poison length	72
Poison shims	
Number, maximum	56
Shape	Rectangular strip
Material	0.20 wt.% boron in 304 S.S.
Shim dimensions, in.	
Thickness	0.10
Width	2 25/32
Poison length	74

Pressure Vessel and Core Structure

The reactor pressure vessel, shown in Fig. VIII-2, has an inside diameter of 11 ft and an overall height of about 36 ft. The vessel and head are designed, constructed, and tested in accordance with Secs. VIII and IX of the *ASME Boiler and Pressure Vessel Code* as modified by Special Code Cases 1270N, 1271N, and 1273N. The design pressure is 700 psig at 500°F, and the integrated fast-neutron flux (>1 Mev) at the point of maximum exposure is calculated to be 2×10^{18} neutrons/cm^2 in 30 years. The vessel shell and lower head sections are fabricated from 3-in.-thick composite plate consisting of ASTM A-212 grade B carbon-steel base material clad on the inside with 1/4-in.-thick type 304L stainless steel. The hemispherical portion of the upper head is formed from 2 3/8-in.-thick A-212 grade B plate with 1/8-in. 304L cladding. The bond between the stainless steel and carbon steel of the composite plate is effected by hot rolling, and weld joints and carbon-steel forgings are clad with weld-deposited niobium-stabilized stainless steel.

The upper vessel opening has a clearance diameter of 7 ft 7 in., which provides sufficient space for the removal of the core grid plate. Three positioning studs in the vessel flange locate the head with respect to the vessel, and the main closure bolting consists of 48 studs and nuts that are 3 in. in diameter. The vessel-closure seal utilizes two concentric, corrugated, stainless-jacketed soft-iron-core gaskets.

The reactor vessel head and closure region are separated from the shield-pool water by a steel cover that contains a layer of metallic thermal insulation. The arrangement of this cover and its connection to the shield-pool floor are shown in Fig. VIII-6. The space between the vessel and concrete biological shield beneath the shield pool is sealed off by the pool floor and a stainless-steel expansion bellows that permits a 1-in. differential expansion between the vessel and shield-pool floor. The vessel proper is insulated with 4 in. of calcium silicate and is held in its cavity by five steel support columns that transfer the vessel load to spread footings embedded in reinforced concrete. Thermal expansion of the vessel in the radial direction is absorbed by flexing of the columns.

The following are the 32 penetrations of the vessel:

Description	No.	Inside diameter, in.	Location
Nozzles to recirculation pumps	3	20 1/2	Below core
Nozzles from recirculation pumps	3	20 1/2	Below core
Steam-outlet nozzle	1	13 1/2	Below superheater
Feedwater nozzle	1	9 3/4	Below core
Boiler-core instrument nozzle	1	6 3/8	Above core
Lower liquid-level nozzle	1	2 3/8	Below core
Control-rod-drive nozzles	20	3 1/2	Vessel head
Superheater core-instrument nozzle	1	1 1/2	Vessel head
Upper liquid-level nozzle	1	1/2	Vessel head

The arrangement of major components within the pressure vessel is illustrated by Figs. VIII-2 and VIII-7. The principal components that are not part of the core structure are the feedwater distribution ring, the steam separators, and the steam dryer.

As shown in Fig. VIII-2, the feedwater distribution ring, which is a 5-in.-diameter pipe, is supported by brackets attached to the vessel wall. Steam separators, shown in Fig. VIII-8, occupy the annular downcomer region in the Pathfinder reactor. These separators, which handle about 20% of the steam produced, help reduce steam carryunder into the recirculation pump suctions to about 0.1% by volume. At normal operating conditions the total maximum-pressure drop through the separators is $5\frac{1}{2}$ ft of water. The steam separators, which are installed in groups, rest on a support shelf mounted on brackets welded directly to the lower portion of the reactor vessel. They are aligned near their tops and are held down axially by brackets that extend under the boiler-element hold-down structure described in a subsequent paragraph.

The steam-dryer assembly, which can be seen in Fig. VIII-2, occupies the annular space between the superheater chimney and the inside

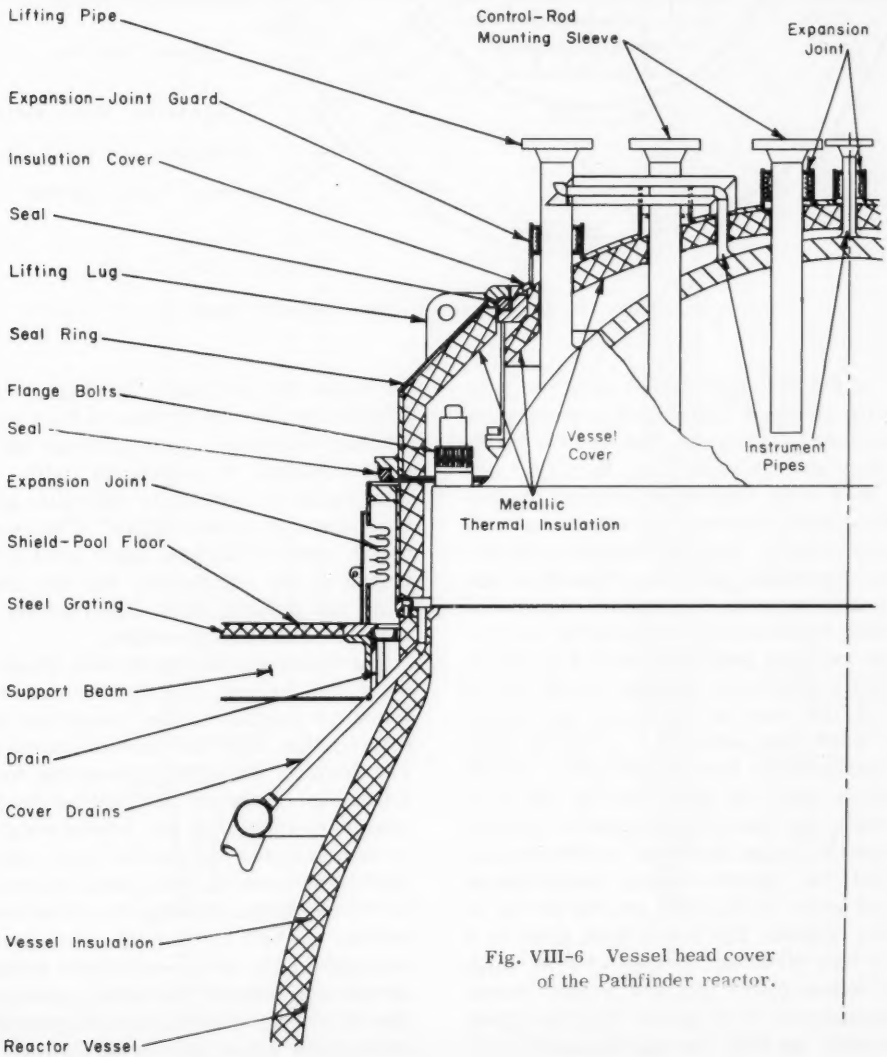

Fig. VIII-6 Vessel head cover of the Pathfinder reactor.

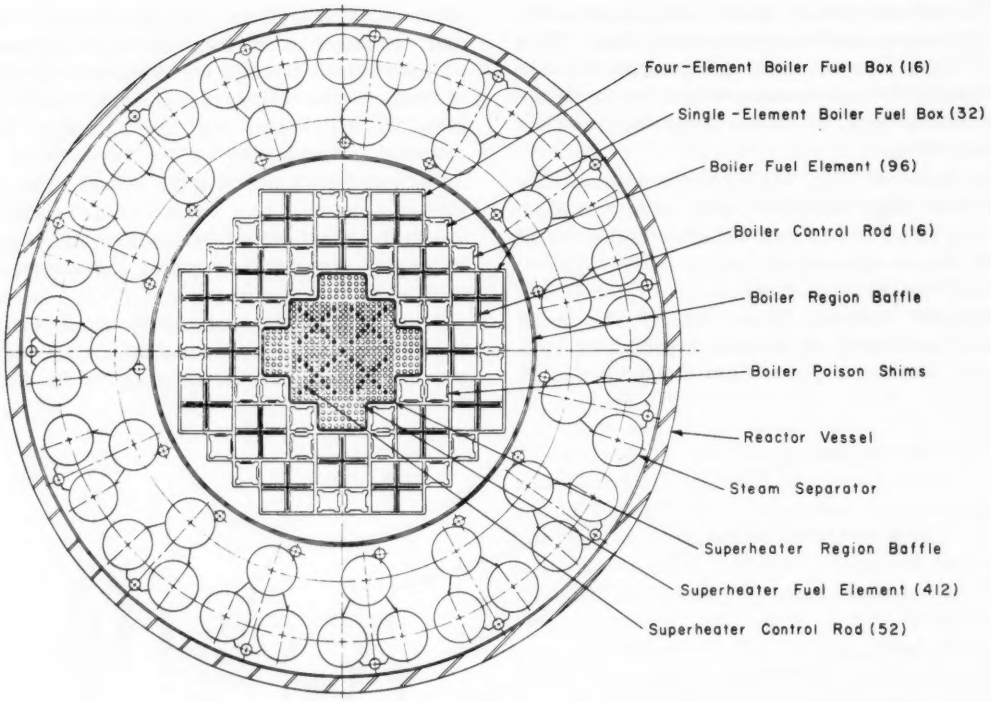

Fig. VIII-7 Horizontal section of the Pathfinder reactor.

surface of the pressure-vessel neck. In addition to its intended function of removing the trace amounts of moisture that remain in the steam after natural separation, the dryer assembly serves the structural purpose of providing a connection between the superheater and the reactor vessel, thereby stabilizing the superheater structural assembly. The dryer assembly also supports the upper control-rod guide tubes, which protect and guide the control-rod-drive rack and latch as shown in Fig. VIII-2.

The basic structural member of the boiler section of the core is the boiler grid plate, which is bolted and doweled to a support skirt welded permanently into the pressure vessel. The support skirt, as shown in Fig. VIII-2, is the member that provides separation between the downward-flowing feedwater and downcomer water and the upward-flowing recirculation water just prior to its entry into the bottom of the boiler region. The boiler grid plate is a sandwich type structure formed by 2-in.-thick top and bottom plates that are welded around their peripheries to a spacer ring that gives the assembly an 8-in. overall thickness. Receptacles for the nozzle portions of the boiler fuel assemblies are formed in the grid plate by welding individual pipes between the top and bottom plates. A cylindrical baffle, which is attached at its bottom to the boiler grid plate, surrounds the boiler region of the core. This baffle, which defines the outer limit of the fueled region of the reactor, is, like the boiler grid plate and support skirt, a permanent piece of the vessel internal structure.

The boiler-element hold-down structure consists of a welded grid of stainless-steel bars which is positioned and locked on top of the boiler baffle after the core is loaded with fuel. The bars of the grid contact the tops of the boiler fuel elements and preload the thermal-expansion springs at the bottom nozzles of the elements. Upper control-rod guide tubes, which shield the control rods from hydraulic loads due to the coolant flowing toward the downcomer region, are held by the hold-down structure, as are lugs of the steam-separator groups in the downcomer annulus. Individual channels for fuel assemblies and control rods are provided in the active core space between the boiler grid plate

and the boiler-element hold-down structure. These channels are formed by components called boiler fuel boxes, which are of two different types. There are 16 four-element boxes and 32 single-element boxes, all formed of Zircaloy-2. The four-element boxes are about $10\frac{3}{4}$ in. square, and contain, in addition to the four square channels for boiler fuel assemblies, a cruciform channel for a boiler control rod. The single-element boxes, which are about 5 in. square and hold one boiler fuel assembly each, have slots milled in their outer surfaces to accommodate burnable-poison shims.

The superheater structure, which resembles a tube type heat exchanger, is shown in Figs. VIII-2 and VIII-7. The assembly contains tubes for fuel elements, for control-rod guidance, and for a neutron source. All tubes are held in vertical alignment by a top tube sheet, by intermediate steady plates, and by a bottom grid plate. The fueled portion of the superheater is surrounded by a vertical baffle, and other vertical structural members extend the overall height of the assembly from a point below the active core region (at the superheater support plate shown in Fig. VIII-2) to the steam-dryer assembly at the top of the reactor vessel. The space between the tubes in the superheater region is filled with water moderator that mixes with the recirculation water above and below the boiler core. Each superheater fuel assembly fits inside a double-walled process tube

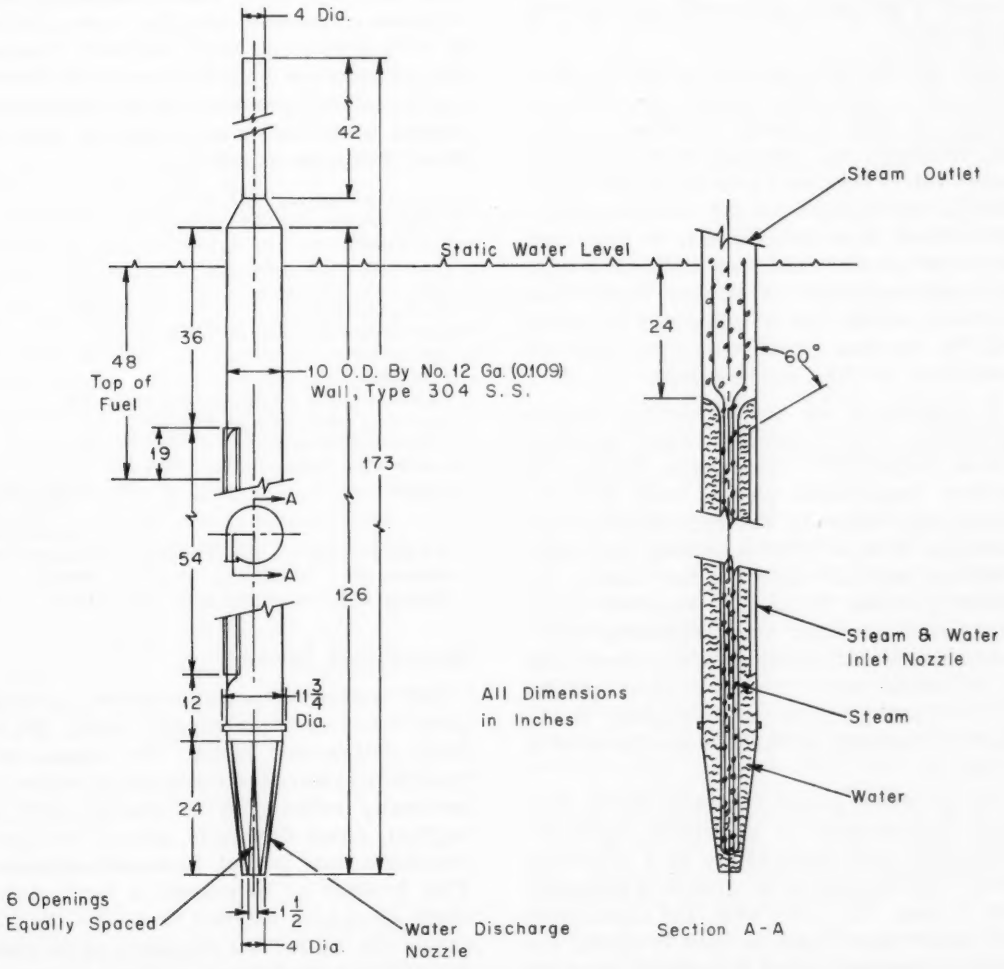

Fig. VIII-8 Steam separator of the Pathfinder reactor.

that contains a layer of stagnant steam for thermal insulation between the water moderator and the superheated-steam coolant.

Control and Instrumentation

The specified mode of operation of the plant calls for manual control of reactivity and for automatic control of pressure. Reactor power is controlled by movement of the control rods or by positioning the recirculation-pump discharge valves (the amount of moderator passing through the core can be varied by throttling recirculation flow with butterfly valves installed on the recirculation-pump discharge side). Reactor pressure is normally controlled by positioning the turbine inlet valves or by a regulating dump valve. If necessary, reactor steam can be dumped to the condenser through the regulating dump valve.

Rate of withdrawal of reactor control rods is limited to a value that causes a reactivity insertion of about 5 cents/sec for any control rod. Similarly, the operators of the pump discharge valves have been selected so that recirculation rate changes will not cause reactivity-insertion rates greater than 5 cents/sec. Interlocks prevent movement of the recirculation-pump discharge valves when control rods are being moved, and no pump may be started with its discharge valve wide open. Only one control rod at a time can be raised.

In addition to the control devices already mentioned, a boron-injection safety shutdown system is provided. This system utilizes two positive displacement pumps, which normally supply seal water to the recirculation-pump discharge pipe at a point between the pump-discharge butterfly valve and the reactor. The system provides 4% negative reactivity under all reactor operating or nonoperating conditions, with or without the reactor vessel open to the shield pool. With the reactor head on, and with both injection pumps running, the 4% negative-reactivity addition is accomplished in 4 min.

The automatic pressure-control system uses steam-line pressure as its primary signal and superheater exit temperature as a secondary signal. The set point of the system is adjustable over a range of 0 to 800 psig. The superheater exit-temperature signal is used to modify the primary pressure signal in order to speed the response of steam flow to reactor power during transients, thereby reducing the temperature rise in the transient.

A block diagram of the Pathfinder nuclear-instrumentation system was given in *Power Reactor Technology*, 5(2): 69, as was the range covered by each of the eight neutron-detecting channels. The two functions of the nuclear instrumentation system are (1) to provide information to the reactor operator so that he can manually adjust the reactivity level in the reactor and (2) to furnish input information to the plant's automatic shutdown system.

Although the first core will contain in-core neutron-flux monitors to obtain experimental information, it is not planned to include such devices in subsequent cores. The first-core installation consists of nine ionization chambers, placed at three radial locations in three superheater process tubes that contain no fuel. At each of the three radial locations, chambers will be placed at three axial positions. Readout instrumentation provides for the simultaneous reading or recording of information from any three of the nine chambers.

Control-rod withdrawal rate, in./min (only one rod may be withdrawn at a time)	
Outer eight boiler rods	72
Inner eight boiler rods	26
Superheater rods	72
Reactivity insertion rate, any single rod, cents/sec	5
Recirculation flow	
Maximum rate of change, gal/min/sec	455
Equivalent rod-withdrawal reactivity insertion, cents/sec	5
Boron-injection system	
Solution	12½% disodium octaborate tetrahydrate
Storage pressure and temperature	Atmospheric
Volume, gal	1000
Injection time for 1000 gal, min	18

Recirculation System

The reactor recirculation system consists of three loops, each containing a pump, two butterfly valves, and piping. The pumps, which provide the forced circulation of coolant and moderator required by the reactor plant, are vertical, mixed-flow units mounted on special structures that permit horizontal movement. This freedom of movement in the horizontal plane minimizes external forces on the pump casing due to thermal expansion of the piping. Bushing type shaft seals, with water injection, prevent leakage of the primary coolant to the

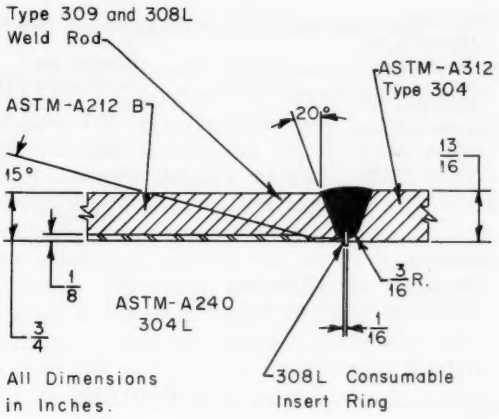

Fig. VIII-9 Transition joint in recirculation piping in the Pathfinder reactor.

atmosphere. Backup sealing is provided by mechanical, spring-loaded face seals and labyrinth bushings on each shaft. Dual seal-injection pumps are provided, with automatic transfer from one pump to the other.

A butterfly valve is located at the suction and another at the discharge of each recirculation pump. The stainless-steel valves, rated for a 50-psi maximum differential pressure across the disk, employ stuffing-box shaft seals. Both the suction and the discharge valves can be closed during shutdown to permit isolation of a recirculation pump for maintenance.

The recirculation piping includes both solid-stainless-steel pipe and stainless-clad carbon-steel pipe. The transition from the stainless pipe to the carbon pipe is accomplished by machining a 15° taper on the end of the clad pipe and then overlaying this taper with stainless steel. The joint is illustrated in Fig. VIII-9.

Recirculation pumps	
Number	3 (one per loop)
Type	Vertical, mixed flow
Nozzle diameter, in.	
Suction	22
Discharge	22
Rated flow each, gal/min	21,600
Developed head at rated flow, ft	71
Drive motor	
Type	600 rpm induction
Power requirements	400 hp, 2300 volt, 3 phase
Butterfly valves	
Number	6 (two per loop)
Pressure rating, psig	700
Maximum ΔP across disk, psi	50
Drives	Electric motors
Piping	
Outside diameter, in.	
Reactor to pumps	22
Pumps to reactor	22
Minimum fundamental natural frequency of piping loops	1.5 × pump rpm

Turbine-Generator, Condensate, and Feedwater Systems

Superheated steam flows from the reactor to the turbine through a single main line. The line is equipped with a motor-operated isolation valve which is located within the reactor building and which is tripped on scrams requiring isolation of the containment building. At the turbine the main steam line divides into two smaller lines, each of which is equipped with a turbine trip valve. Four bellows-sealed safety valves, installed on a common 10-in. header, are located in the main steam line between the reactor and the isolation valve. The safety valves discharge through flexible connections to a common 14-in. discharge line that connects to the condenser desuperheater pipe.

The turbine is a tandem-compound double-flow unit that utilizes special shaft seals supplied with nonradioactive sealing steam from a gland steam evaporator. The regular gland steam evaporator utilizes reactor steam to boil demineralized water, and an auxiliary gland steam generator, fired with oil or gas, is used during startup and shutdown and as a standby for the regular unit. The turbine supplies steam to four feedwater heaters as indicated in Fig. VIII-1.

The two-pass surface condenser is equipped with an oversized hot well that provides storage space for the water used to flood the reactor steam dome and superheater during shutdown. A desuperheater pipe, which is located above the hot well, accepts steam which is bypassed around the turbine or which is relieved through the reactor safety valves. Temperature of the bypassed or relieved steam is reduced in the desuperheater by condensate that is injected into the steam through spray nozzles. Condenser circulating water comes from the basin of a cross-flow induced-draft cooling tower, and makeup water for the cooling tower is pumped from the Big Sioux River.

After being drawn from the hot well by condensate pumps, the feedwater passes through three low-pressure heaters, a full-flow filter,

a feed pump, and a high-pressure heater. A parallel arrangement is employed for all pumps and filters, and, since each unit is sized for full normal flow, a standby is provided. Each feedwater heater is equipped with a bypass line. Makeup water is supplied to the condenser hot well from a demineralized-water storage tank.

An emergency shutdown condenser, cooled by shield-pool water, is used to condense reactor steam following a scram that requires isolation of the containment building.

Steam line	
Diameter, in.	16
Thickness	Schedule 60
Steel	A-335 grade P11
Insulation thickness, in.	5
Turbine-generator	
Speed, rpm	3600
Rating, Mw(e)	66
Generator	Direct-coupled hydrogen-cooled type
Condenser	
Design heat load, 10^6 Btu/hr	435
Vacuum for design heat load, in. Hg	28.5

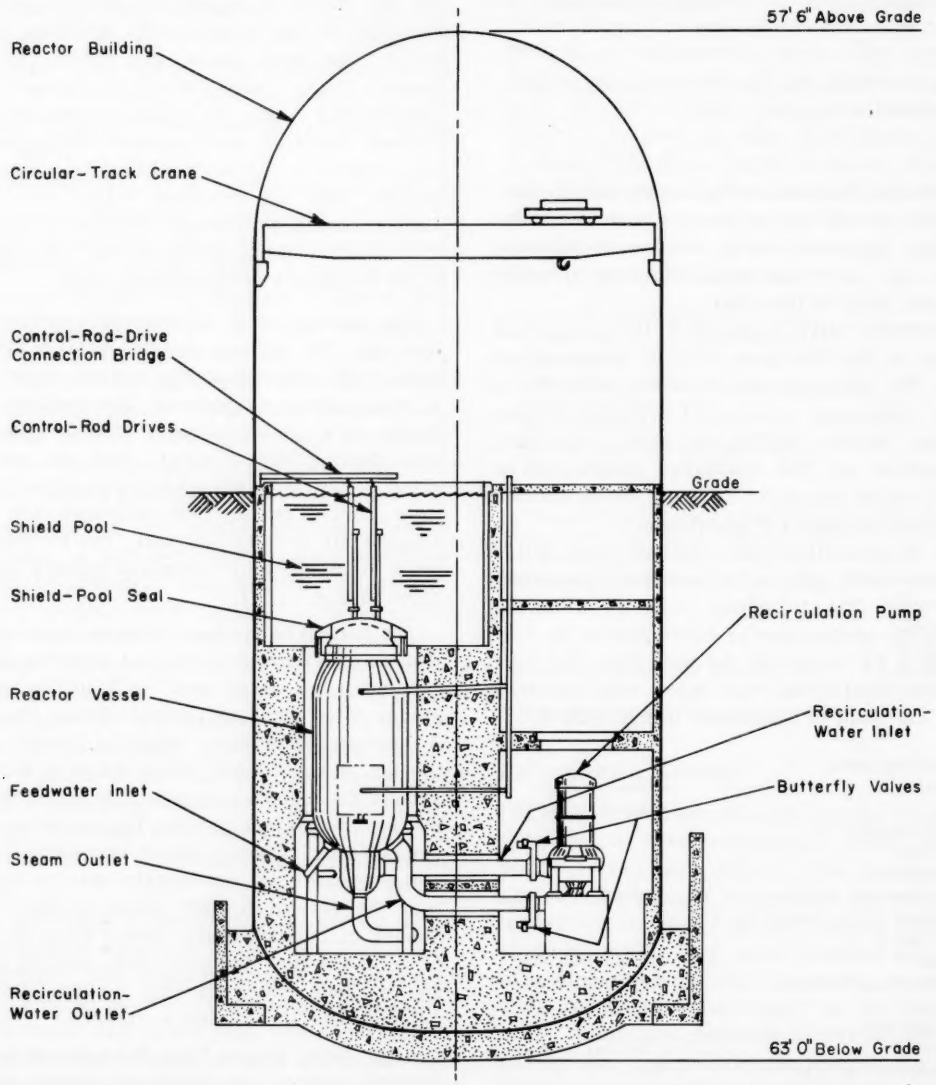

Fig. VIII-10 Vertical section through the containment building of the Pathfinder Atomic Power Plant.

Plant Arrangement and Containment

The reactor and recirculation system are enclosed in a cylindrical containment vessel. Figure VIII-10, a vertical section through the containment vessel, and Fig. VIII-11, a horizontal section through the plant, illustrate the arrangement of the major components. Access to the containment is through a normal airlock, an emergency airlock, or an 11-ft-diameter circular equipment door that is bolted and sealed to the shell. Approximately the bottom half of the reactor containment vessel is below grade: the upper half of the vessel is insulated on its outside down to an elevation 5 ft below ground level.

Containment vessel	
Shape	Cylindrical, with hemispherical top and ellipsoidal bottom
Inside diameter, ft	50
Inside height, ft	120.5
Height of cylindrical section, ft	83
Height of portion below grade, ft	63
Material	Carbon steel
Thickness, in.	
Top	$\frac{11}{16}$
Walls and bottom	$1\frac{3}{8}$
Design internal pressure, psig	78
Maximum leakage rate at design pressure, % of contained volume per day	0.2

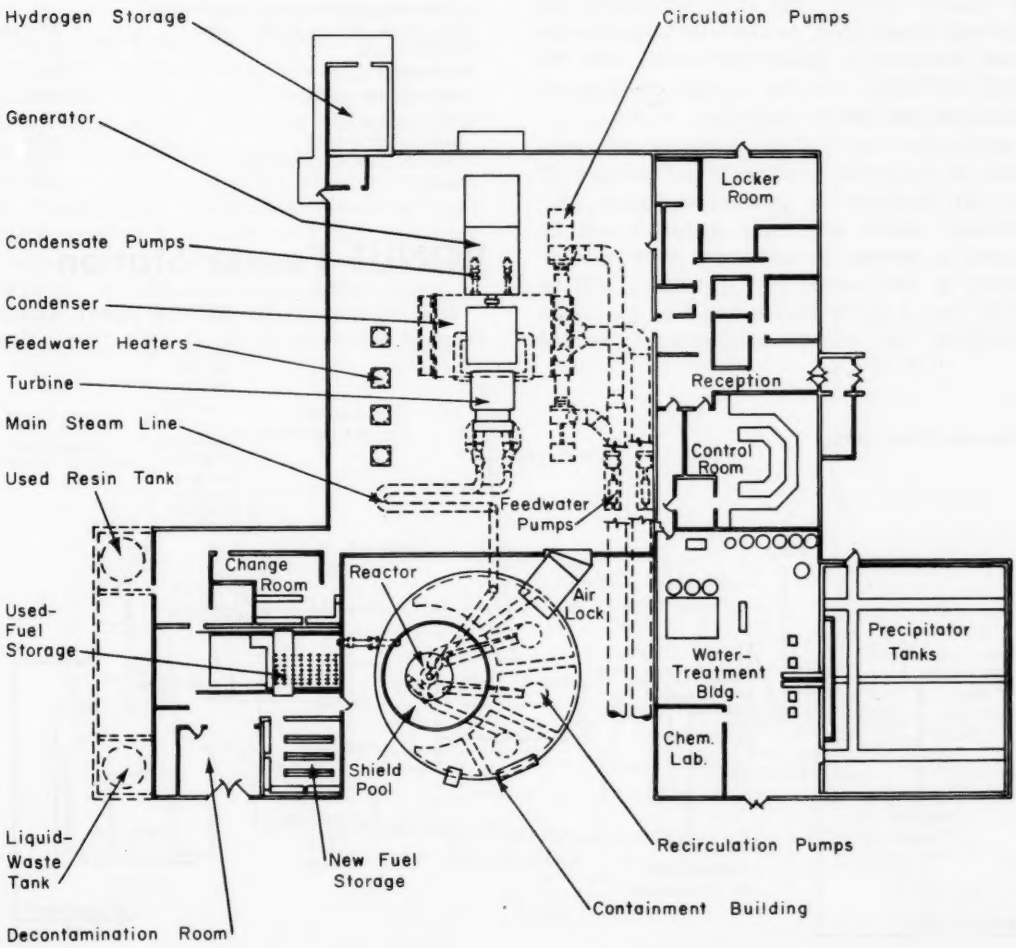

Fig. VIII-11 Horizontal section of the Pathfinder Atomic Power Plant.

Purification and Radioactive Waste Disposal

Noncondensable radioactive gases, which originate in the reactor, pass with the steam to the main condenser where they are removed by air ejectors. The oxygen and hydrogen formed by dissociation of water in the reactor are passed through a catalytic recombiner located after the second-stage nozzle of the air ejector, as shown in Fig. VIII-12. The discharged gas stream from the recombiner is passed through a shielded holdup pipe that provides decay time for short-lived radioactive nuclides. The gases are then moved by a compressor through a baffled holdup tank that provides additional decay time, thence through a filter, and finally to the plant stack. Ventilation air from the area around the reactor proper, and from equipment and tank-vent discharges, is also discharged to the stack. Radioactive gases introduced into the stack are mixed with the normal containment ventilation flow before discharge.

Radioactive solid-waste material will generally be collected, packaged, and shipped off site for disposal or processing. Spent ion-exchange resins and filter material will be sluiced to storage tanks where, after concentrating by sedimentation, the wastes will be stored for a decay period and then placed in containers for off-site shipment. Estimated quantities of solid waste are shown in the tabulation below.

Radioactive liquid wastes will be processed by filtration, demineralization, sedimentation, decay, and/or dilution. After processing has reduced radioactivity levels to acceptable values, the processed water will be returned to its system for reuse or will be discharged to the river. The capacities of tanks in the liquid-waste systems are given in the following tabulation:

Plant stack	
Height above grade, ft	107
Minimum flow during operation, cfm	25,000
Estimated quantities of solid wastes	
Combustible wastes, lb/year	10,000
Noncombustible wastes, lb/year	2000
Filter cartridges, lb/year	1000
Spent resins, cu ft/year	350
Filter backwash materials, lb/year	1000
Liquid-waste system tank capacities, gal	
Four tanks for low solids holdup	3000 each
Waste surge	1000
Reclaimed water	3000
Neutralizing holdup	300
Neutralizing tank	1500
High-solids holdup	2000
Concentrated waste storage	2000
Sumps	7200

BONUS Power Station

The reactor of the BONUS power station[3] reached criticality in April 1964. The follow-

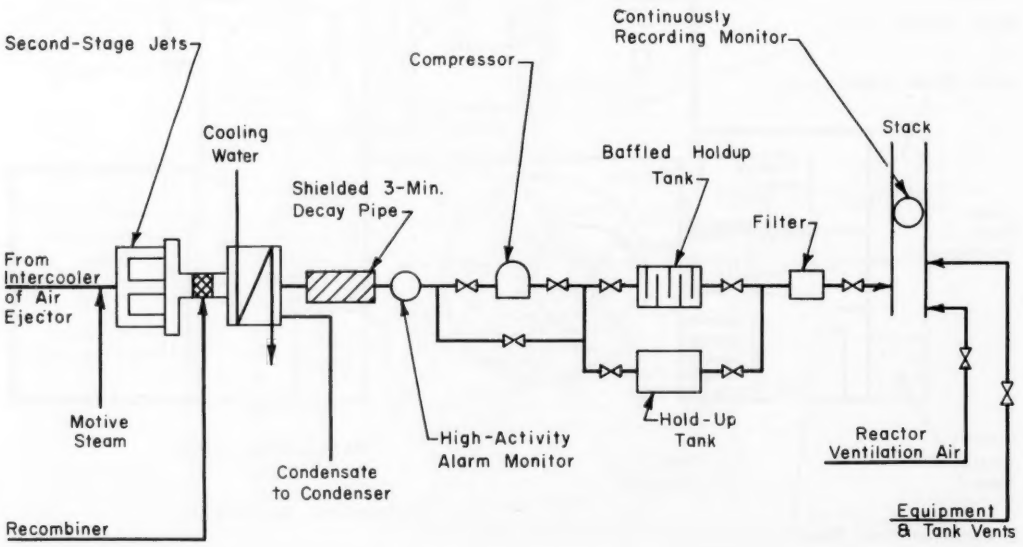

Fig. VIII-12 Gaseous waste-disposal system of the Pathfinder Atomic Power Plant.

ing material on BONUS is presented, for the reader's convenience, in the same general format as in the above description of the Pathfinder plant. Another review, in considerably less detail, appeared in *Power Reactor Technology*, 3(4): 68-74.

The BONUS plant, a joint construction project of the Puerto Rico Water Resources Authority (PRWRA) and the USAEC, is located at Punta Higuera, near Rincon, P. R. It was designed by the General Nuclear Engineering Corporation and PRWRA. Its operation, after testing, will be the responsibility of the PRWRA.

The two-region core of the reactor consists of a central boiler region and a peripheral superheater region. Superheated steam produced in the reactor is fed directly to a condensing steam turbine, and feedwater from the condensate system is returned to the reactor vessel, where it mixes with the reactor recirculating water. Recirculation loops located external to the reactor vessel provide forced coolant flow through the boiler region of the core. The Zircaloy-2-clad boiler fuel elements contain natural or slightly enriched uranium dioxide. The Inconel-clad superheater elements also contain uranium dioxide but of a slightly higher enrichment. The entire power plant is housed in a large, low-pressure containment vessel.

A simplified flow diagram of the plant is given in Fig. VIII-13, and the following are the principal characteristics:

Power, boiler region, kw	37,000
Power, superheater region, kw	13,000
Total core power, kw	50,000
Gross electrical capability, kw	17,500
Net electrical output, kw	16,500
Net efficiency, %	33
Steam outlet pressure, psig	865
Reactor operating pressure, psig	950
Temperature, boiler region, °F	540
Outlet temperature, superheater region, °F	900
Reactor steam flow at rated power (approximate), lb/hr	152,000
Recirculation rate, gal/min	8660
Containment-vessel size, ft	Hemisphere on top of short cylinder, 167 (dia.)
Reactor vessel size, ft	7.5 (OD) by 27
Overall core dimensions, height and diameter, ft	4.55 by 4.83
Fuel, boiler region (Zircaloy-clad)	Natural and 2.4% enriched UO_2
Fuel, superheater region (Inconel-clad)	3.25% enriched UO_2
Fuel loading, boiler region, kg ^{235}U	61.2
Fuel loading, superheater region, kg ^{235}U	52.8
Average heat flux, boiler region, Btu/(hr)(sq ft)	106,000
Average heat flux, superheater region Btu/(hr)(sq ft)	66,000
Maximum heat flux, boiler region, Btu/(hr)(sq ft)	367,000
Maximum heat flux, superheater region, Btu/(hr)(sq ft)	201,000

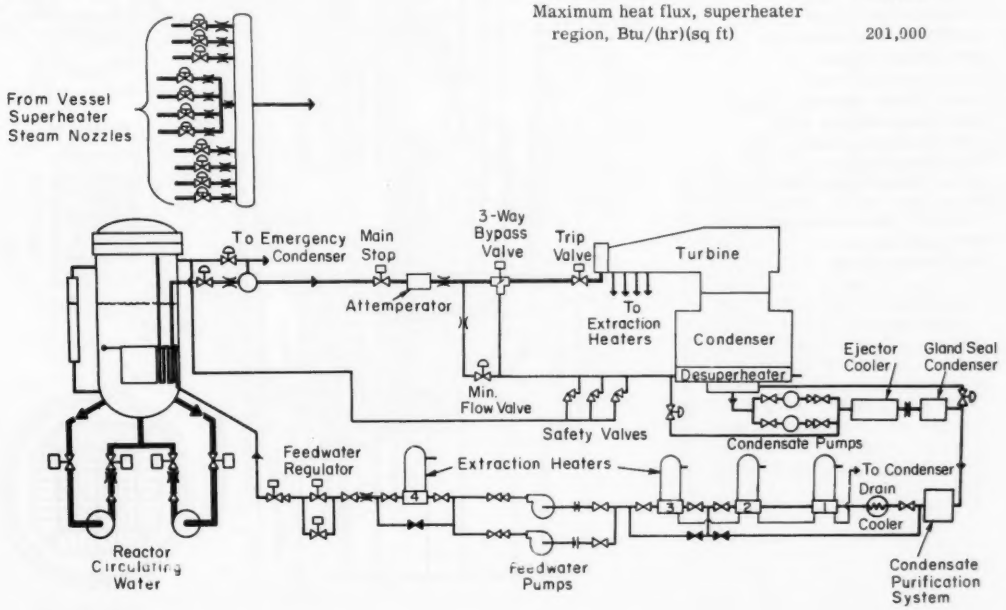

Fig VIII-13 Simplified flow diagram, BONUS power station.

General Reactor Features

The arrangement of the major reactor components and the locations of piping connections to the pressure vessel are shown in Figs. VIII-14 and VIII-15. Recirculation water enters the reactor vessel through a bottom central nozzle and flows upward within the vessel to enter the bottom of the boiler fuel assemblies. The slightly subcooled water is heated as it progresses upward through the boiler assemblies, and a net steam generation occurs. The steam-water mixture formed in the boiler fuel assemblies continues to move upward after it leaves the active core region and passes through the cells of the eggcrate superstructure. At the steam-water interface and in the steam dome above the interface, gravitational separation of water and steam takes place. The water then passes downward through the annular down-

1 Control-Rod Actuator Assembly
2 Closure Head
3 Boiler Spray
4 Steam-Dryer Preheater Assembly
5 Upper Emergency Cooling Pipe
6 Center Emergency Cooling Pipe
7 Superheater Outlet Connector Pipe
8 Superheater Inlet Connector Pipe
9 Reactor Vessel
10 Core Structure
11 Boiler Fuel Holddown Assembly
12 Thermal Shield
13 Boiler Fuel Assembly
14 Feedwater Spray Ring
15 Cruciform Control Rod (2 thru 9)
16 Superheater Fuel Assembly
17 Core Support Barrel
18 Boron Injection Pipe
19 Charpy Impact Specimen Holder
20 Core-Support-Barrel Shim
21 Lower Emergency Cooling Pipe
22 Slab Control Rod
23 Boiler Superheater Shim
24 Boiler Shim
25 Cruciform Control Rod No.1
26 Neutron Source
27 Superheater Shim

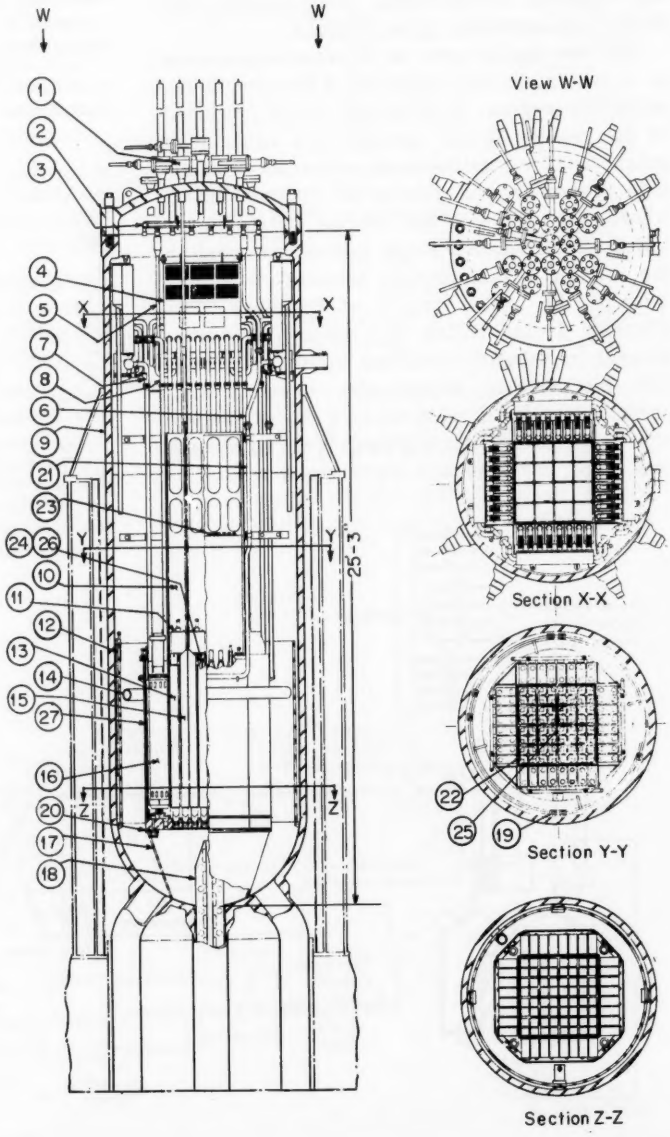

Fig. VIII-14 Pressure-vessel cross sections of the BONUS reactor.

comer region between the reactor core and the pressure-vessel wall, where it mixes with the feedwater. The recirculation flow, consisting of the downcomer and feedwater flows, then leaves the pressure vessel through two outlet pipes. The steam, which still contains traces of water, passes through dryer/preheater units located near the top of the reactor vessel, after which it enters individual superheater inlet pipes. It then flows downward through these individual pipes to the superheater fuel assemblies that are at the elevation of the active core. The steam passes through the superheater fuel assemblies and then returns, through individual superheater-assembly outlet pipes, to the upper portion of the pressure vessel. It is then fed from the outlet pipes to collection headers, from which several small pipes leave the reactor vessel through superheated-steam outlet nozzles.

The boiler region of the core contains 64 fuel assemblies, each about $4\frac{1}{2}$ in. square by $5\frac{1}{2}$ ft long. The 32 fuel assemblies of the superheater region are arranged in 4 groups of 8 assemblies each around the square boiler region of the core. Reactor power level is controlled by a system of control rods that are located in the boiler region and in the space between the

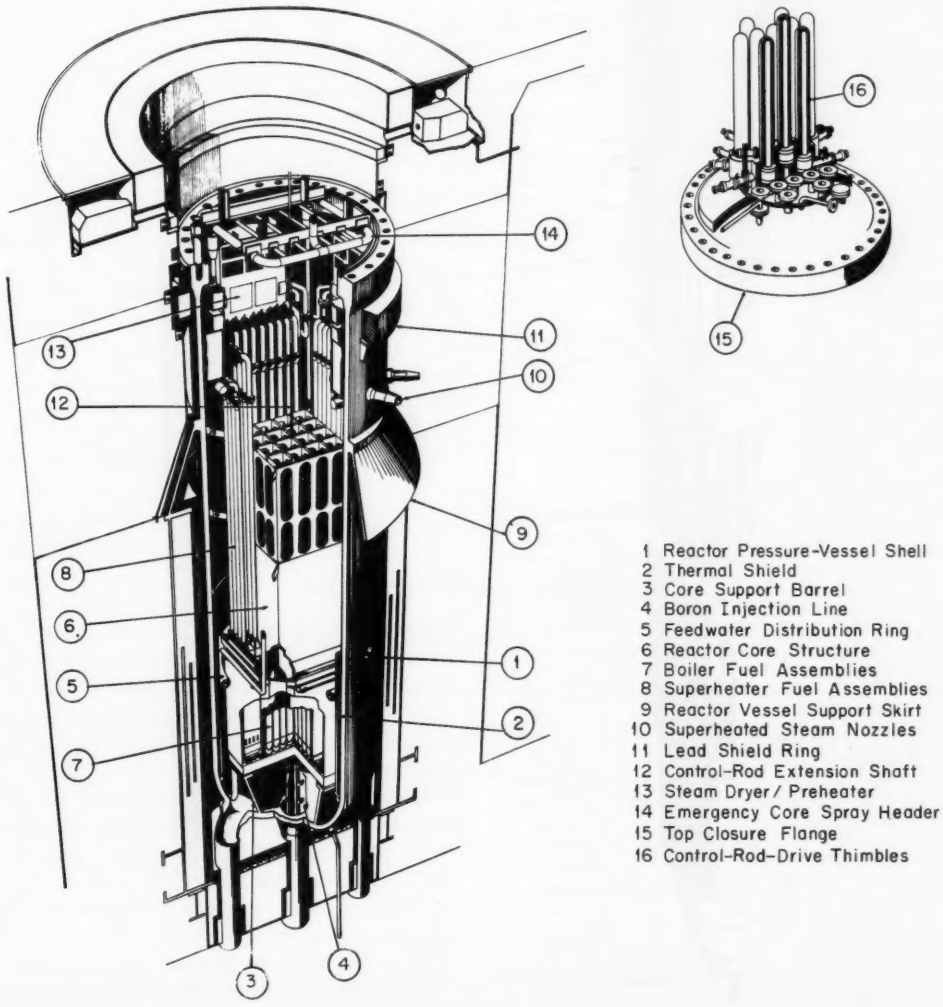
1 Reactor Pressure-Vessel Shell
2 Thermal Shield
3 Core Support Barrel
4 Boron Injection Line
5 Feedwater Distribution Ring
6 Reactor Core Structure
7 Boiler Fuel Assemblies
8 Superheater Fuel Assemblies
9 Reactor Vessel Support Skirt
10 Superheated Steam Nozzles
11 Lead Shield Ring
12 Control-Rod Extension Shaft
13 Steam Dryer/ Preheater
14 Emergency Core Spray Header
15 Top Closure Flange
16 Control-Rod-Drive Thimbles

Fig. VIII-15 Perspective view of pressure vessel and internals of the BONUS reactor.

boiler and superheater regions. The rods are top-driven, and their actuators are mounted on the reactor vessel head.

The reactor vessel is carbon steel and is clad internally with stainless steel; the major internal structural members and the recirculation piping are stainless steel.

Boiler Fuel

A boiler fuel assembly and a boiler fuel rod are shown in perspective in Fig. VIII-16, and horizontal cross sections through the rod and the assembly are given in Fig. VIII-17. Each assembly consists of a square Zircaloy-2 outer box, stainless-steel top and bottom end fittings, and two bundles of Zircaloy-clad fuel rods. The two bundles of rods are placed one on top of the other inside the Zircaloy-2 outer box, and each bundle consists of an inner and an outer Zircaloy-2 grid plate, a central square Zircaloy-2 tube, and 32 Zircaloy-clad fuel rods that contain the UO_2 fuel. The inner grid plates are those which occupy positions nearer the

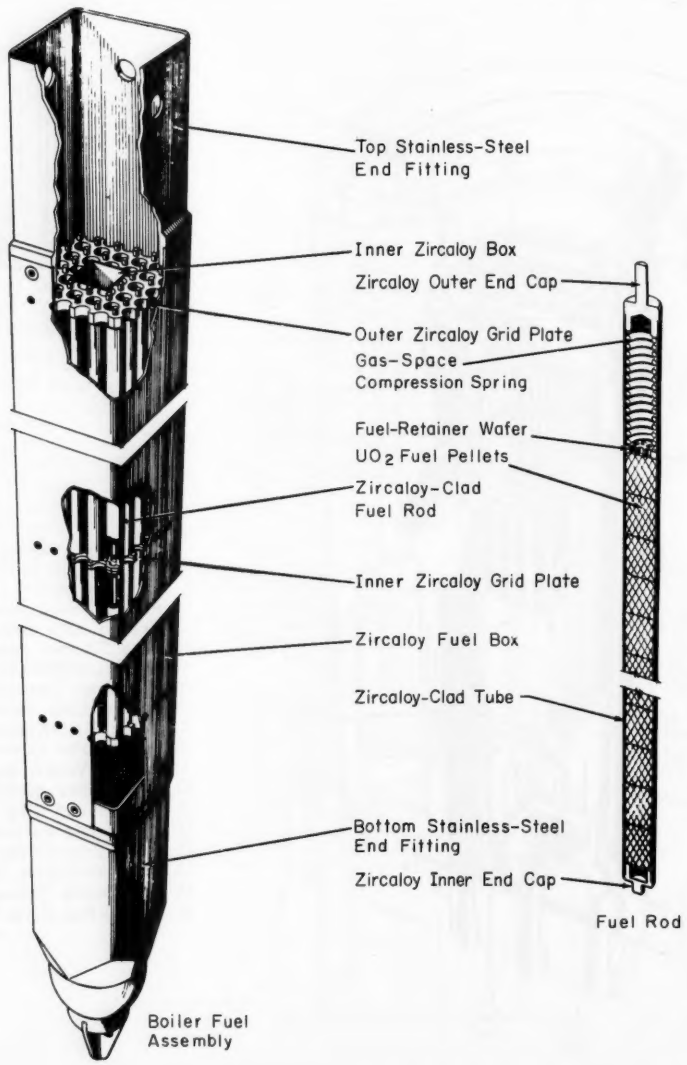

Fig. VIII-16 Perspective view of boiler fuel assembly of the BONUS reactor.

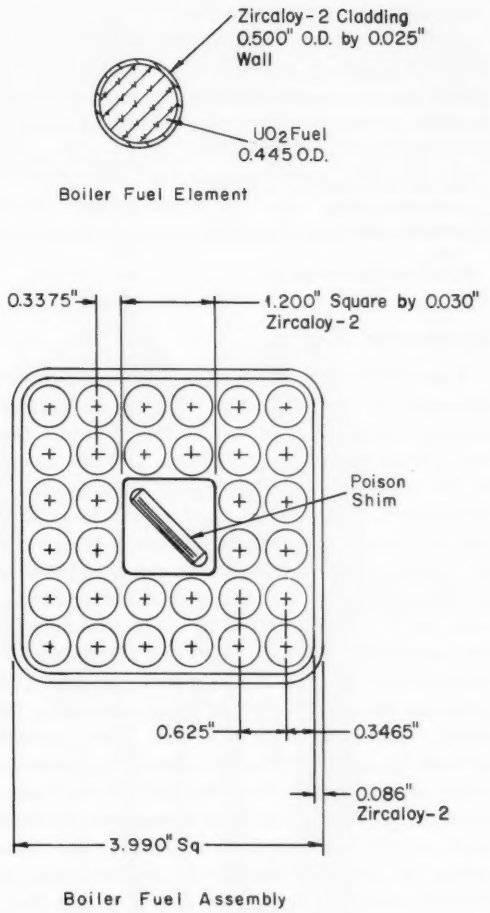

Fig. VIII-17 Boiler fuel-assembly cross sections of the BONUS reactor.

vertical midpoint of the fuel assembly, and the outer grid plates are those which are located at the top and bottom of the fuel assembly. The fuel rod shown in Fig. VIII-16 is in the vertical orientation of those rods which comprise the upper bundle. In the lower bundle the end of the fuel rod which contains the internal spring would be located at the bottom of the bundle. The fuel rods in each bundle are welded at their inner end caps to their inner grids. The inner grids as well as the outer grids of each bundle are welded to the fuel-assembly outer box, but the fuel rods are not welded to their outer grid plates; consequently the outer grid plates provide only radial spacing of the fuel rods, and the rods are free to expand axially to accommodate differential thermal growth. The upper-bundle rods expand upward, whereas the lower-bundle rods expand downward from the center of the boiler fuel assembly.

The fuel rods are arranged in 6 by 6 square lattice with the four central rods removed. This nonfueled axial region along the center line of the fuel assembly is occupied by a central Zircaloy box. The volume inside the central box is occupied by water that enters the region through an orifice at the inlet end of the bottom fuel bundle. The flow to the region is sufficient to prevent formation of steam by gamma and neutron heating. The central-box region can also contain removable poison shims that are used for axial and radial shaping of the power pattern in the boiling zone.

Boiler-region-component specifications and performance data are given in the following table.

Boiler core region	
Size and geometry of active core, in.	35.4 square by 54.6 high
Effective outside diameter, ft	3.34
Moderator and reflector material	H_2O
Structural metal within active core	Zircaloy-2
Fuel material	UO_2, sintered pellets
Number of fuel assemblies	64
Fuel loading, tons uranium element	2.81
Initial fuel enrichment, wt.% ^{235}U	0.71 (natural U) in four central assemblies; 2.4 in remaining 60 assemblies
Average specific power, Mw(t)/ton uranium element	13.2
Average region power density, kw(t)/liter of region	33.6
H_2O/UO_2 volume ratio (without control rods; superheater unflooded)	2.4
Total steam flow from coolant channels, lb/hr	143,000
Total steam flow from moderator, lb/hr	9000
Total water flow to coolant channels, lb/hr	3.226×10^6
Total water flow to moderator, lb/hr	134,000
Total water flow to reactor vessel, lb/hr	3.360×10^6
Volume composition of active core, %	
Water moderator other than coolant	25.2
UO_2 fuel	25.4
Coolant, steam-water	35.1
Structural metal, Zircaloy-2	7.6
Fuel cladding, Zircaloy-2	6.1
Helium fuel-to-cladding thermal bond	0.6

Boiler fuel assembly	
Fuel elements per assembly	32
Fuel-element pitch, in.	0.625
Assembly structural material	Zircaloy-2
Assembly-can outside dimensions, in.	3.990 square
Can wall thickness, in.	0.086
Central-moderator tube	Square
Moderator-tube outside dimensions, in.	1.200 by 1.200
Moderator-tube wall thickness, in.	0.030
Fuel-cladding outside diameter, in.	0.500
Boiler fuel element	
Element type	Rod, segmented
Fuel type	UO_2, sintered pellets
Total length of fuel, in.	54.0
Fuel length per rod segment, in.	27.0
Fuel-cladding material	Zircaloy-2
Fuel-cladding outside diameter, in.	0.500
Fuel-cladding thickness, in.	0.025
Fuel-to-cladding thermal bond	Helium
Thermal bond thickness, in.	0.0025
UO_2 fuel-pellet diameter, in.	0.445
Boiler heat transfer and fluid flow	
Net heat generation in fuel at 100% full power, Mw(t)	37.0
Heat loss to moderator by gamma and neutron radiation, Mw(t)	0.44
Heat transferred through fuel cladding, Mw(t)	36.3
Net heat transferred to moderator, Mw(t)	0.7
Average heat flux, Btu/(hr)(sq ft)	106,000
Maximum heat flux, Btu/(hr)(sq ft)	367,000
Burnout heat flux, Btu/(hr)(sq ft)	>750,000
Nominal operating pressure, psig	950 (exit)
Water saturation temperature, °F	540
Coolant exit temperature, °F	540
Coolant inlet temperature, °F	532
Feedwater temperature, °F	354
Inlet subcooling, °F	8
Inlet subcooling, Btu/lb	9.8
Average inlet velocity in coolant channels, water, ft/sec	6.3
Average exit velocity in coolant channels, water, ft/sec	9.3
Maximum exit velocity in coolant channels, water, ft/sec	16.0
Maximum fuel-cladding temp., °F	650
Fuel-cladding melting point, °F	3350
Maximum UO_2 fuel centerline temp., °F	4140
Maximum UO_2 fuel surface temperature, °F	1040
Average UO_2 fuel temperature over region, °F	1200
UO_2 fuel melting point, °F	5000
Fraction of total active coolant-channel height in boiling	0.80
Fraction of water-coolant-channel volume in total water of region	0.58
Average steam volume fraction in total water of region	0.147
Average steam volume fraction over total active height of coolant channels	0.23
Average steam volume fraction in boiling section of coolant channels	0.28
Average steam volume fraction at exit of coolant channels	0.42
Maximum steam volume fraction at exit of coolant channels	0.450
Average exit steam volume fraction in total water of region	0.290
Average steam quality at exit of coolant channels	0.0443
Minimum inlet operating pressure, psig	950
Region pressure drop, psi	8.4

Superheater Fuel

A perspective drawing of the superheater fuel assembly is given as Fig. VIII-18, and cross-section dimensions of the assembly and a fuel rod are shown in Fig. VIII-19. Overall height of the assembly, including the standpipes and connectors, is 18 ft 8 in., and its total weight is 325 lb. Steam makes four passes in traversing the superheater assembly, so the flow velocity is relatively high and the heat-transfer coefficient is relatively good. Steam is channeled to the assembly through the inlet standpipe and commences its first pass through the assembly from the top. At the bottom of the assembly, the steam reverses direction and flows upward through the second-pass fuel elements, reverses again at the top of the assembly, flows downward through the third-pass elements, reverses again at the bottom of the assembly, and completes its passage through the fueled region by flowing upward through the fourth-, and final, pass elements to the outlet standpipe. Each of the four passes in an individual fuel assembly contains eight superheater fuel rods spaced in two clusters of four each, as shown in Fig. VIII-19. The standpipes are equpped with connectors that permit the fueled portion of the assembly to be uncoupled, rotated 180°, and recoupled, thereby reversing the position of the individual fuel rods relative to the radial power distribution and permitting a more nearly uniform burnup of the fuel.

The basic flow channels in the superheater assembly are formed by stainless-steel pressure tubes that are brazed to top and bottom tube-sheet structures. The stainless-steel castings that form the top and bottom tube-sheet assemblies are similar in design except for the number and location of pass-divider walls. The lower tube sheet has a single, split-wall pass divider that separates the crossover plenum for the first and second passes from the cross-

over plenum of the last two passes. The upper tube sheet has two divider walls that separate the inlet and outlet connection plenums from the crossover plenum between the second and third passes. Each plenum in the assembly is lined with a thin-walled member that prevents contact between the superheated steam and the relatively cool walls of the tube-sheet structure. The space between the liner and the structural walls is filled with stagnant steam and acts as an insulator to reduce heat losses to the moderator. The liners slide over the coolant tubes to accommodate differential expansion. The tube portion of the superheater fuel assembly is enclosed by a protective Zircaloy-2 shroud.

The basic fuel element of the superheater assembly consists of a clad fuel rod, formed from cylindrical pellets of UO_2, and a concen-

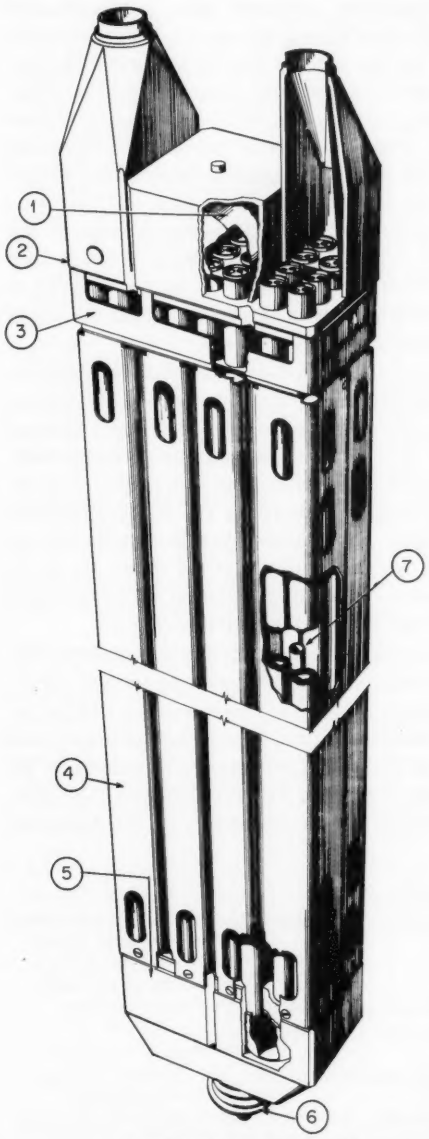

Superheater Fuel Assembly

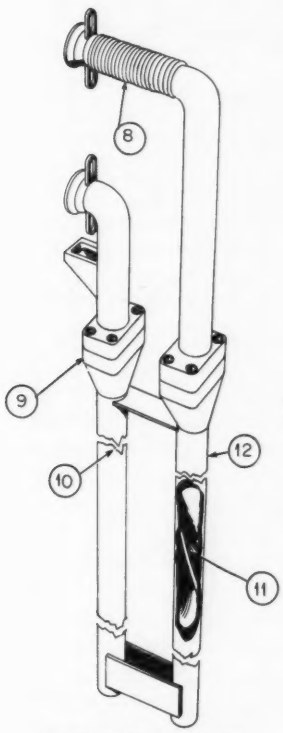

Superheater Standpipes & Connectors

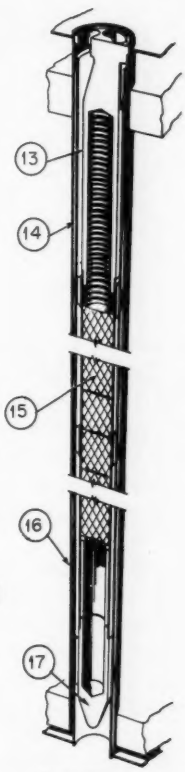

Superheater Fuel Element

1 Pass Crossover Flow Liner
2 Upper Tube Sheet
3 Emergency Spray Pan
4 Protective Shroud
5 Lower Tube Sheet
6 Support Spring
7 Tube Support Ferrules
8 Extension Bellows
9 Connectors for Rotating Fuel Assembly
10 Superheated-Steam Outlet Standpipe
11 Steel Radiation Shield
12 Saturated-Steam Inlet Standpipe
13 Upper End Cap
14 Coolant Tube
15 Fuel Pellet
16 Pressure Tube
17 Lower End Cap

Fig. VIII-18 Perspective view of superheater fuel assembly of the BONUS reactor.

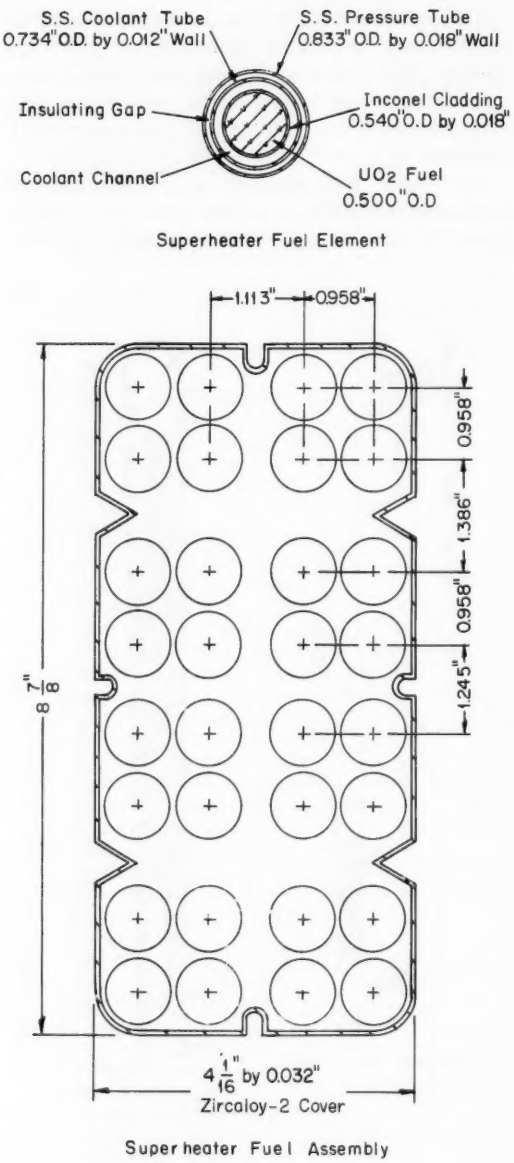

Fig. VIII-19 Superheater fuel-assembly details, BONUS reactor.

tric coolant tube that forms an annular flow channel. The pellets are concave at each end to permit thermal growth of the central, hottest zone of the pellet relative to the cooler, cladding-restrained surface. Fission-gas space is provided at each end of the fueled portion of the rod between the last pellet and the welded end closure.

The coolant tube, which forms the flow annulus around the superheater rod, is welded to the top end closure of the rod. Radial positioning of the coolant tube relative to the fuel rod is accomplished by four spacer rings with radial guides that are brazed to the fuel cladding and by similar type radial lugs that are cast integral with the bottom closure of the rod. The coolant tube is not affixed to these radial guides.

Each fuel element is brazed to its superheater-assembly pressure tube at the top, and four split-ring spring spacers are brazed to the outside of the coolant tube to maintain concentricity between the fuel element and the pressure tube. The space between the coolant tube and the pressure tube is occupied by stagnant steam that acts as insulation between the superheated steam within the flow tube and the saturated moderator water on the outside of the pressure tube. Thermal expansion of the coolant tube and fuel tube relative to each other and to the pressure tube is downward from the top of the assembly.

Both the saturated-steam inlet and superheated-steam outlet pipes, which are welded to the top tube-sheet structure of the fuel assembly, are concentric-tube units that contain radiation shield plugs within the inner tube. The insulating steam gap between the concentric tubes of the inlet and outlet pipes is maintained by spacers that are welded to the inner, or liner, tube, which, in turn, is welded at its midpoint to the outer tube of the assembly.

Differential expansion of the superheater assembly relative to the pressure vessel is accommodated by the spring mounting that is integral with the bottom tube-sheet assembly and by the deflection of an expansion bellows in the horizontal leg of the saturated-steam inlet line.

Superheater data are given in the following table:

Superheater core region	
Size and geometry of active core	Four slabs adjacent to boiler region; 35.2 in. by 9.8 in. by 54.6 in. each
Effective outside diameter, ft	4.83
Moderator and reflector material	H_2O
Structural metal within active core	Inconel, S.S. and Zircaloy-2
Fuel material	UO_2, sintered pellets
Number of fuel assemblies	32
Fuel loading, tons of uranium element	1.79
Initial fuel enrichment, wt.% ^{235}U	3.25

Average specific power, Mw(t)/ton of uranium element	7.25
Average region power density, kw(t)/liter of region	11.5
H_2O/UO_2 volume ratio (without control rods; superheater unflooded)	3.85
Total steam flow from coolant channels, lb/hr	152,000
Total steam flow from moderator, lb/hr	9000
Approximate volume composition of active core, %	
Water moderator other than coolant	58
UO_2 fuel	15
Coolant, steam	13
Steam insulation	6
Structural metal	2 Zircaloy-2; 5 S.S.
Fuel cladding	2 Inconel
Superheater fuel assembly	
Fuel elements per assembly	32
Fuel-element pitch, in.	0.958
Assembly structural material	Type 348 S.S.
Assembly-can outside dimensions, in.	8.87 by 4.05
Can wall thickness, in.	0.032
Thermal insulation within assembly	Stagnant steam
Composition of pressure and coolant tubes	Type 348 S.S.
Pressure tube outside diameter, in.	0.833
Pressure tube inside diameter, in.	0.797
Thickness of steam insulation annulus, in.	0.0315
Coolant tube outside diameter, in.	0.734
Coolant tube inside diameter, in.	0.710
Fuel cladding outside diameter, in.	0.540
Thickness of steam coolant annulus, in.	0.089
Superheater fuel element	
Element type	Full length
Fuel type	UO_2, sintered pellets
Total length of fuel, in.	54.6
Fuel length per rod segment, in.	54.6
Fuel cladding material	Inconel 600
Fuel cladding outside diameter, in.	0.540
Fuel cladding thickness, in.	0.018
UO_2 fuel-pellet diameter, in.	0.500
Superheater heat transfer, fluid flow	
Net heat generation in fuel at 100% full power, Mw(t)	13.0
Heat loss to moderator by gamma and neutron radiation, Mw(t)	0.50
Heat transferred through fuel cladding, Mw(t)	13.0
Insulation heat loss to moderator from coolant, Mw(t)	0.9
Net heat transferred to coolant, Mw(t)	11.6
Net heat transferred to moderator, Mw(t)	1.4
Average heat flux, Btu/(hr)(sq ft)	66,000
Maximum heat flux, Btu/(hr)(sq ft)	201,000
Nominal operating pressure, inlet, psig	950
Water-saturation temperature, °F	540
Coolant exit temperature, °F	900
Coolant inlet temperature, °F	540
Average inlet velocity in coolant channels, steam, ft/sec	76.0
Average exit velocity in coolant channels, steam, ft/sec	122
Maximum exit velocity in coolant channels, steam, ft/sec	145
Maximum fuel cladding temperature, °F	1175
Maximum UO_2 fuel centerline temperature., °F	3160
Maximum UO_2 fuel surface temperature, °F	1300
Average UO_2 fuel temperature over region, °F	1400
UO_2 fuel melting point, °F	5000
Region pressure drop, psi	79.3

Control Elements

Reactivity control elements in the BONUS core include cruciform control rods located in the boiler region, slab control rods in the space between the boiler and superheater regions, boiler poison shims, boiler-superheater poison shims, and, possibly, superheater poison shims. In addition, the four natural-uranium boiler fuel assemblies located at the center of the core serve as rather massive elements which shim the reactivity and flatten the power.

The poison subassembly of the cruciform control rod consists of four thin, boron–stainless-steel angles that are spot welded together to form a member with a cruciform cross section. The cruciform poison section is joined to a cruciform guide shaft that in turn is welded to an extension shaft equipped with a disconnect fitting for the drive mechanism. In the fully inserted position, the cruciform control rods extend downward to a level 2 in. above the bottom of the fuel region. When fully withdrawn from the core, the rods extend downward to a point 3 in. above the top of the fuel region.

The slab control rods, which occupy channels located between the boiler and superheater regions of the core, are formed from boron–stainless-steel plate. The slab, which is stiffened by a tee reinforcement, is joined to a tee-section guide shaft. As with the cruciform rods, the guide shaft of the slab rod is joined to an extension shaft that has the lower half of the

drive-mechanism disconnect fitting at its upper end. Vertical disposition of the slab control rods relative to the active core region, in the fully inserted and the fully withdrawn positions, is the same as for the cruciform control rods.

The boiler shim assemblies are positioned diagonally inside the central boxes of the boiler fuel assemblies as shown in Fig. VIII-17. The shim assembly, shown in perspective in Fig. VIII-20*a*, is basically a holder of boron–stainless-steel strips. The assembly is designed so that different thicknesses and widths of shim strip may be accommodated in a standard mechanical unit. Consequently the shim loading

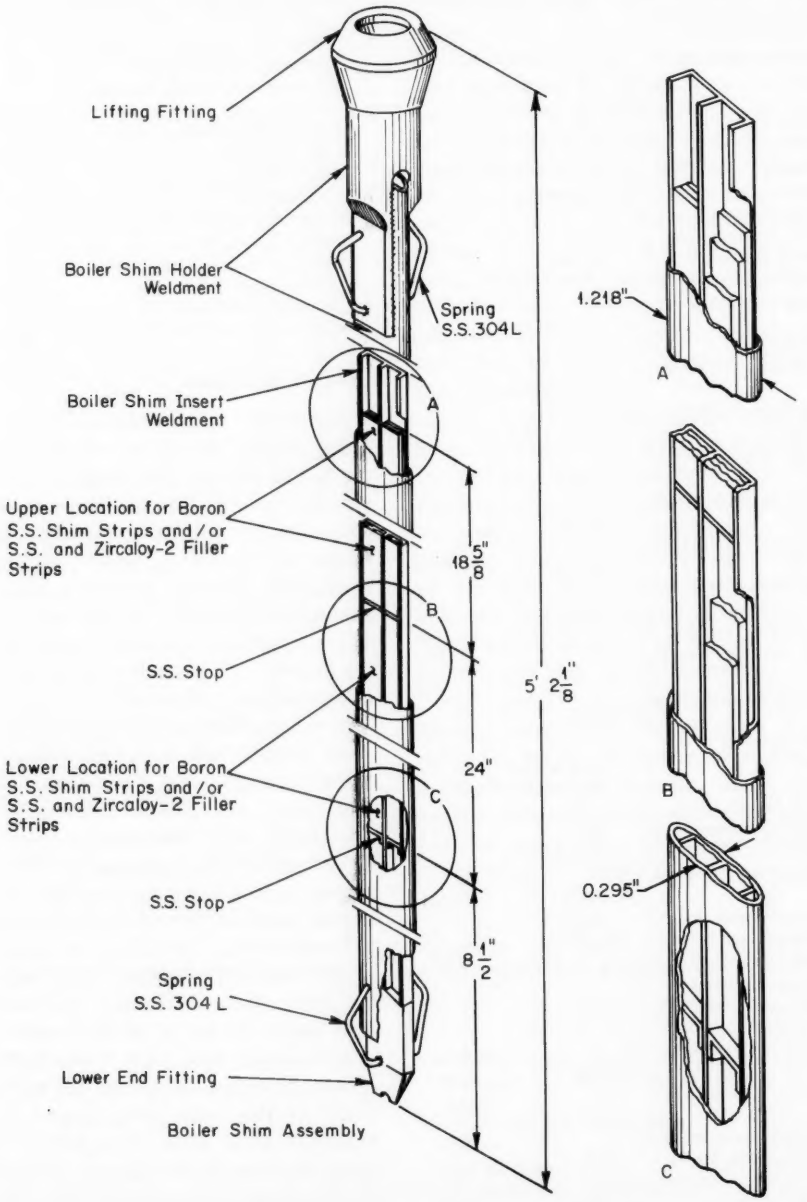

Fig. VIII-20*a* Boiler shim assembly of the BONUS reactor.

can be adjusted in fine steps to match closely the requirements for power shaping, etc.

The boiler-superheater shim assembly, shown in Fig. VIII-20*b*, is used to maintain the proper power distribution between the boiler and the superheater regions during the approach to equilibrium fuel cycle. As in the boiler shim assemblies, the poison strength of the assembly can be preselected by loading it with various combinations of shim strips.

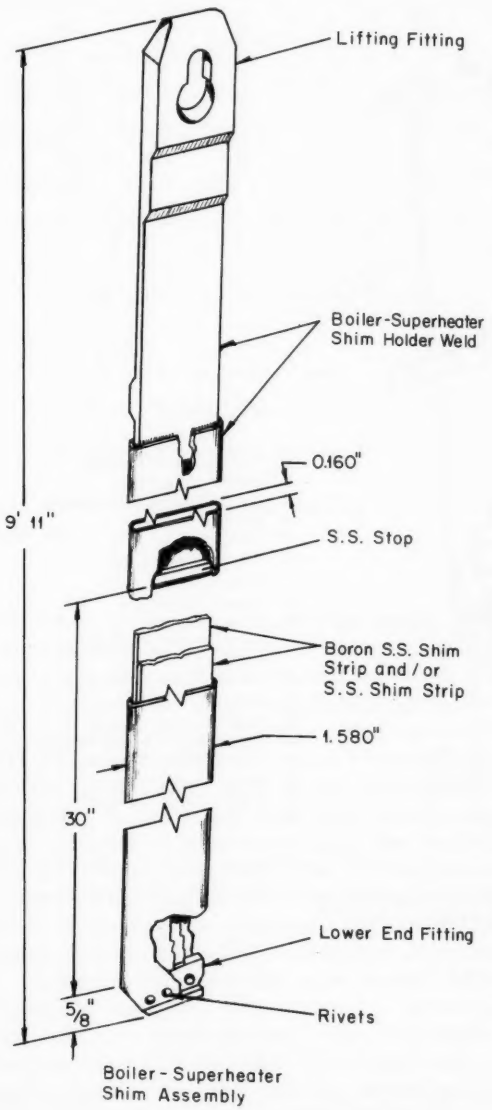

Fig. VIII-20*b* Boiler-superheater shim assembly of the BONUS reactor.

If it is necessary to decrease the power generation in the superheater fuel zone relative to power generation in the boiler fuel zone, superheater shim assemblies will be employed. The superheater shim assembly is a relatively simple piece, consisting of a boron–stainless-steel shim bar attached to a lifting fitting.

Boiler control rods	
Number	9
Number of drives	9
Shape	Cruciform
Material	1.09 wt.% enriched boron S.S. (92 wt.% ^{10}B)
Span, in.	$7\frac{3}{4}$
Blade thickness, in.	0.125
Poison length, in.	$62\frac{3}{8}$
Superheater control rods	
Number	8
Number of drives	8
Shape	Slab
Material	1.09 wt.% enriched boron S.S. (92 wt.% ^{10}B)
Span, in.	$14\frac{1}{4}$
Blade thickness, in.	0.125
Poison length, in.	$62\frac{3}{8}$
Boiler and boiler-superheater shims	
Poison material	1.25 wt.% natural boron S.S. or type 304L S.S.
Superheater shims	
Width, in.	1.0
Thickness, in.	$\frac{1}{2}$
Material	0.5 wt.% natural boron S.S.

Pressure Vessel and Core Structure

The BONUS reactor pressure vessel is a hollow right-circular cylinder with an integral lower head and a removable upper head. The structural material of the vessel is carbon steel, and a weld-overlaid stainless-steel inside lining provides long-term corrosion resistance. At the closure end of the vessel, where the clear opening is 6 ft 4 in. in diameter, the seal is effected by double, stainless-steel O-rings. Thirty-six $3\frac{1}{2}$-in.-diameter studs are used to secure the vessel top to the shell, and a leak-off connection is provided between the O-ring seal members to prevent leakage outside the vessel. The vessel is supported by a conical steel skirt welded to its outer wall. The skirt rests on a portion of the external shield and is welded to it to prevent lifting of the reactor vessel in the event of a primary-system rupture accident.

An internal thermal shield, consisting of a cylindrical piece of stainless steel, is supported

by brackets welded to the lower portions of the vessel wall. A unique feature in the BONUS reactor vessel is the arrangement in the superheated-steam outlet nozzles; the connecting steam piping not only extends outward from the nozzles but internal piping extends inward to the superheated-steam headers. The internal piping, which carries the superheated steam, is insulated from the nozzle forging by seven layers of stainless-steel foil. A summary of reactor-vessel data and a list of nozzles are given at the end of this section.

Figure VIII-21 is a perspective drawing of the reactor core structure. As shown in this figure and in Figs. VIII-14 and VIII-15, the load of the reactor core structure is transferred to the bottom of the reactor pressure vessel by a conical support barrel. This barrel, which is

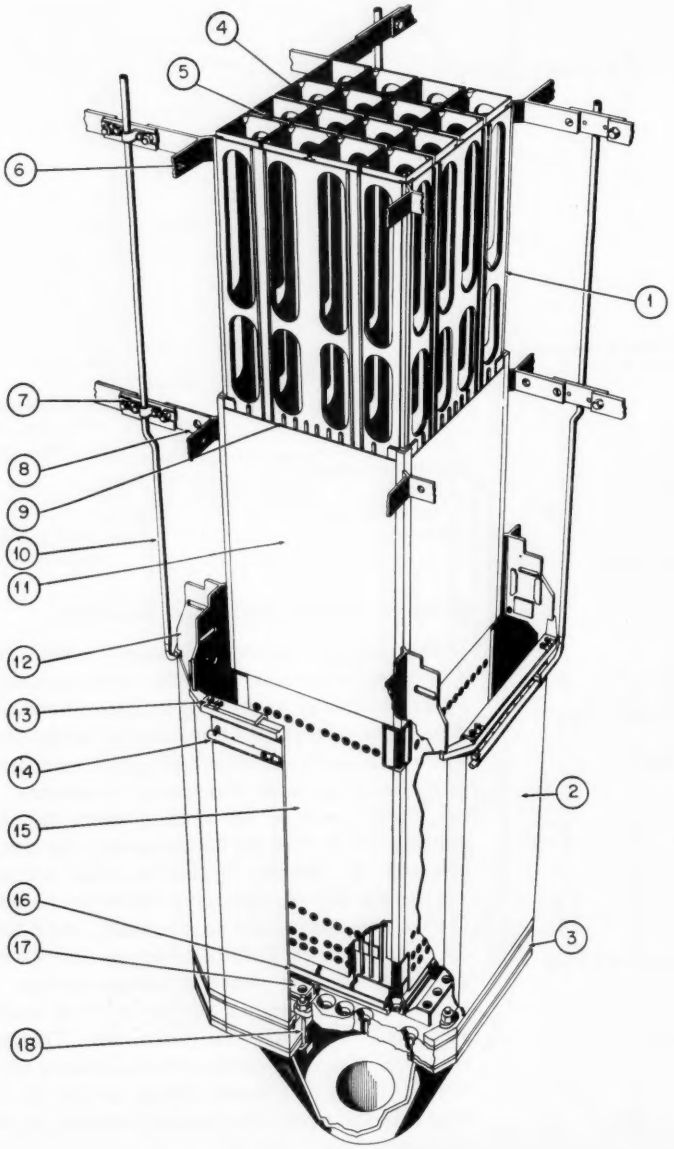

1 Rod Guide Structure
2 Baffle Support
3 Core Plate & Attachments
4 Boxes
5 Spacer Bar
6 Upper Sway Lug
7 Sway Link
8 Lower Sway Lug
9 Shim Channel
10 Superheater Emergency Coolant Pipe
11 Upper Panel Assembly
12 Support Lug
13 Superheater Spacer
14 Emergency Coolant Header
15 Lower Panel Assembly
16 Panel Support
17 Superheater Support
18 T Bolt

Fig. VIII-21 Perspective view of core structure of the BONUS reactor.

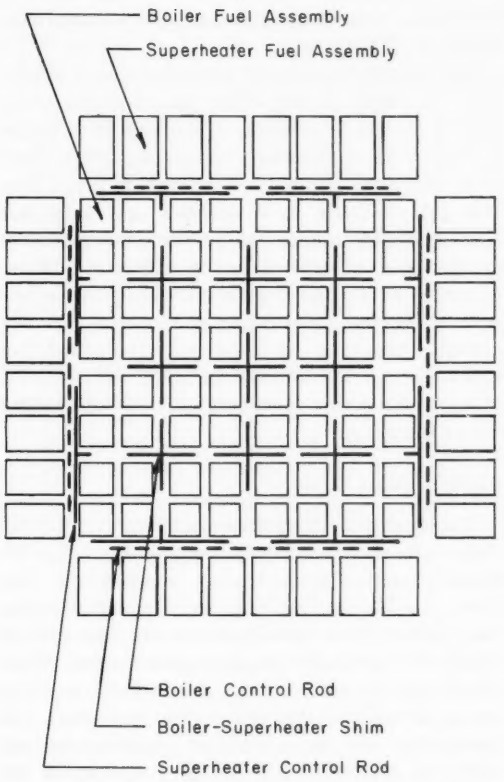

Fig. VIII-22 Control-element locations in the BONUS reactor.

welded to the carbon-steel reactor vessel, contains an Inconel section that acts as a welded transition piece between the stainless-steel upper section of the barrel and the reactor vessel so that stresses due to differential expansion are minimized. The core support barrel is attached at its upper end to the core support plate and supports this plate and the full core load. The barrel also serves as a flow barrier between the coolant-water inlet and the recirculation-water outlets. The stainless-steel core plate contains holes that accept the bottom fittings of the boiler fuel assemblies, provides a mounting space for the superheater fuel-assembly supports, and furnishes a mounting for the core baffle support. The core baffle support transmits the load of the upper superheater grid structure and the control-guide structure to the core support grid. Sway lugs are attached to brackets welded to the vessel wall at two elevations, and four emergency cooling line brackets are welded to the vessel wall. Superheated-steam headers are mounted high in the reactor vessel, as are superheated-steam outlet pipes. Each header has four connector flanges to which superheater-assembly outlet standpipes are attached, and each superheated steam outlet pipe has a single connector flange. The headers are supported by brackets that also serve to support the dryer/preheaters and to furnish the main alignment surface for the reactor-vessel internals.

A boiler emergency spray header is attached by brackets to the underside of the vessel closure head.

Each boiler fuel assembly is supported directly by the bottom grid and is held in place by a hold-down assembly that exerts a lateral force on each of four boiler assemblies through a wedging and spacing action. This force aligns the assemblies under the control-rod guide structure so that they cannot be removed as long as the hold-down assembly is in place.

At each slab type control-rod position, Zircaloy-2 double-walled panels extend downward from the upper guide structure to the bottom grid. These panels serve the dual purpose of defining the slab control-rod channels and providing positions for the boiler-superheater shims. A horizontal cross section through the reactor core, which shows the locations of fuel and control assemblies, is shown in Fig. VIII-22.

Pressure vessel	
Vessel shape	Cylindrical
Vessel wall composition	ASTM A-212 grade B carbon steel; S.S. weld overlay type ER 308L over type ER 309
Vessel inside diameter	7 ft
Vessel overall height	26 ft 7 in.
Vessel wall thickness, base metal	$3\frac{1}{8}$ in.
Vessel cladding thickness	$\frac{1}{4}$ in.
Design pressure	1150 psig
Design temperature	600°F
Operating pressure	950 psig
Operating temperature	540°F
Internal thermal-shield material	AISI type 304 S.S.
Internal thermal-shield thickness	1 in.
External thermal insulation	Fiberglass
External thermal-insulation thickness	$3\frac{1}{2}$ in.
Nozzle list	
Recirculating-water inlet	1, 16-in. schedule 100
Recirculating-water outlets	2, 12-in. schedule 100
Feedwater inlet	1, 4-in. schedule 80
Large superheated-steam outlets	1, 3-in. schedule 80

Small superheated-steam outlets	4, 2-in. schedule 160
Control-rod thimbles	17, 3-in. double extra heavy
Instrumentation thimbles	4, 3-in. double extra heavy
Pressure-relief nozzle	1, 6-in. schedule 80
Upper liquid-level nozzle	1, 2-in. schedule 80S
Lower liquid-level nozzle	1, 2-in. schedule 80S
Vent nozzle	1, 1-in. schedule 80S
Emergency coolant inlet	1, 2-in. schedule 80S
Gasket leak-off nozzle	2, 1-in. schedule 80S
Spare nozzle	1, 2-in. schedule 80S

Control and Instrumentation

The control concept employed in the BONUS station is one in which the reactor establishes the plant output, and control of the turbine admission valves is made responsive to reactor pressure. The turbine accepts the steam generated by the reactor and maintains a load such that the reactor pressure is held constant at its set point. Control of reactor power level is accomplished by movement of the cruciform-shaped and slab type control rods. Although the recirculation flow loops in the BONUS plant are provided with flow-control valves that can be used for making initial adjustments of the recirculation rate, reactor power will not normally be controlled by varying recirculation flow.

The superheated-steam exit temperature of the reactor is allowed to vary between 900 and 950°F, and an automatic attemperator spray-control system is provided in the main steam-supply line to maintain steam temperature at the inlet of the turbine essentially constant and equal to a nominal value of 900°F.

Pressure control is accomplished by an integrated master system composed of three valve-control systems: the turbine-admission-valve control system, the turbine-bypass-valve control system, and the minimum-flow bypass-valve control system. The functional interconnection of these systems, which provides control of reactor pressure, is such that the proper system or combination of systems is brought into use as the particular pressure set point and operating conditions demand.

A block diagram of the 10-channel nuclear instrumentation system of the BONUS reactor was given in *Power Reactor Technology*, 5(2): 68. The reactor contains no in-core instrumentation.

All control rods are provided with rack-and-pinion type top-mounted drives. Only one rod can be moved at a time, which results in a maximum reactivity-addition rate of approximately 0.01% k_{eff}/sec.

The reactor system is provided with a manually operated, gravity-flow liquid-poison system. A 20 wt.% solution of boric acid in water is stored in a pressure vessel mounted about 18 ft above the normal reactor water level. The 114 gal of boric acid solution are kept hot (193°F) during storage to prevent thermal shock to the reactor vessel during poison injection. Injection of all the poison solution into the reactor requires about 3 min and results in a reactivity decrease of such magnitude that the reactor is 1.5% subcritical when cold, clean, with normal water level, and all rods and shims out of the core.

Recirculation System

The major components of the recirculation loops are shown schematically in Fig. VIII-13. Slightly subcooled water is pumped into the core via the bottom inlet nozzle and plenum. The water rises through the boiler assemblies where it is heated to saturation, after which steam is separated from the water, and the water flows radially outward and then down between the reactor core and pressure-vessel wall. As the saturated water descends in the vessel, it mixes with relatively cold feedwater that reduces the overall temperature of the recirculation mixture to a subcooled level. The subcooled water leaves the vessel at the bottom through two nozzles and descends through downcomers to the reactor circulating-water pumps, which are located in a pump room beneath the reactor vessel. Discharge lines from the circulating pumps feed a common, single riser that returns the recirculation water to the reactor vessel.

The two downcomer pipes are equipped with motor-operated gate valves, and the discharge line from each pump is equipped with a motor-operated gate valve, a check valve, and a flowmeter. Either pump can be isolated from the reactor by closing its gate valves. The check valves prevent reverse flow through a pump if it fails, and the other pump continues to operate.

Of the total water flow to the reactor vessel, 95% passes through the coolant channels and the remaining 5% flows to the moderator and to the control-rod channels between the boiler fuel-assembly boxes. Characteristics of the recirculation-system components are listed in the following table:

Recirculation pumps	
Number	2 (one per loop)
Type	Vertical, single stage, single volute, centrifugal
Nozzle diameter	
Suction	12 in.
Discharge	10 in.
Rated flow each	4500 gal/min
Developed head at rated flow	67 ft
Piping diameter	
Reactor to pumps	12 in.
Pumps to riser	10 in.
Riser to reactor	16 in.

Turbine-Generator, Condensate, and Feedwater Systems

The power-conversion cycle and equipment of the BONUS plant are essentially the same as those of a conventional power plant. Steam flows from the reactor through the main steam line to the turbine-condenser unit. Condensate pumps take water from the condenser hot well and pump it through the air ejector after coolers, a gland-seal condenser, condensate purification units, and three low-pressure feedwater heaters, to the main feed pumps. The feed pumps raise the pressure of the condensate and force it through the high-pressure feedwater heater and the feedwater regulating valve back into the reactor.

The single-casing single-flow turbine, which has four extraction openings for feedwater heating, drives a standard 13.8-kv 3-phase 60-cycle hydrogen-cooled generator. The gland-seal system used for the turbine shaft seals is a standard pressure-breakdown type. Steam leakoff from the high-pressure packing at the high-pressure end of the turbine is fed to the extraction line leading to feedwater heater No. 1. During turbine operation the seal gland at the low-pressure end of the turbine is normally fed by steam that is bled from the leak-off connection on the high-pressure seal gland; however, with the turbine shut down, reactor steam is supplied to the seals through the seal steam regulator. The outer chamber of all seal glands is maintained at a negative pressure with respect to the building atmosphere by means of gland-seal exhausters.

The reactor is equipped with a saturated steam line that leads to an emergency condenser, and on a branch from this line a series of safety valves is installed to prevent excessive pressures in the reactor system. The location of these valves is shown in Fig. VIII-13.

The two-pass main condenser is capable of condensing the full output of the reactor when the turbine bypass valves are open and a condenser pressure of 3.5 in. Hg abs. is available. The condenser has a divided hot well and divided water boxes, and its condensate storage capacity is sufficient for a 4- to 9-min holdup at full-flow conditions. Condenser cooling is accomplished with pumped seawater.

Turbine	
Number	1
Description	Single-casing ASME-AIEE preferred standard
Nameplate rating	16,500 kw
Turbine throttle conditions at full full load	
Superheated-steam weight flow	151,000 lb/hr
Pressure	850 psig
Temperature	900°F
First extraction	163 psia; 6734 lb/hr
Second extraction	64 psia; 7312 lb/hr
Third extraction	27.2 psia; 8251 lb/hr
Fourth extraction	8.14 psia; 7703 lb/hr
Exhaust-steam enthalpy, CEP	1010.3 Btu/lb
Exhaust-steam weight flow	117,285 lb/hr
Generator	
Number	1
Description	13,800-volt, 3ϕ, 60 cps, 3600 rpm, ASME-AIEE preferred standard
Terminal output	17,506 kw
Capability at 0.85 lb-ft and 30 psig H_2 pressure	22,059 kva
Main condenser	
Number	1
Description	Two-pass single-shell divided waterbox and hot well
Heat-transfer surface	20,000 sq ft
Capacity	119,000 lb/hr
Operating pressure with 85°F cooling water	2 in. Hg abs.
Tube description	
Material	Aluminum and brass
Number	4368
Outside diameter	$\frac{7}{8}$ in.
Wall thickness, BWG	16
Length	20 ft
Cooling-water flow rate	17,800 gal/min
Cooling-water temperature, inlet	85°F

Plant Arrangement and Containment

A total-containment design philosophy is employed in the BONUS plant. The general containment type that results from this philosophy was compared to other types in *Power Reactor Technology*, 5(1): 34-35, and a discussion of the actual BONUS containment appeared in *Power Reactor Technology*, 5(2): 54-55.

The basic components of the containment building are a steel dome, a short cylindrical steel section, and a concrete foundation slab. A perspective view of the building, showing the arrangement of plant equipment, is given as Fig. VIII-23, and dimensions and specifications are listed in the following table:

Containment building	
Shape	Cylindrical steel and concrete wall, hemispherical steel dome, flat concrete-floor slab
Overall dimensions	
Diameter	166 ft 8 in.
Height inside	107 ft 4 in.
Building height above ground	84 ft 4 in.
Concrete-wall dimension	
Minimum thickness	18 in.
Height	26 ft 6 in.
Dome	
Diameter	166 ft 8 in.
Wall thickness	$\frac{5}{16}$ in.
Material	Carbon steel, ASTM A-201 grade B
Cylindrical shell	
Height	26 ft 4 in.
Wall thickness	$\frac{3}{8}$ in.
Material	Carbon steel, ASTM A-201 grade B

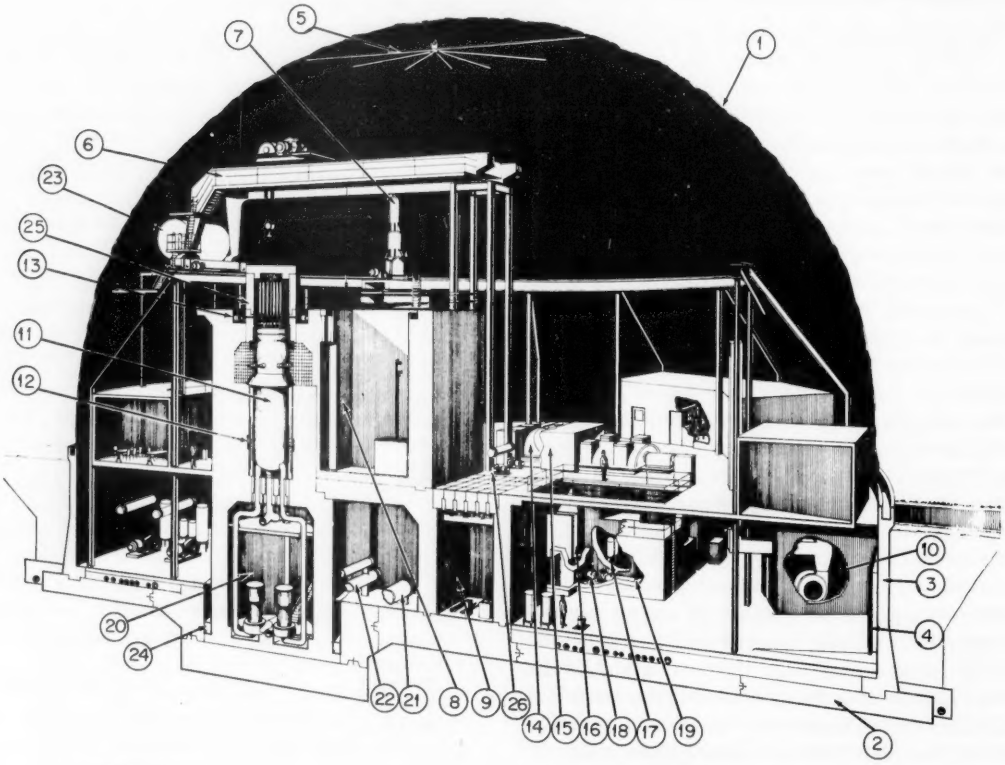

1 Steel Dome
2 Foundation Mat
3 Retainer Wall
4 Freight Door
5 Building Spray
6 Polar Gantry Crane
7 Fuel Unloading Coffin
8 Spent-Fuel Storage Pool
9 Solid Radioactive-Waste Storage
10 Building Ventilation Intake Fan
11 Reactor Pressure Vessel
12 Neutron Shield Tank
13 Control-Rod-Drive Motor Trench
14 Turbine Generator
15 Turbine Shield
16 Condenser
17 Condensate Pumps
18 Evactor Pump
19 Gland Seal Condenser
20 Reactor Circulating-Water Pump Room
21 Startup Heater
22 Reactor Water-Purification Coolers
23 Emergency Condenser
24 Reactor Pit Water Moat
25 Removable Concrete Shield
26 Fuel Pool Cooling System

Fig. VIII-23 Perspective view of containment building, BONUS power station.

Design pressure	5 psig
Design temperature	140°F
Free volume of containment barrier	1.59×10^6 cu ft
Design leak rate of steel shell, % of building vol./day at 5 psig	0.2
Maximum permissible leak rate, including floor slab and all penetrations, % of building vol./day at 5 psig	0.4

Purification and Radioactive Waste Disposal

The scheme of disposing of the noncondensable gases formed during reactor operation is one in which radiolytic and radioactive gases are removed from the main condenser by the air ejector and then are subjected to a series of holdups and filtrations before being discharged to the reactor building exhaust. A schematic diagram of the system is shown in Fig. VIII-24.

The principal liquid wastes are expected to be low-level wastes that can be processed at the plant and discharged to the sea. Any liquid wastes containing high levels of radioactivity will be converted to solid waste by the addition of absorbent solids or by casting in cement.

Solid wastes from the BONUS plant will be handled by bailing or by drum storage. A hot-waste storage area, with sufficient capacity to handle the waste generated over a period of several years, will be used as a collection point for material awaiting off-site shipment for permanent disposal. The estimated rates of generation of solid wastes are given in the following table:

Waste source	Quantity of waste, 66-gal drums/year
Filters, condensate, reactor, and pool	5
IX resins	4
Charcoal traps	1
Liquid-waste concentrate	6
Baled-paper waste	7
Miscellaneous, air filters, etc.	2
Total (estimated)	25

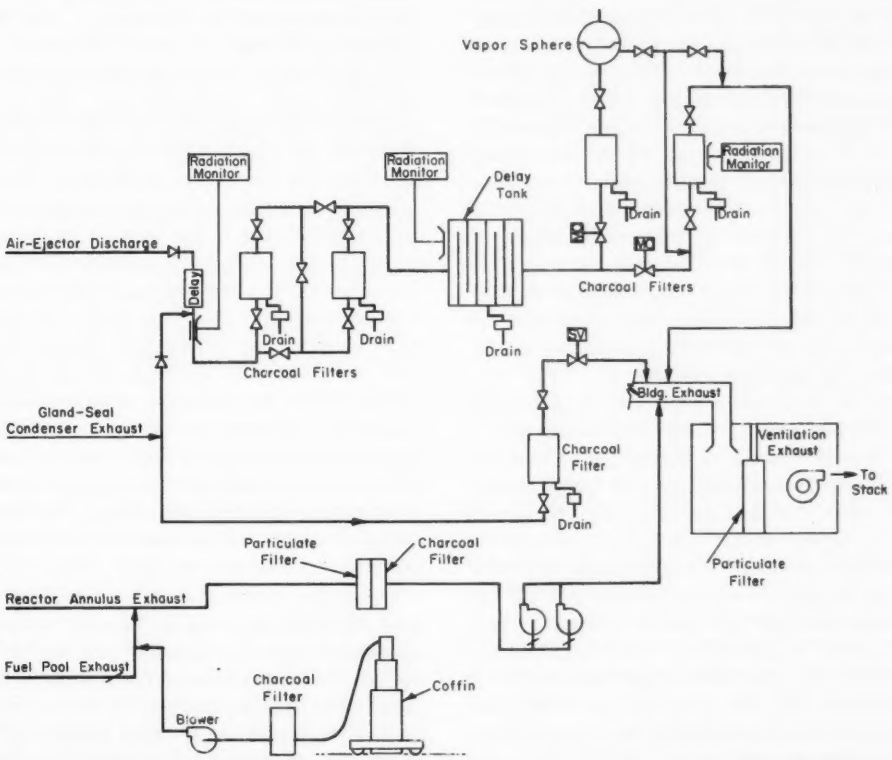

Fig. VIII-24 Gaseous waste-disposal system of the BONUS power station.

Discussion

The incorporation of integral nuclear superheat into the basic concept of the direct-cycle boiling-water reactor appears to be the most straightforward way of attaining the modern steam conditions that are generally regarded as an important goal for nuclear steam generation. Designers can build on the established boiling-water technology to eliminate some of the developmental problems that usually accompany the proving of a new concept and can use the direct cycle (no heat exchangers) to minimize the reactor temperatures necessary for a given steam temperature, although the direct-cycle steam may prove to be a difficult reactor coolant.

Relative to the direct-cycle saturated-steam boiling reactor, the provision of integral nuclear superheat seems to have added at least the four new questions of feasibility that follow.

1. Effective steam-water separation, and, in particular, the problem of water carry-over in the steam, assumes much greater importance, probably to the point of becoming a feasibility problem. This is because nonvolatile impurities carried by entrained water can be deposited in the superheater coolant passages when the water finally evaporates. The most obvious sources of trouble in such a case would be the chlorides, which are known to promote stress corrosion in stainless steels even when present in very small amounts. The problem may be accentuated in superheaters using reactor-generated steam because of the relatively high concentration of oxygen from the radiolytic decomposition of water; the presence of oxygen is known to enhance chloride stress corrosion.

2. Suitable fuel elements must be provided for superheater service. This problem is, of course, closely related to the preceding one, as well as to the rather high surface temperature required. The latter must evidently be about 1200°F or higher if the steam is to be superheated to the desired temperatures. At these temperatures the strength and ductility of the jacket material, as well as its corrosion resistance, are questions of real importance. Currently there are no low-cross-section materials suitable for this service, and even the stainless steels are suspect because of the stress-corrosion problem.

3. The question of radioactive carry-over into the turbine and the off-gas system of the superheat reactor cannot be assumed to be settled by the favorable past experience with direct-cycle saturated-steam boiling reactors. This is true because the boilers benefit from a large decontamination factor: when the steam evaporates, nearly all the nonvolatile impurities are left behind in the water. The boiler sections of integral superheat reactors will enjoy the same effect, but any radioactive products that are added to the steam in the superheater—as from a failed or leaky fuel element—will pass on into the turbine.

4. The coupling of the two sections of the reactor—the boiler and the superheater—in terms of both the neutron chain reaction and the coolant flow introduces unique relations of core design and plant operation. It is essential to provide means for adjusting and maintaining the division of power between the boiler and the superheater, over the reactivity lifetime of both, at proper values to yield the desired steam outlet temperature.

The superheater normally has no independent coolant supply of its own, but is dependent upon steam generated by the boiler. Therefore the designer, although he must thermally insulate the superheater coolant passages from the surrounding water moderator in order to prevent excessive heat loss from the superheated steam, must not insulate too effectively; this heat leakage into the moderator will be the only means of shutdown cooling after the power has decayed to the point that there is no significant steam production in the boiler section of the core. Aside from the considerations of emergency and shutdown cooling, the dependence of the superheater upon the boiler for coolant flow must also be taken into account in operating procedures. Thus, for example, if some unusual circumstance causes overheating in the superheater, a reduction of total reactor power may not be a very effective countermeasure, for it reduces the coolant flow to the superheater at the same time that it reduces the superheater power.

When the development of integral boiling-superheating reactors was begun, the problems connected with the nuclear coupling of the two regions were considered to be feasibility problems. Now that the designs of two reactors have been worked out and checked by critical experiments, the problems are no longer in that category, but the measures taken for their solution have played important roles in determining the

core designs and must be taken into account in any assessment of the designs.

The nature of the preceding problems is such that they cannot be completely resolved except by operation of the reactor itself. For this reason the performances of the Pathfinder and BONUS reactors will be of great interest, and if utilized effectively these reactors may provide invaluable information for reactor development for some years to come.

For the successful development of a reactor type, it is not enough that the feasibility problems be solved; rather, they must be solved in a manner that will make the reactor type economically competitive. Since the integral nuclear superheat reactor represents an extension of direct-cycle boiling-water technology, the economic requirements in this case can perhaps be stated more directly than in most cases of a new reactor type. Economic advantages will accrue from the higher thermal efficiency and from the savings in cost of the turbine and associated equipment. For economic success of the reactor type, it is necessary that these advantages not be nullified by costs associated with the superheating feature. Conceivable sources of such costs include:

—increased capital costs due to lower power density in the reactor core or to the need for very effective steam-water separation

—increased fuel-cycle costs due to shorter fuel-element life, more expensive fuel-element construction, or greater neutron losses to highly absorbing cladding materials

—increased costs of siting, off-gas control, or maintenance due to higher radioactivity levels in the steam

It would be unreasonable to expect the first reactors of a type to solve the economic as well as the feasibility problems. Indeed, more advanced design studies for nuclear superheat have indicated very favorable prospects for avoiding the above-mentioned sources of possible cost problems. These designs differ quite widely from both Pathfinder and BONUS, although they involve the same feasibility questions. These studies have been reviewed briefly in *Power Reactor Technology*, 4(3): 71-85 (June 1961); 6(2): 75-80 (March 1963); 6(4): 97-105 (Fall 1963). In assessing the designs of Pathfinder and BONUS, it is reasonable to ask whether they advance the technology in the directions that are most likely to lead to good economic performance.

The differences between the two designs are substantial. Some of these differences are due to the design power output, and some are rather incidental. It would not be feasible, for example, to employ the BONUS system of superheater power-level control, which utilizes sheets (blades) of absorbing material between the boiler and superheater, in a very much larger reactor. On the other hand, the use of this system rather than a set of control rods within the superheater is a rather incidental design choice. The difference in reactor size may have been of greater significance in fostering a somewhat bolder approach in the smaller BONUS reactor. This approach is reflected by the higher design values of steam temperature and pressure in BONUS relative to Pathfinder.

The question of a central or peripheral location for the superheater section generates many pros and cons for each approach. When the question is considered in a general way, the central location is usually credited with requiring a relatively small volume for a given power, with having a relatively flat radial power distribution, and with causing some reduction in the overall reactor maximum-to-average power ratio. The central location does, however, result in relatively high heat fluxes and fuel temperatures in the superheater and does lead to relatively large effects on reactivity. Just the opposite advantages and disadvantages are usually given for the peripheral superheater. The calculated values for Pathfinder and BONUS show some of these effects. The Pathfinder superheater does produce a good deal of power in a relatively small volume (its power density is about three times that of the BONUS superheater) but not without penalty. In Pathfinder the maximum fuel-cladding temperature is 1270°F for an outlet steam temperature of 725°F; in BONUS the corresponding value is 1175°F for 900°F steam. The relatively small difference between maximum cladding temperature and steam exit temperature in BONUS is due partly to the in-out multipass design of the superheater, in which the steam traverses regions of lower power density as its temperature increases.

Although the Pathfinder fuel operates at a somewhat higher maximum surface temperature than the BONUS fuel, its required lifetime is much shorter (nine months, about one-sixth

that of the BONUS fuel). This is due partly to the shorter reactivity lifetime of the highly enriched superheater fuel. From the long-range standpoint, it is questionable whether highly enriched fuel has an economic future in central-station power reactors, and in this respect the BONUS development, if it is successful, may represent a more direct approach to ultimate economic success. In some ways the oxide-pellet slightly enriched fuel appears also to offer advantages in solving the corrosion problems, for it allows considerable flexibility in the choice of jacket material. It was a relatively straightforward matter, for example, to modify the BONUS fuel-element jacket, from stainless steel to Inconel, after the seriousness of the stress-corrosion problem in stainless steel became apparent.

The nuclear designs of the two reactors are characteristic of their basic geometrical arrangements. As mentioned above, the power split between boiler and superheater is controlled in BONUS by means of blade type control rods at the boiler-superheater boundary, whereas Pathfinder has control rods in both the boiler and the superheater. The nuclear design of each reactor is such that reactivity effects from flooding or voiding of the superheater regions are minimized by suitable choice of the fuel-to-water ratio. Under operating conditions, flooding of the Pathfinder superheater causes a reactivity change of $-0.66\%\ \Delta k/k$, whereas flooding of the BONUS superheater results in a reactivity gain of $0.16\%\ k_{\text{eff}}$.

The problem of obtaining the required degree of steam-water separation is handled differently in the two plants. Pathfinder has centrifugal separators in its downcomer region to remove entrained steam from the recirculation water, whereas BONUS, with no such mechanical devices, relies on gravitational separation. Pathfinder has a mesh type steam dryer through which saturated steam must pass on its way to the superheater region of the core, and BONUS has dryer units in the same relative location and preheats the steam slightly before its entrance to the superheater proper by regenerative heat exchange with the exit steam.

The BONUS reactor is provided with a gravity-actuated emergency core spray that will cool the boiler and superheater fuel elements in the event all primary cooling water is lost from the vessel. Pathfinder, on the other hand, relies on the normal feedwater supply to provide cooling water to the reactor vessel faster than it is lost.

In summary, it can be said that the integral-superheat reactors of the Pathfinder and BONUS plants show originality of concept and reflect interesting differences in design approach. With the plants now in the process of startup, speculation as to their probable performance is pointless, since experience should soon provide the answers to questions of operational capabilities.

References

1. Northern States Power Co., Pathfinder Atomic Power Plant Safeguards Report, Part II. License Application, USAEC Report ACNP-5905, Jan. 15, 1962, and addenda.
2. Northern States Power Co., Technical Specifications for Pathfinder Atomic Power Plant, May 28, 1963.
3. General Nuclear Engineering Corp. and the Puerto Rico Water Resources Authority, Boiling Nuclear Superheater (BONUS) Power Station, Final Hazards Summary Report, USAEC Report PRWRA-GNEC-5, Feb. 1, 1962, and addenda.

Section

IX

Power Reactor Technology

Operating Experience

Consolidated Edison Nuclear Steam-Generating Station

The Consolidated Edison Thorium Reactor (CETR) was described in detail in *Power Reactor Technology*, 6(3): 28-40. Since that review a number of articles dealing with the operating experience of the CETR have been published.[1-6] Reference 1 is a paper from a conference on operating experience with power reactors; the conference was sponsored by the International Atomic Energy Agency in June 1963. References 2 to 6 are papers that were presented at the Winter Meeting of the American Nuclear Society, November 1963. In 1962, the provisional operating license for the CETR was issued in March, the facility was completed in May, criticality was achieved on August 2, and the unit was placed on-line on September 16. Operation at full power occurred on Jan. 25, 1963; as of March 1964, a total of about 1.2×10^6 Mw-hr had been generated.

An early trouble was experienced with the coating of the fuel-transfer canal. This coating was a phenolic paint, and leakage of water occurred through defects in the paint or around inadequately sealed points of attachment of anchors. A similar problem was also experienced at the Shippingport reactor and is reviewed in *Power Reactor Technology*, 6(3): 51. In Ref. 2 it is stated that work was done on the CETR fuel-transfer pool during August and September of 1963; however, no details of this work are given. Difficulties were noted in the ability to produce and maintain water in the fuel-transfer-system pool of sufficient visual clarity for satisfactory handling of the core and core components. The fuel-transfer system was designed to be flooded with water from condensed bleed steam; before power operation the system used treated water. Algae were found to be present in the fuel pools, and it is postulated[2] that the algae fed on the cyclohexylamine present in water as a corrosion inhibitor. The following temporary measures were instituted to clarify the water:[2]

1. Drain the pools and treat the pool walls with hydrogen peroxide for algae control.
2. Abandon cyclohexylamine treatment of the particular tank furnishing makeup water for this purpose.
3. Install a temporary wood cellulose filter to remove the fine silt and corrosion products present in the unevaporated makeup water. These steps were successful in making fuel loading under a full head of water possible.

Tests of the reactor head joint revealed a leak-free seal. Although provision had been made for seal-welding the top head closure, the seal ring was welded to the head only and not to the body of the vessel. However, other bolted-joint components were seal welded. These items included the pressurizer vent-valve bonnet and the hinge-pin covers on all eight discharge check valves for the primary coolant pumps. Not all hinge-pin covers experienced leakage, but all were welded as a precaution.

During the first six months of operation, 187 automatic shutdowns occurred. They were not occasioned by a reactor safety problem but were the result of malfunctions of associated equipment and conservative settings of the nuclear instruments. Of these shutdowns, about 20% were from malfunctions in nuclear instrumentation systems, 25% originated in the control system for the control-rod drives, and about 30% were caused by malfunctions in the conventional plant equipment. The remaining 25% were from miscellaneous causes, generally non-repetitive in nature.

The control-rod-drive system appears to be the most interesting area of operating experience reported. The drive system, shown in Fig. V-6 of *Power Reactor Technology*, 6(3), is sealed in an 1800-psi pressure-tight housing. Experience demonstrated that the small amount of leakage past the shaft seal, plus the water that was carried down into the housing by a wet shaft, produced a high-humidity condition. This atmosphere seemed particularly hard on the miniature switch that reported disengagement of the drive shaft from its carriage and the one that operated when full insertion was reached. The following is quoted from Ref. 2:

> ... Various corrective measures were made including the use of a switch redesigned to reduce its susceptibility to moisture interference, and a system to purge the drive mechanism housing with dry nitrogen to limit humidity. These measures were partially successful, and recently, further improvements have been made to provide for an arrangement allowing individual nitrogen flow control to each housing in accordance with certain electrical circuit resistance readings periodically made as an indicator of moisture in the housing, and to provide a new set of hermetically sealed switches.

Reference 1 reports the virtual elimination of troubles with the rod-drive system as a result of these actions.

A number of the difficulties experienced were peculiar to the CETR. These included some piping reruns and failures of tubes in the fossil-fired superheater. Some activity has been detected on the secondary side of the primary steam generators. Up to the time Ref. 2 was written, a level of about 10^{-5} μc/ml had been detected, and this appeared to be steadily rising. This activity leak apparently occurred within the period from June to November 1963, since a particular point made in Ref. 1 is that no measurable leakage had been observed.

The ion-exchange and filtration portions of the primary coolant purification system have been kept in almost continuous operation, but the purification gas stripper was not required to be in operation.[2] At the outlet of the mixed-bed ion exchanger, the activity was about 2×10^{-5} μc/ml due to noble-gas activity; operation of the degasser decreased this to about 10^{-5} μc/ml. No gaseous waste had been discharged as of the writing of Ref. 1, and the ventilation of the containment building, prior to access, has required no exceptional precautions.

The operation of the automatic control system for the CETR is briefly described in Ref. 3. The plant was designed to accept a ± 18% power step or a ± 9% per minute power ramp. Although an actual step could not be studied because the turbine throttle could not be stepped, a power change of 50 Mw(e) in 12 sec was reviewed. Figures IX-1 and IX-2 show the results with the steam-flow gain constant set at its recommended design value. The author concludes that the plant can actually accept a step of ± 27% in power or a ramp of ± 15% per minute.

References 4 to 6 present results of physics and thermal measurements done on the CETR. Temperature coefficients of reactivity were determined by doubling time differences for several temperatures, both with and without boric acid in the moderator. Control-rod worths were determined, and power coefficients were measured. Table IX-1 shows a summary of the CETR reactivity coefficients.

A series of flow measurements and heat balances were made on the CETR, and it was of interest to find that the heat balances indicated that the actual flow was higher than the design flow by about 13%. The actual flow, which is equivalent to 60×10^6 lb/hr, is obtained with eight pumps in operation and at

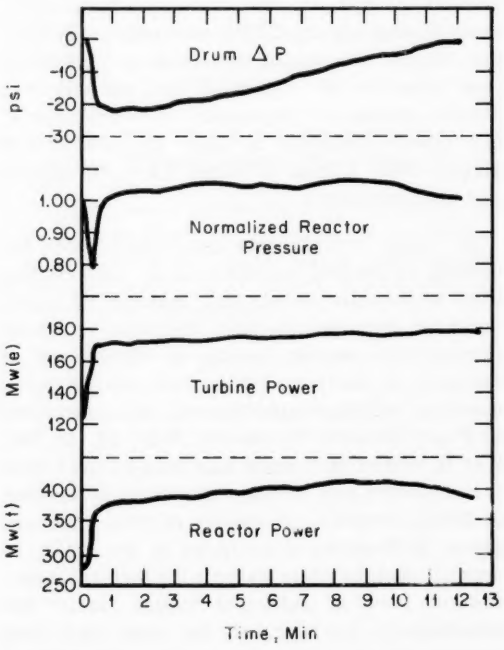

Fig. IX-1 Response of the CETR plant to a simulated step in power of +5 Mw(e).[3]

temperatures between 475 and 500°F. The measured core pressure drop was 49 psi, compared to the predicted value of 54 psi. Deddens concludes that[6]

> ...most of the decreased core pressure drop is accounted for by a revised method for computing pressure drop in the flow annulus between the fuel element bundle and the fuel element can... The significance of this is that not all of the increased flow is effective in cooling the fuel rods...

Deddens also concludes that the steam-generator performance is "significantly" better than predicted and that the CETR has excess thermal capacity; therefore the CETR could be operated at rated power [585 Mw(t)] with six pumps in three boiler loops in operation.[6]

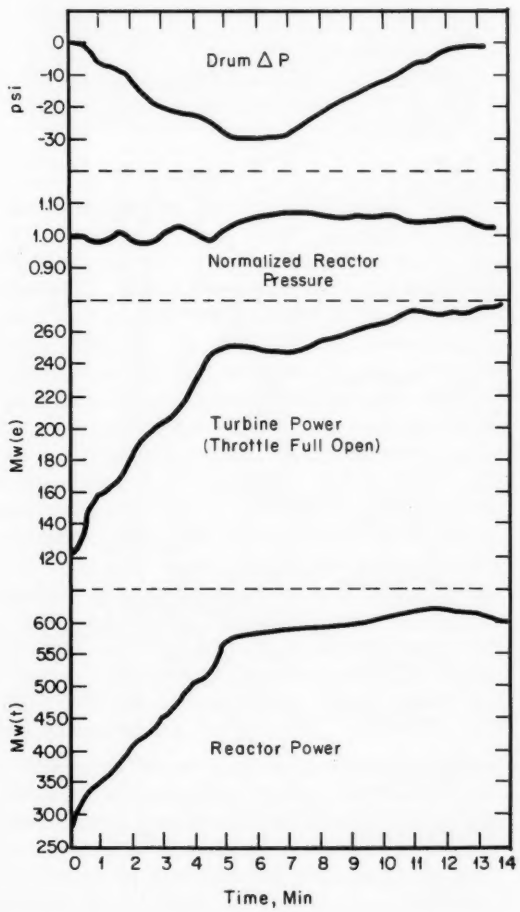

Fig. IX-2 Response of the CETR plant to a ramp[3] of +25 Mw(e)/min.

Table IX-1 SUMMARY OF CETR REACTIVITY COEFFICIENTS[5]

Parameter	Reactivity coefficient $dk/k \times 10^5$	Core conditions
Temperature, uniform	−17.1/°F ± 8%	Initial, 450°F, no poison
Boric acid	−14.8 ± 0.7/10 ppm	Initial, 450°F
Pressure coefficient	+13.3/100 psi	Initial, 450°F, 1450 to 1650 psig
Power coefficient	−2.2 ± 0.07/Mw	Initial

Plutonium Recycle Test Reactor: Primary Coolant Pumps

The Plutonium Recycle Test Reactor (PRTR) is not a power reactor in the strict sense, but the primary coolant pressure and temperature are high enough to be representative of power-reactor conditions. The PRTR primary coolant is heavy water at a temperature of about 480°F and a pressure of 1050 psi. Prototypes of the PRTR primary coolant pumps have been extensively tested, and these earlier tests have been reviewed in *Power Reactor Technology*, 4(4): 71-73. Reference 7 is a report on the operating experience with the pumps used with the reactor. The reader may wish to consult Fig. XI-1 in the previously mentioned article in *Power Reactor Technology* for a schematic diagram of the mechanical pump seals used on the prototype PRTR pumps and, presumably, the actual pumps used with the reactor.

The problems encountered with the pumps are summarized as follows:

1. Stationary mechanical seal face distortion.
   (a) Differential thermal expansion of the massive pump cover plate which supported this member.
   (b) Hydraulic-pressure distortion of the stationary face.
2. Large amounts of corrosion products collected in the mechanical seal chamber from carbon-steel test loops.
3. Misalignment of mechanical seal faces from insert cocking; unseating the seal face from O-ring expansion.
4. Excessive vibration of the pump rotating assembly which includes the 2400-lb flywheel; vibration resulting from hydraulic instability of

the pumps causing lack of positive seating in the thrust bearings; and motor vibration.
5. Helium evolving between seal faces.
6. Inadequate venting of the seal chamber and the pump bowl.

Of these problems, all but the last two were encountered and corrected during the test program; the last two were peculiar to operation of the PRTR. In the reference are several tables that give detailed comments on pump-seal failures during PRTR operations. The helium that is dissolved in the PRTR coolant comes from the pressurization of the primary coolant with helium,[8] and this caused rapid failure of the pump seals during initial PRTR operations. The problem was solved by injecting helium-free water into the seal chamber and venting the pump bowl and seal chamber to remove helium collected at these points during primary system cooldown, depressurization, or other circumstances resulting in excessive gassing. The PRTR primary pumps are located at a high point of the piping and serve as collection points for any evolved helium. The vent flow is 3 gal/min from the pump bowl, and the vent pipe is drilled into the highest point of the high-pressure seal chamber to allow seal venting during pump operation.

As a result of the studies just described, the life of the PRTR pump seals has been improved. The following quotation serves to define the improvement:[7]

> Seal life has increased from an average of 1250 for 15 of the first 20 PRTR runs to an average of 2050 hr for the last completed run of each pump. The longest completed run was for 7 months with 4094 hr total operation. Mockup runs have shown seal life of more than a year attainable. Longer than average runs are currently in progress. It should be noted that PRTR is a test reactor with operating periods of 1 week to 10 days. Longer life, as with the test loop, is predicted for continual operation.

Heavy-Water Components Test Reactor: Control- and Safety-Rod Drive Systems

The Heavy-Water Components Test Reactor (HWCTR) also is not a power reactor but, like the PRTR, has the capability of operation with coolant pressure and temperatures approaching those of a power reactor. The HWCTR is cooled with D_2O at 1500 psi and 600°F, nominally, and is equipped with 18 control rods and 6 safety rods. Reference 9 reports on operating experience with the HWCTR rod-drive systems.

The rod drives are motor-driven rack-and-pinion drives located at the top of the reactor. Pressure breakdown, floating-ring labyrinth seals are employed. Figure IX-3 shows a simplified section of the safety-rod-drive arrangement. The six central control rods are arranged in a cluster and are attached to a common rack-drive housing. The remaining control rods and the safety rods are individually driven. The rack-drive housings are about 20 ft long and consist of a stainless-steel drive housing welded to two sections of 2-in. stainless-steel pipe. Latches for gripping the rod poison sections

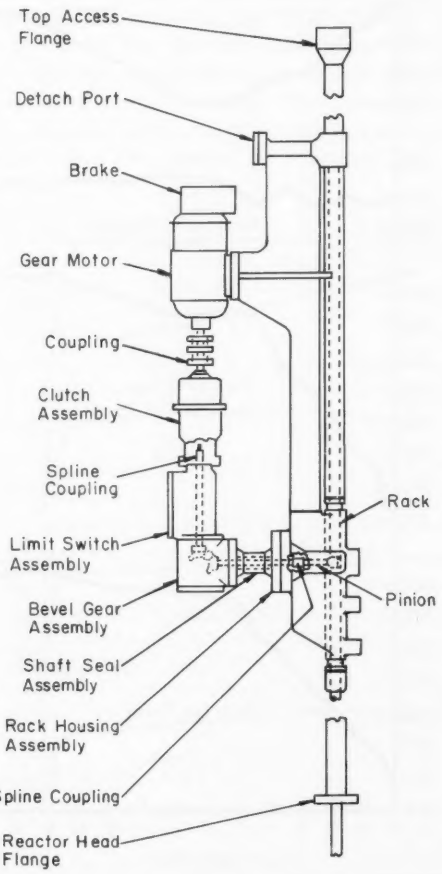

Fig. IX-3 Safety-rod-drive arrangement for the HWCTR.[9]

are at the lower end of the rack assembly, but the latch-actuating mechanism is located in the upper end, where it can be operated through the delatch port (Fig. IX-3).

During the first 1.5 years of operation of the HWCTR, there have been 34 incidents involving abnormal operation of the rod drives. These are summarized in Table IX-2. Most of the incidents (19) occurred during the first month of operation at low power, and 25, including the 19, occurred before power operation. Table IX-3 shows the breakdown of failures and operating difficulties. The seized clutch and seal that caused the stuck rods during scram were repaired and modified to prevent further difficulties. On four occasions (Table IX-3) the rods drove in an uncontrolled manner, although the reference does not say in which direction. This action was caused by a broken rod-drive control switch at the reactor control panel. The switches originally were double-block selector switches with a stiff spring return. No mechanical stops were incorporated, and, if the operator applied too much torque to the handle of the switch, the plastic cam mechanism causing the rod motion could be broken in the last-demanded position. All switches were replaced in March 1962 with ones employing metal cams and mechanical stops.

Table IX-2 SUMMARY OF HWCTR ROD-DRIVE DIFFICULTIES[8]

Operating difficulties	
Mechanical failures	10
Electrical failures	18
Others	6
Difficulties occurring in March 1962	19
Total rod drops (approximate)	1200
Failures to drop properly	
Slow times	6
Stuck	3
Electrical component revisions	4
Mechanical component revisions	4

Table IX-3 LIST OF HWCTR FAILURES AND OPERATING DIFFICULTIES[8]

Description	Causes
Failure of safety rod to scram completely (3 times)	Unknown; seized clutch; seized seal
Broken and bent latch fingers; rod could not be driven out of reactor	Rack scrammed six times without attached poison section; broken finger jammed in guide tube
Broken limit switch actuating cam nut (3 times)	Understrength cam surface; switches improperly adjusted
Rod drove in or out uncontrolled (4 times)	Broken control switch actuating the cam jammed the switch
Inoperative electrical system (16 times)	Shorted clutch coils, shorted relay coils, faulty relays, loose wires
Broken limit switch "Microswitch" (3 times)	Cracked during assembly and improper adjustment
Difficulty in latch or delatching rods (5 times)	Guide tubes too long; improper use of latching tool
Control rod driving abnormally (4 times)	Unknown
Failure of safety rod to scram within time limits (6 times)	Gear misalignment; inadequate limit switch lubrication; improper switch adjustment

Table IX-4 SEAL LEAK RATES FOR THE HWCTR

Total seal outleakage, lb/hr	7.1
Average seal outleakage, lb/hr per seal	0.3
Smallest outleakage of any seal, lb/hr	0.1
Total seal inleakage to reactor, lb/hr	171.0
Average seal inleakage to reactor, lb/hr per seal	7.1

The performance of the seals was satisfactory. Table IX-4 illustrates the seal leak rates. One case of seal failure was found. The failure was due to improper seal assembly. The seal leakage is especially important for reactors employing heavy water as a coolant, and it should be noted that the total seal outleakage in the HWCTR was collected. Inspection of the seals indicated absence of crud. This was due to the filtration of the seal water before injection into the seal.

Performance of the EBWR at Powers Up to 100 Mw(t)

As originally designed, the Experimental Boiling-Water Reactor (EBWR) was to be a prototype boiling-water reactor to produce 20 Mw(t) in the form of 600-psig steam. It eventually attained a power level of 61.7 Mw(t).

Information is given in Refs. 10 and 11 on modifications to the EBWR and on results of experiments in an attempt to reach a power of 100 Mw(t). Since Ref. 10 is a more up-to-date report, its review will be emphasized here.

Figure IX-4 is a schematic of the EBWR pressure vessel and internals as modified for operation up to 100 Mw(t). One of the basic changes made was to increase the number of fuel elements from 110 to 147, still maintaining a 4-ft core height. As shown in the figure, the core was encased in a shroud to prevent bypass flow, and a riser was installed. Increased riser height was provided to step up the flow rate through the core, since the reactor was operated as a natural-circulation device. A new feedwater ring was installed near the top of the riser to attempt to rapidly quench any steam carried over into the downcomer, and a new steam discharge duct was provided. The new steam duct withdrew the steam from the very top of the reactor in order to obtain as large a distance as practical between the water level and the steam-withdrawal point. The thermal power of the EBWR was distributed as follows: 20 Mw(t) was utilized by the turbine plant, and the balance [up to 80 Mw(t)] was absorbed by the reboiler plant. Steam generated in the boilers was condensed in air-cooled condensers. A steam dryer, which was part of the original EBWR equipment, was utilized to ensure a supply of dry steam for the turbine. Performance characteristics of the EBWR from zero to 100 Mw(t) are given in Ref. 12.

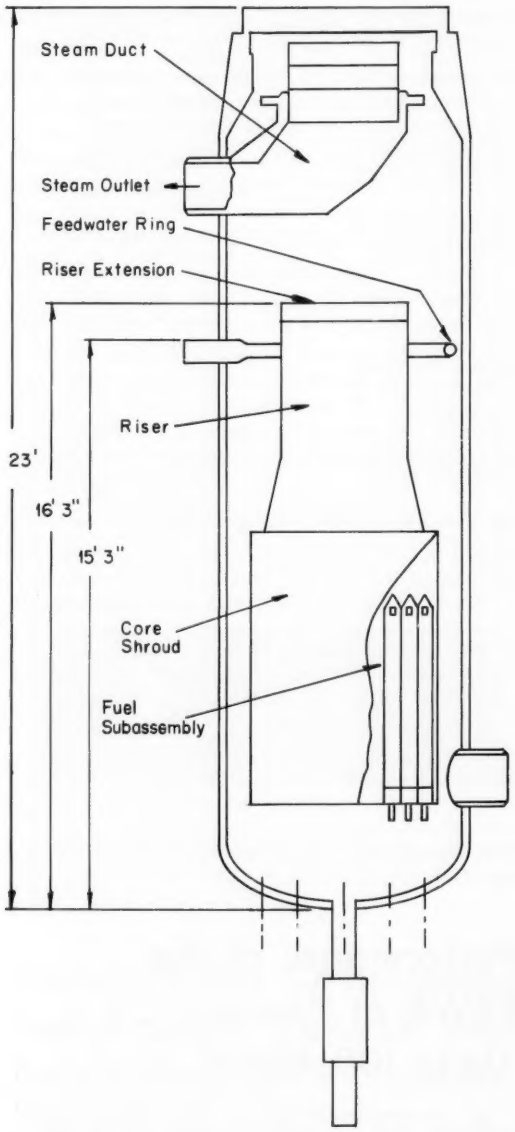

Fig. IX-4 Schematic of the EBWR pressure vessel and internals as modified for operation at power levels up to 100 Mw(t).[10]

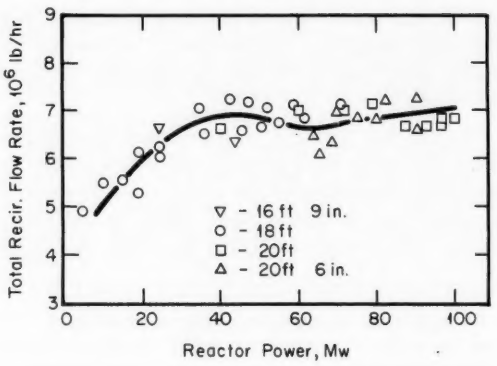

Fig. IX-5 Total recirculation flow rate as a function of reactor power at 600 psig and various true-mixture interface levels.[10]

Extensive instrumentation was installed within the vessel to provide data on the recirculation flow rate, volumetric and weight fraction of vapor carry-under in the downcomer, reactor subcooling, riser void fractions, quenching rate of the entrained vapor in the downcomer, location of the true two-phase mixture interface within the reactor, and liquid carry-over in the effluent steam. The reader's attention is

directed to the references[10,11] for design details on the instrumentation.

Three series of tests were conducted with the modified EBWR. The first series was of an exploratory nature and was run at 300 psig to simulate operation at higher power density. The maximum power level attained during the series was 20 Mw(t). During test series 2, the reactor power was varied from 5 to 60 Mw(t), and the pressure was held at 600 psig. Prior to the start of the second series of tests, the top foot of the riser was removed to increase the steam dome volume, and the saturated water level was maintained 7 in. above the top of the riser during the series. Test series 2 ended with all control rods fully out of the core and with some boric acid (equivalent to 0.5% k) remaining in the coolant. Boron strips were removed from some of the fuel elements in order to attain the desired 100-Mw(t) power level during test series 3.

The more important results of the test series are contained in Figs. IX-5 through IX-8. These figures, in general, show how the performance characteristics of the EBWR are governed by steam carry-under in the downcomer, liquid carry-over in the effluent steam and, indirectly, by the location of the water-steam interface in the pressure vessel. For example, Fig. IX-5 illustrates the total recirculation flow rate as a function of reactor power. Although the data pertinent to operation with the old riser configuration are not shown in the figure, they are illustrated in Ref. 10. The additional riser height was successful in

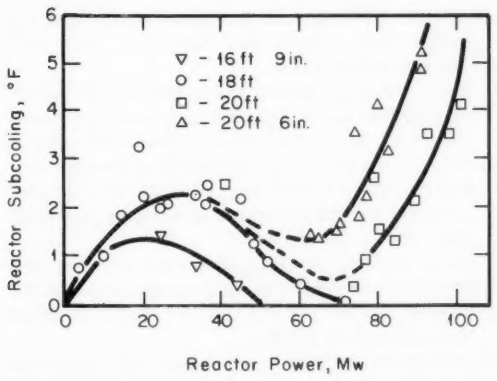

Fig. IX-6 Map of reactor subcooling as a function of reactor power and various true-mixture interface levels.[10]

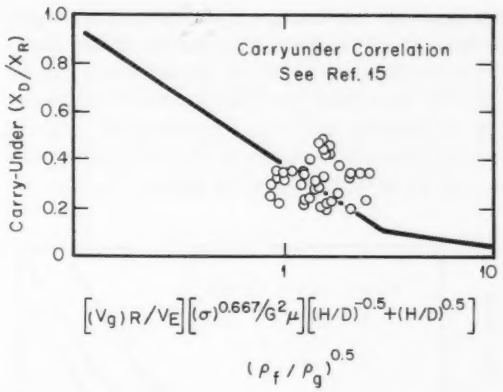

Fig. IX-7 Comparison of carry-under data with the correlation, using measured steam volume fraction.[10]

increasing the recirculation flow rate. The reason for the inflection point of the flow rate vs. power curve (Fig. IX-5) can be explained by a consideration of Fig. IX-6. This latter figure is a map of the subcooling of the reactor coolant, and an understanding of the figure is most helpful in gaining an insight into the operation of the EBWR at high power.

For reactor operation with no carry-under of steam into the downcomer, the core inlet subcooling increases continuously with power. This can be qualitatively explained by considering the data shown in Fig. IX-5 for powers up to about 20 Mw(t)—as power doubles, say from 10 to 20 Mw, the recirculation flow rate increases somewhat, but not by a factor of 2. A doubling of power is accompanied, however, by a doubling of the flow rate of the relatively cold feedwater, if steady state exists. Thus, as power increases, the core subcooling increases until the point is reached where steam starts to be carried into the downcomer. The effect of carry-under can be noticed in Fig. IX-6 at powers of about 20 to 30 Mw(t). The carry-under of saturated steam decreases the subcooling as power is increased. It can be seen from Fig. IX-6 that the subcooling increases sharply at a power of about 70 Mw(t) for an interface height of 20 ft. At this point liquid carry-over in the steam commences, and its effect is noticed in Fig. IX-6 by a rapidly increasing subcooling at the core inlet. It is of interest to note the sensitivity of the reactor subcooling to the interface height. At an interface height of 20 ft 6 in., the point of carry-over is reached at a lower power level (about 60 Mw)

because of the reduced steam dome height. Reference 10 presents a prediction of the reactor subcooling curve in the region where carry-over is important, and the agreement between the prediction and the experimental data (a typical example is shown in Fig. IX-6 at powers in excess of 60 to 70 Mw) is good.

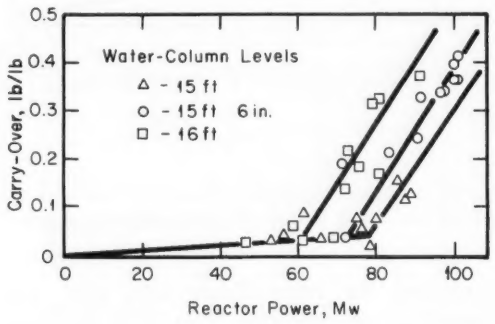

Fig. IX-8 Liquid carry-over as a function of reactor power and various water-column levels. (Data from Heat Balance on Primary Reboiler)[10]

In Fig. IX-5 the shape of the flow vs. power curve can be explained by the effect of inlet subcooling; as subcooling increases, the recirculation flow rates tend to increase.[10] Between roughly 40 and 60 Mw(t), Fig. IX-6 shows decreasing subcooling due to carry-under, and this is reflected in Fig. IX-5 in decreasing recirculation flow rates. Above about 60 Mw(t), subcooling increases due to carry-over, and this is reflected in Fig. IX-5 by increasing recirculation flow rates.

The vapor carry-under in the EBWR was calculated with the aid of a heat balance, using measured flow rates and subcooling. The carry-under in this reactor was substantial, even at low power, and varied from about 20% at 10 Mw to about 40% at 100 Mw. The value of 40% means that 40 wt.% of all steam generated in the core ends up entrained in the downcomer. What is of particular value, however, is the comparison of the analytical carry-under prediction given in Ref. 13 with the experimental data derived from the EBWR operation. This comparison is shown in Fig. IX-7. Steam-water separation was reviewed in *Power Reactor Technology*, 6(2): 69-74, and Ref. 13 was included in this earlier review. The scatter of the data shown in Fig. IX-7 is believed[10] to be caused by inaccuracies in determining the steam volume fraction in the upper part of the downcomer because of the quenching process and the resulting high degree of turbulence around the measuring probe.

Figure IX-8 illustrates liquid carry-over as a function of reactor power and water-column level. The water-column level is a measure of the true fluid-interface level, and, in the power range from 70 to 100 Mw, other data presented in Ref. 10 show that the true mixture interface is about 4.8 ft above the water-column-level readings. The figure illustrates that the initiation of carry-over, the break-points in the curves, occurs at different power levels for different interface heights. The figure also illustrates the large amount of carry-over that attended the operation of the modified EBWR at high power.

References

1. W. C. Beattie and R. H. Freyberg, Operating Experience with Indian Point Nuclear Electric Generating Station, in *Operating Experience with Power Reactors*, Vol. 1, pp. 307-324, International Atomic Energy Agency, Vienna, 1963.
2. R. H. Freyberg, Jr., Operating Experience at Indian Point, Consolidated Edison Company of New York, *Trans. Am. Nucl. Soc.*, 6(2): 340 (November 1963).
3. S. H. Esleeck, Performance of the Indian Point Reactor Plant, *Trans. Am. Nucl. Soc.*, 6(2): 341 (November 1963).
4. M. L. Batch and F. E. Fisher, Indian Point Reactor Reactivity and Flux-Distribution Measurements, *Trans. Am. Nucl. Soc.*, 6(2): 343 (November 1963).
5. R. M. Ball, J. M. Makepeace, and J. P. Farrar, Operating Coefficients and Reactivity Behavior at Indian Point, *Trans. Am. Nucl. Soc.*, 6(2): 343-344 (November 1963).
6. J. C. Deddens, Indian Point Reactor Primary-System Thermal and Hydraulic Evaluation, *Trans. Am. Nucl. Soc.*, 6(2): 340-341 (November 1963).
7. P. A. Scott, Plutonium Recycle Test Reactor Primary Coolant Pumps, Paper No. 63-WA-234 presented at the Winter Annual Meeting of the ASME, Nov. 17–22, 1963.
8. N. G. Wittenbrock (Ed.), Plutonium Recycle Test Reactor Preliminary Safeguards Analysis, USAEC Report HW-48800 (Rev.), Hanford Atomic Products Operation, June 5, 1958.
9. S. H. Kale, HWCTR Control-Rod and Safety-Rod Drive Systems, Paper No. 63-WA-257 presented at the Winter Annual Meeting of the ASME, Nov. 17–22, 1963.
10. M. Petrick and E. A. Spleha, Thermal Hydraulic

Performance Characteristics of EBWR [0 to 100 Mw(t)], USAEC Report ANL-6693, Argonne National Laboratory, May 1963.

11. D. Miller (Ed.), Thermal Operating Performance of Nuclear Reactors, A Panel Discussion Held at the Fifth National Heat Transfer Conference, Houston, Texas, August 8, 1962, USAEC Report TID-7669.
12. E. A. Wimunc, M. Petrick, W. C. Lipinski, and H. Iskenderian, Performance Characteristics of EBWR from 0–100 Mwt, USAEC Report ANL-6775, Argonne National Laboratory, September 1963.
13. M. Petrick, A Study of Vapor Carryunder and Associated Problems, USAEC Report ANL-6581, Argonne National Laboratory, July 1962.

Section

X

Power Reactor Technology

Specific Reactor Types

Pressurized Water: Study of Zircaloy Core Structure for N.S. Savannah

The reactor for the N. S. *Savannah* was described in detail in *Power Reactor Technology*, 6(1): 43-54. As built, the reactor contained a stainless-steel core structure, and Ref. 1 is an evaluation of the substitution of Zircaloy in the fuel-element containers.

Figure X-1 shows the core structure for the reactor. The boxlike structures contain the fuel elements and presently account for about one-third of the total quantity of stainless steel in the active core. The remaining steel (which is type 304) is accounted for primarily by the cladding of the fuel rods. The substitution of Zircaloy for the element containers would be expected to lower the ^{235}U inventory for a given reactivity lifetime and increase the control-rod worth. Physics calculations and structural analyses were done for the various core compositions considered, and the results were used in an economic study of the fuel cycle. Supporting studies were on the compatibility of Zircaloy with the reactor environment, and a brief safeguards analysis was made.

The results of the nuclear calculations are summarized in Table X-1. The four cases studied were the reference case, S-420, which

Table X-1 SUMMARY OF CALCULATED NUCLEAR CHARACTERISTICS[1] FOR VARIOUS FUEL-ELEMENT CONTAINERS

	Stainless-steel containers, reference case S-420*	Zircaloy fuel-element containers		
		Case Z-420†	Case Z-386‡	Case Z-338§
One-zone enrichment, wt. % ^{235}U	4.20	4.20	3.86	3.38
Multiplication factor of clean core with rods out (followers in)				
Cold	1.132	1.195	1.172	1.135
Hot	1.079	1.138	1.114	1.079
Multiplication factor of clean core with rods in				
Cold	0.972	0.991	0.969	0.934
Hot	0.882	0.910	0.886	0.848
Cold worth of all control rods, % Δk	16	20	20	20
Shutdown margin of cold, clean core with central rod out, % Δk	1.4	Supercritical	1.4	4.9
Lifetime, years at 63 Mw(t)	1.63	3.20	2.52	1.63

*Case S-420 was the reference case, with core 1 type fuel elements (uniform enrichment of 4.20 wt. %) in stainless-steel containers.

†Case Z-420 was the same as the reference case except that the containers were Zircaloy.

‡Case Z-386 had core 1 type fuel elements (uniform enrichment of 3.86 wt. %) in Zircaloy containers; enrichment was adjusted to give the same shutdown margin with the central rod out as the reference case.

§Case Z-338 had core 1 type fuel elements (uniform enrichment of 3.38 wt. %) in Zircaloy containers; enrichment was adjusted to give the same lifetime as the reference case.

represented the as-designed reactor, and three cases employing Zircaloy fuel-element boxes, cases Z-420, Z-386, and Z-338. These cases are described in the table. The results of the economic evaluation of the various cases are summarized in Table X-2. The savings are substantial in all the cases; it was concluded that the Zircaloy boxes would cost about $ 130,000 more than the stainless-steel boxes, but this cost was amortized over a 20-year core life and was insignificant in the final results.

Zircaloy-2 and Zircaloy-4 were evaluated for applicability over the expected 20-year life of the core. Corrosion, wear, and long-lived crud activity were found to be acceptable with the only area of uncertainty being the susceptibility of Zircaloy to fretting corrosion. This problem might be accentuated on the N. S. *Savannah* reactor because of its mobile nature, but the problem of fretting corrosion is potentially present in any reactor employing Zircaloy as structural material. Reference 1 includes a review of previous investigations on fretting corrosion of Zircaloy, which are considered inconclusive for the proposed application. The material appears susceptible to impact corrosion that might arise owing to repeated contact between fuel elements and their Zircaloy containers. The conclusion[1] is that this can only be answered by testing a mockup of a portion of the core under the proposed system conditions.

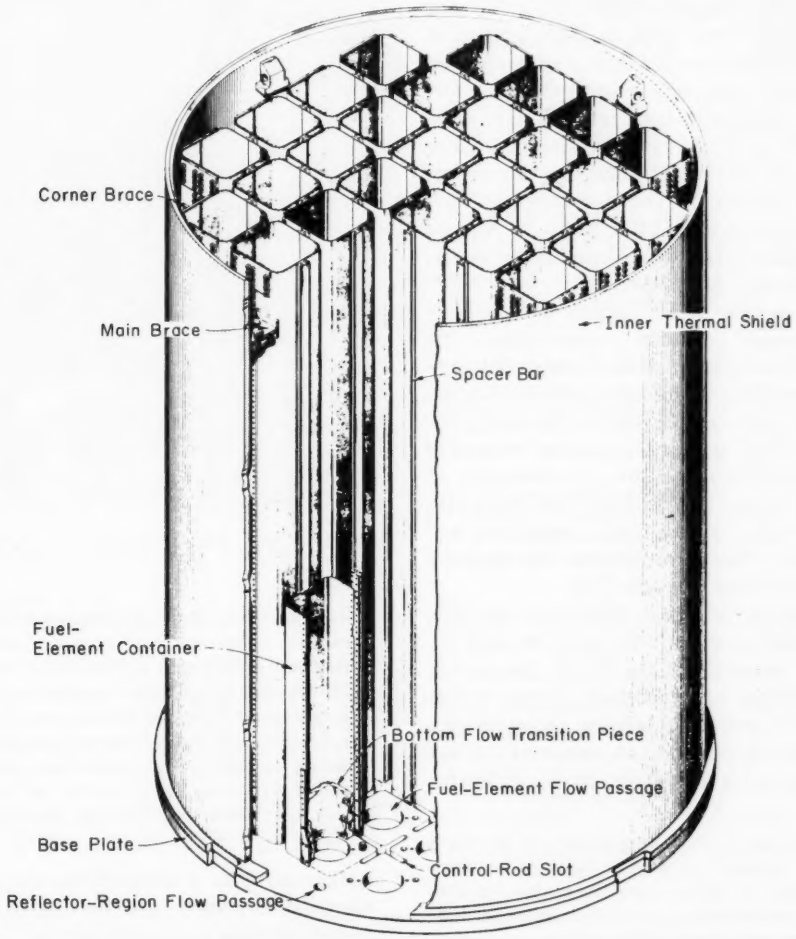

Fig. X-1 Fuel-element container assembly.[1]

Table X-2 COST REDUCTIONS RESULTING FROM SUBSTITUTING ZIRCALOY FOR STAINLESS STEEL IN FUEL-ELEMENT CONTAINERS[1]

Cost component	Cost reduction, % (based on cost for reference case S-420)*		
	Case Z-420	Case Z-386	Case Z-338
Fabrication	49	38	9
Net burnup	1	4	2
Reprocessing	49	37	7
Uranium use charge	7	15	26
Working capital	2	5	9
Total fuel cycle	32	26	10

*See the Table X-1 footnotes for a description of the cases.

Organic-Cooled Reactors: The Tripartite Meeting

The Tripartite Organic-Cooled Heavy-Water Reactor Meeting was held in June 1962, and Ref. 2 is the collection of the papers presented at this meeting. Although most of the information is now rather old, the document does contain a collection of papers from Atomic Energy of Canada, Ltd. (AECL), which are not otherwise widely available. The participants at the meeting were from the AECL, the U. S. Atomic Energy Commission, and the Communauté Européene de l'Énergie Atomique.

An early design of an organic-cooled deuterium-moderated reactor experiment, the OCDRE, is described in Ref. 3. After this design was reworked to include some additional experimental features, it was termed the OTR. It is now called the WR-1 and is scheduled for completion[4] in late 1964. A schematic of the WR-1 is shown in Fig. X-2. The basic aim of the reactor is to test fuels, materials, and coolants under reactor conditions. Parameters of interest are given in Table X-3.

A key problem is one of materials, and sintered aluminum powder (SAP) is to be used for the cladding material of the WR-1. Because of the susceptibility of zirconium alloys to hydriding, their use for cladding and pressure tubes in the organic-cooled reactors is not straightforward, as evidenced by the following quotation:[4]

> Zirconium alloys were considered in the early days of the organic program in the USA but were discarded due to unfavorable corrosion results. However, re-examination of the data showed a wide scatter in the results with some indication of promise under certain conditions. Over the past two-year period several in-reactor and out-reactor tests have been done at Chalk River with promising results. In the last and most severe test two fuel elements of UO_2 clad in Zircaloy-2 were irradiated for 3 weeks in an organic coolant with sheath temperatures of 460°C. No visible change occurred and a detailed examination showed that the sheaths had picked up essentially no hydrogen. This makes the use of zirconium alloy sheaths and pressure tubes look very attractive, although there still is a great deal of work to be done.

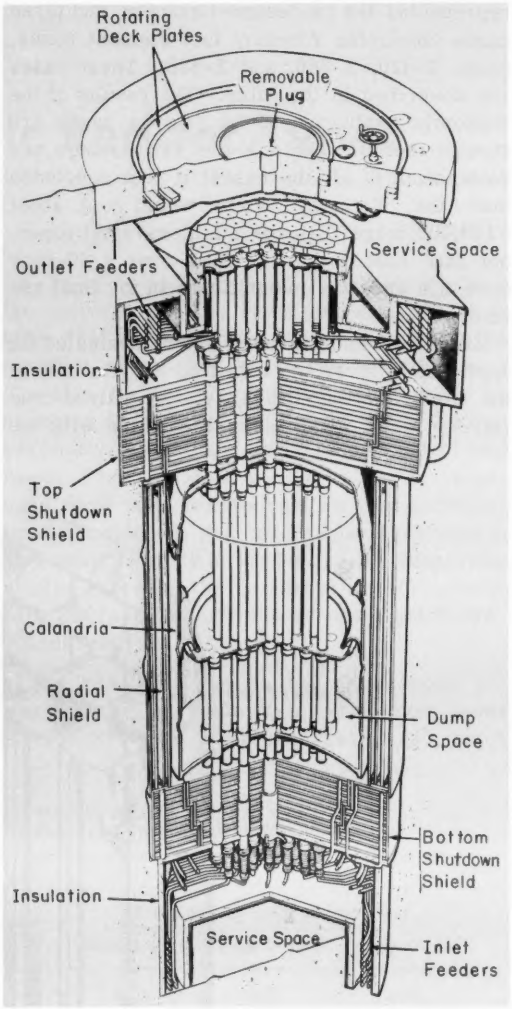

Fig. X-2 Cutaway[4] of the WR-1.

Reference 6 is a study of the use of zirconium alloys in organics, and the following are suggested as ways to use the alloys:

—insulate the zirconium alloy from the organic material

Table X-3 DESIGN PARAMETERS FOR THE WR-1 REACTOR

Reactor type	Uranium oxide fuel, heavy-water moderator, organic coolant, vertical construction
Total nuclear power, Mw(t)	30.0
Reactor power, Mw(t)	28.6
Number of fuel sites	37 at 2.23% enrichment
Power per site, maximum fuel rating, Mw	1.07
Core data	
Lattice type	Triangular
Lattice pitch, in.	9.25
Cell area, cm^2	478
Nominal hot core radius, in.	29.54
Nominal core height, ft	7
Actual core height, ft	8
Maximum thermal-neutron flux, neutrons/(cm^2)(sec)	1.08×10^{14}
Average/maximum axial flux	0.637
Average/maximum radial flux	0.776
Fuel-channel assembly	
Geometry	
Internal diameter, core region, in.	3.25
Overall length	33 ft 1.5 in.
Minimum wall thickness, core region, in.	0.0315
Approximate dry weight, lb	
Without fuel	400
With fuel and coolant	700
Material	S.S. (initially)
Fuel closure	Standard mechanical type closure
Fuel support	Fuel is hung from the fuel closure
Calandria form	Vertical cylinder tapered on top side with dished top and bottom
Material	304L S.S.
Nominal inside diameter	8 ft 10 in.
Overall height, ft	16.5
Wall thickness, in.	$\frac{1}{2}$
Top head thickness, in.	$\frac{3}{4}$
Bottom head thickness, in.	$1\frac{3}{8}$
Dry weight, less extensions, lb	32,200
Calandria tubes	
Material	ASTM B-210-60T-alloy 5052 aluminum
Quantity	13
Inside diameter, in.	4.755
Wall thickness, in.	0.060
Quantity	24
Inside diameter, in.	3.695
Wall thickness, in.	0.050
Heavy-water inventory at 120°F, lb	
Calandria	31,500
Moderator system pipes	2470
Main pumps	120
Demineralizer circuit	323
Heat exchanger	1050
Helium pumps	106
Instrumentation system	20
Approximately 3% reserve	1111
Total	36,700
Reactor heat transport system	
Total flow, lb/hr $\times 10^{-6}$	3.3
Outlet temperature, °F	700
Inlet temperature, °F	640
Maximum velocity through coolant tubes, ft/sec	30
Design pressure drop across fuel, psi	150
Channel outlet pressure, psi	165
Fuel	
Fuel density at 20°C, g/cm^3	10.4 to 10.7
Sheath material	SAP
Type of assembly	19-element bundle
Bundles/site	1
Number of bundles in core	37
Fuel length, hot, in.	96
Overall bundle length, approximate in.	106
Sheath outside diameter, maximum cold and hot, in.	0.6035 and 0.6095
Sheath thickness, average in.	0.0235
Fuel temperature and ratings	
Maximum fuel temperature, °F	
At surface	1380
At center	3730
Maximum sheath surface temperature, °F	895
Maximum internal pressure, psia	350 to 450
Maximum surface heat flux, Btu/(hr) (sq ft)	298,000
Linear power rating, normal	
Of bundle, kw/cm	7.85
Of element, $Q/4\pi$, watts/cm	36.4
Heat flux distribution	Sinusoidal in axial direction
Coolant	
Material	Mixture by weight of 70% Santowax OM and 30% radiolytic tars
Final melting point, °F	152
Vapor pressure at 700°F, psia	39
Moisture content, ppm	Less than 100
Estimated organic damage rate at 30 Mw nominal and 30% high boiler, lb/hr	11.2

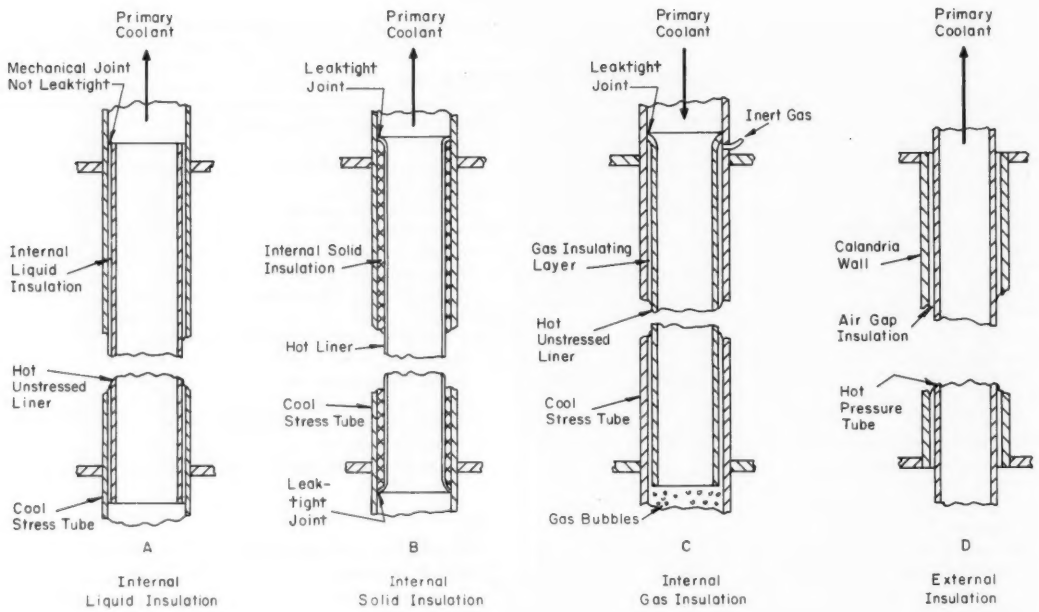

Fig. X-3 Pressure-tube designs.[4]

— coat the alloy with a material impervious to hydrogen, to prevent hydrogen pickup

— control coolant conditions to maintain a protective oxide film on the zirconium alloy

— reduce the hydrogen content until pickup is reduced to a tolerable rate

Reference 6 is a progress report. It discusses experiments done with Zircaloy-2 and a Zirconium – 0.5 copper–0.4 molybdenum alloy, called "ATR." The authors came to the decision that the evidence is not conclusively against the use of zirconium alloys in organic environments.

The basic design problem of a pressure-tube reactor is that of the pressure tube. The WR-1 utilizes, for example, an aluminum calandria tube to keep the relatively cool moderator (90–200°F) from contacting the pressure tube (about 650°F). In contrast, the Carolinas-Virginia Tube Reactor (the CVTR, a D_2O-cooled reactor) uses internal insulation between the fuel bundle and the pressure tube, so that the pressure-tube temperature approaches that of the moderator [see *Power Reactor Technology*, 6(4): 63-81]. Several possible approaches are summarized in Fig. X-3. The design employing the internal liquid insulation is simple in concept but difficult in practice; it is the concept used in the CVTR, which employs a multiplicity of thermal baffles, some attached to the pressure tube and some to the fuel bundle. The design employing internal solid insulation poses materials problems. The Canadian workers have been studying the use of fibrous compressed silica insulation, known as MinK, for this application.[7] The internal gas insulation approach is not a natural one for a liquid-cooled reactor and did not receive much attention in Refs. 4 and 7. The external insulation concept, which is used for the WR-1, results in operation with a hot pressure tube. Operation of the tube at elevated temperature accentuates corrosion problems and reduces greatly the probability of finding a successful zirconium alloy for the application. It also reduces the strength of the tube material and increases the required wall thickness. This consideration may be a less important one when an organic coolant is used, since the coolant pressure is not high.

References

1. T. D. Anderson, E. E. Gross, H. C. McCurdy, L. D. Schaffer, L. R. Shobe, and C. L. Whitmarsh, Summary Report, An Evaluation of the Substitution of Zircaloy for Stainless Steel in N.S. *Savannah* Fuel-

Element Containers, USAEC Report ORNL-3476, Oak Ridge National Laboratory, Nov. 6, 1963.
2. The Tripartite Organic Cooled Heavy Water Reactor Meeting, Santa Monica, California, June 11–13 1962, USAEC Report TID-7648 (Pt. 1).
3. I. MacKay, Organic-Cooled Deuterium-Moderated Reactors, *Nucleonics*, 18(10): 78 (October 1960).
4. W. M. Campbell, Canada's Organic Cooled Reactor Program, in The Tripartite Organic Cooled Heavy Water Reactor Meeting, Santa Monica, California, June 11–13, 1962, USAEC Report TID-7648 (Pt. 1), pp. 1-16.
5. L. R. Haywood, WR-1 Station Data, in The Tripartite Organic Cooled Heavy Water Reactor Meeting, Santa Monica, California, June 11–13, 1962, USAEC Report TID-7648 (Pt. 1), pp. 137-161.
6. A. Sawatzky and F. H. Krenz, Zirconium Alloys in Organics: A Possibility, in The Tripartite Organic Cooled Heavy Water Reactor Meeting, Santa Monica, California, June 11–13, 1962, USAEC Report TID-7648 (Pt. 1), pp. 72-91.
7. E. J. Adams, OCDR Coolant Tube Assembly Development, in The Tripartite Organic Cooled Heavy Water Reactor Meeting, Santa Monica, California, June 11–13, 1962, USAEC Report TID-7648 (Pt. 1), pp. 41-56.

LEGAL NOTICE

This journal was prepared under the sponsorship of the U. S. Atomic Energy Commission. Neither the United States, nor the Commission, nor any person acting on behalf of the Commission:

A. Makes any warranty or representation, expressed or implied, with respect to the accuracy, completeness, or usefulness of the information contained in this journal, or that the use of any information, apparatus, method, or process disclosed in this journal may not infringe privately owned rights; or

B. Assumes any liabilities with respect to the use of, or for damages resulting from the use of any information, apparatus, method, or process disclosed in this journal.

As used in the above, "person acting on behalf of the Commission" includes any employee or contractor of the Commission, or employee of such contractor, to the extent that such employee or contractor of the Commission, or employee of such contractor prepares, disseminates, or provides access to, any information pursuant to his employment or contract with the Commission, or his employment with such contractor.

NUCLEAR SCIENCE ABSTRACTS

The U. S. Atomic Energy Commission, Division of Technical Information, publishes *Nuclear Science Abstracts (NSA)*, a semimonthly journal containing abstracts of the literature of nuclear science and engineering.

NSA covers (1) research reports of the U. S. Atomic Energy Commission and its contractors; (2) research reports of government agencies, universities, and industrial research organizations on a world-wide basis; and (3) translations, patents, books, and articles appearing in technical and scientific journals.

Complete indexes covering subject, author, source, and report number are included in each issue. These are cumulated quarterly, semiannually, and annually providing a detailed and convenient key to the literature.

Availability of *NSA*

SALE *NSA* is available on subscription from the Superintendent of Documents, U. S. Government Printing Office, Washington, D. C., 20402, at $30.00 per year for the semimonthly abstract issues and $22.00 per year for the four cumulated-index issues. Subscriptions are postpaid within the United States, Canada, Mexico, and all Central and South American countries, except Argentina, Brazil, British and French Guiana, Surinam, and British Honduras. Subscribers in these Central and South American countries, and in all other countries throughout the world, should remit $37.00 per year for subscriptions to semimonthly abstract issues and $25.00 per year for the four cumulated-index issues.

EXCHANGE *NSA* is also available on an exchange basis to universities, research institutions, industrial firms, and publishers of scientific information. Inquiries should be directed to the Division of Technical Information Extension, U. S. Atomic Energy Commission, P. O. Box 62, Oak Ridge, Tennessee, 37831.

TECHNICAL PROGRESS REVIEWS may be purchased from Superintendent of Documents, U. S. Government Printing Office, Washington, D. C., 20402. *Isotopes and Radiation Technology* at $2.00 per year for each subscription or $0.55 per issue; the other four journals at $2.50 per year and $0.70 per issue. The use of the coupon below will facilitate the handling of your order.

POSTAGE AND REMITTANCE: Postpaid within the United States, Canada, Mexico, and all Central and South American countries except as hereinafter noted. Add $0.50 per year, or $0.15 per single issue for the *Isotopes and Radiation Technology* journal and $0.75 per year or $0.20 per single issue for the other four journals for postage to all other countries, including Argentina, Brazil, British and French Guiana, Surinam, and British Honduras. Payment should be by check, money order, or document coupons, and MUST accompany order. Remittances from foreign countries should be made by international money order, or draft on an American bank, payable to the Superintendent of Documents, or by UNESCO book coupons.

order form

SUPERINTENDENT OF DOCUMENTS
U. S. GOVERNMENT PRINTING OFFICE
WASHINGTON , D. C., 20402

Enclosed:
document coupons ☐ check ☐ money order ☐

Charge to Superintendent of Documents No. _____

Please send a one-year subscription to

☐ NUCLEAR SAFETY

☐ POWER REACTOR TECHNOLOGY

☐ REACTOR FUEL PROCESSING

☐ REACTOR MATERIALS

(Each subscription $2.50 per year; $0.70 per issue.)

☐ ISOTOPES AND RADIATION TECHNOLOGY

(Each subscription $2.00 a year; $0.55 per issue.)

SUPERINTENDENT OF DOCUMENTS
U. S. GOVERNMENT PRINTING OFFICE
WASHINGTON, D. C., 20402

(Print clearly)

Name _____

Street _____

City _____ Zone ____ State _____